Iterative Receiver Techniques for Data-Driven Channel Estimation and Interference Mitigation in Wireless Communications

Ming Zhao

M.Eng. (National University of Singapore)
B.Eng. (First Class Hons)(National University of Singapore)

June 2009

A thesis submitted for the degree of Doctor of Philosophy
in Research School of Information Sciences and Engineering,
College of Engineering and Computer Science
of The Australian National University

Declaration

The contents of this thesis are the results of original research and have not been submitted for a higher degree to any other university or institution.

Much of the work in this thesis has been published or has been submitted for publication as patent, journal papers or conference proceedings.

The research work presented in this thesis has been performed jointly with Dr. Zhenning Shi and Dr. Mark C. Reed. The substantial majority of this work was my own.

Ming Zhao
Department of Information Engineering,
Research School of Information Sciences and Engineering,
College of Engineering and Computer Science,
The Australian National University,
Canberra,
ACT 0200,
Australia.

Acknowledgements

The work presented in this thesis would not have been possible without the support of a number of individuals and organizations and they are gratefully acknowledged below:

- My supervisors Dr. Mark C. Reed and Dr. Zhenning Shi
- My teammates Matt (Ming) Ruan, David Shepherd, Raymond Chan, Nipun Bhaskar, and Milind Neharkar
- My friends Andrew (Jian) Zhang, Eric (Xiang) Yuan, Lin Luo, Ying Chen and Wen Zhang
- The Australian National University for the funding support in stipend and travel allowance during my Ph.D period
- NICTA Canberra for the facilities to carry out my research
- The ARC Communications Research Network for funding support to attend local and international conferences, and research visits

And to all my friends although I may not list their names here, I sincerely thank them for giving me another way of support.

Finally, I would like to thank Sha for encouraging me to complete the PhD, from the start to finish. Without her trust and support, none of this would have been possible. The rest of my thanks is to my parents. They are always wishing the best for me. Their love and never-ending support are things that I treasure the most.

Abstract

Wireless mobile communications were initially a way for people to communicate through low data rate voice call connections. As data enabled devices allow users the ability to do much more with their mobile devices, so to will the demand for more reliable and pervasive wireless data. This is being addressed by so-called 4^{th} generation wireless systems based on orthogonal frequency division multiplexing (OFDM) and multiple-input multiple-output (MIMO) antenna systems. Mobile wireless customers are becoming more demanding and expecting to have a great user experience over high speed broadband access at any time and anywhere, both indoor and outdoor. However, these promising improvements cannot be realized without an efficient design of the receiver.

Recently, receivers utilizing iterative detection and decoding have changed the fundamental receiver design paradigm from traditional separated parameter estimation and data detection blocks to an integrated iterative parameter estimator and data detection unit. Motivated by this iterative data driven approach, we develop low complexity iterative receivers with improved sensitivity compared to the conventional receivers, this brings potential benefits for the wireless communication system, such as improving the overall system throughput, increasing the macro cell coverage, and reducing the cost of the equipments in both the base station and mobile terminal.

It is a challenge to design receivers that have good performance in a highly dynamic mobile wireless environment. One of the challenges is to minimize overhead reference signal energy (preamble, pilot symbols) without compromising the performance. We investigate this problem, and develop an iterative receiver with enhanced data-driven channel estimation. We discuss practical realizations of the iterative receiver for SISO-OFDM system. We utilize the channel estimation from soft decoded data (the *a priori* information) through frequency-domain combining and time-domain combining strategies in parallel with limited pilot signals. We analyze the performance and complexity of the iterative receiver, and show that

the receiver's sensitivity can be improved even with this low complexity solution. Hence, seamless communications can be achieved with better macro cell coverage and mobility without compromising the overall system performance.

Another challenge is that a massive amount of interference caused by MIMO transmission (spatial multiplexing MIMO) reduces the performance of the channel estimation, and further degrades data detection performance. We extend the iterative channel estimation from SISO systems to MIMO systems, and work with linear detection methods to perform joint interference mitigation and channel estimation. We further show the robustness of the iterative receivers in both indoor and outdoor environment compared to the conventional receiver approach.

Finally, we develop low complexity iterative spatial multiplexed MIMO receivers for nonlinear methods based on two known techniques, that is, the Sphere Decoder (SD) method and the Markov Chain Monte Carlo (MCMC) method. These methods have superior performance, however, they typically demand a substantial increase in computational complexity, which is not favorable in practical realizations. We investigate and show for the first time how to utilize the *a priori* information in these methods to achieve performance enhancement while simultaneously substantially reducing the computational complexity.

In our modified sphere decoder method, we introduce a new accumulated *a priori* metric in the tree node enumeration process. We show how we can improve the performance by obtaining the reliable tree node candidate from the joint Maximum Likelihood (ML) metric and an approximated *a priori* metric. We also show how we can improve the convergence speed of the sphere decoder (i.e., reduce the complexity) by selecting the node with the highest *a priori* probability as the starting node in the enumeration process.

In our modified MCMC method, the *a priori* information is utilized for the first time to qualify the reliably decoded bits from the entire signal space. Two new robust MCMC methods are developed to deal with the unreliable bits by using the reliably decoded bit information to cancel the interference that they generate. We show through complexity analysis and performance comparison that these new techniques have improved performance compared to the conventional approaches, and further complexity reduction can be obtained with the assistance of the *a priori* information. Therefore, the complexity and performance tradeoff of these nonlinear methods can be optimized for practical realizations.

List of Publication

Journal Papers

Ming Zhao, Zhenning Shi and Mark C. Reed, "Iterative Turbo Channel Estimation for OFDM System over Rapid Dispersive Fading Channel.", *IEEE Trans. Wireless Commun.*, vol. 7, no. 8, pp. 3174-3184, Aug 2008.

Conference Papers

Ming Zhao, Zhenning Shi and Mark C. Reed, "Iterative Turbo Channel Estimation for OFDM System over Rapid Dispersive Fading Channel.", in *Proc. IEEE Int. Conf. Communications (ICC).*, Glasgow, Scotland, Jun 24-28, 2007, pp. 4849-4854.

Ming Zhao, Zhenning Shi and Mark C. Reed, "An Iterative Receiver with Channel Estimation for MIMO-OFDM System over Time and Frequency Dispersive Channel.", in *Proc. IEEE Globecom.*, Washington, DC, USA, Nov 26-30, 2007, pp. 4155-4159.

Ming Zhao, Zhenning Shi and Mark C. Reed, "Modified Schnorr-Euchner Sphere Decoding for Iterative Spatial Multiplexing MIMO Receiver.", in *Proc. IEEE Int. Symp. Spread Spectrum Techniques and Applications (ISSSTA).*, Bologna, Italy, Aug 25-28, 2008, pp. 118-123.

Ming Zhao, Zhenning Shi and Mark C. Reed, "On Performance of Sphere Decoders for Iterative Spatial Multiplexing MIMO Receiver," in *Proc.* 5^{th} *Int. Symp. Turbo Codes.*, Lausanne, Switzerland, Sep 1-5, 2008, pp. 113-117.

Ming Zhao, Zhenning Shi and Mark C. Reed, "A Reduced State Space Markov Chain Monte Carlo Method for Iterative Spatial Multiplexing MIMO," submitted to *IEEE Globecom.*, Hawaii, U.S.A., 30 Nov-4 Dec, 2009.

Preliminary Patent

Ming Zhao, Zhenning Shi and Mark C. Reed, "Detection of a Communication Signal.", Australian Provisional Patent, May 2008.

Ming Zhao, Zhenning Shi and Mark C. Reed, "Channel Estimation for Future Mobile Communication System.", Australian Provisional Patent, Apr 2006.

List of Acronyms

16-QAM	16-quadrature amplitude modulation
APP	a posteriori probability
AWGN	additive white Gaussian noise
BEM	basis expansion model
BER	bit error rate
BLAST	Bell laboratories-layered-space-time
BPSK	binary phase shift keying
CDMA	code division multiple access
CFO	carrier frequency offset
CLT	central limit theorem
CP	cyclic prefix
CRC	cyclic redundancy check
CRLB	Cramér-Rao lower bound
CSI	channel state information
DAB	digital audio broadcasting
DFE	decision feedback equalizer
DFT	discrete Fourier transform
DS-CDMA	direct sequence CDMA
DVB	digital video broadcasting
EM	expectation-maximization
FER	frame error rate
FFT	fast Fourier transform
FP	Fincke-Pohst
FST	force-state-transitions
GS	gibbs sampler
ICI	inter-carrier interference
IDD	iterative detection and decoding
IDFT	inverse discrete Fourier transform

IFFT	inverse fast Fourier transform
i.i.d	independent and identically distributed
IMT-2000	international mobile telecommunications-2000
ISI	inter-symbol interference
ITU	international telecommunication union
LLR	log likelihood ratio
LMMSE	linear minimum mean-square-error
LS	least square
LTE	long term revolution
MAN	metropolitan area network
MAP	maximize a posteriori
MCMC	markov chain monte carlo
MF	matched filter
MIMO	multiple-input-multiple-output
ML	maximum likelihood
MLE	maximum likelihood estimator
MMSE	minimum mean-square-error
MMSEE	minimum mean-square-error estimator
MRC	maximum ratio combing
MSE	mean square error
MUV	minimum-variance unbiased
OFDM	orthogonal frequency division multiplexing
OFDMA	orthogonal frequency division multiple access
PAM	pulse amplitude modulation
PDF	probability density function
P/S	parallel to serial
QPSK	quadrature phase shift keying
QoS	quality of service
QRD	QR decomposition
RSS	reduced-state-space
SCC	serial concatenated code
SCM	spatial channel model
SD	sphere decoder
SE	Schnorr-Euchner
SINR	signal-to-interference-plus-noise ratio
SISO	single-input-single-output
SM	spatial multiplexing

SNR	signal to noise ratio
S/P	serial-to-parallel
SPIC	soft parallel interference cancelation
STBC	space-time block-coded
STC	space-time coded
STTC	space-time trellis-coded
SVD	singular value decomposition
UMTS	universal mobile telecommunications system
V-BLAST	vertical BLAST
WCDMA	wideband code-division-multiple-access
WiMAX	worldwide interoperability for microwave access
WLAN	wireless local area network
WSSUS	wide sense stationary uncorrelated scattering
ZF	zero forcing

Notations and Symbols

$\mathbf{A}^H$	complex conjugate transpose of matrix $\mathbf{A}$
$\mathbf{a}^H$	complex conjugate transpose of vector $\mathbf{a}$
$\mathbf{A}^T$	transpose of matrix $\mathbf{A}$
$\mathbf{a}^T$	transpose of vector $\mathbf{a}$
$\mathbf{A}^*$	complex conjugate of matrix $\mathbf{A}$
$\mathbf{a}^*$	complex conjugate of vector $\mathbf{a}$
$[\mathbf{A}]_{i,j}$	the $(i,j)^{th}$ elements of matrix $\mathbf{A}$
$[\mathbf{a}]_i$	the i^{th} elements of vector $\mathbf{a}$
$\{x\}$	the sequence $\{x_0, x_1, \ldots\}$
$\arg(\cdot)$	argument
$diag(\cdot)$	diagonal matrix
$E\{\cdot\}$	expectation
$\Im(\cdot)$	imaginary component
$\mathcal{J}$	cost function
$J_0(\cdot)$	the first kind of Bessel function of zero order
$\mathcal{K}$	arbitrary constant
$\lim(\cdot)$	limits
$\ln(\cdot)$	natural logarithm
$\max(\cdot)$	maximization
$\min(\cdot)$	minimization
$p(\cdot)$	probability density function
$p(\cdot\|\cdot)$	conditional probability density function
$p(\cdot,\cdot)$	joint probability density function
$P(\cdot)$	probability
$P(\cdot\|\cdot)$	conditional probability
$P(\cdot,\cdot)$	joint probability

$\mathcal{Q}(\cdot)$	Q-function
$\mathcal{Q}^{-1}(\cdot)$	inverse Q-function
$\Re(\cdot)$	real component
$Tr(\cdot)$	trace operator

Contents

List of Figures

List of Tables

Chapter 1

Introduction

1.1 Motivations and Summary of Contributions

Modern wireless communication systems promise to support users with high data rates in a highly mobile environments. No matter which environment (or channel) the wireless communication system is experiencing, the signal processing at the receiver is attempting to make the correct decision on the transmitted data to minimize packet loss and maintain a reliable link for the appropriate application, whether that is a voice call or data messaging. However, such dynamic wireless systems with sparse spectrum resource impose many challenges in system design, which therefore requires the investigation of enabling signal processing techniques. As an example, high mobility users suffers from unstable channel quality, which makes data detection almost impossible without advanced signal processing techniques. Hence, how to manage mobility to fulfill the quality of service (QoS) requirement becomes an open question in modern receiver design.

Under the conventional receiver design framework, channel estimation requires a reference signal, i.e. preamble and/or pilot symbols, to be transmitted in parallel with the information data. The system performance heavily depends on the quality of the reference signal, and the system throughput is compromised as the reference signal occupies a certain amount of bandwidth or power, especially in severe channel environments. Nevertheless, with the iterative detection and decoding, the availability of the *a priori* information of the transmitted signal changes the receiver design paradigm dramatically as the data is no longer a passive quantity which the receiver uses to make a decision on but it can also take the initiative to improve the overall system performance by enhancing other modules such as channel estimation, etc. In the first part of this thesis, an iterative data-driven

channel estimator, which utilizes channel estimation from soft data (the *a priori* information) in parallel with the pilot-aided channel estimation is developed. A standardized Orthogonal Frequency Division Multiplexing (OFDM) system is used to show these techniques are realizable in practice.

Another important technical breakthrough in modern wireless communications is the use of multiple antenna at both transmitting and receiving ends. Compared to single-input-single-output (SISO) system, MIMO systems provide both capacity and diversity enhancements, however, it also introduces a large amount of interference between data streams from different antennas. Improperly managed interference from multiple antennas at the receiver makes channel estimation and data detection a challenging problem, especially in the high mobility environment. In this thesis, the analysis of the channel estimation for the SISO-OFDM system is extended, and an iterative receiver based on soft parallel interference cancelation (SPIC) with channel estimation is proposed for the MIMO-OFDM system.

Furthermore, as mentioned before, data detection is a fundamental block in the iterative detection and decoding. Hence, the second part of this thesis is focusing on developing the advanced data-driven technique to perform the interference mitigation in a interference limited system. The developed technique can be applied to any specific system that needs interference mitigation. Recently, a technique known as sphere decoder (SD) is proposed for data detection in the MIMO spatial multiplexing (SM) environment. The sphere decoder technique provides promising performance, which is close to the ML detector. It also has less complexity than the ML detector because unlike the ML detector searching the entire signal space, the sphere decoder avoids the exhaustive search by restricting the signal search to a limited signal enumeration set, known as the search sphere. Efficient sphere decoder algorithms are developed in the literature, however, they do not make full use of the *a priori* information in the iterative decoding. In this thesis, efficient sphere decoder algorithms are developed for the iterative receiver with spatial multiplexed MIMO system by utilizing the *a priori* information to improve the performance as well as the complexity.

Finally, a statistical data detection method known as Markov Chain Monte Carlo (MCMC) Gibbs sampler (GS) is proposed primarily for the iterative receiver in a code division multiple access (CDMA) system [1–3]. It has been applied for the MIMO spatial multiplexing system as well and compared to the sphere decoder. Unlike the sphere decoder which performs the deterministic search for the solution close to the transmitted signal, the MCMC method walks though random samples

and performs the data detection by selecting statistically significant signal samples. The MCMC method performs very well in low signal to noise ratio (SNR), however, it suffers from an error floor in the high SNR region. In this thesis, two novel MCMC methods are developed for the iterative receiver in the spatial multiplexed MIMO system. Both MCMC methods can remove the error floor at high SNR while one of the MCMC methods can also achieve significant complexity reduction through interference cancelation.

In summary, this thesis investigates the application of the iterative data-driven technique with the assistance from the evolution of the data information for wireless communications. This thesis demonstrates that the data-driven channel estimation and interference mitigation techniques can achieve significantly better receiver sensitivity compared to conventional receivers. The improved coverage and capacity lowers the cost per bit to users and wireless operators where this improvement is simply achieved by the low cost data-driven receivers without any significant alteration of the system architecture.

1.2 Turbo Receiver with Iterative Detection and Decoding

The turbo principle [4–7] has recently emerged as one of the significant technical breakthroughs in the modern wireless communication since the invention of the powerful Turbo codes [8, 9]. Analogous to the original parallel turbo code is serial turbo decoding where the encoding is performed by a Serial Concatenated Code (SCC) [10], the turbo principle can be also utilized to model a wireless communication system as a serial concatenation of an inner code and a outer code, which are separated by an interleaver. Fig. 1.1 shows the wireless communication system with transmitter in the SCC structure and a generic iterative receiver. The inner code refers to the combination of the data modulator and wireless communication channels, which can be either inter-symbol interference (ISI) channel, multiple-access channel, or multiple-input-multiple-output (MIMO) channel. The outer code is realized by the conventional channel encoder. The interleaver serves the purpose of removing correlation between the inner and outer code. Obviously, the optimal performance of the receiver can only be obtained by performing data detection and decoding jointly. However, such joint detection and decoding would result an unrealizable solution with prohibitive complexity, which is exponential in terms of the system dimension, modulation order and channel code memory.

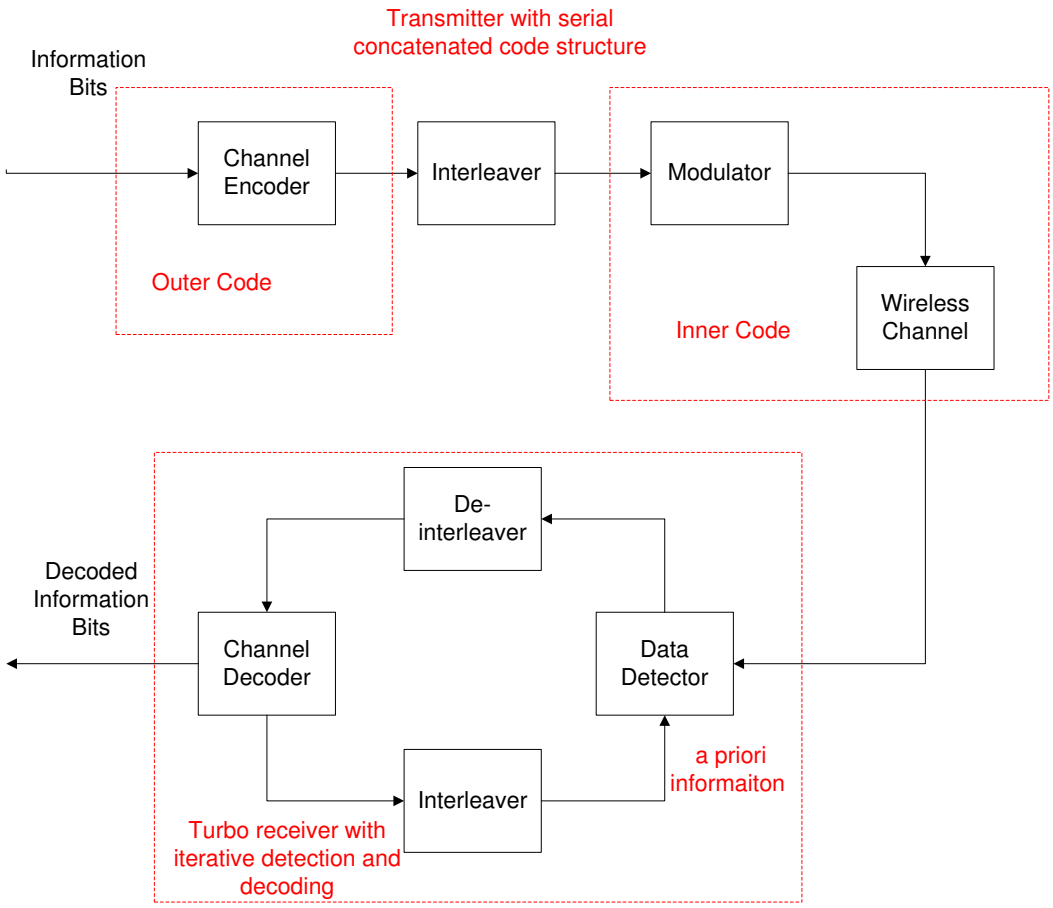

Figure 1.1: Wireless communication system with transmitter and iterative receiver

Conventional receiver performs data detection and decoding as individual units in a non-iterative (sequential) manner, which is not an optimal solution. Recently, iterative receivers based on the Turbo principle have been shown to be able to provide near-optimal performance with linearly increasing additional complexity introduced by iterations. The main characteristics of the iterative receiver are the utilization of the *a priori* probability of the transmitted signal over decoding iterations.

More specifically, it is well known that the data detection rules are developed from the optimal *maximum a posteriori* (MAP) probability detection criteria, which is to find the signal with the maximum *a posteriori probability* (APP) of the transmitted signal. The conventional receiver does not have the knowledge of the *a priori* probability of the transmitted signal, hence, the detection rule is reduced to maximum likelihood (ML) detection criteria, which assumes the trans-

mitted signals are equally probable. On the other hand, from iterative detection and decoding point of view, after the data detection and decoding are performed, the receiver has the knowledge of the transmitted signal. This knowledge of the transmitted signal is treated as *a priori* information. Hence, the iterative receiver can utilize this *a priori* information to perform the data detection with true MAP criteria by updating *a priori* probability of the transmitted signal. This is known as the iterative detection and decoding (IDD) strategy.

Technically, the iterative receiver performs data detection and decoding not just once, but over many iterations. Each iteration consists of one independent data detection and decoding between which the "soft" information of the decoding data is exchanged. By soft we mean that real valued data are used, as opposed to the hard zeros and ones. This information exchanging process runs over iterations between detector and decoder, which are sub-optimal on their own but after a number of iterations, the results converge to the optimum. In this thesis, several iterative receiver techniques are developed for wireless communication systems to improve both the system performance and the complexity. Although this work focuses on the single-user communications, we believe that the data-driven techniques developed can be employed to multi-user communications easily.

1.3 Literature Review and Detailed Contributions

1.3.1 Iterative Receiver with Channel Estimation for SISO-OFDM System

OFDM [11–14] is an attractive technique for high data rate transmission over wireless channels. The most important advantage of an OFDM system over a single carrier system is that it transforms the frequency selective channel into a parallel collection of flat fading subchannels, which simplifies the equalization at the receiver for a small penalty in performance due to a guard interval. OFDM has been adopted in several wireless standards such as digital audio broadcasting (DAB), digital video broadcasting (DVB-T), the IEEE 802.11a [15] Wireless Local Area Network (WLAN) standard and the IEEE 802.16a/e [16,17] Metropolitan area network (MAN) standard. OFDM is also a potential candidate for the next generation mobile wireless communications.

With the knowledge of channel state information (CSI), coherent detection can be performed on OFDM symbols. Realistic mobile radio channels are characterized

by the time and frequency dispersive nature due to the multipath delay profile and the Doppler spread of the channel. It has been shown in Chapter 2 Section 2.2.3 that the channel variation becomes more significant in both time and frequency domain as the mobility and the delay spread increase. Therefore, rapid dispersive fading channel with time and frequency selectivity makes channel estimation and tracking a challenging problem in OFDM system design.

Generally speaking, in order to estimate time and frequency selective channels, training signals are employed in OFDM packets, which are known as preamble channel estimation and pilot-aided channel estimation [18, 19]. Another channel estimation technique, known as blind adaptive technique [20–22], which does not apply any training signals, is also well explored in the literature. However, the blind estimation approach does not align with the practical systems which adopt training signal based approach. Hence, this thesis is focusing on the training signal based approach.

In the practical OFDM system, the training signal arrangements are different for the uplink and downlink. In the uplink, pilot signals are inserted in OFDM data symbols, while a preamble is transmitted prior to the data symbols in the downlink OFDM frames. More specifically, conventional OFDM systems [15–17] assume the channel is static within one frame, and only use channel estimates obtained from the preamble for data symbol detection. Such an approach performs well in static channels but incurs a severe performance degradation in the rapidly dispersive fading channel. Dowler *et al.* [23] proposed a data derived method, which uses decoded hard decision data of the current symbol to adjust the channel estimate for the next symbol. This method partially tracks the channel variation, but also introduces delays and error propagation.

In the uplink transmission, pilots are often multiplexed into the data sequence and channel estimation can be performed by interpolation. Negi *et al.* [24] proposed least square (LS) based channel estimation and discussed optimal pilot spacing. In the papers [25–27], channel estimators for OFDM system have been proposed based on the singular value decomposition (SVD) and frequency domain filtering. Time domain filtering has been proposed in [28] to further improve the channel estimator. Extended from Beek's work, Li *et al.* [29]investigated the correlation of channel frequency response over times and frequency and proposed a robust minimum mean-square-error (MMSE) channel estimator. Robertson *et.al* [18] proposed a two-dimensional Wiener filtering pilot symbol channel estimation. However, complexity prohibits their application to practical systems.

In order to resolve time selective channels, Stamoulis *et al.* [30] developed a channel estimator based on linear interpolation of partial channel information. Shin *et al.* [31], Zemen *et.al* [32, 33] and Kim *et.al* [34] approximated LMMSE estimation by representing the channel in basis expansion model (BEM) [35–37] to obtain the channel impulse response from interpolation of the partial channel information. Schniter *et.al* [38, 39] proposed channel estimation using FFT and specific time-domain pilot signals, however, due to the utilization of time-domain pilot signals, it may not be compatible with existing OFDM standards. Furthermore, although above methods can track the rapid dispersive channel, system throughput is sacrificed due to the enormous amount of pilots inserted.

Song *et al.* [43] proposed iterative joint zero forcing (ZF) channel estimation and signal detection algorithm based on hard decision feedback. To address dispersive channels, Park *et al.* [44] proposed an iterative channel estimator by employing time and frequency domain MMSE filters for mobile radio channels. Tomasin *et al.* [45] proposed an iterative receiver with inter-carrier interference (ICI) cancelation and MMSE channel estimation for extremely high mobility condition. These receivers are computationally complex and infeasible for practical systems.

As we can see, in the rapid dispersive channel environment, conventional preamble-based and pilot-aided channel estimation require numerous reference signals, which significantly compromises the system throughput. On the other hand, data signals are also part of transmission. In the iterative detection and decoding, soft data signals are available and can be considered as reference signals but with limited reliability. Therefore, a fundamental question is could the soft data signals make contribution in the channel estimation? We believe that better channel estimation will improve the data detection, and vice versa, the improved data detection could benefit the channel estimation. Hence, a novel low complexity iterative turbo channel estimation technique is developed, which makes use of preamble, pilots and soft decoded data information in an iterative fashion to improve the system performance over the time and frequency selective fading channel while maintaining the system throughput.

1.3.2 Iterative Receiver with Channel Estimation for MIMO-OFDM System

Digital communications using MIMO [3] have recently been proposed as one of the most significant technical breakthroughs in modern communications. It also attracts a lot of research attentions and many state-of-art results are published in

the literature. Surprisingly, in a few year time after the invention, MIMO technology has been adopted in large-scale standards-driven commercial wireless products and networks such as Worldwide Interoperability for Microwave Access (WiMAX), WLAN, 3G long term evolution (LTE) [46] and beyond.

MIMO systems can be defined a link for which the transmitting and receiving ends are equipped with multiple antenna elements. The idea behind this is that the signals on the transmitting antennas and receiving antennas are combined in such a way that the quality of the communication can be improved from diversity benefit [3]. MIMO systems also provide a capacity improvement of N times, where N is the minimun number of antennas at either end of the link [47]. In a MIMO system, channel modeling is particularly critical to properly determine algorithm performance because of sensitivity with respect to correlations and system model matrix rank properties, which are some fundamental differences compared to SISO system.

The combination of MIMO and OFDM is a promising approach for broadband wireless communication [15–17]. The difference between the MIMO-OFDM system and the SISO-OFDM system is the additional space-time processing module [47], which is applied to improve both the data rate and reliability of wireless link by taking advantage of the spatial diversity achieved by spatially separated antennas in a dense multipath scattering environment. The space-time processing techniques typically fall into two categories: data rate maximization and diversity maximization, although there has been some effort toward unification recently [48]. In the first category, the data rate maximization is achieved through spatial multiplexing data streams to different transmitting antennas, a particular example is the vertical Bell labs layered space time (V-BLAST) system [49]. On the other hand, the individual streams could be encoded jointly in order to protect transmission against errors caused by channel fading and noise plus interference. This leads to a second kind of category in which one tries also to put a level of redundancy through the space-time coding (STC) [50]. Effectively, a number of coded data symbols equal to the number of transmitting antennas are generated and transmitted simultaneously, one symbol per antenna. These coded data symbols are generated by the space-time encoder such that by using the appropriate signal processing and decoding procedure at the receiver, the diversity gain and/or the coding gain is maximized. Hence, each transmitting antenna sees a differently encoded, redundant version of the same transmitting signal. In this case, the multiple antennas are only used as a source of spatial diversity and not to increase the data rate.

In practical MIMO-OFDM system, two mandatory MIMO space-time processing profiles [51], namely the Alamouti STC [52] and Spatial Multiplexing (SM), are employed. The typical example is IEEE 802.16e Mobile WiMAX system [17]. In both STC and SM systems, the received signal at each receiving antenna is the superposition of the fading signals from all transmitting antennas. In time and frequency dispersive fading environment, the channel is time varying over symbols. The massive interferences and channel variations make channel estimation and tracking a challenging problem and affect data detection significantly.

Conventional MIMO-OFDM receiver usually adopted one-shot channel estimation and data detection, which can be achieved through well known signal processing techniques [53] such as maximum ratio combing (MRC) for Alamouti STC system, and ZF or MMSE for SM system. An important assumption made in the STC-OFDM system is that the channel is static within the two consecutive OFDM symbol period, then one-shot channel estimation from preamble can be done and used for rest of OFDM symbols in a two-symbol STC block basis. The static channel assumption does not hold any more if the channel coherence time is shorter than the radio frame. As seen in Fig 3.6 of Chapter 3 Section 3.3, the correlation among consecutive OFDM symbols fades away when other OFDM symbols are far away from the OFDM symbol of interest. In this case, the MRC receiver will suffer from severe channel estimation mismatch. On the other hand, in SM-OFDM system, the received signal is the superposition of the fading signals from all transmitting antennas. In time and frequency dispersive fading environment, the channel is time varying over symbols. The massive interference and channel variations make channel estimation and tracking a challenging problem and affect data detection significantly. In other words, the conventional channel estimation fails in the mobile radio channel with time and frequency variations.

Li *et al.* [40–42] proposed decision-directed LS and MMSE channel estimators for OFDM system with multiple antennas. Song *et al.* [43] proposed iterative joint ZF channel estimation and signal detection algorithm based on hard decision feedback, error propagation may exist to degrade the receiver performance. Wang *et al.* [54,55] proposed an iterative receiver for space-time block-coded (STBC) OFDM system based on expectation-maximization (EM) approach. Such receiver assumes that the fading process is constant over the duration of one STBC code word to reduce the receiver complexity. Juntti *et al.* [56–59] also applied EM based channel estimator in MIMO-OFDM system. The EM channel estimator works in an iterative procedure to avoid direct matrix inversion, which is necessary for the ZF

channel estimator. However, the EM channel estimator is designed to approximate the ZF channel estimator. It only achieves complexity reduction and doesn't bring further channel estimation improvement. Lim *et al.* [60] approximated a time varying channel as polynomials, which is not practical due to high computation complexity. Moon *et al.* [61] developed an iterative receiver well suited for WLAN. However, the effectiveness of above mentioned systems substantially decreases under high mobility situations. Hu *et.al* [62] discussed the optimal pilot sequence and proposed a nonuniform distributed pilot arrangement for channel estimation in MIMO-OFDM systems, which is not able to handle mobility environment.

In Chapter 3, an receiver with iterative turbo channel estimation has been developed, which are able to provide near-optimal channel estimation and data detection performance in the realistic mobile radio channel environment with rapid time and frequency dispersive fading characteristics. Hence, we are going to apply the proposed receiver with iterative turbo channel estimation to MIMO-OFDM systems. More specifically, a novel low complexity channel estimator with time-domain and frequency-domain combining of channel estimates from preamble, pilots and soft decoded data information is proposed to track the dynamics of channel frequency response. This channel estimator is integrated with MRC receiver for Alamouti STC system and interference canceler for the system with spatial multiplexing.

1.3.3 Iterative Receiver on Sphere Decoder

MIMO spatial multiplexing systems have been applied to improve both the data rate and the reliability of wireless link. It takes the advantage of the multiplexing gain and spatial diversity by spatially separated antennas in a dense multipath scattering environment. A variety of detection algorithms have been proposed for MIMO systems. The ML detection is an optimal detector compared to the conventional ZF detector, decision feedback equalizer (DFE), and MMSE detector [63]. However, the complexity of ML detection grows exponentially with the number of antennas.

Recently, a technique called sphere decoder [64] was proposed for MIMO systems. The sphere decoder provides the approximation of ML estimate of the transmitted signal sequence by restricting the search range to a limited enumeration set rather than to the entire signal space. It is generally agreed that the sphere decoder technique has polynomial [65] computational complexity only for high SNRs.

Sphere decoder algorithms can be identified into three categories in the literature. The first category is known as depth-first algorithms [66–68], the second

category is known as breadth-first algorithms [69], and the third category is known as the metric-first algorithms [70]. Graphically, if the sphere decoder algorithms are considered as a systematic procedure to perform a tree search, the depth-first algorithms perform the search first vertically then horizontally. On the other hand, the breadth-first algorithms perform the tree search first horizontally then vertically. Juntti *et al.* [58] developed efficient breadth-first algorithm, known as iterative K-best sphere decoder. Compared to the conventional K-best sphere decoder [69] which initialized the tree search by QR decomposition (QRD), authors in [58] initializes the K-best sphere decoder by LMMSE estimate to obtain better convergence behavior to reduce the complexity. Another difference is that authors in [58] also introduced decision feedback to the K-best sphere decoder. Finally, the metric-first algorithm is same as finding the shortest path in graph theory, which is far more complex in the practical implementation. In this chapter, we focus on the depth-first sphere decoder algorithms. The breadth-first and metric-first sphere decoder algorithms are out of the scope of this thesis. Hence, unless otherwise stated, the "sphere decoder" refers to the depth-first algorithms in the rest of the thesis.

Fincke-Pohst (FP) enumeration [66] is a well known sphere decoding algorithm to evaluate all the lattice points within a sphere. It consists of spanning the tree search by defining a admissible interval at each level. All symbol hypotheses are enumerated at each level between the lower and upper bounds determined by the interval. Nevertheless, the FP algorithm has a prohibitive complexity which is exponential with the dimension of the tree search in the worst case. The Schnorr-Euchner (SE) enumeration [67] is a variation of the FP algorithm. Instead of enumerating all the lattice points within the interval, the SE algorithm performs the tree node search in a zig-zag order, starting from the zero forcing solution. Numerical results in [71] showed that the SE enumeration is more efficient than the FP implementation.

In [68], the authors made the connection between the sphere decoding and stack sequential decoding, and applied the SE algorithm [67] in the tree search. Such an approach could offer significant reductions in the computational complexity compared to the FP enumeration-based sphere decoder. Although the SE algorithm is not sensitive to the initial radius, there is a performance loss due to the poor ZF-DFE estimate at the beginning of the tree search. Reference [68] proposed a number of preprocessing algorithms to enhance the initial estimate, such as those using ordered ZF-DFE and MMSE estimates.

Iterative detection and decoding has been introduced to sphere decoding, known as list sphere decoding [72]. Instead of finding the ML point, a list of candidates with a specified radius close to ML points are generated by the a soft MIMO detector. Reference [73] had a similar approach but included the *a priori* information to generate the list. Yuan *et al.* [74] proposed an approximated MAP-based iterative receiver with modified sphere detection. The sphere decoder used in these works is based on the FP enumeration, which is less efficient compared to the SE algorithm [68].

Unlike previous approaches, we think that the *a priori* information metric could play a significant role in the enumeration process, i.e. the tree node search, rather than contributing as a term in the *a posteriori* probability evaluation. Firstly, the sphere decoder is defined to estimate the MAP probability of the received symbol sequence. Secondly, the FP and SE algorithms are modified by accumulating the *a priori* information metric in the enumeration process. More specifically, the Algorithms I and II in [68] are extended to iterative reception by including an accumulated *a priori* information metric. Thirdly, for Algorithm II, an improved ZF-DFE symbol estimation is developed by approximating the *a priori* information with a quadratic metric in the sphere decoder tree search. Furthermore, an improved tree search is developed to adjust the starting point in *a priori* zig-zag fashion. These two novel schemes aim to improve the performance and reduce the computational complexity even further over iterations.

1.3.4 Iterative Receiver on Markov Chain Mento Carlo Methods

MIMO spatial multiplexing system has similar characteristics as a multiple access system [75, 76], where each transmit antenna may be viewed as a user and the channel gains between one transmit antenna and multiple receive antennas can be viewed as spreading code for the corresponding user. Conventional suboptimal MIMO detection methods, e.g., ZF detector, DFE detector, MMSE detector, and sphere decoder are proposed to perform deterministic search of the near ML candidate in the signal space with a reduced complexity.

Recently, a statistical method called Gibbs sampling [22, 77–79] that is a particular realization of Markov Chain Monte Carlo simulation [80] has been applied to MIMO detection. In MCMC, statistical inferences are developed by simulating the underlying process through Markov chain. The Gibbs sampling is a particular Markov chain process that searches the state space defined by the transmitted

signal. The basic idea is to draw random samples of unknown transmitted signal from their conditional posterior distribution and then to calculate the marginal *a posteriori* distribution by averaging over the random samples. Hence, Gibbs Sampling starts from uniformly distributed samples and walks through the transmitted signal space in a stochastic manner to look for the important/significant samples close to the transmitted signal.

Hence, the MCMC method is an alternative search technique which is unique in two ways. Firstly, the MCMC method is a stochastic approach. Secondly, the growth of the size of the candidates (analogy to the nodes visited in sphere decoder) that Gibbs sampling walks through and thus the complexity of the MIMO detector is not exponential with the number of bits per channel users (analogy to the dimensions in sphere decoder). In fact, the complexity of the MIMO detector with MCMC is approximately linear [81].

Authors in [82] made the comparison between the MCMC detector and the sphere decoder detector [72]. The results in [82] show that the MCMC detector outperforms the sphere decoder in low SNR region with a significant reduction in the complexity. However, it has been found that the MCMC detector has degraded performance as the SNR increases, and the method suffers from error floors at the high SNR [79, 81]. Authors in [79] proposed two solutions by running multiple Markov chains in parallel and assuming a higher noise variance. These solutions show performance improvement in the medium levels of SNRs.

The reason for this high SNR problem has been investigated in [81], that is the samples, which are associated with large *a priori* probabilities (so called "ill conditioned" bits), dominate the Markov chain process and stop the Markov chain from converging to the correct result. In other words, the Markov chain is trapped in the bad states, which is considered as equilibrium state although it is not, and will never move out of this state. Such phenomenon challenges the fundamental principle of the MCMC methods, as the Markov chain should cover as many states as possible so that it can finally converge to the desired distribution. Authors in [81] also proposed a number of *ad-hoc* methods, such as using ZF or MMSE solution to initialize the Gibbs sampler, and run more iterations with increased number of samples if error occurs after Cyclic Redundancy Check (CRC). These methods are effective, however, the complexity inevitably increases.

Unlike the above mentioned *ad-hoc* methods, a better approach would be to minimize the influence from the "ill conditioned" bits, the Markov chain should be able to move forward as desired. And the *a priori* information should provide

us the knowledge of quality of the samples. Hence, two novel MCMC methods for the MIMO detector are developed, namely the reduced-state-space MCMC (RSS-MCMC) detector and the force-state-transitions MCMC (FST-MCMC). Two novel reliability constraints are first proposed to separate the reliable bits from the unreliable ones. The RSS-MCMC cancels the interference from the reliable bits obtained from previous iteration while keep running MCMC for undesired samples. After canceling the interference from reliable bits, a heavily loaded MIMO system is transformed into a channel with less interference. And the RSS-MCMC detector draws random samples for the unreliable bits using the improved signal. For the FST-MCMC, the preliminary work as shown in [83], while our method differs from [83] in two ways. Firstly, the method in [83] flips the bit with the minimum variance, which is not feasible because the "good bits" may also have minimum variance. Our approach is to flip the "ill conditioned" bits only from the unreliable signal set. Secondly, the method in [83] flips only one bit per sample, where one sample is equivalent to the entire transmitted signal vector. This may not be sufficient to move Markov chain out from the trapped state. Our approach is to flip all "ill conditioned" bits so that the Markov chain could visit more states. Theoretical analysis and simulation results show that both RSS-MCMC and FST-MCMC improve the performance at the high SNR while the RSS-MCMC also reduces the complexity from drawing less samples in the Gibbs sampler.

1.4 Outline of The Thesis

The rest of the thesis is organized as follows:

In Chapter 2, the system model employed for the rest of the chapters in this thesis is presented. The system model for SISO system is introduced first, followed by the modeling of SISO-OFDM system. Then the SISO channel characteristics in terms of time selectivity and frequency selectivity are discussed and a three-dimensional channel response with various mobilities is presented. After that, MIMO system is introduced as a natural extension of the SISO counterpart. Two popular MIMO system configurations, namely the space-time coded MIMO and spatial multiplexed MIMO systems are presented. Based on these two configurations, OFDM and MIMO are combined into a MIMO-OFDM system. After defining all the systems models, the generic structure of the iterative detection and decoding is introduced, followed by the soft parallel interference cancelation approach.

In Chapter 3, the iterative receiver with channel estimation for the SISO-OFDM system is presented. Firstly, the channel estimation for SISO-OFDM system is formulated, followed by the investigation of the inter-carrier interference (ICI) caused by the mobilities in the channel estimation. A solution to minimize the influence from the ICI is developed. Secondly, the conventional frequency domain preamble and pilot-aided channel estimation techniques and their mean square error (MSE) analysis are discussed, particularly for the ML and MMSE channel estimator. Thirdly, the iterative turbo channel estimation technique for SISO-OFDM system is developed. We start with a brief outline of the iterative receiver, then introduce the three-stage iterative channel estimation technique. Furthermore, the MSE bounds and complexity of the iterative channel estimation technique are analyzed. Finally, the simulation results are presented by comparing the proposed iterative receiver with the conventional receiver in terms of downlink performance, uplink performance, performance under various mobilities, and performance with carrier frequency offset.

In Chapter 4, the iterative receiver with channel estimation for MIMO-OFDM system is presented. The conventional receivers are introduced first followed by the development of the novel iterative MRC and iterative interference cancelation based receivers for space time coded and spatial multiplexed OFDM systems, respectively. The three-stage iterative channel estimation is modified for the MIMO-OFDM systems, and the MSE bounds analysis is presented. Furthermore, the complexity of the iterative receivers including the complexity of the iterative channel estimation is discussed. Finally, the simulation results are presented by comparing the proposed iterative receivers with the conventional MRC and MMSE receivers. The performance is compared in the space time coded OFDM system and the spatial multiplexed OFDM system.

In Chapter 5, the iterative receiver using a sphere decoder is presented. The MIMO system model is modified from the complex domain to the real domain followed by the review of the original FP and SE sphere decoder algorithms. Based on the original sphere decoder algorithms, the iterative receivers with modified FP and SE algorithms are developed. To further improve the performance of the SE sphere decoder algorithm, two schemes are developed by utilizing the *a priori* information. After that, the complexity of the iterative receiver with modified sphere decoder algorithms are briefly discussed. Finally, the simulation results are presented to show the performance and complexity of iterative receiver with modified sphere decoder algorithms.

In Chapter 6, the iterative receivers on MCMC methods are presented. The new MCMC methods are developed by first introducing the novel reliability constraints, followed by the RSS-MCMC and FST-MCMC methods. And the complexity of the different MCMC methods are discussed as well. Finally, the simulation results are presented to compare the RSS-MCMC, FST-MCMC and the conventional MCMC methods.

In Chapter 7, the general conclusion of the thesis and future research directions are presented.

Chapter 2

System Model

2.1 Introduction

Given an arbitrary wireless communication system using a single point to point connection, also known as a single-input single-output (SISO) channel, the wireless link for which the transmitting end and the receiving end is equipped with single antenna, and the information is sent over a single channel. The single channel can be characterized in types of flat fading channel, frequency selective channel, slow fading channel, or fast fading channel [84]. The performance of a SISO system can be seriously degraded due to the lack of diversity in a wireless link. This lack of diversity means that if the particular link has a poor link budget or is capacity inhibited, then there is no other link that could be used.

In the wireless communication system with a MIMO configuration, multiple antenna elements are adopted at both transmitter and receiver. Each transmitter and receiver link can be modeled as a single channel, hence, the information is sent over multiple channels in parallel. The advantage of MIMO system over conventional SISO is promising due to two reasons [47]. Firstly, the capacity enhancement is achieved from spatial multiplexed data streams at each transmitting antenna. And secondly, the reliability improvement from spatial diversity as information is transmitted and received over multiple wireless links, which can increase the network's QoS dramatically.

In this chapter, the SISO and MIMO system models used in this thesis are discussed. In order to make the connection between generic and practical systems, the OFDM system is introduced to illustrate a practical SISO-OFDM and MIMO-OFDM system model. Furthermore, the notation of the iterative receiver techniques used in this thesis are introduced.

2.2 Single-Input-Single-Output (SISO) System

In a wireless communication system with SISO configuration, both transmitting and receiving ends are equipped with single antenna element. Fig. 2.1 shows the transmitter, receiver and channel in the generic SISO system. The binary source generates information bit sequence $\{b\}$. The information bit sequence $\{b\}$ is encoded by channel encoder, and becomes coded bit sequence $\{d\}$. After passing the coded bit sequence $\{d\}$ through interleaver, the interleaved bit sequence $\{c\}$ is permutated and then modulated by the data modulator. The modulator outputs transmitted data symbol sequence $\{x\}$, which is sent through the communication channel.

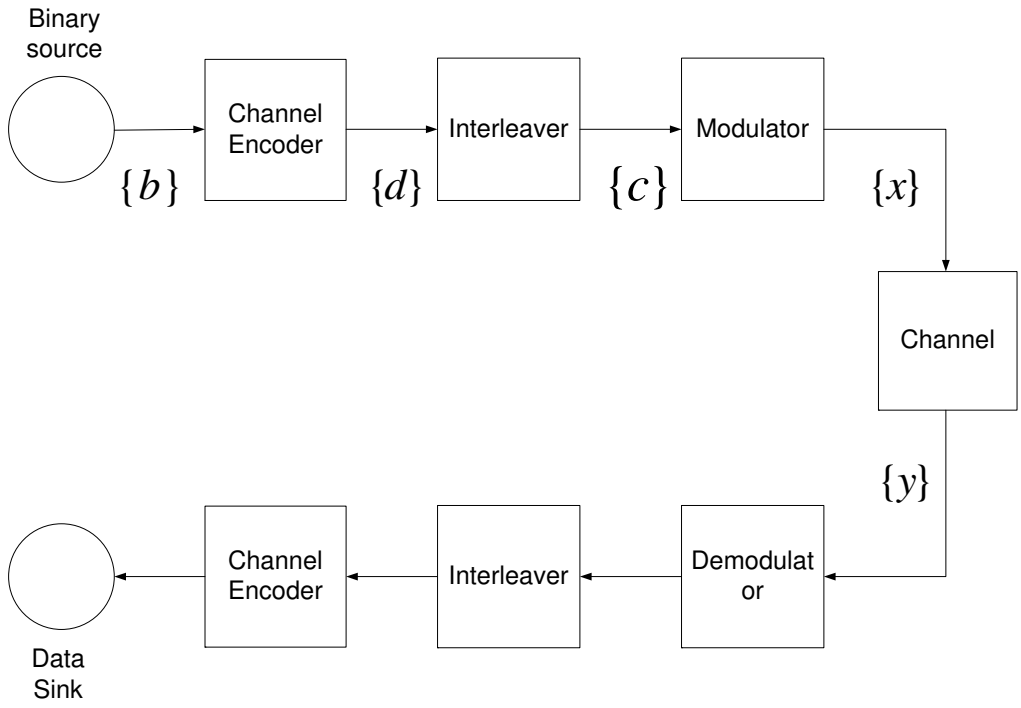

Figure 2.1: SISO system model with transmitter, receiver and channel

At the receiver end, the received data symbol sequence $\{y\}$ can be expressed as:

$$\mathbf{y} = \mathbf{H}\mathbf{x} + \mathbf{w}, \tag{2.1}$$

where $\mathbf{H}$ is channel response and $\mathbf{w}$ is the additive noise, which can be modeled by Gaussian distribution with zero mean and variance σ^2. The channel response

h can be additive white Gaussian noise (AWGN) channel, multiple access channel, ISI channel, flat fading channel, and frequency selective channel. It is also worth noting that expression (2.1) does not necessarily have to be restricted to a SISO system, it can also represent a MIMO system with multiple inputs and outputs. The received data symbol sequence **y** is demodulated and deinterleaved, and finally decoded by the channel decoder. In the conventional non-iterative receiver, the interleaver and deinterleaver spread the data bits across the transmission frame the error bits for the channel decoder, which helps in the task to correct the bursty errors in the fading channel. Furthermore, in the iterative receiver, the interleaver and deinterleaver also decorrelate the adjacent coded bits in order to make them independent to each other.

2.2.1 Orthogonal Frequency Division Multiplexing (OFDM)

OFDM is an attractive technique for high data rate transmission over wireless channels. OFDM system is a special realization of the multi-carrier [13] communication system as shown in Fig. 2.2. In the multi-carrier system, the high-speed data is serial to parallel multiplexed in to N data streams. Data streams $X_0, X_1, \ldots, X_{N-1}$ are modulated with different carrier frequency $e^{j\omega_0}, e^{j\omega_1}, \ldots, e^{j\omega_{N-1}}$ correspondingly, hence, the entire system bandwidth is divided into N narrow bands. It transforms the frequency selective channel into a parallel collection of flat fading subchannels, which simplifies the equalization at the receiver, and thus makes it possible to realize high speed data modems that wouldn't have been possible to build with single carrier systems. Fig. 2.3 shows the practical realization of the multi-carrier system through OFDM technology. The multi-carrier modulation/demodulation operations are realized by using both the inverse fast Fourier transform (IFFT) and the fast Fourier transform (FFT) in the transmitter and receiver. The cyclic prefix (CP) that is longer than the channel delay spread is attached at the beginning of each symbol to prevent inter-symbol interference (ISI).

2.2.2 SISO-OFDM System

In this thesis, we consider the discrete-time OFDM system with N subcarriers. The information bits $\{b^{(i)}\}$ are first encoded into coded bits $\{d^{(i)}\}$, where i is the time index. These coded bits are interleaved into a new sequence of $\{c^{(i)}\}$, mapped into M-ary complex symbols and serial-to-parallel (S/P) converted to a data sequence of $\{X_d^{(i)}\}$. Pilot sequence $\{X_P^{(i)}\}$ are inserted into data sequence $\{X_d^{(i)}\}$ at pilot subcar-

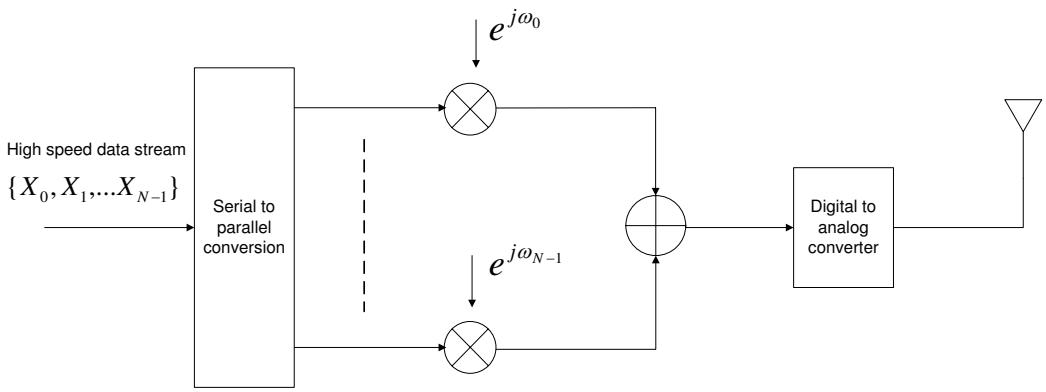

Figure 2.2: Multi-carrier system

riers to form an OFDM symbol represented as $\mathbf{X}^{(i)} = [X^{(i)}(0), X^{(i)}(1), \cdots, X^{(i)}(N-1)]^T$. N-point inverse discrete Fourier transform (IDFT) is performed on $\mathbf{X}^{(i)}$ given by:

$$x^{(i)}(n) = \frac{1}{\sqrt{N}} \sum_{k=0}^{N-1} X^{(i)}(k) \cdot \exp \frac{j2\pi kn}{N}, \tag{2.2}$$

where $0 \leq n \leq N-1$. After adding the CP of length G, the OFDM symbol is converted into a time domain sample vector $\mathbf{x^{(i)}} = [x^{(i)}(-G), x^{(i)}(-G+1), \cdots, x^{(i)}(N-1)]^T$, where $x^{(i)}(-k) = x^{(i)}(N-G+k), k = 1, \ldots, G$. These time domain samples are then digital to analog converted and transmitted over the multi-path fading channel.

The fading channel can be modeled by the time-variant discrete impulse response with $h^{(i)}(n, l)$ representing the fading coefficient of the l^{th} path at n^{th} sample for i^{th} OFDM symbol. Assuming that the CP is longer than or at least equal to the maximum channel delay spread L, i.e. $L \leq G$, after removing the CP, the sampled received signal can be characterized in the following tapped-delay-line model [85]:

$$y^{(i)}(n) = \sum_{l=0}^{L-1} h^{(i)}(n, l) x^{(i)}(n-l) + w^{(i)}(n), \tag{2.3}$$

where $w^{(i)}(n)$ is the AWGN with zero mean and variance σ_w^2. In the range of $0 \leq n \leq N-1$, the received signal $y^{(i)}(n)$ is immune to the interference by previous OFDM symbol due to the CP. The demodulated signal in the frequency domain is

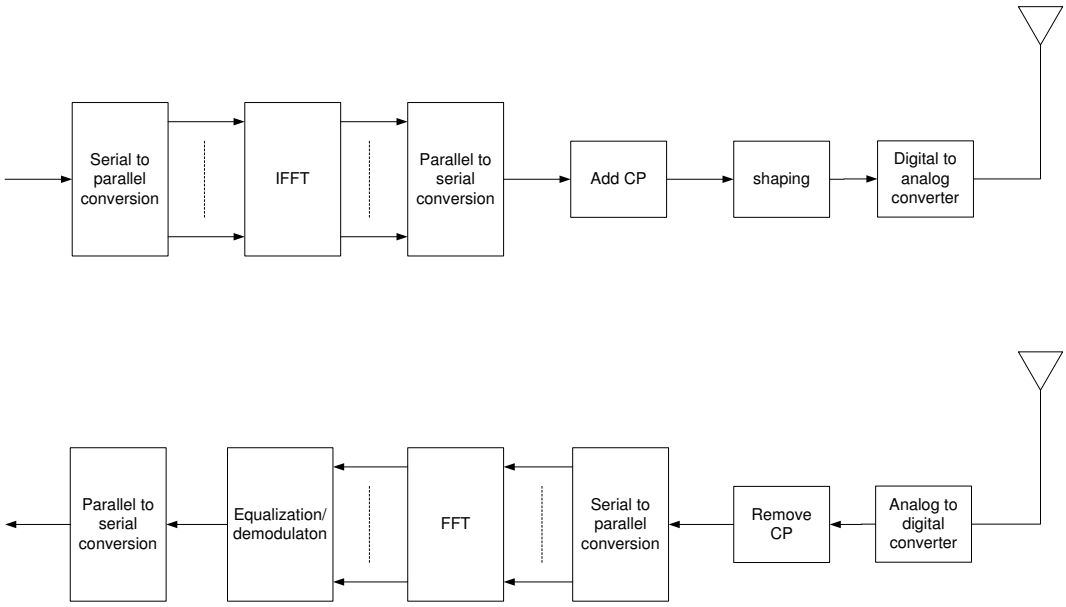

Figure 2.3: Practical OFDM system with transmitter and receiver

obtained by taking N-point DFT of $y^{(i)}(n)$ as:

$$\begin{aligned} Y^{(i)}(m) &= \frac{1}{\sqrt{N}} \sum_{n=0}^{N-1} y^{(i)}(n) e^{-j2\pi mn/N} = H_{m,m}^{(i)} X^{(i)}(m) \\ &\quad + \sum_{k \neq m}^{N-1} H_{m,k}^{(i)} X^{(i)}(k) + W^{(i)}(m), \end{aligned} \tag{2.4}$$

where

$$\begin{aligned} H_{m,m}^{(i)} &= \frac{1}{N} \sum_{n=0}^{N-1} \sum_{l=0}^{L-1} h^{(i)}(n,l) e^{-j2\pi lm/N} \\ &= \frac{1}{N} \sum_{n=0}^{N-1} \hbar_m^{(i)}(n), \end{aligned} \tag{2.5}$$

$$\begin{aligned} H_{m,k}^{(i)} &= \frac{1}{N} \sum_{n=0}^{N-1} \{ \sum_{l=0}^{L-1} h^{(i)}(n,l) e^{-j2\pi lk/N} \} e^{-j2\pi (m-k)n/N} \\ &= \frac{1}{N} \sum_{n=0}^{N-1} \hbar_k^{(i)}(n) e^{-j2\pi (m-k)n/N}, \end{aligned} \tag{2.6}$$

and

$$W^{(i)}(m) = \frac{1}{\sqrt{N}} \sum_{n=0}^{N-1} w^{(i)}(n) e^{-j2\pi mn/N}, \tag{2.7}$$

are the multiplicative distortion at the desired subcarrier m, the neighboring subcarrier k, and the noise after DFT respectively. In (2.5), $\hbar_m^{(i)}(n)$ is the channel frequency response of subcarrier m at time n in i^{th} OFDM symbol. If the channel is assumed to be time-invariant during one OFDM symbol period, $\hbar_k^{(i)}(n)$ is constant in (2.6), and $H_{m,k}^{(i)}$ vanishes. In this case, $Y^{(i)}(m)$ in (2.4) only contains the multiplicative distortion at the desired subcarrier, which can be easily compensated by a one-tap frequency domain equalizer.

2.2.3 SISO Channel Modeling

Realistic mobile radio channels are characterized by the time and frequency dispersive nature. The channel time dispersive characteristic is determined by the multi-path delay profile. In the time-domain, the channel impulse response has a multi-path delay spread. In the frequency-domain, the channel frequency response is varying with frequency. Fig. 2.4 illustrates the channel time dispersive nature. Under such condition, the narrow band signal will experience flat fading whereas the wideband signal will encounter frequency selective fading.

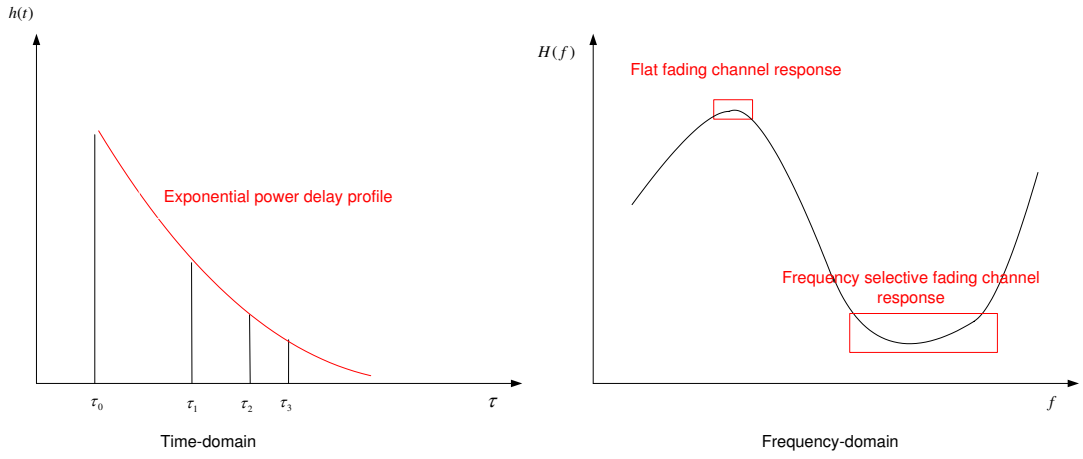

Figure 2.4: Time dispersive/Frequency selective dual channel

The channel frequency dispersive characteristic is determined by the Doppler

spread of the channel. In frequency-domain, Doppler spread is a measure of the spectral broadening effect caused by the changing time rate of the mobile radio channel. When the mobile station and base station are in movement relative to each other, the received signal spectrum will have the frequency offset within doppler spread in addition to that on the desired frequency as shown in Fig. 2.5. The amount of the doppler spread depends on the relative velocity of the movement and the angle between the direction of motion of the mobile and the base station. In the time-domain, the channel frequency response is varying in time. If the transmitted signal bandwidth is much greater than the Doppler spread, i.e. the symbol period is shorter than the channel time variation, the effect of Doppler spread is negligible at the receiver and the signal is classified as being under slow fading conditions. Otherwise, if the transmitted signal bandwidth is much smaller than the Doppler spread, i.e. the symbol period is longer than the channel time variation, the signal is under fast fading.

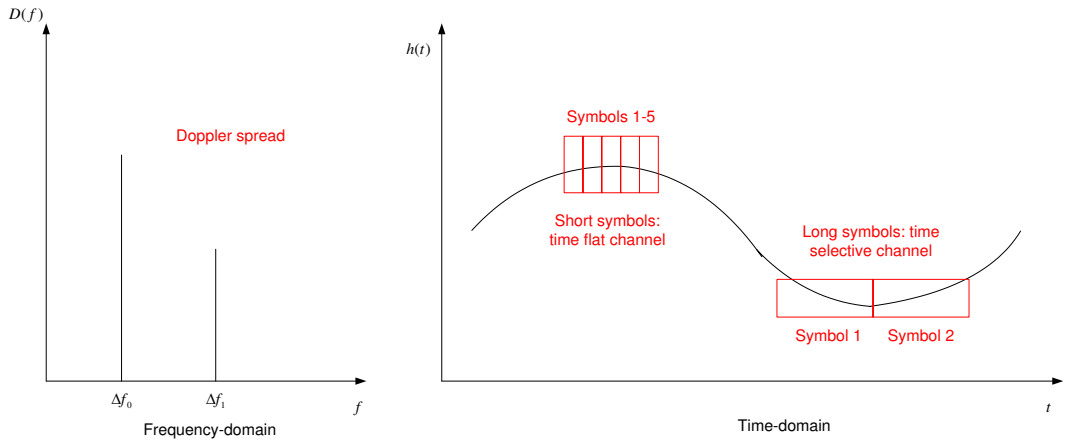

Figure 2.5: Frequency dispersive/Time selective dual channel

In the literature, the fading channel can be modeled by the time-variant discrete impulse response with $h(n,l)$ representing the coefficient of the l^{th} path at n^{th} sample. The fading coefficients are modeled as zero mean complex Gaussian random variables. Based on the wide sense stationary uncorrelated scattering (WSSUS) assumption [84], the fading coefficients for different paths are statistically independent, while the fading coefficients for a particular path are correlated over time. The time-domain autocorrelation function of $h(n,l)$ is given by [86]:

$$E\{h(n,l) \cdot h^*(m,l)\} = \alpha_l \cdot J_0(2\pi(n-m)f_m T_s), \tag{2.8}$$

where $J_0(\cdot)$ is the first kind of Bessel function of zero order, $T_s = 1/BW$ is the sample time, BW is the bandwidth of the system, f_m is the maximum Doppler spread and α_l is the average power of the l^{th} path. The channel gain is normalized as given by:

$$\sum_{l=0}^{L-1} E\{\|h^{(i)}(n,l)\|^2\} = \sum_{l=0}^{L-1} \alpha_l = 1, \tag{2.9}$$

where the number of fading taps $L = \lceil \tau_{max}/T_s \rceil$ is the maximum delay in terms of OFDM samples. And the frequency-domain correlation is given by:

$$\begin{aligned} E\{H_{r,s} \cdot H^*_{p,q}\} &= \frac{1}{N^2} \sum_{l=0}^{L-1} \alpha_l \cdot e^{-j2\pi(s-q)l/N} \cdot \sum_{n=0}^{N-1} \sum_{m=0}^{N-1} J_0[2\pi f_m(n-m)T_s] \\ &\quad \cdot e^{-j2\pi(r-s)n/N} e^{j2\pi(p-q)m/N}, \end{aligned} \tag{2.10}$$

where $H(\cdot)$ is channel frequency response, $\{r,p\}$ is the time index and $\{s,q\}$ is the frequency index.

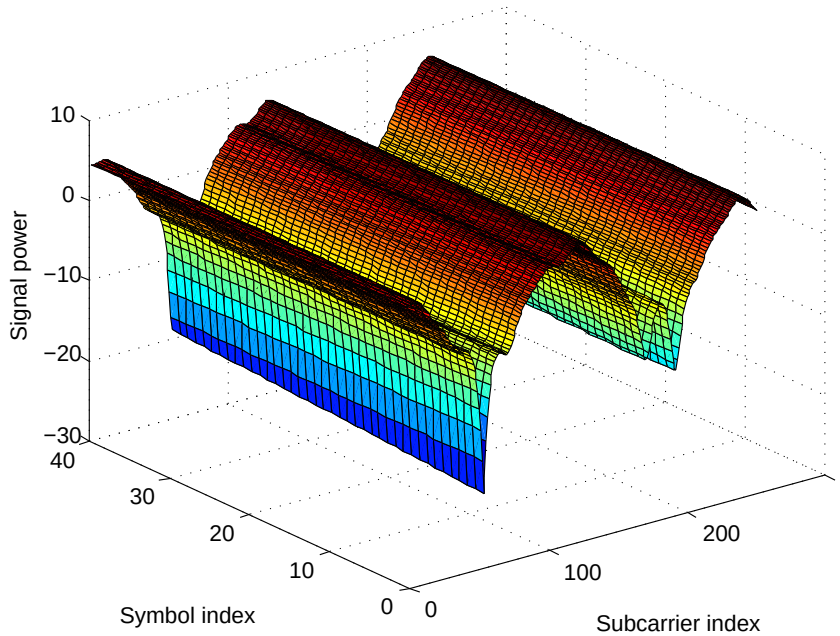

Figure 2.6: Channel time and frequency response at 3kmh

In OFDM system, data symbols are transmitted in both time and frequency domain. Fig. 2.6, Fig. 2.7, and Fig. 2.8 show the channel frequency response of ITU IMT-2000 vehicular-A channel [87] over subcarriers and OFDM symbols at vehicular speeds 3kmh, 120kmh, and 333kmh respectively for the carrier frequency

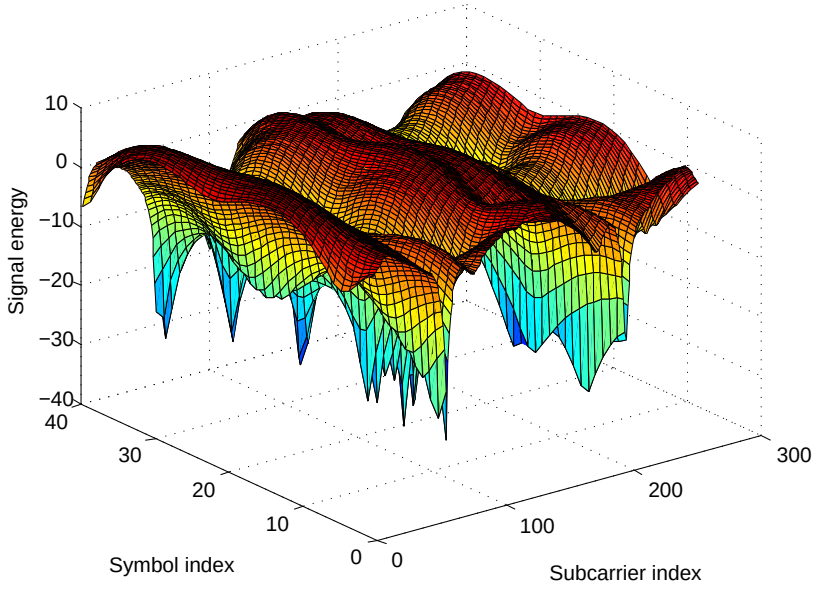

Figure 2.7: Channel time and frequency response at 120kmh

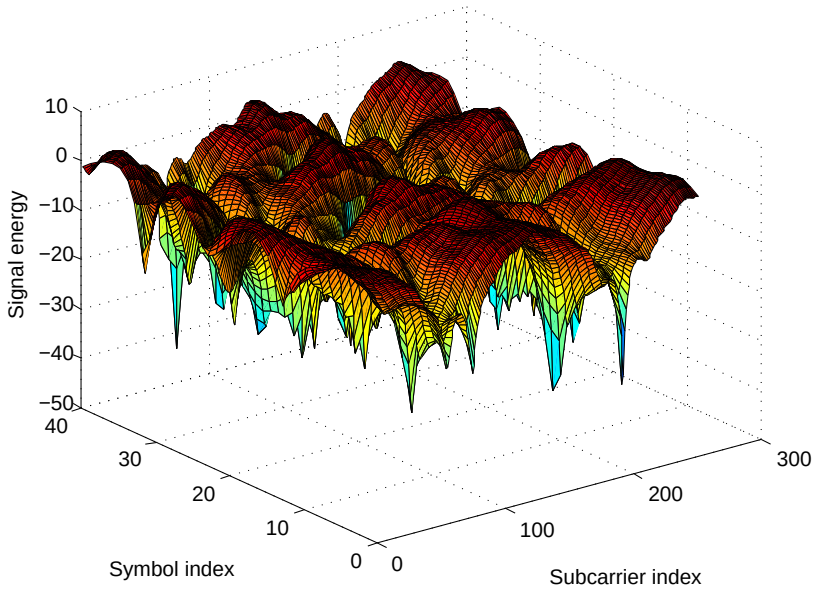

Figure 2.8: Channel time and frequency response at 333kmh

of 5GHz. It can be seen that the channel variation becomes more significant in both time and frequency domain as mobility increases.

2.3 Multiple-Input Multiple-Output (MIMO) System

The MIMO system can be considered as further extension from SISO system. Both transmitter and receiver are equipped with multiple antenna elements. Such a setup is illustrated in Fig. 2.9. Two mandatory MIMO profiles, namely the Alamouti STC and SM, are employed in practical MIMO system [17]. The idea behind MIMO system configuration is that the signals at the receive antennas are combined in such a way that the quality or the data rate will be enhanced. As discussed in Section 2.2, the generic MIMO system modeling is expressed as:

$$\mathbf{Y} = \mathbf{HX} + \mathbf{W}, \tag{2.11}$$

where $\mathbf{Y}$ is the received signal vector, $\mathbf{W}$ is the AWGN vector over receiving antennas, and $\mathbf{H}$ is the MIMO channel matrix, which can be either a Alamouti STC channel matrix or a SM channel matrix.

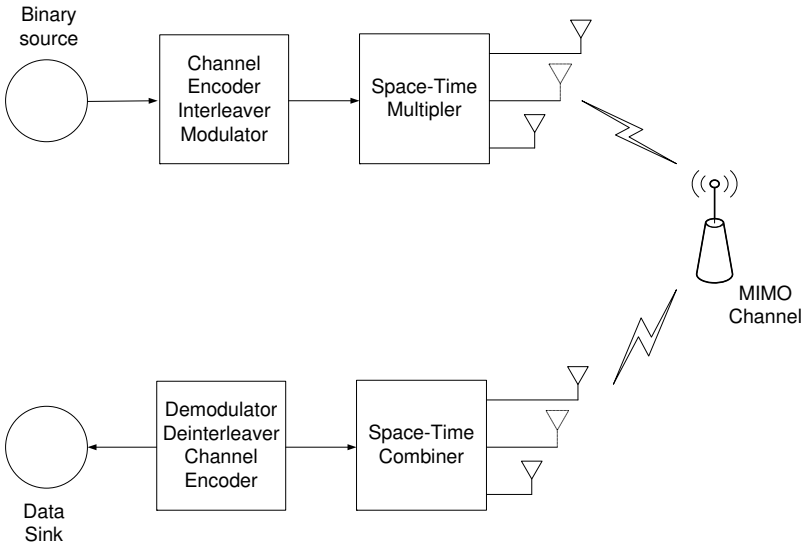

Figure 2.9: MIMO system model with transmitter, receiver and channel

2.3.1 Alamouti Space-Time Coding (STC) System

The Alamouti STC [52] is a remarkable STBC scheme for transmission with two transmitting antennas and one receiving antenna. This scheme supports ML detection based only on linear processing at the receiver. Such a simple transmission

structure and linear processing of the detection makes it a very attractive scheme that is currently part of both the UMTS/WCDMA [84]. Another typical example is IEEE 802.16e Mobile WiMAX system [17].

In the Alamouti STC system, the space-time multiplexer block in Fig. 2.9 is implemented by a space-time block encoder, which divides the input symbols into groups of two symbols each. At a given symbol period, the symbols in each group $\{X_0, X_1\}$ are transmitted simultaneously from both antennas, where the signal transmitted from antenna 0 is X_0 and the signal transmitted from antenna 1 is X_1. In the next symbol period, the signal $-X_1^*$ is transmitted from antenna 0 and the signal X_0^* is transmitted from antenna 1. Hence, two symbols are transmitted in two symbol periods, which means the coding rate of the space-time block encoder is one. Let h_0 and h_1 be the channel responses from the first and second transmitting antennas to the receiving antenna. It is critical to assume that the channel responses are constant over two consecutive symbol periods, i.e.

$$\begin{aligned} h_0(2nT) &\approx h_0((2n+1)T) \\ h_1(2nT) &\approx h_1((2n+1)T), \end{aligned} \tag{2.12}$$

where T is the symbol duration. Denoting the received signal over two consecutive symbol periods at receiving antenna as y_0 and y_1, the received signal can be expressed as:

$$\begin{bmatrix} y_0 \\ y_1 \end{bmatrix} = \begin{bmatrix} X_0 & -X_1^* \\ X_1 & X_0^* \end{bmatrix} \cdot \begin{bmatrix} h_0 \\ h_1 \end{bmatrix} + \begin{bmatrix} w_0 \\ w_1 \end{bmatrix}. \tag{2.13}$$

By taking the conjugate of y_1, equation (2.13) can be rewritten as:

$$\begin{bmatrix} y_0 \\ y_1^* \end{bmatrix} = \begin{bmatrix} h_0 & h_1 \\ h_1^* & -h_0^* \end{bmatrix} \cdot \begin{bmatrix} X_0 \\ X_1 \end{bmatrix} + \begin{bmatrix} w_0 \\ w_1^* \end{bmatrix}. \tag{2.14}$$

Link equation (2.14) to equation (2.11), it can be easily found that:

$$\mathbf{Y} = \begin{bmatrix} y_0 \\ y_1^* \end{bmatrix}, \mathbf{H} = \begin{bmatrix} h_0 & h_1 \\ h_1^* & -h_0^* \end{bmatrix}, \mathbf{X} = \begin{bmatrix} X_0 \\ X_1 \end{bmatrix}, \mathbf{W} = \begin{bmatrix} w_0 \\ w_1^* \end{bmatrix}.$$

Alamouti STC can also be applied with two receiving antennas. In such 2×2 configuration, similar to the 2×1 configuration, the received signals are taken from two consecutive symbol periods but from both receiving antennas. Denoting y_j^i and n_j^i as the received signal and noise for the i^{th} symbol at the j^{th} receiving antenna,

and $h_{m,n}$ as the channel responses from the n^{th} transmitting antenna to the m^{th} receiving antenna, the 2×2 Alamouti STC system model can be expressed as:

$$\begin{bmatrix} y_0^0 & y_0^1 \\ y_1^0 & y_1^1 \end{bmatrix} = \begin{bmatrix} h_{0,0} & h_{0,1} \\ h_{1,0} & h_{1,1} \end{bmatrix} \cdot \begin{bmatrix} X_0 & -X_1^* \\ X_1 & X_0^* \end{bmatrix} + \begin{bmatrix} w_0^0 & w_0^1 \\ w_1^0 & w_1^1 \end{bmatrix}. \tag{2.16}$$

By taking the conjugate of y_0^1 and y_1^1, equation (2.16) can be rewritten as:

$$\begin{bmatrix} y_0^0 \\ y_1^0 \\ (y_0^1)^* \\ (y_1^1)^* \end{bmatrix} = \begin{bmatrix} h_{0,0} & h_{0,1} \\ h_{1,0} & h_{1,1} \\ h_{0,1}^* & -h_{0,0}^* \\ h_{0,0}^* & -h_{1,0}^* \end{bmatrix} \cdot \begin{bmatrix} X_0 \\ X_1 \end{bmatrix} + \begin{bmatrix} w_0^0 \\ w_1^0 \\ (w_0^1)^* \\ (w_1^1)^* \end{bmatrix}. \tag{2.17}$$

Link equation (2.17) to equation (2.11), it can be easily found that:

$$\mathbf{Y} = \begin{bmatrix} y_0^0 \\ y_1^0 \\ (y_0^1)^* \\ (y_1^1)^* \end{bmatrix}, \mathbf{H} = \begin{bmatrix} h_{0,0} & h_{0,1} \\ h_{1,0} & h_{1,1} \\ h_{0,1}^* & -h_{0,0}^* \\ h_{0,0}^* & -h_{1,0}^* \end{bmatrix}, \mathbf{X} = \begin{bmatrix} X_0 \\ X_1 \end{bmatrix}, \mathbf{W} = \begin{bmatrix} w_0^0 \\ w_1^0 \\ (w_0^1)^* \\ (w_1^1)^* \end{bmatrix}.$$

Equation (2.13) and (2.16)can be used for the channel estimation if symbols X_0 and X_1 are training symbols and equation (2.14) and (2.17) can be used for data detection if channel responses h_0 and h_1 are known.

2.3.2 Spatial Multiplexing (SM) System

In MIMO spatial multiplexing system, streams of independent data are transmitted over different antennas to maximize the average data rate over the MIMO system. Unlike the Alamouti STC system, the symbols are transmitted from different transmitting antennas in every symbol period. Hence, the space-time block encoder has a coding rate of two. Considering a 2×2 MIMO SM system, denoting X_0 and X_1 as the symbols transmitted in a symbol period for transmitting antennas, and $h_{m,n}$ as the channel responses from the n^{th} transmitting antenna to the m^{th} receiving antenna, the received signal y_0 and y_1 from each receiving antenna can be expressed as:

$$\begin{bmatrix} y_0 \\ y_1 \end{bmatrix} = \begin{bmatrix} h_{0,0} & h_{0,1} \\ h_{1,0} & h_{1,1} \end{bmatrix} \cdot \begin{bmatrix} X_0 \\ X_1 \end{bmatrix} + \begin{bmatrix} w_0 \\ w_1 \end{bmatrix}. \tag{2.19}$$

Link equation (2.19) to equation (2.11), it can be easily found that:

$$\mathbf{Y} = \begin{bmatrix} y_0 \\ y_1 \end{bmatrix}, \mathbf{H} = \begin{bmatrix} h_{0,0} & h_{0,1} \\ h_{1,0} & h_{1,1} \end{bmatrix}, \mathbf{X} = \begin{bmatrix} X_0 \\ X_1 \end{bmatrix}, \mathbf{W} = \begin{bmatrix} w_0 \\ w_1 \end{bmatrix}.$$

Unlike the STC approach which can recover the symbols without interference the SM technique suffers significant interference which will be discussed in more detail later in this thesis.

2.3.3 MIMO-OFDM System

The application of Alamouti STC or SM on the top of OFDM could be trivial because each subcarrier of OFDM system can be considered as an independent Alamouti STC or SM sub-system. In each subcarrier, the received signal is the superposition of the fading signals from all transmitting antennas.

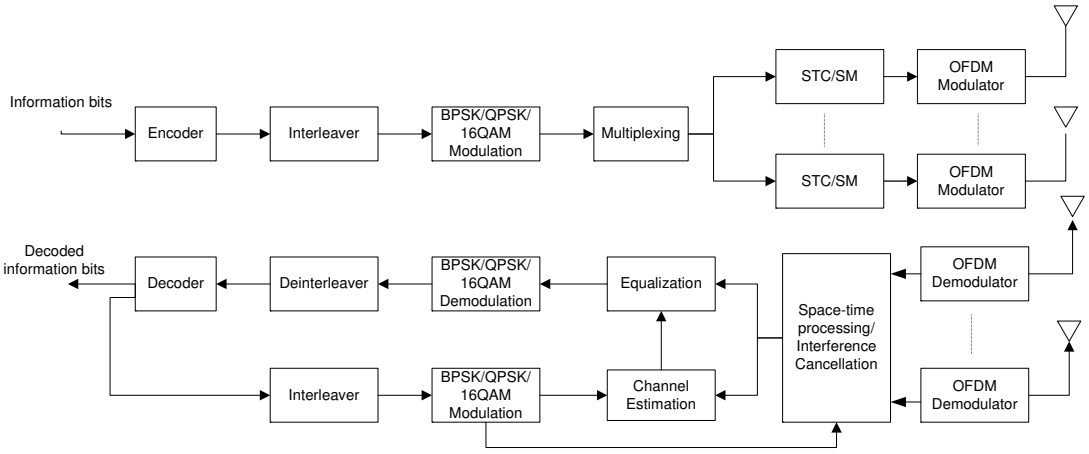

Figure 2.10: MIMO-OFDM system with transmitter, iterative receiver and channel

The MIMO-OFDM system with N subcarriers considered in this thesis is shown in Fig. 2.10. There are N_T transmitting antennas and N_R receiving antennas. The information bits $\{b_i\}$ are first encoded into coded bits sequences $\{d_i\}$, where i is the time index. These coded bits are interleaved into a new sequence of $\{c_i\}$, mapped into M-ary complex symbols and serial-to-parallel converted to a data sequence. A pilot sequence is inserted into data sequence to form an OFDM symbol of N frequency-domain signals represented as a $(N \times N_T) \times 1$ vector $\underline{\mathbf{X}}_i = [\mathbf{X}_{i,0}^T, \mathbf{X}_{i,1}^T, \cdots, \mathbf{X}_{i,N-1}^T]^T$, where $\mathbf{X}_{i,m} = [X_{i,m}^0, X_{i,m}^1, \cdots, X_{i,m}^{N_T-1}]^T$ is the $N_T \times 1$ for the frequency-domain signals transmitted at the m^{th} subcarrier for all transmitting antennas.

In the 2×1 Alamouti STC-OFDM system, the frequency-domain signal is multiplexed into the STC encoder at each transmitting substreams. The STC encoder will output coded symbols as discussed in Section 2.3.1. After adding the CP of length G, the whole OFDM symbol is converted into time domain sample vector. These time domain samples are transmitted over the multipath fading channel, which can be modeled by the time-variant discrete impulse response. After removing the CP at the receiver end, the demodulated frequency-domain signal is defined as:

$$\underbrace{\begin{bmatrix} Y^0_{i-1,m} \\ (Y^0_{i,m})^* \end{bmatrix}}_{\mathbf{Y}_m} = \underbrace{\begin{bmatrix} H^{0,0}_{i,m} & H^{0,1}_{i,m} \\ (H^{0,1}_{i,m})^* & -(H^{0,0}_{i,m})^* \end{bmatrix}}_{\mathbf{H}_m} \cdot \underbrace{\begin{bmatrix} X_{i-1,m} \\ X_{i,m} \end{bmatrix}}_{\mathbf{X}_m} + \underbrace{\begin{bmatrix} W^0_{i-1,m} \\ (W^0_{i,m})^* \end{bmatrix}}_{\mathbf{W}_m}, \tag{2.21}$$

where $Y^r_{i,m}$ as the received signal at r^{th} receiving antenna for m^{th} subcarrier of the i^{th} OFDM symbol, $X_{i,m}$ as the transmitted signal at both transmitting antennas for m^{th} subcarrier of the i^{th} OFDM symbol, $H^{r,t}_{i,m}$ is the channel frequency response between t^{th} transmitting antenna and r^{th} receiving antenna for the m^{th} subcarrier of i^{th} OFDM symbol, and $W^r_{i,m}$ as the noise signal at r^{th} receiving antenna for m^{th} subcarrier of the i^{th} OFDM symbol. Similarly, in a 2×2 Alamouti STC-OFDM system, we can easily obtain the demodulated frequency-domain signal as:

$$\underbrace{\begin{bmatrix} Y^0_{i-1,m} \\ Y^1_{i-1,m} \\ (Y^0_{i,m})^* \\ (Y^1_{i,m})^* \end{bmatrix}}_{\mathbf{Y}_m} = \underbrace{\begin{bmatrix} H^{0,0}_m & H^{0,1}_m \\ H^{1,0}_m & H^{1,1}_m \\ (H^{0,1}_m)^* & -(H^{0,0}_m)^* \\ (H^{0,0}_m)^* & -(H^{1,0}_m)^* \end{bmatrix}}_{\mathbf{H}_m} \cdot \underbrace{\begin{bmatrix} X_{i-1,m} \\ X_{i,m} \end{bmatrix}}_{\mathbf{X}_m} + \underbrace{\begin{bmatrix} W^0_{i-1,m} \\ W^1_{i-1,m} \\ (W^0_{i,m})^* \\ (W^1_{i,m})^* \end{bmatrix}}_{\mathbf{W}_m}. \tag{2.22}$$

On the other hand, in the SM-OFDM system, after removing the CP at the receiver end, the demodulated frequency-domain signal is defined as $(N \times N_R) \times 1$ vector $\underline{\mathbf{Y}}_i = [\mathbf{Y}^T_{i,0}, \mathbf{Y}^T_{i,1}, \cdots, \mathbf{Y}^T_{i,N-1}]^T$, where $\mathbf{Y}_{i,m} = [Y^0_{i,m}, Y^1_{i,m}, \cdots, Y^{N_R-1}_{i,m}]^T$ is the $N_R \times 1$ signal vector at m^{th} subcarrier for all receiving antennas. Hence, the overall system model can be expressed as:

$$\underline{\mathbf{Y}}_i = \underline{\mathbf{H}}_i \underline{\mathbf{X}}_i + \underline{\mathbf{W}}_i, \tag{2.23}$$

$\underline{\mathbf{H}}_i$ is $(N \times N_R) \times (N \times N_T)$ channel frequency response matrix. If the channel is assumed to be time-invariant during an OFDM symbol period, $\underline{\mathbf{H}}_i$ can be defined

as:

$$\underline{\mathbf{H}}_i = diag(\mathbf{H}_{i,m}), \tag{2.24}$$

where

$$\mathbf{H}_{i,m} = \begin{bmatrix} H_{i,m}^{0,0} & H_{i,m}^{0,1} & \dots & H_{i,m}^{0,N_T-1} \\ H_{i,m}^{1,0} & H_{i,m}^{1,1} & \dots & H_{i,m}^{1,N_T-1} \\ \vdots & \vdots & \ddots & \vdots \\ H_{i,m}^{N_R-1,0} & H_{i,m}^{N_R-1,1} & \dots & H_{i,m}^{N_R-1,N_T-1} \end{bmatrix}, \tag{2.25}$$

is the channel frequency response matrix of m^{th} subcarrier with each element representing channel frequency response for a particular transmitter and receiver link. On the other hand, if the channel is time variant, which occurs in real wireless channels, then $\underline{\mathbf{H}}_i$ is a full matrix where the off-diagonal items cause ICI [88,89]. A central limit theorem (CLT) argument is used to model ICI as a Gaussian random process, which is included in the $(N \times N_R) \times 1$ AWGN vector $\underline{\mathbf{W}}_i$ with covariance $\sigma_w^2 \mathbf{I}_{(N \times N_R)}$. For a particular subcarrier m of interest, the received frequency-domain signal from the t^{th} transmitting antenna can be expressed as:

$$\begin{aligned} \mathbf{Y}_{i,m} &= \mathbf{H}_{i,m}\mathbf{X}_{i,m} + \mathbf{W}_{i,m} \\ &= \underbrace{\mathbf{H}_{i,m}^{t} X_{i,m}^{t}}_{\text{desired signal}} + \underbrace{\sum_{k \neq t} \mathbf{H}_{i,m}^{k} X_{i,m}^{k}}_{\text{interference}} + \mathbf{W}_{i,m}, \end{aligned} \tag{2.26}$$

where $\mathbf{H}_{i,m}^{k}$ is the k^{th} column of $\mathbf{H}_{i,m}$.

2.4 Iterative Detection and Decoding (IDD)

In this section, we first present an overview of IDD with definitions of special terms and notations used widely in the literature. A detailed mathematical formulation for these special terms and notations are presented thereafter. Fig. 2.11 shows the generic iterative receiver applied in this thesis. The core structure of an iterative receiver consists of a soft-input-soft-output detector, interleaver π, deinterleaver π^{-1}, and a soft-input-soft-output decoder, which exchange the detection and decoding information in an iterative fashion. Depending on the applications, other receiver modules could be included in the receiver, such as iterative channel estimator.

In Turbo decoder nomenclature [4], λ_1, λ_1^e, and λ_2^e are referred to as the *a posteriori* information, extrinsic information, and *a priori* information, respectively. The subscript "1" in λ_1 and λ_1^e means it is the output of the detector. The sub-

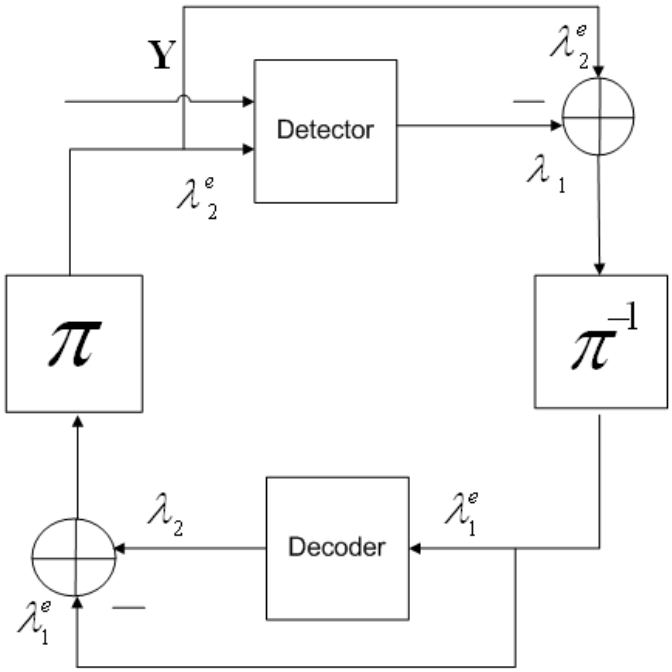

Figure 2.11: Generic iterative receiver

script "2" in λ_2^e means it is the output of channel decoder, which is fedback as input of the detector. The superscript "e" means extrinsic information. The main idea of an iterative receiver is that the detector takes the received signal $\mathbf{Y}$ and the *a priori* information λ_2^e as input, and outputs the reliability of the coded bits. This reliability is fed back as a form of extrinsic information λ_1^e to the channel decoder. The channel decoder takes the extrinsic information λ_1^e from the detector as the *a priori* input and decodes the information bits. At the same time, the channel decoder outputs the reliability of the coded bits and feeds them back to the detector as input, i.e., the *a priori* information λ_2^e. The above operations complete one iteration. The extrinsic information and the *a priori* information are also known as soft information.

Now we present the concepts of "extrinsic LLRs", "*a priori* information", and "*a posteriori* information" mathematically. Given the SISO system in equation (2.1) or the MIMO system model in equation (2.11), in the conventional non-iterative receiver, the detector tries to maximize the likelihood of the transmitted signal, that is, to minimize the Euclidian Distance to the received signal, which is

given by:

$$\widehat{\mathbf{X}} = \arg\max_{\mathbf{X}\in\mathcal{A}} P(\mathbf{Y}|\mathbf{X}) = \arg\min_{\mathbf{X}\in\mathcal{A}} \|\mathbf{Y} - \mathbf{H}\mathbf{X}\|^2, \tag{2.27}$$

where $\mathcal{A}$ is the signal set with M-ary data modulation. On the other hand, in the iterative receiver, the detector aims to maximize the *a posteriori* probability of transmitted signal sequence, which is given by:

$$\widehat{\mathbf{X}} = \arg\max_{\mathbf{X}\in\mathcal{A}} P(\mathbf{X}|\mathbf{Y}) = \arg\max_{\mathbf{X}\in\mathcal{A}} \frac{P(\mathbf{Y}|\mathbf{X})P(\mathbf{X})}{P(\mathbf{Y})}. \tag{2.28}$$

Assuming that the transmitted bits $d_0, d_1 \ldots, d_{\log_2 M-1}$ are independent, $P(\mathbf{X})$ can be expressed as:

$$P(\mathbf{X}) = \prod_{k=0}^{\log_2 M-1} P(d_k(\mathbf{X})). \tag{2.29}$$

Since $P(\mathbf{Y})$ as a constant which is common to all $\mathbf{X}$ over $\mathcal{A}$, (2.28) can be reformulated as:

$$\begin{aligned} \widehat{\mathbf{X}} &\approx \arg\max_{\mathbf{X}\in\mathcal{A}}\{P(\mathbf{Y}|\mathbf{X})P(\mathbf{X})\} \\ &\approx \arg\max_{\mathbf{X}\in\mathcal{A}}\{P(\mathbf{Y}|\mathbf{X}) \prod_{k=0}^{\log_2 M-1} P(d_k(\mathbf{X}))\}. \end{aligned} \tag{2.30}$$

In the iterative detection and decoding, the soft information [90] rather than the hard decision is computed for $\widehat{\mathbf{X}}$. The soft information is measured by the log likelihood ratio (LLR) [4] of the transmitted bit. The LLR $\lambda(d_k)$ of the coded bit d_k is computed by the log ratio of the probability of the bit to be 1 over the probability of the information bit to be 0, i.e.

$$\lambda(d_k) = \ln \frac{P(d_k = 1)}{P(d_k = 0)}. \tag{2.31}$$

Hence, denoting $\widehat{\mathbf{X}}_{\setminus k} = \{d_0, d_1 \ldots, d_{k-1}, d_{k+1}, \ldots, d_{\log_2 M-1}\}$ as the transmitted bits excluding the bit of interest d_k, the detector will output the *a posteriori* LLRs of the transmitted bits $d_0, d_1 \ldots, d_{\log_2 M-1}$ as:

$$\lambda_1(d_k(\widehat{\mathbf{X}})) = \ln \frac{P(d_k = 1|\widehat{\mathbf{X}})}{P(d_k = 0|\widehat{\mathbf{X}})}$$

$$
\begin{aligned}
&= \underbrace{\ln \frac{P(\mathbf{Y}|d_k=1,\widehat{\mathbf{X}}_{\setminus k}) \prod_{l\neq k}^{\log_2 M-1} P(d_l(\widehat{\mathbf{X}}))}{P(\mathbf{Y}|d_k=0,\widehat{\mathbf{X}}_{\setminus k}) \prod_{l\neq k}^{\log_2 M-1} P(d_l(\widehat{\mathbf{X}}))}}_{\text{Extrinsic information}} + \underbrace{\ln \frac{P(d_k(\widehat{\mathbf{X}})=1)}{P(d_k(\widehat{\mathbf{X}})=0)}}_{a\ priori\ \text{information}} \\
&= \lambda_1^e(d_k(\widehat{\mathbf{X}})) + \lambda_2^e(d_k(\widehat{\mathbf{X}})). \qquad (2.32)
\end{aligned}
$$

As seen from equation (2.32), the *a posteriori* information $\lambda_1(d_k(\widehat{\mathbf{X}}))$ is the summation of the extrinsic information $\lambda_1^e(d_k(\widehat{\mathbf{X}}))$ and the *a priori* information $\lambda_2^e(d_k(\widehat{\mathbf{X}}))$. The extrinsic information is the reliability measured from the Euclidian Distance between the received signal and the hypothesis, and the *a priori* probability of other bits as seen by the bit of interest. The *a priori* information $\lambda_2^e(d_k(\widehat{\mathbf{X}}))$ is the reliability measured by the probability fed back by the channel decoder on the bit of interest only. In the iterative detection and decoding, only the extrinsic information is the reliability measure obtained from the detector in the current iteration, the *a priori* information is the reliability measure from the previous iteration. Hence, the extrinsic information $\lambda_1^e(d_k(\widehat{\mathbf{X}}))$

$$\lambda_1^e(d_k(\widehat{\mathbf{X}})) = \lambda_1(d_k(\widehat{\mathbf{X}})) - \lambda_2^e(d_k(\widehat{\mathbf{X}})) \qquad (2.33)$$

rather than the *a posterior* information $\lambda_1(d_k(\widehat{\mathbf{X}}))$ is passed to the channel decoder as input, as shown in Fig. 2.11.

The channel decoder takes $\lambda_1^e(d_k(\widehat{\mathbf{X}}))$ as input and output $\lambda_2^e(d_k(\widehat{\mathbf{X}}))$, which is also the extrinsic information. In the next iteration, $\lambda_2^e(d_k(\widehat{\mathbf{X}}))$ is considered as the *a priori* information to the detector as one of the inputs. It is worth noting that in the first iteration, the *a priori* information from the channel decoder is not available. Therefore, the coded bits are considered to have equal *a priori* probability of 0.5, i.e. $\lambda_2^e(d_k(\widehat{\mathbf{X}})) = 0$, for $k = 0, 1, \ldots, \log_2 M - 1$. In this thesis, the channel decoder is implemented as a MAP decoder based on the BCJR algorithm [91]. BCJR algorithm involves a double recursion, i.e. one in forward direction and the other in the reverse direction. Consequently, it has four times the complexity on average and at least twice the complexity of the Viterbi algorithm [92,93] in its most general form. However, it produces soft outputs, which is critical in the iterative detection and decoding mechanism.

In summary, the main difference of the non-iterative receiver and iterative receiver is the usage of the *a priori* information. This difference is reflected in the ML detector and MAP detector. The non-iterative receiver assumes there is no *a*

priori knowledge of coded bits, hence, all the coded bits are assumed with equal probability. Therefore, the ML detector is the optimal detector in non-iterative receiver. On the other hand, in the iterative receiver, the *a priori* knowledge of coded bits becomes available from the channel decoder after first iteration. From second iteration onwards, the MAP detector can be utilized. Over iterations the *a priori* probability $P(\mathbf{X})$ makes a significant contribution in improving the *a posteriori* probability of the coded transmitting bits in the detection mechanism as shown in equation (2.28).

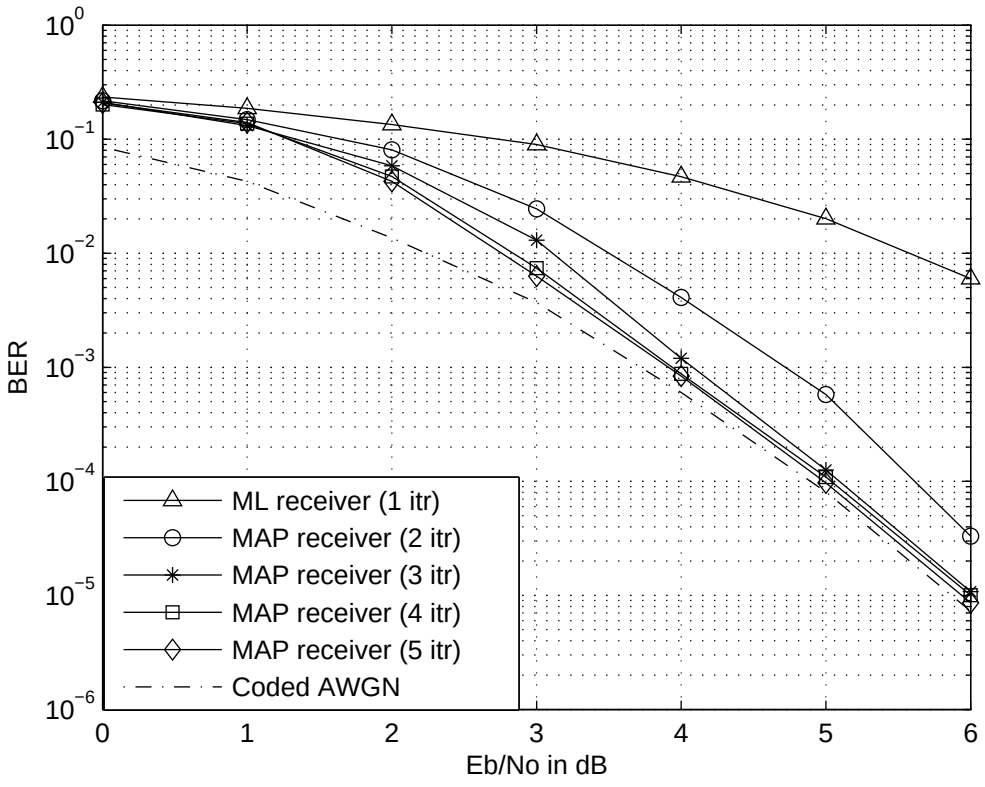

Figure 2.12: ML and MAP receivers over ISI channel

Fig. 2.12 shows the bit error rate (BER) performance of ML detector based non-iterative receiver and MAP detector based iterative receiver over a ISI channel. The ISI channel response is ISI channel-B [0.407 0.815 0.407] [94]. The channel code is the $(5, 7)_8$ convolutional code, the data modulation is binary phase shift keying (BPSK), and there are five iterations in the iterative receiver. The non-iterative receiver is basically equivalent to the first iteration in the iterative receiver. This is because in the first iteration, the *a priori* information is not available, hence, the MAP detector is essentially reduced to ML detector. The dotted line is the

AWGN channel performance which acts as the benchmark because it is the best performance a receiver can achieve if it can entirely remove the effect of the ISI channel. The x-axis shows the signal to noise ratio defined as E_b/N_0, which is computed in Appendix A.1. From the Fig. 2.12, it can be seen that the BER performance improves over iterations. The most performance gain can be obtained in the second iteration. And in later iterations, the performance gain is marginal. And finally, the iterative receiver approaches AWGN performance at $E_b/N_0 = 5$dB, which the non-iterative receiver will not be able to achieve.

2.5 Soft Parallel Interference Cancelation (SPIC)

As discussed in the previous section, the *a priori* information can be generated from iterative detection and decoding. Another advantage of using the *a priori* information is to generate soft bits or symbols. In the interference limited system, with soft bits or symbols, the interference can be reconstructed at the receiver and removed from the received signal. Therefore, instead of performing joint detection on the full set of coded bits as in equation (2.32), the individual data stream can be separated and decoded so that a low complexity implementation is feasible.

Given the generic SISO/MIMO system model (2.1) and (2.11), we can extend the formulation in equation (2.26) for MIMO-OFDM system by removing the time and frequency index for brevity as:

$$\begin{aligned} \mathbf{Y} &= \mathbf{HX} + \mathbf{W} \\ &= \underbrace{\mathbf{H}_t X_t}_{\text{desired signal}} + \underbrace{\sum_{k \neq t} \mathbf{H}_k X_k}_{\text{interference}} + \mathbf{W}, \end{aligned} \tag{2.34}$$

where $\mathbf{H}_k$ is the k_{th} column of $\mathbf{H}$. Assuming that the soft symbol $\widehat{X}_k$ for $k \neq t$ can be generated from the *a priori* information, the interference can be reconstructed and removed from the received signal as:

$$\mathbf{Y}_t = \underbrace{\mathbf{H}_t X_t}_{\text{desired signal}} + \underbrace{\sum_{k \neq t} \mathbf{H}_k (X_k - \widehat{X}_k)}_{\text{residual interference}} + \mathbf{W}, \tag{2.35}$$

where $\widehat{X}_k$ is the soft symbol of X_k. Therefore, single-user detection methods can be applied to detection in equation (2.35).

The soft symbol $\widehat{X}_k$ is defined as the Bayesian estimate [95], which is the mean value of X_k as given by:

$$\widehat{X}_t = \sum_{s_j \in \mathcal{A}} s_j \cdot P(X_t = s_j), \tag{2.36}$$

where s_j is one of the constellation points, which is formed by $\{d_0, d_1, \ldots, d_{\log_2 M-1}\}$ in the signal set $\mathcal{A}$ and

$$P(X_t = s_j) = \prod_{k=0}^{\log_2 M-1} P(d_k(X_t)). \tag{2.37}$$

As discussed before, the soft symbol is computed by the *a priori* information in the form of LLR value. Recalling the definition of the LLR value in equation (2.31), and we also know that:

$$P(d_k(X_t) = 1) + P(d_k(X_t) = 0) = 1, \tag{2.38}$$

$P(d_k(X_t))$ can be obtained from the LLR value of $\lambda(d_k(X_t))$ as follows:

$$P(d_k(X_t) = 1) = \frac{e^{\lambda(d_k(X_t))}}{1 + e^{\lambda(d_k(X_t))}}, \tag{2.39}$$

$$P(d_k(X_t) = 0) = \frac{1}{1 + e^{\lambda(d_k(X_t))}}. \tag{2.40}$$

In practical communication system, the computation of the soft symbol depends on the data modulation scheme. In the case of BPSK and Gray-coded QPSK, the soft data symbol can be obtained by:

$$\widehat{X}_t = \tanh(\lambda(d_0(X_t))/2), \tag{2.41}$$

$$\widehat{X}_t = \frac{1}{\sqrt{2}}(\tanh(\lambda(d_0(X_t))/2) + j \tanh(\lambda(d_1(X_t))/2)). \tag{2.42}$$

The detailed derivation is shown in Appendix A.2.

2.6 Summary

This chapter has investigated the SISO and MIMO system models used in this thesis in later chapters. Both SISO and MIMO system can be expressed by a single expression (2.1) or (2.11). In SISO system modeling, the channel channel time

selectivity and frequency selectivity characteristics are discussed in detail. The channel response can be shown in both time-domain and frequency-domain. It has been shown that a realistic mobile radio channel varies significantly in time-domain at high mobility and in frequency-domain with long multi-path delay spread. In MIMO system modeling, two space-time transmission techniques, namely Alamouti STC and SM are discussed. The Alamouti STC is designed to use the MIMO diversity to enhance signal reliability. The modeling of Alamouti STC is based on the assumption that the channel is not varying for two-symbol period. In this case, the channel matrix can be reformulated with orthogonal columns, hence, the Alamouti STC receiver only needs the linear processing to perform MRC for optimal detection. The SM is designed to improve MIMO system capacity, however suffers significant interference which needs to be removed and will be discussed in the following chapters. Benefits from diversity still remain in SM, however, the massive interference dominates the system performance. By taking the analogy to multi-user systems, the MIMO SM system is reformulated to a multiple access channel by considering each transmitting antenna as a user. Therefore, the interference cancelation technique is introduced, which can be used for detection.

In addition to the generic SISO/MIMO systems, the practical SISO-OFDM and MIMO-OFDM system model are introduced, which are used in transmission over wireless channels. The most important advantage of an OFDM system over a single carrier system is that it transforms the frequency selective channel into a collection of parallel flat fading subchannels, which simplifies the equalization at the receiver. However, realistic mobile radio channels with rapid dispersive fading in both time and frequency make channel estimation and tracking a challenging problem in OFDM system design.

Furthermore, the notations of the iterative receiver techniques used in this thesis are introduced. Iterative receiver realizes MAP detection by utilizing the *a priori* information. The main idea behind the iterative receiver is to exchange of extrinsic information between decoding blocks and enhance each block with the *a priori* information. The simulation results show the step-by-step (iteration over iteration) performance improvement achieved through the iterative detection and decoding. Finally, the soft parallel interference cancelation is introduced. The concept of soft information/symbol is introduced and how to compute the soft symbol from soft information is discussed. The soft interference cancelation will be applied in the iterative detection and decoding for MIMO systems.

Chapter 3

Iterative Receiver for SISO-OFDM System

3.1 Introduction

This chapter presents a novel iterative receiver with channel estimation. The channel estimation for a SISO-OFDM system is investigated and the iterative detection and decoding technique is applied to the channel estimation problem. A novel low complexity iterative turbo channel estimation technique is proposed, which makes use of preamble, pilots and soft decoded data information in an iterative fashion to improve the system performance over the time and frequency selective fading channel while maintaining the system throughput.

3.2 Frequency Domain Channel Estimation for OFDM System

The literature on OFDM channel estimation is abundant, most of which can be categorized into time-domain channel estimation and frequency-domain channel estimation. In the time-domain channel estimation, the channel impulse response is obtained from the time-domain training samples. The channel frequency response is then obtained by taking the Fourier transform of the channel impulse response. Many time-domain channel estimation techniques [96] initially designed for single carrier system can be used directly for the OFDM system. However, additional complexity is introduced due to the pilot insertion in the time domain and the Fourier transform of the channel impulse response. Furthermore, the time-domain

channel estimation has another drawback besides high complexity, which is the error propagation due to the FFT. This is because any error in the channel impulse response for a particular path in the time-domain will produce error in the channel frequency response across all subcarrier in the frequency-domain. On the other hand, in the frequency-domain estimation approach, the training sequence is embedded as frequency-domain signal samples. The channel frequency response is obtained directly. Hence, the frequency-domain estimation approach usually has less complexity. In this thesis, the frequency-domain estimation is investigated.

3.2.1 Channel Frequency Response for OFDM System

The channel estimation problem can be treated as a parameter estimation problem [97]. The basic idea is to estimate the channel response using maximum likelihood criteria, which is known as the ML estimator (MLE) [98], or alternatively, the minimum mean square error criteria, which is known as MMSE estimator (MMSEE) [98]. we denote the transmitted frequency-domain signal by a $N \times 1$ vector $\mathbf{X}^{(i)} = [X^{(i)}(0), X^{(i)}(1), \cdots, X^{(i)}(N-1)]^T$, and the received time-domain signal in (2.3) by a $N \times 1$ vector $\mathbf{y}^{(i)} = [y^{(i)}(0), y^{(i)}(1), \cdots, y^{(i)}(N-1)]^T$, where (i) means i^{th} OFDM symbol, the IDFT coefficients by a $N \times N$ matrix whose $(m,n)^{th}$ element is $[\mathbf{F}]_{m,n} = e^{j2\pi mn/N}/\sqrt{N}$, AWGN as $N \times 1$ vector $\mathbf{w}^{(i)} = [w^{(i)}(0), w^{(i)}(1), \cdots, w^{(i)}(N-1)]^T$, and time-domain channel matrix by $N \times N$ matrix

$$\mathbf{h}^{(i)} = \begin{bmatrix} h_{0,0}^{(i)} & 0 & 0 & \dots & 0 & h_{0,L-1}^{(i)} & h_{0,L-2}^{(i)} & \dots & h_{0,1}^{(i)} \\ h_{1,1}^{(i)} & h_{1,0}^{(i)} & 0 & \dots & 0 & 0 & h_{1,L-1}^{(i)} & \dots & h_{1,2}^{(i)} \\ \vdots & \vdots & \vdots & \ddots & \ddots & \ddots & \ddots & \ddots & \vdots \\ 0 & 0 & 0 & \dots & h_{N-1,L-1}^{(i)} & h_{N-1,L-2}^{(i)} & \cdots & \dots & h_{N-1,0}^{(i)} \end{bmatrix}, \quad (3.1)$$

(2.3) can be expressed as:

$$\mathbf{y}^{(i)} = \mathbf{h}^{(i)}\mathbf{F}\mathbf{X}^{(i)} + \mathbf{w}^{(i)}. \quad (3.2)$$

And for the IDFT matrix $\mathbf{F}$, we have following relation:

$$\mathbf{F}^H\mathbf{F} = \mathbf{I}_N, \quad (3.3)$$

where $\mathbf{F}^H$ is the DFT matrix with element $[\mathbf{F}^H]_{m,n} = -\exp^{j2\pi mn/N}/\sqrt{N}$. The received frequency-domain signal after DFT is given by:

$$\begin{aligned}\mathbf{Y}^{(i)} &= \mathbf{F}^H\mathbf{y}^{(i)} \\ &= \mathbf{F}^H\mathbf{h}^{(i)}\mathbf{F}\mathbf{X}^{(i)} + \mathbf{F}^H\mathbf{w}^{(i)} \\ &= \mathbf{H}^{(i)}\mathbf{X}^{(i)} + \mathbf{W}^{(i)}, \end{aligned} \tag{3.4}$$

where $\mathbf{H}^{(i)} = \mathbf{F}^H\mathbf{h}^{(i)}\mathbf{F}$ and $\mathbf{W}^{(i)} = \mathbf{F}^H\mathbf{w}^{(i)}$. For a general time-varying channel, $\mathbf{H}^{(i)}$ has non-trivial off-diagonal elements $[\mathbf{H}^{(i)}]_{m,k}$ given by (2.6). This off-diagonal term leads to the ICI, which is caused by time varying nature of the channel rather than the carrier frequency offset (CFO) in the synchronization. If the channel is time invariant, these off-diagonal terms will vanish. In practice, estimation of the entire $N \times N$ channel matrix incurs a prohibitive computational complexity. In the literature, only the diagonal coefficients of $\mathbf{H}^{(i)}$ are estimated [24, 25, 29]. Obviously, a performance degradation occurs by ignoring the ICI due to channel time variation. In the next section, we will look at how severe the ICI is.

With above approach, we reformulate the OFDM system channel estimation model in (3.4) as:

$$\mathbf{Y}^{(i)} = \mathbf{X}'^{(i)}\mathbf{H}'^{(i)} + \mathbf{W}'^{(i)}, \tag{3.5}$$

where $\mathbf{X}'^{(i)} = diag(X_0^{(i)}, X_1^{(i)}, \ldots, X_{N-1}^{(i)})$ is the $N \times N$ diagonal matrix with the assumption that pilot and data symbols are taken from a constellation with unit mean energy, i.e.,$E\{|X_m^{(i)}|^2\} = 1$. $\mathbf{H}'^{(i)}$ is the $N \times 1$ channel frequency response (diagonal terms of $\mathbf{H}^{(i)}$) vector under investigation, and $\mathbf{W}'^{(i)}$ is the equivalent $N \times 1$ noise vector with $\sigma_{w'}^2 = \sigma_w^2 + \sigma_{ICI}^2$.

3.2.2 Degradation from Inter-Carrier Interference

The degradation caused by ignoring the off-diagonal ICI terms in $\mathbf{H}^{(i)}$ can be evaluated by investigating the cross-correlation between elements in $\mathbf{H}^{(i)}$ as shown in (2.10). The power of ICI for a particular subcarrier m is expressed as:

$$\begin{aligned}P_{ICI}^m &= E\{|\sum_{k\neq m} H_{m,k}^{(i)} X^{(i)}(m)|^2\} \\ &= \sum_{m\neq k} |H_{m,k}^{(i)}|^2 \\ &= \frac{1}{N^2}\sum_{k\neq m}\sum_{l=0}^{L-1}\alpha_l\{N + 2\sum_{p=1}^{N-1}(N-p)\end{aligned}$$

$$\cdot J_0(2\pi f_m p T_s) cos[\frac{2\pi(m-k)p}{N}]\}, \tag{3.6}$$

and the average power of ICI over all subcarriers is given by:

$$\begin{aligned} P_{ICI} &= \frac{1}{N}\sum_{m=0}^{N-1} P_{ICI}^{m} \\ &= \frac{N-1}{N} + \frac{4}{N^3}\sum_{l=0}^{L-1}\alpha_l \sum_{p=1}^{N-1}(N-p)J_0(2\pi f_m p T_s) \\ &\quad \cdot \sum_{q=1}^{N-1}(N-q)cos(\frac{2\pi pq}{N}). \end{aligned} \tag{3.7}$$

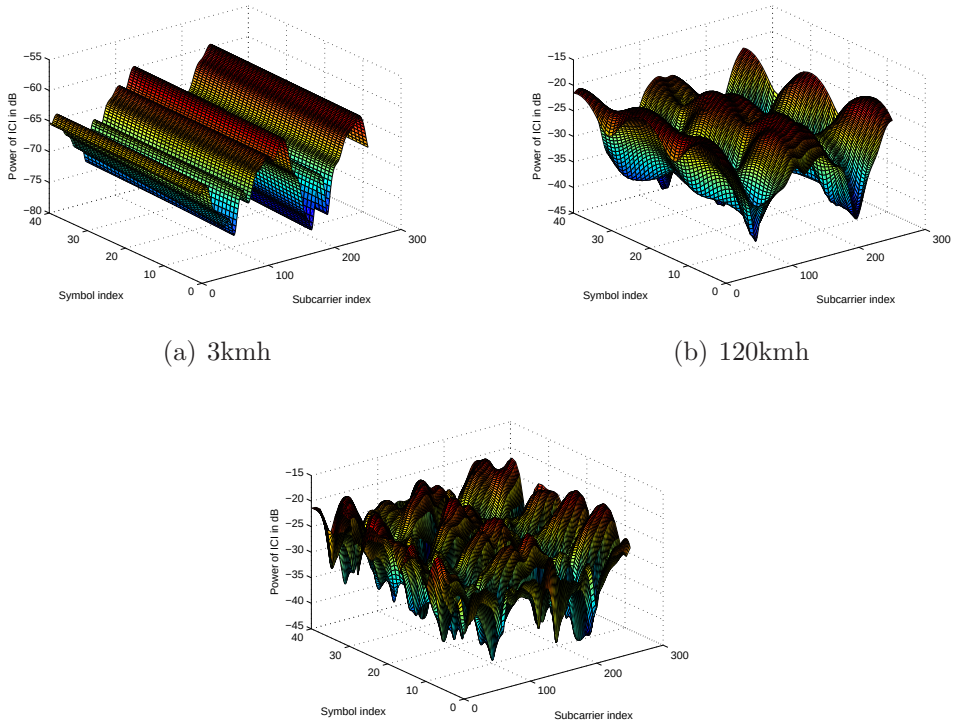

(a) 3kmh

(b) 120kmh

(c) 333kmh

Figure 3.1: Power of ICI at 3kmh, 120kmh, and 333kmh

Fig. 3.1(a), Fig. 3.1(b), and Fig. 3.1(c) show the ICI power of IMT-2000 vehicular-A channel [87] model over subcarriers and OFDM symbols at vehicular speeds 3kmh, 120kmh, and 333kmh respectively for the carrier frequency of 5GHz. The bandwidth is 5MHz, and there are 256 subcarriers. The subcarrier spacing is around 20KHz. It can be seen that in the low mobility environment, the power

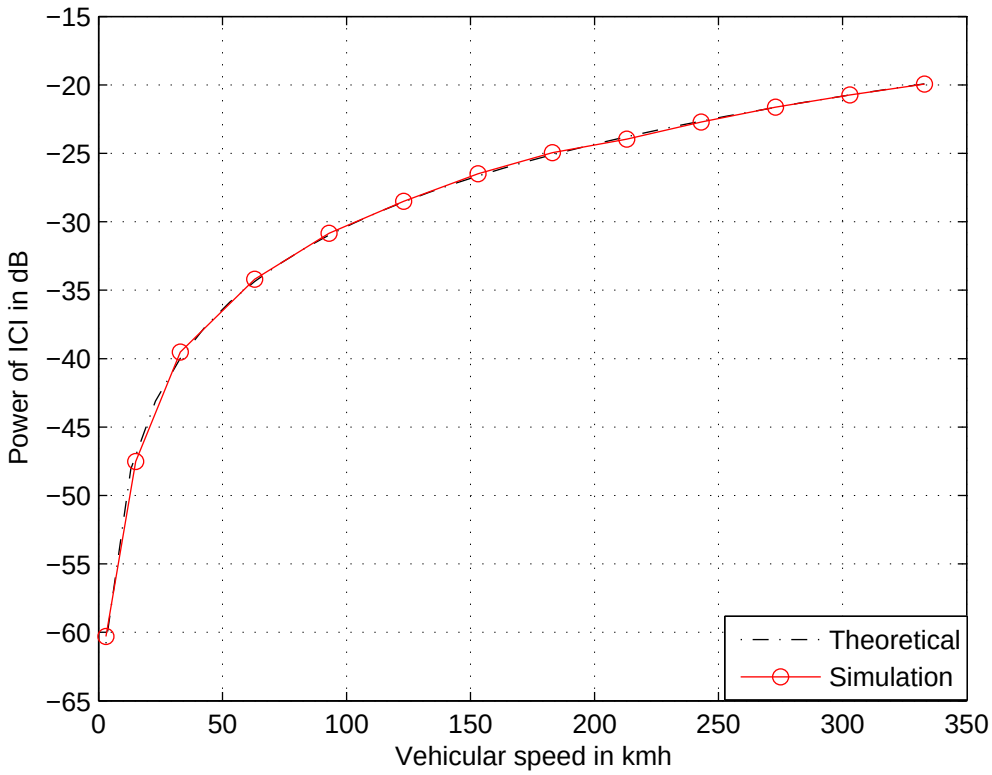

Figure 3.2: ICI Power at different vehicular speeds

of ICI is so small that the off-diagonal term in $\mathbf{H}^{(i)}$ vanishes. As the mobility increases, the power of ICI becomes larger and larger. However, such increasing of the ICI power saturates at -20dB as shown in Fig. 3.1(b) and Fig. 3.1(c).

To validate the findings, the power of ICI in terms of vehicular speed is plotted in Fig. 3.2. The dashed line shows the theoretical computation of the ICI power by equation (3.7), and the red solid line with circle mark is the simulated ICI power. The theoretical and simulated results coincide with each other. It can be seen that the power of ICI for the mobile channel in most practical Doppler spreads is below -20dB. Due to the very minor influence that the ICI has on the receiver, we focus on the diagonal channel frequency response in $\mathbf{H}^{(i)}$ and treat the ICI term as an additional embedded Gaussian noise, according to the central limit theorem [95]. The ICI variance is computed by equation (3.7), assuming that the maximum doppler spread is estimated by the method developed in [99].

3.2.3 Conventional Maximum Likelihood Estimator

In this section, the conventional ML estimator [97] is derived from first principles. The same approach will be utilized in the derivation of the developed final stage ML estimator in Section 3.3.4 and analysis of performance bonds in Section 3.4.

In the ML estimation criteria, the channel estimator tries to maximize the probability $P(\mathbf{H}'^{(i)}|\mathbf{Y}^{(i)})$ without any knowledge of $\mathbf{H}'^{(i)}$, which is equivalent to finding the channel frequency response such that the received signal can be reconstructed with minimum error, i.e.

$$\begin{aligned}
\widehat{\mathbf{H}'^{(i)}_{ML}} &= \arg\max_{\mathbf{H}'^{(i)}}\{P(\mathbf{H}'^{(i)}|\mathbf{Y}^{(i)})\} \\
&= \arg\max_{\mathbf{H}'^{(i)}}\{P(\mathbf{Y}^{(i)}|\mathbf{H}'^{(i)})\} \\
&= \arg\min_{\mathbf{H}'^{(i)}}\|\mathbf{Y}^{(i)} - \mathbf{X}'^{(i)}\widehat{\mathbf{H}'^{(i)}}\|^2 \\
&= \arg\min_{\mathbf{H}'^{(i)}}\{(\mathbf{Y}^{(i)} - \mathbf{X}'^{(i)}\widehat{\mathbf{H}'^{(i)}})^H(\mathbf{Y}^{(i)} - \mathbf{X}'^{(i)}\widehat{\mathbf{H}'^{(i)}})\}, \qquad (3.8)
\end{aligned}$$

where $\mathbf{X}'$ works as training sequence and is known at the receiver. To solve equation (3.8), the cost function for a ML channel estimation can be defined as:

$$\begin{aligned}
\mathcal{J}_{ML} &= (\mathbf{Y} - \mathbf{X}'\mathbf{H}'^H)(\mathbf{Y} - \mathbf{X}'\mathbf{H}) \\
&= \mathbf{Y}^H\mathbf{Y} - \mathbf{Y}^H\mathbf{X}'\mathbf{H}' - \mathbf{H}'^H\mathbf{X}'^H\mathbf{Y} + \mathbf{H}'^H\mathbf{X}'^H\mathbf{X}'\mathbf{H}', \qquad (3.9)
\end{aligned}$$

where the symbol index (i) is dropped for brevity. By taking the derivative of cost function $\mathcal{J}_{ML}$ with respect to $\mathbf{H}'$, we have

$$\frac{\partial \mathcal{J}_{ML}}{\partial \mathbf{H}'} = -2\mathbf{X}'^H\mathbf{Y} + 2\mathbf{X}'^H\mathbf{X}'\mathbf{H}'. \qquad (3.10)$$

Hence, the ML channel estimation solution is given by taking the equation (3.10) to equal to zeros, i.e., $\frac{\partial \mathcal{J}_{ML}}{\partial \mathbf{H}'} = 0$, and the solution is obtained as:

$$\widehat{\mathbf{H}'_{ML}} = (\mathbf{X}'^H\mathbf{X}')^{-1}\mathbf{X}'^H\mathbf{Y}. \qquad (3.11)$$

Substituting equation (3.5) into equation (3.11) with symbol index (i) dropped, the ML channel estimator can be expressed as:

$$\begin{aligned}
\widehat{\mathbf{H}'_{ML}} &= (\mathbf{X}'^H\mathbf{X}')^{-1}\mathbf{X}'^H(\mathbf{X}'\mathbf{H}' + \mathbf{W}') \\
&= \mathbf{H}' + (\mathbf{X}'^H\mathbf{X}')^{-1}\mathbf{W}'. \qquad (3.12)
\end{aligned}$$

It is worth noting that from estimation theory [97, 98], the channel frequency response estimated by the MLE is viewed as a *deterministic but unknown* quantity. The ML approach minimizes the Euclidean Distance between the original received signal and the reconstructed received signal with estimated channel frequency response. the MSE is understood as an average over the observed data. Hence, the mean value of $\widehat{\mathbf{H}^{'}_{ML}}$ is taking over the effective noise $\mathbf{W}^{'}$ as:

$$E\{\widehat{\mathbf{H}^{'}_{ML}}\} = \mathbf{H}^{'}, \tag{3.13}$$

and the covariance matrix is given by:

$$\begin{aligned} C_{ML} &= E\{(\widehat{\mathbf{H}^{'}_{ML}} - \mathbf{H}^{'})(\widehat{\mathbf{H}^{'}_{ML}} - \mathbf{H}^{'})^{H}\} \\ &= E\{(\mathbf{X}^{'H}\mathbf{X}^{'})^{-1}\mathbf{W}^{'}\mathbf{W}^{'H}((\mathbf{X}^{'H}\mathbf{X}^{'})^{-1})^{H}\} \\ &= ((\mathbf{X}^{'H}\mathbf{X}^{'})^{-1}E\{\mathbf{W}^{'H}\mathbf{W}^{'}\}(\mathbf{X}^{'H}\mathbf{X}^{'})^{-1})^{H} \\ &= \sigma^{'2}_{w}(\mathbf{X}^{'H}\mathbf{X}^{'})^{-1}((\mathbf{X}^{'H}\mathbf{X}^{'})^{-1})^{H}. \end{aligned} \tag{3.14}$$

The MSE of the MLE can be obtained by taking the average of the summed covariance matrix elements as:

$$\begin{aligned} \varepsilon_{ML} &= \frac{Tr(C_{ML})}{N} \\ &= \frac{\sigma^{'2}_{w}}{N} Tr((\mathbf{X}^{'H}\mathbf{X}^{'})^{-1}((\mathbf{X}^{'H}\mathbf{X}^{'})^{-1})^{H}), \end{aligned} \tag{3.15}$$

where $Tr(\cdot)$ is the trace operator.

3.2.4 Conventional Minimum Mean Square Error Estimator

In this section, the conventional MMSE estimator [97] is derived from first principles. The same approach will be utilized in the derivation of the developed final stage MMSE estimator in Section 3.3.4 and analysis of performance bonds in Section 3.4.

In the minimum mean square error (MMSE) estimation criteria, the channel estimator tries to find the possible channel frequency response such that the error between the estimated channel frequency response and the true channel frequency

response is minimized, i.e.,

$$\begin{aligned}\widehat{\mathbf{H}^{'(i)}_{MMSE}} &= \arg\min_{\mathbf{H}^{'(i)}} E\{\|\widehat{\mathbf{H}^{'(i)}} - \mathbf{H}^{'(i)}\|^2\} \\ &= \arg\min_{\mathbf{H}^{'(i)}} E\{(\widehat{\mathbf{H}^{'(i)}} - \mathbf{H}^{'(i)})^H(\widehat{\mathbf{H}^{(i)}} - \mathbf{H}^{'(i)})\}, \end{aligned} \tag{3.16}$$

To solve equation (3.16), a linear filter can be designed as:

$$\widehat{\mathbf{H}^{'(i)}_{MMSE}} = \mathcal{F}_{MMSE}\mathbf{Y}. \tag{3.17}$$

Substitute equation (3.17) into equation (3.16), we have the cost function for MMSEE as:

$$\mathcal{J}_{MMSE} = E\{(\mathcal{F}_{MMSE}\mathbf{Y} - \mathbf{H}^{'})^H(\mathcal{F}_{MMSE}\mathbf{Y} - \mathbf{H}^{'})\}, \tag{3.18}$$

where the symbol index (i) is dropped for brevity. As similar in Section 3.2.3, the solution of MMSEE can be obtained by taking the derivative of $\mathcal{J}_{MMSE}$ with respect to $\mathcal{F}_{MMSE}$. An alternative approach is to use the *Orthogonal Principle* [100] as follows:

$$E\{(\mathcal{F}_{MMSE}\mathbf{Y} - \mathbf{H}^{'})\mathbf{Y}^H\} = 0. \tag{3.19}$$

Both approaches end up with the solution:

$$\mathcal{F}_{MMSE} = E\{\mathbf{H}^{'}\mathbf{Y}^H\}E\{\mathbf{Y}\mathbf{Y}^H\}^{-1}, \tag{3.20}$$

where

$$\begin{aligned} E\{\mathbf{H}^{'}\mathbf{Y}^H\} &= E\{\mathbf{H}^{'}(\mathbf{X}^{'}\mathbf{H}^{'} + \mathbf{W}^{'})^H\} \\ &= E\{\mathbf{H}^{'}\mathbf{H}^{'H}\mathbf{X}^{'H}\} + E\{\mathbf{H}^{'}\mathbf{W}^{'H}\} \\ &= E\{\mathbf{H}^{'}\mathbf{H}^{'H}\}\mathbf{X}^{'H}, \end{aligned} \tag{3.21}$$

and

$$\begin{aligned} E\{\mathbf{Y}\mathbf{Y}^H\} &= E\{(\mathbf{X}^{'}\mathbf{H}^{'} + \mathbf{W}^{'})(\mathbf{X}^{'}\mathbf{H}^{'} + \mathbf{W}^{'})^H\} \\ &= E\{\mathbf{X}^{'}\mathbf{H}^{'}\mathbf{H}^{'H}\mathbf{X}^{'H}\} + E\{\mathbf{W}^{'}\mathbf{W}^{'H}\} \\ &= \mathbf{X}^{'}E\{\mathbf{H}^{'}\mathbf{H}^{'H}\}\mathbf{X}^{'H} + \sigma_w^{'2}\mathbf{I}_N. \end{aligned} \tag{3.22}$$

Hence, substitute equation (3.20) into equation (3.17), the channel frequency re-

sponse estimated by the MMSEE is given by:

$$\widehat{\mathbf{H}^{'(i)}_{MMSE}} = (\mathbf{X}^{'H}\mathbf{X}^{'} + \sigma_w^{'2} E\{\mathbf{H}^{'}\mathbf{H}^{'H}\}^{-1})^{-1}\mathbf{X}^{'H}\mathbf{Y}. \tag{3.23}$$

From estimation theory [97, 98], the channel frequency response estimated by the MMSEE is viewed as a *a random* quantity whose particular realization we want to estimate. Hence, the MSE is understood as an average taken over not only the observed data but also the channel frequency response probability density function as well. By substituting equation (3.5) into equation (3.20), the mean value of $\widehat{\mathbf{H}^{'}_{MMSE}}$ can be obtained by:

$$E\{\widehat{\mathbf{H}^{'}_{MMSE}}\} = (\mathbf{X}^{'H}\mathbf{X}^{'} + \sigma_w^{'2} E\{\mathbf{H}^{'}\mathbf{H}^{'H}\}^{-1})^{-1}\mathbf{X}^{'H}\mathbf{X}^{'}E\{\mathbf{H}^{'}\}, \tag{3.24}$$

and the covariance matrix of $\widehat{\mathbf{H}^{'}_{MMSE}}$ can be obtained by *Bayesian Gauss-Markov Theorem* [97]:

$$\begin{aligned} C_{MMSE} &= E\{(\widehat{\mathbf{H}^{'}_{MMSE}} - \mathbf{H}^{'})(\widehat{\mathbf{H}^{'}_{MMSE}} - \mathbf{H}^{'})^{H}\} \\ &= \sigma_w^{'2}(\mathbf{X}^{'H}\mathbf{X}^{'} + \sigma_w^{'2} E\{\mathbf{H}^{'}\mathbf{H}^{'H}\}^{-1})^{-1}. \end{aligned} \tag{3.25}$$

Similar to MLE, the MSE of the MMSEE can be obtained by taking the average of the summed covariance matrix elements as:

$$\begin{aligned} \varepsilon_{MMSE} &= \frac{Tr(C_{MMSE})}{N} \\ &= \frac{\sigma_w^{'2}}{N} Tr((\mathbf{X}^{'H}\mathbf{X}^{'} + \sigma_w^{'2} E\{\mathbf{H}^{'}\mathbf{H}^{'H}\}^{-1})^{-1}). \end{aligned} \tag{3.26}$$

Some remarks regarding MLE and MMSEE are worth noting. Realistic mobile radio channels vary in both frequency and time, and such variation becomes more and more significant across sub-carriers and symbols in high mobility environment, which requires more training signals to be embedded across time and frequency. As in the derivations, we assume that the training sequence $\mathbf{X}^{'} = diag(X_0^{(i)}, X_1^{(i)}, \ldots, X_{N-1}^{(i)})$ is known to the receiver for MLE and MMSEE. However, it is impossible to introduce large amount of training signals in practical systems, as the OFDM system throughput needs to be maintained. Hence, a fundamental problem is the trade off between channel estimation performance and the system throughput. To obtain better data detection performance in a channel environment which has both time and frequency selectivity, conventional preamble-based and pilot-aided channel estimation require numerous reference signals, which

significantly compromises the system throughput. On the other hand, system capacity will be significantly limited due to poor channel estimation performance based on limited number of training signals.

In this thesis, estimates of the information bits are also utilized in the channel estimation. As discussed in Chapter 2 Section 2.4, soft data information can be obtained from the iterative detection and decoding. These soft data values are computed from the feedback information from channel decoder and immediately available after the first iteration. Hence, similar to the training signals, the soft data can be applied as training signals. However, unlike the training signals which are 100% reliable (as they are known at the receiver), the soft data information should be treated differently in the channel estimation as their reliability will vary.

3.3 Iterative Receiver with Three-Stage Turbo Channel Estimation

In this section, a novel iterative receiver with three-stage turbo channel estimation technique is presented.

3.3.1 Receiver Structure Outline

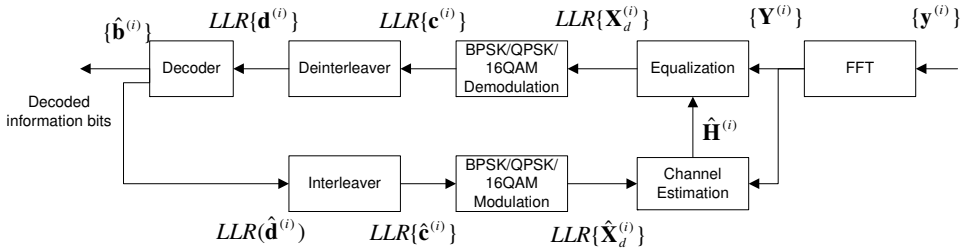

Figure 3.3: Iterative channel estimation for SISO-OFDM system

Assuming that OFDM symbols are transmitted on a frame by frame basis. In the downlink transmission, each frame consists of one preamble followed by a number of data symbols. In each data symbol, pilots are evenly distributed across available subcarriers. In the uplink transmission, there is no preamble but only

pilots. The example configurations we utilize are specified in [16, 17]. The proposed iterative receiver structure is shown in Fig. 3.3, where a three-stage turbo channel estimator, a demapper module, and a MAP decoder work in an iterative fashion. For each OFDM symbol, at each iteration, the three-stage turbo channel estimator estimates the channel frequency response based on the soft decoded data information from previous iteration, the demapper computes the a *posteriori* probability $P(X(m)|Y(m), \widehat{H_{m,m}})$, $0 \leq m \leq N-1$ given the channel estimates $\widehat{H_{m,m}}$ and received symbol $Y(m)$, and outputs extrinsic information for the coded bits in symbol $X(m)$. More specifically, the demapper outputs LLR λ_1^e of the k^{th} coded bits c_k in symbol $X(m)$ as in (3.27),

$$\lambda_1^e(c_k(X(m))) = \ln \frac{\sum_{s_j \in U_k^+(\mathcal{A})} P(X(m) = s_j | Y(m), \widehat{H_{m,m}}, \lambda_2^e)}{\sum_{s_j \in U_k^-(\mathcal{A})} P(X(m) = s_j | Y(m), \widehat{H_{m,m}}, \lambda_2^e)}, \tag{3.27}$$

where

$$\begin{aligned} P(X(m) = s_j | Y(m), \widehat{H_{m,m}}, \lambda_2^e) &= \frac{1}{2\pi\sigma_{w'}^2} \exp(-\frac{|Y(m) - \widehat{H_{m,m}} X(m)|^2}{2\sigma_{w'}^2}) \\ &\quad \cdot \prod_{l \neq k} p(c_l(X(m))), \end{aligned} \tag{3.28}$$

and $U_k^+(\mathcal{A})$ is the constellation set that contains all the symbols whose k^{th} bit is 1, and $U_k^-(\mathcal{A})$ is the constellation set that contains all the symbols whose k^{th} bit is 0. The conditional probability is computed using (3.28).

The LLRs on the coded bits are de-interleaved and passed to the MAP decoder for decoding. The MAP decoder feedbacks the extrinsic information $\lambda_2^e(c_k(X(m)))$, which is used to compute the soft data symbol as shown in equation (2.41) for BPSK, equation (2.42) for Gray-coded QPSK, and equation (A.13)(A.14) for 16QAM. The soft symbols will be used in channel estimation as detailed in the following section.

Fig. 3.4 shows the three-stage turbo channel estimator, which estimates the channel based on the improved *a priori* information of the decoded data, preamble and the pilots by adaptively weighting the statistics according to the respective levels of reliability. The performance of channel estimation is significantly enhanced which in turn leads to improved system performance. The proposed receiver also allows for high throughput transmission since there is a substantial saving on the number of preambles and pilots required.

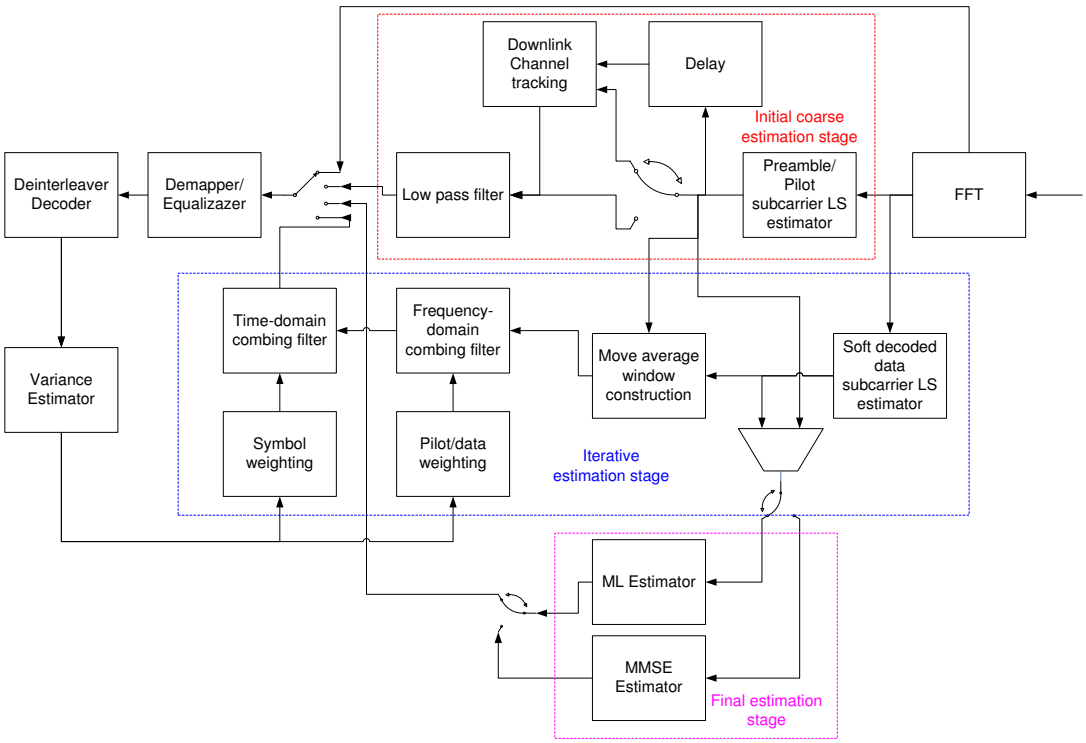

Figure 3.4: Three-stage turbo channel estimator

3.3.2 Initial Coarse Estimation Stage

Initial coarse estimation stage is performed at the first iteration. Denoting the pilot symbol at p^{th} subcarrier and the data symbol at n^{th} subcarrier for i^{th} OFDM symbol as $X_P^{(i)}(p)$ and $X_d^{(i)}(n)$ respectively, the system model for pilot symbol transmission is given by:

$$\begin{aligned} Y^{(i)}(p) &= H_{p,p}^{(i)}\sqrt{E_p}X_P^{(i)}(p) + \sum_{q\neq p} H_{p,q}^{(i)}\sqrt{E_p}X_P^{(i)}(q) \\ &\quad + \sum_{n\neq p,q} H_{p,n}^{(i)}\sqrt{E_d}X_d^{(i)}(n) + W^{(i)}(p), \end{aligned} \tag{3.29}$$

where second and third terms on the right side of equation (3.29) are ICI from other pilot subcarriers and data subcarriers, E_p and E_d are the energy of pilot and data symbol, respectively. Channel frequency response at pilot subcarrier is obtained by the LS approach:

$$\widehat{H_{p,p}^{(i)}} = Y^{(i)}(p)\frac{(X_P^{(i)}(p))^*}{\sqrt{E_p}}$$

$$
\begin{aligned}
&= H_{p,p}^{(i)} + \sum_{q \neq p} H_{p,q}^{(i)} X_P^{(i)}(q)(X_P^{(i)}(p))^* \\
&\quad + \sum_{n \neq p,q} H_{p,n}^{(i)} \sqrt{\frac{E_d}{E_p}} X_d^{(i)}(n)(X_P^{(i)}(p))^* + \frac{W^{(i)}(p)(X_P^{(i)}(p))^*}{\sqrt{E_p}} \\
&= H_{p,p}^{(i)} + W_P^{'(i)}(p), \qquad (3.30)
\end{aligned}
$$

Assuming pilots and data symbols are independent, it can be shown in Appendix B.1 that:

$$E\{W_P^{'(i)}(p)\} = 0, \qquad (3.31)$$

and

$$E\{(W_P^{'(i)}(p))^*(W_P^{'(i)}(p))\} = \frac{\sigma_w^2 + \sigma_{ICI}^2}{E_p}. \qquad (3.32)$$

For OFDM data symbols, channel tracking is applied to obtain initial coarse channel estimates. In the downlink transmission, channel estimates for the i^{th} symbol is given by:

$$\widehat{\mathbf{H}^{(i)}} = \widehat{\mathbf{H}^{(i-1)}} + \mathcal{F}(\widehat{\mathbf{H}_P^{(i)}} - \widehat{\mathbf{H}_P^{(i-1)}}), \qquad (3.33)$$

where $\widehat{\mathbf{H}_P}$ is the channel estimates at pilot subcarriers. $\mathcal{F}(\cdot)$ denotes the interpolation filter, which can be FFT based [25], MMSE based [29], or linear interpolation based [101]. In this thesis, linear interpolation is employed due to its low complexity. More specifically, assuming the pilot spacing is δ, $\widehat{H_{p,p}^{(i)}}$ and $\widehat{H_{p+\delta,p+\delta}^{(i)}}$ are the channel estimates from two adjacent pilots. The channel estimate $\widehat{H_{m,m}^{(i)}}$ at subcarrier m, which is between pilot subcarrier p and $p+\delta$ is given by:

$$\widehat{H_{m,m}^{(i)}} = \begin{bmatrix} 1 - \frac{m-p}{\delta} & \frac{m-p}{\delta} \end{bmatrix} \cdot \begin{bmatrix} \widehat{H_{p,p}^{(i)}} \\ \widehat{H_{p+\delta,p+\delta}^{(i)}} \end{bmatrix}, \qquad (3.34)$$

In contrast, in the uplink transmission, the initial channel estimates for the i^{th} symbol is given by:

$$\widehat{\mathbf{H}^{(i)}} = \mathcal{F}(\widehat{\mathbf{H}_P^{(i)}}), \qquad (3.35)$$

where the design of the interpolation filter is based on the pilots allocation in practical OFDM systems.

3.3.3 Iterative Estimation Stage

In the iterative estimation stage, LS estimation is first performed for both pilot and data subcarriers, followed by frequency-domain combining and time-domain combining. Similar to the pilot tones, the system model for data symbol transmission is given by:

$$\begin{aligned} Y^{(i)}(m) &= H^{(i)}_{m,m}\sqrt{E_d}X^{(i)}_d(m) + \sum_{n\neq m} H^{(i)}_{m,n}\sqrt{E_d}X^{(i)}_d(n) \\ &\quad + \sum_{p\neq m} H^{(i)}_{m,p}\sqrt{E_p}X^{(i)}_P(p) + W^{(i)}(m), \end{aligned} \tag{3.36}$$

and the LS channel estimation for data symbol is given by:

$$\widehat{H^{(i)}_{m,m}} = Y^{(i)}(m)\frac{(\widehat{X^{(i)}_d}(m))^*}{\sqrt{E_d|\widehat{X^{(i)}}(m)|^2}}. \tag{3.37}$$

However, the data detection in previous iterations may not be reliable such that the energy of soft decoded data symbol in (2.41) and (2.42) may be less than unity. If the soft decoded data symbol is directly applied to LS estimation, the channel estimates are subject to a bias due to the imperfect decoding information. To overcome this problem, channel estimate at the m^{th} subcarrier is normalized by the average energy of the soft decoded data symbols within a moving average window (MAW) Θ as:

$$\begin{aligned} \widehat{H^{(i)}_{m,m}} &= Y^{(i)}(m)\frac{(\widehat{X^{(i)}_d}(m))^*}{\sqrt{E_d|\widehat{X^{(i)}_{d\in\Theta}}|^2}} \\ &= H^{(i)}_{m,m}\frac{X^{(i)}_d(m)(\widehat{X^{(i)}_d}(m))^*}{\sqrt{|\widehat{X^{(i)}_{d\in\Theta}}|^2}} + \sum_{n\neq m} H^{(i)}_{m,n}\frac{X^{(i)}_d(n)(\widehat{X^{(i)}_d}(m))^*}{\sqrt{|\widehat{X^{(i)}_{d\in\Theta}}|^2}} \\ &\quad + \sum_{p\neq m} H^{(i)}_{m,p}\frac{\sqrt{E_p}X^{(i)}_P(p)(\widehat{X^{(i)}_d}(m))^*}{\sqrt{E_d|\widehat{X^{(i)}_{d\in\Theta}}|^2}} + \frac{W^{(i)}(m)(\widehat{X^{(i)}_d}(m))^*}{\sqrt{E_d|\widehat{X^{(i)}_{d\in\Theta}}|^2}} \\ &\approx H^{(i)}_{m,m}\sqrt{|\widehat{X^{(i)}_{d\in\Theta}}|^2} + W^{'(i)}_d(m), \end{aligned} \tag{3.38}$$

where

$$|\widehat{X^{(i)}_{d\in\Theta}}|^2 = E\{\widehat{X^{(i)}_{d\in\Theta}}(m)(\widehat{X^{(i)}_{d\in\Theta}}(m))^*\}, \tag{3.39}$$

is the average energy of soft coded data information in the MAW Θ. Similar in the pilot symbol channel estimation, assuming pilots and data symbols are independent, it can be shown in Appendix B.2 that:

$$E\{W_d^{'(i)}(m)\} = 0, \tag{3.40}$$

and

$$E\{(W_d^{'(i)}(m))^*(W_d^{'(i)}(m))\} = \frac{\sigma_w^2 + \sigma_{ICI}^2}{E_d}. \tag{3.41}$$

Mobile radio channel shows natural phenomenon of delay spread in the time-domain, which is caused by the reflected and scattered propagation paths. In the frequency-domain, the channel frequency response shows correlation, which is measured by coherent bandwidth [84]. Coherent bandwidth is the range of frequencies over which two frequency components are likely to be correlated in amplitude and phase. Fig. 3.5 shows the frequency-domain correlation between the 5^{th} subcarrier and other subcarriers for IMT-2000 vehicular-A channel model in SISO-OFDM system with 256 subcarrier over 5MHz bandwidth. The blue line is the theoretical correlation result, and the black doted line with cross is the simulation results. It can be seen that the channel frequency response at the adjacent subcarriers near the 5^{th} subcarriers are highly correlated. Knowing this property can be used to improve the channel estimation technique.

More specifically, due to the correlation in the frequency domain, low pass filtering can be performed by combining channel estimates from both pilot tones and soft coded data information within a MAW to generate improved channel estimates. In the OFDM system, the size of the MAW is determined by the system coherent bandwidth and subcarrier spacing. For example, in the system configuration as mentioned in Section 2.2.3, the subcarrier spacing is 5.12kHz, while the coherent bandwidth is 54kHz for the channel considered in this thesis. Therefore, it is reasonable to define a MAW of size 9. In practical system, the coherent bandwidth can be derived from channel delay profile, which can be obtained by taking the inverse Fourier transform of channel frequency response estimated by reference signals, such as preamble or pilots, in the training period [14]. Furthermore, the idea of the combining strategies in the OFDM system can be generalized to other systems too, such as 3GPP DS-CDMA system. In that case, the combining strategy can be applied between control and data channel, where the size of MAW is determined by the chip rate and channel coherence time.

Assuming within the MAW, the channel frequency response is highly correlated,

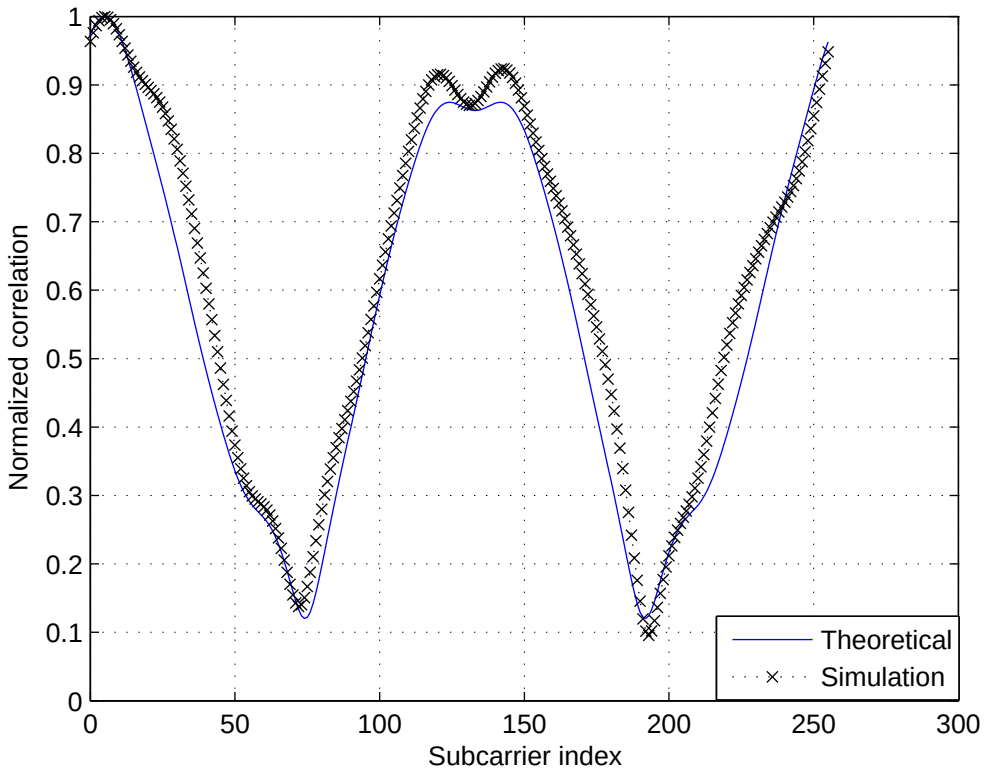

Figure 3.5: Frequency-domain correlation between the 5^{th} subcarrier and other subcarriers for IMT-2000 vehicular-A channel model in SISO-OFDM system

i.e. $H_{p,p}^{(i)} \approx H_{d,d}^{(i)} \approx H_{m,m}^{(i)}$, the weighted average for the channel frequency response at subcarrier m is given by:

$$\begin{aligned}
\widetilde{H^{(i)}}_{m,m} &= \omega_p \sum_{p\in\Theta} \widehat{H_{p,p}^{(i)}} + \omega_d \sum_{d\in\Theta} \widehat{H_{d,d}^{(i)}} \\
&= \omega_p \sum_{p\in\Theta} (H_{m,m}^{(i)} + W_P^{'(i)}) + \omega_d \sum_{d\in\Theta} (H_{m,m}^{(i)} \sqrt{\widehat{|X_{d\in\Theta}^{(i)}|^2}} + W_d^{'(i)}) \\
&= (N_p\omega_p + N_d\omega_d \sqrt{\widehat{|X_{d\in\Theta}^{(i)}|^2}}) H_{m,m}^{(i)} \\
&\quad + \underbrace{(\omega_p \sum_{p\in\Theta} W_P^{'(i)} + \omega_d \sum_{d\in\Theta} W_d^{'(i)})}_{\mathcal{N}(0, N_p\omega_p^2 \frac{\sigma_{w'}^2}{E_p} + N_d\omega_d^2 \frac{\sigma_{w'}^2}{E_d})},
\end{aligned} \tag{3.42}$$

where N_p and N_d are the number of pilot and data symbols within the MAW. It can be observed from equation 3.42 that the channel estimate after frequency-main

combining is the true channel frequency response $H_{m,m}^{(i)}$ distored by a factor $(N_p\omega_p + N_d\omega_d\sqrt{|\widehat{X_{d\in\Theta}^{(i)}|^2}})$, and with noise added on $(\omega_p \sum_{p\in\Theta} W_P^{'(i)} + \omega_d \sum_{d\in\Theta} W_d^{'(i)})$. Hence, an convex optimization problem can be defined as follows: the optimal weight values $\{\omega_p, \omega_d\}$ should be obtained in such as way that the added on noise should have mimimun variance subject to the constraint that the distortion factor is unity. The optimal weight values $\{\omega_p, \omega_d\}$, can be determined using the MRC principle, which is mathematically formulated into the following Lagrange multiplier problem:

$$\begin{aligned}\{\omega_p, \omega_d\} &= \arg\min_{\omega_p,\omega_d}\{(N_p\omega_p^2\frac{\sigma_{w'}^2}{E_p} + N_d\omega_d^2\frac{\sigma_{w'}^2}{E_d}) + \lambda(N_p\omega_p \\ &\quad + N_d\omega_d\sqrt{|\widehat{X_{d\in\Theta}^{(i)}|^2}} - 1)\},\end{aligned} \tag{3.43}$$

where λ is the Lagrange multiplier. Hence, the optimal weights $\{\omega_p, \omega_d\}$ can be derived as:

$$\omega_p = \frac{1}{N_p + N_d\frac{E_d}{E_p}|\widehat{X_{d\in\Theta}^{(i)}|^2}}, \tag{3.44}$$

$$\omega_d = \frac{\sqrt{|\widehat{X_{d\in\Theta}^{(i)}|^2}}}{N_p\frac{E_p}{E_d} + N_d|\widehat{X_{d\in\Theta}^{(i)}|^2}}. \tag{3.45}$$

To further improve channel estimates, time-domain MAW combining can be applied to the channel frequency response. The time-domain combining is designed from the observation that the channel impulse response has correlated fading gains within the coherence time [84]. The coherence time is the time duration over which two channel fading gains have a strong likelihood of amplitude and phase correlation. Hence, in the OFDM system, after transforming the correlated channel impulse response within the coherence time to the frequency-domain, the channel frequency response within the coherence time are correlated as well.

Fig. 3.6 shows the frequency response correlation at the 5^{th} subcarrier over 20 OFDM symbols period between for IMT-2000 vehicular-A channel model at 333kmh in SISO-OFDM system. The blue solid line is the theoretical correlation result, and the black doted line with cross is the simulation results. It can be seen that channel frequency response for a particular subcarrier for the adjacent OFDM symbols are highly correlated. This property can be used to improve the channel estimation.

Therefore, based on the observation that OFDM channel frequency responses are highly correlated in the time-domain for consecutive OFDM symbols, i.e.

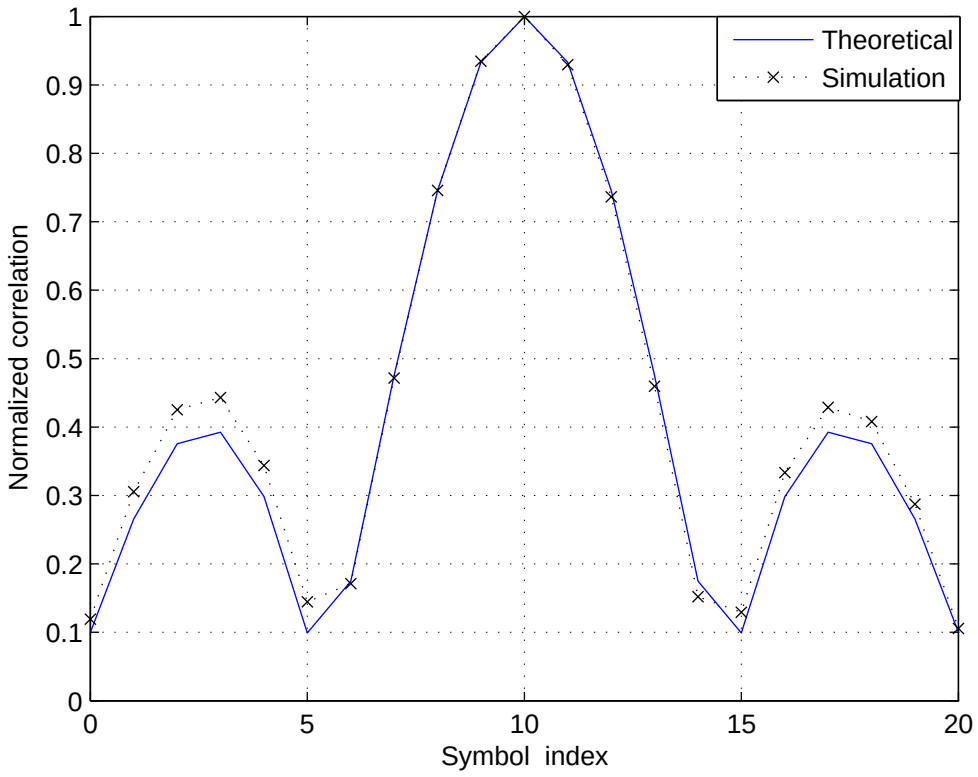

Figure 3.6: Frequency response correlation at the 5^{th} subcarrier over 20 consecutive symbols for IMT-2000 vehicular-A channel model at 333kmh in SISO-OFDM system

$H_{m,m}^{(i-1)} \approx H_{m,m}^{(i)}$. Therefore, another MRC can be performed, which is given by:

$$\begin{aligned} \widetilde{\widehat{H}_{m,m}^{(i)}} &= \alpha \widetilde{H^{(i-1)}}_{m,m} + \beta \widetilde{H^{(i)}}_{m,m} \\ &= (\alpha+\beta) H_{m,m}^{(i)} + \underbrace{(\alpha W^{''(i-1)}(m) + \beta W^{''(i)}(m))}_{\mathcal{N}(0, \alpha^2 \sigma^2_{w^{''(i-1)}} + \beta^2 \sigma^2_{w^{''(i)}})}, \end{aligned} \tag{3.46}$$

where α and β are weighting parameters obtained by minimizing the estimation error, that is:

$$\{\alpha, \beta\} = \underset{\alpha,\beta}{\operatorname{argmin}} \{(\alpha^2 \sigma^2_{w^{''(i-1)}} + \beta^2 \sigma^2_{w^{''(i)}}) + \lambda(\alpha + \beta - 1)\}, \tag{3.47}$$

and $\sigma^2_{w^{''(i-1)}}$ and $\sigma^2_{w^{''(i)}}$ are the variances after the frequency-domain combining for the $(i-1)^{th}$ and i^{th} OFDM symbols, respectively.

$\sigma^2_{w^{''(i-1)}}$ and $\sigma^2_{w^{''(i)}}$ are obtained from the variance estimator in Fig. 3.4. Here, we illustrate how the variance estimator computes $\sigma^2_{w^{''(i)}}$ for the i^{th} OFDM symbol.

The variance $\sigma^2_{w''(i-1)}$ for the $(i-1)^{th}$ OFDM symbol can be obtained similarly. As shown in equation (3.42), the variance after the frequency-domain combining is approximated as:

$$\begin{aligned}\sigma^2_{w''(i)} &\approx (\omega_p \sum_{p\in\Theta} W_P^{'(i)} + \omega_d \sum_{d\in\Theta} W_d^{'(i)}) \\ &\approx N_p\omega_p^2 \frac{\sigma^2_{w'}}{E_p} + N_d\omega_d^2 \frac{\sigma^2_{w'}}{E_d}. \end{aligned} \tag{3.48}$$

Substituting equations (3.44) and (3.45) in equation (3.48), the variance estimator will output the variance for the time-domain combining as:

$$\sigma^2_{w''(i)} \approx \frac{N_p\sigma^2_{w'}}{E_p(N_p + N_d\frac{E_d}{E_p}\widehat{|X^{(i)}_{d\in\Theta}|^2})^2} + \frac{N_d\sigma^2_{w'}\widehat{|X^{(i)}_{d\in\Theta}|^2}}{E_d(N_p\frac{E_p}{E_d} + N_d\widehat{|X^{(i)}_{d\in\Theta}|^2})^2}. \tag{3.49}$$

Hence, the optimal solution for α and β in the time-domain combining are obtained as:

$$\alpha = \frac{\sigma^2_{w''(i)}}{\sigma^2_{w''(i-1)} + \sigma^2_{w''(i)}}, \tag{3.50}$$

$$\beta = \frac{\sigma^2_{w''(i-1)}}{\sigma^2_{w''(i-1)} + \sigma^2_{w''(i)}}. \tag{3.51}$$

The advantage of the proposed method is that the weights in (3.44), (3.45), (3.50) and (3.51) are adaptive to the number and power of pilots and data symbols in the MAW, and most importantly, the reliability of the specific OFDM symbols. Therefore, the combining is performed in proportion to the available information. As the iterations proceed, the available *a priori* information on data signals improves, the weights associated with the data-aided channel estimates increase accordingly, where the decoding data serve as virtual reference signals.

It is worth mentioning that the frequency-domain combining and time-domain combining strategies are developed based on the assumption that time and frequency correlations remain valid. As discussed in both theoretical and practical perspectives, time and frequency correlations are widely accepted concepts. This assumption has been verified in the Fig. 3.5 and 3.6, and other references [14, 84] in the literature as well. The impact of error in channel time and frequency correlations is out of the scope of this chapter.

3.3.4 Final Estimation Stage

The final estimation stage is performed on the final iteration, where the decoding information from MAP decoder becomes very reliable, and is almost as reliable as reference pilot signals. For an OFDM symbol with estimated reference signals, the MLE or MMSEE techniques are able to provide a further improvement over the LS based MRC channel estimator discussed in the previous section. Extended from the reformulated OFDM system channel estimation model in (3.5), if $\mathbf{X}^{'(i)}$ is perfectly known, the LS estimation is given by:

$$\begin{aligned}\widetilde{\mathbf{H}^{'(i)}}_{LS} &= [(\mathbf{X}^{'(i)})^H\mathbf{X}^{'(i)}]^{-1}(\mathbf{X}^{'(i)})^H\mathbf{Y}^{(i)} \\ &= \mathbf{H}^{'(i)} + [(\mathbf{X}^{'(i)})^H\mathbf{X}^{'(i)}]^{-1}(\mathbf{X}^{'(i)})^H\mathbf{W}^{'(i)} \\ &= \mathbf{H}^{'(i)} + (\mathbf{X}^{'(i)})^{-1}\mathbf{W}^{'(i)}, \end{aligned} \tag{3.52}$$

where $(\mathbf{X}^{'(i)})^{-1}\mathbf{W}^{'(i)}$ is statistically equivalent to $\mathbf{W}^{'(i)}$ for a PSK constellation. Hence, a new signal model [97] based on (3.52) is used for estimating $\mathbf{H}^{'(i)}$, given by:

$$\begin{aligned}\widetilde{\mathbf{H}^{'(i)}}_{LS} &= \mathbf{H}^{'(i)} + [(\mathbf{X}^{'(i)})^H\mathbf{X}^{'(i)}]^{-1}(\mathbf{X}^{'(i)})^H\mathbf{W}^{'(i)} \\ &= \mathbf{G}\mathbf{h}^{'(i)} + [(\mathbf{X}^{'(i)})^H\mathbf{X}^{'(i)}]^{-1}(\mathbf{X}^{'(i)})^H\mathbf{W}^{'(i)} \\ &= \mathbf{G}\mathbf{h}^{'(i)} + (\mathbf{X}^{'(i)})^{-1}\mathbf{W}^{'(i)}, \end{aligned} \tag{3.53}$$

where $\mathbf{G}$ is the $N \times L$ matrix with element $[\mathbf{G}]_{n,l} = e^{-j2\pi nl/N}$, $0 \le n \le N-1$ and $0 \le l \le L-1$. $\mathbf{h}^{'(i)} = [h_0^{'(i)}, h_1^{'(i)}, \cdots, h_{L-1}^{'(i)}]^T$ is a $L \times 1$ channel impulse response vector, where $h_n^{'(i)}$ is given by:

$$h_l^{'(i)} = \frac{1}{N}\sum_{n=0}^{N-1} h^{(i)}(n,l), \tag{3.54}$$

As shown in Section 3.2.3, if $\mathbf{H}^{'(i)}$ is assumed to be a deterministic and unknown vector, the MLE can be derived following the invariance property [98], given by:

$$\begin{aligned}\widehat{\mathbf{H}^{'(i)}_{MLE}} &= \mathbf{G}(\mathbf{G}^H\mathbf{G})^{-1}\mathbf{G}^H\widetilde{\mathbf{H}^{'(i)}}_{LS} \\ &= \mathbf{G}(\mathbf{G}^H\mathbf{G})^{-1}\mathbf{G}^H[(\mathbf{X}^{'(i)})^H\mathbf{X}^{'(i)}]^{-1}(\widehat{\mathbf{X}^{'(i)}})^H\mathbf{Y}^{(i)} \\ &= \frac{1}{N}\mathbf{G}\mathbf{G}^H(\widehat{\mathbf{X}^{'(i)}})^{-1}\mathbf{Y}^{(i)}, \end{aligned} \tag{3.55}$$

where $\widehat{\mathbf{X}'^{(i)}}$ is soft coded OFDM symbol from the last second iteration with pilot tones. On the other hand, as $\mathbf{H}'^{(i)}$ is random in nature, Bayesian estimators are able to improve the performance by exploiting the priori knowledge on channel statistics. Hence, similar in Section 3.2.4, we consider the MMSEE [97], given by:

$$\begin{aligned}\widehat{\mathbf{H}'^{(i)}_{MMSE}} &= \mathbf{G}\mathbf{R}_{\mathbf{h}'\mathbf{h}'}(\mathbf{G}^H\mathbf{G}\mathbf{R}_{\mathbf{h}'\mathbf{h}'} + \sigma^2_{w'}\mathbf{I_L})^{-1}\mathbf{G}^H\widetilde{\mathbf{H}'^{(i)}}_{LS} \\ &= \mathbf{G}\mathbf{R}_{\mathbf{h}'\mathbf{h}'}(N\mathbf{R}_{\mathbf{h}'\mathbf{h}'} + \sigma^2_{w'}\mathbf{I_L})^{-1}\mathbf{G}^H\widetilde{\mathbf{H}'^{(i)}}_{LS} \\ &= \mathbf{G}\mathbf{R}_{\mathbf{h}'\mathbf{h}'}(N\mathbf{R}_{\mathbf{h}'\mathbf{h}'} + \sigma^2_{w'}\mathbf{I_L})^{-1}\mathbf{G}^H(\widehat{\mathbf{X}'^{(i)}})^{-1}\mathbf{Y}^{(i)}, \end{aligned} \tag{3.56}$$

where $\mathbf{R}_{\mathbf{h}'\mathbf{h}'} = E\{\mathbf{h}'\mathbf{h}'^H\} = diag(\alpha_l)$ is the $L \times L$ covariance matrix of $\mathbf{h}'$ based on the WSSUS assumption. $\mathbf{I_L}$ is the $L \times L$ identity matrix, and $\mathbf{G}^H\mathbf{G} = N\mathbf{I_L}$.

3.4 Mean Square Error Analysis of Turbo Channel Estimation

In this section, we derive the lower bound of MSE for the three-stage turbo channel estimator. It is difficult to analyze the MSE of the proposed iterative turbo channel estimation technique because of the exchange of soft information and MAP decoder. Instead, the MSE lower bounds are calculated for MLE and MMSEE in Section 3.3.4.

Extended from (3.55), the MLE can be expressed as:

$$\widehat{\mathbf{H}'^{(i)}_{MLE}} = \mathbf{H}'^{(i)} + \mathbf{G}(\mathbf{G}^H\mathbf{G})^{-1}\mathbf{G}^H(\mathbf{X}'^{(i)})^{-1}\mathbf{W}'^{(i)}, \tag{3.57}$$

whose mean can be obtained as $E\{(\widehat{\mathbf{H}'^{(i)}_{MLE}})\} = \mathbf{H}'^{(i)}$, and the covariance matrix can be obtained as:

$$\begin{aligned} C_{\widehat{\mathbf{H}'^{(i)}_{MLE}}} &= E\{(\widehat{\mathbf{H}'^{(i)}_{MLE}} - \mathbf{H}'^{(i)})(\widehat{\mathbf{H}'^{(i)}_{MLE}} - \mathbf{H}'^{(i)})^H\} \\ &= \sigma^2_{w'}\mathbf{G}((\mathbf{G}^H\mathbf{G})^{-1})^H\mathbf{G}^H \\ &= \frac{\sigma^2_{w'}}{N}\mathbf{G}\mathbf{G}^H, \end{aligned} \tag{3.58}$$

where $(\mathbf{X}'^{(i)})^{-1}((\mathbf{X}'^{(i)})^{-1})^H = \mathbf{I}_N$ for PSK constellation considered in this thesis. Hence, the corresponding MSE for MLE is given by:

$$MSE_{MLE} = \frac{1}{N}Tr(C_{\widehat{\mathbf{H}'^{(i)}_{MLE}}}) = \frac{1}{N}Tr(\frac{\sigma^2_{w'}}{N}\mathbf{G}\mathbf{G}^H) = \frac{\sigma^2_{w'}L}{N}. \tag{3.59}$$

As shown in the Appendix C.1, the proposed iterative turbo MLE achieves the Cramér-Rao lower bound (CRLB), which is the lower bound for the performance that the minimum-variance unbiased (MVU) estimator [97, 98] can achieve. The MVU estimator is known as the optimal estimator for the estimation of the deterministic quantity. Since the proposed iterative turbo MLE achieves CRLB, it is a MVU estimator.

Similarly, for the MMSEE, substitute equation (3.56) into equation (3.25), the covariance matrix of $\widehat{\mathbf{H}'^{(i)}_{MMSE}}$ is given by:

$$C_{\widehat{\mathbf{H}'^{(i)}_{MMSE}}} = \sigma^2_{w'}\mathbf{G}\mathbf{R}_{\mathbf{h}'\mathbf{h}'}(N\mathbf{R}_{\mathbf{h}'\mathbf{h}'} + \sigma^2_{w'}\mathbf{I}_{\mathbf{L}})^{-1}\mathbf{G}^H, \tag{3.60}$$

and the Bayesian MSE is given by:

$$\begin{aligned} MSE_{MMSE} &= \frac{1}{N}Tr(C_{\widehat{\mathbf{H}'^{(i)}_{MMSE}}}) \\ &= \sigma^2_{w'}Tr\{\mathbf{R}_{\mathbf{h}'\mathbf{h}'}(N\mathbf{R}_{\mathbf{h}'\mathbf{h}'} + \sigma^2_{w'}\mathbf{I}_{\mathbf{L}})^{-1}\} \\ &= \frac{\sigma^2_{w'}}{N}Tr\{diag(\frac{\alpha_l}{\alpha_l + \sigma^2_{w'}/N})\} \\ &= \frac{\sigma^2_{w'}}{N}\sum_{l=0}^{L-1}\frac{1}{1+\sigma^2_{w'}/(N\alpha_l)}. \end{aligned} \tag{3.61}$$

MSEs in (3.59) and (3.61) will be used as benchmarks to evaluate the performance for proposed channel estimator in the following section. It can be shown that $MSE_{MMSE} \leq MSE_{MLE}$ as the MMSE estimator utilizes channel statistical information to enhance the performance.

3.5 Complexity Analysis for Turbo Channel Estimation

In this section, the computational complexity of the proposed iterative turbo channel estimation is evaluated by determining the number of multiplications. Assuming there are altogether N_{itr} iterations, and N subcarriers. In the initial estimation stage, pilot estimation requires N_p multiplications. To obtain the coarse channel frequency response at data tones, the linear interpolation between pilot tones requires $(N - N_p)$ multiplications.

In the iterative estimation stage, every iteration requires the same computational complexity. More specifically, in each iteration, the soft data channel estima-

tion requires $(N-N_p)$ multiplications. The calculation of ω_p, ω_d coefficients requires $N \times N_\Theta^{FD}$ multiplications, frequency-domain filtering requires $N \times N_\Theta^{FD}$ multiplications, where N_Θ^{FD} is the frequency-domain MAW size. The calculation of α, β coefficients is a single multiplication. The time-domain filtering requires $2N$ complex multiplications. Therefore, there are totally $(N_{itr}-2) \times (3N - N_p + 2N \times N_\Theta^{FD} + 1)$ multiplications.

Table 3.1: Computational Complexity for Iterative Channel Estimation in SISO-OFDM System

Operations	First Stage	Second Stage (per iteration)	Final Stage
Pilot Estimation	N_p	0	0
Soft Data Estimation	0	$N - N_p$	$N - N_p$
Linear Interpolation	$N - N_p$	0	0
ω_p, ω_d Calculation	0	$N \times N_\Theta^{FD}$	0
Frequency-domain Filtering	0	$N \times N_\Theta^{FD}$	0
α, β Calculation	0	1	0
Time-domain Filtering	0	$2N$	0
ML Estimation	0	0	$\mathcal{O}(N^2)$
MMSE Estimation	0	0	$\mathcal{O}(N^3)$
Total for each stage	$\mathcal{O}(N)$	$\mathcal{O}(N)$	$\mathcal{O}(N^2) or \mathcal{O}(N^3)$

In the final estimation stage, only soft data channel estimation and MLE or MMSE operation are performed. Similar to iterative estimation stage, soft data channel estimation requires $(N - N_p)$ multiplications. MLE operation requires $\mathcal{O}(N^2)$ multiplications and MMSE operation requires $\mathcal{O}(N^3)$. Therefore, the total complexity is $N + O(N^2)$ for MLE and $N + \mathcal{O}(N^3)$ for MMSE estimator. Table 3.1 summarizes the number of multiplications involved in each stage. It can be seen that if the final estimation stage is excluded, the complexity of initial coarse estimation stage and iterative estimation stage is $N + (N_{itr}-2) \times (3N - N_p + 2N \times N_\Theta^{FD} + 1)$, which is in the order of $\mathcal{O}(N)$. Fig. 3.7 shows the number of multiplications in the different estimation stages for $N_{itr} = 4$, $N_p = 8$, and $N_\Theta^{FD} = 9$. Compared to conventional MLE or MMSE estimation, the additional complexity from iterative channel estimation remains low.

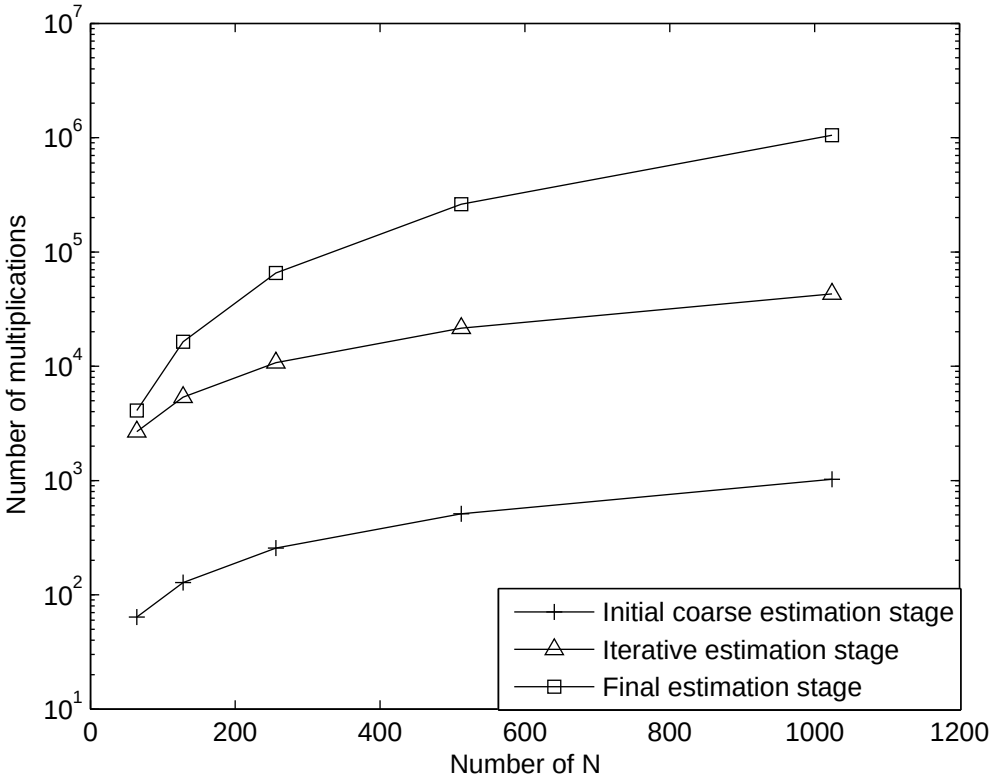

Figure 3.7: Number of multiplications in the initial coarse, iterative, and final estimation stages for $N_{itr} = 4$, $N_p = 8$, and $N_{\Theta}^{FD} = 9$

3.6 Numerical Results

3.6.1 Simulation Setup

In this section, an OFDM system with $N = 256$ subcarriers, and 8 pilot tones as used in [17] is considered. The carrier frequency is 5GHz, and the bandwidth is 5MHz. The subcarrier spacing is approximately 19.53kHz. The IMT-2000 vehicular-A channel [87] is generated by Jakes model [86], with exponential decayed power profile {0, -1, -9, -10, -15, -20} in dB and relative path delay {0, 310, 710, 1090, 1730, 2510} in ns. The coherent bandwidth is approximately 54kHz. The frequency-domain MAW size is set to 9 to ensure that the correlation of channel frequency response within the window is sufficiently high. Unless stated otherwise, the vehicular speed is 333kmh, which is translated to a Doppler frequency of $f_m = 1540.125Hz$. The CP duration is 16 samples. A rate-1/2 $(5, 7)_8$ convolutional code is used for channel coding. Random interleaving is adopted in the simulation and the modulation scheme is QPSK. The maximum number of itera-

tions is set to 6. There are ten OFDM symbols per frame transmission. The energy of the pilot symbols is same as data symbols. Pilot tones are evenly distributed across subcarriers. We demonstrated the performance under the simulation environment that frame by frame transmission is adopted, which is the same setup as the practical system. Hence, we think that frame error rate (FER) is the most suitable performance metric to show the benefits of our technique. In the following sections, performance comparisons are made in terms of FER and channel estimation MSE. Performance of MSE will be compared to lower bounds for MLE and MMSE estimators respectively, which are derived in Section 3.4. We refer the iterative receivers as "turbo...", the conventional receivers as "conventional...", and the receiver performance with perfect CSI as "Perfect...".

3.6.2 Downlink Performance

For the downlink transmission, the OFDM receiver with iterative turbo channel estimation technique is compared to the OFDM receiver with preamble-based channel estimation [14] and iterative data derived channel estimation [23]. Fig. 3.8 and Fig. 3.9 show the downlink FER and MSE of the iterative receiver over a number of iterations altogether with that using conventional preamble channel estimation and data derived channel estimation. The conventional receiver with just preamble estimation fails at such high mobility. The OFDM receiver with data derived channel estimation performs much better than the conventional preamble estimation, while the OFDM receiver with the iterative channel estimation achieves the best performance among the three, and approaches that with perfect CSI. As shown in Fig. 3.9, in the last iteration, the MSE of iterative turbo channel estimation approaches MLE lower bound. This verifies the observations shown in Fig. 3.8.

3.6.3 Uplink Performance

For the uplink transmission, the receiver is compared to the conventional OFDM receiver with pilot-aided channel estimation [14,98] using $P = 64$ pilot tones. Hereafter, the iterative turbo MLE channel estimation and MMSE channel estimation refer to the iterative methods with ML estimation and MMSE estimation performed in the last iteration respectively.

Fig. 3.10 and Fig. 3.11 show the uplink FER and MSE of the iterative receiver together with that using conventional pilot-aided channel estimation. Eight pilots are embedded in each OFDM symbol for the iterative system while 64 subcarriers

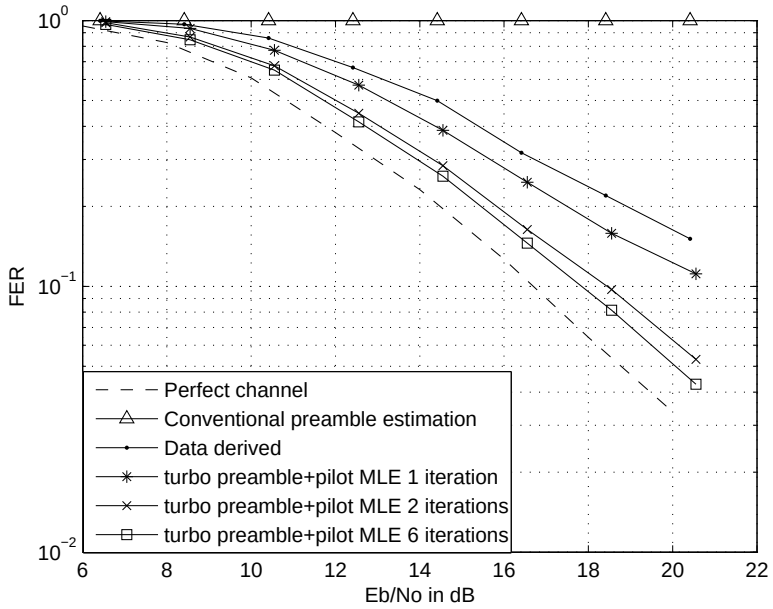

Figure 3.8: Downlink FER performance between OFDM receiver with iterative turbo channel estimation and OFDM receiver with conventional preamble channel estimation and data derived channel estimation

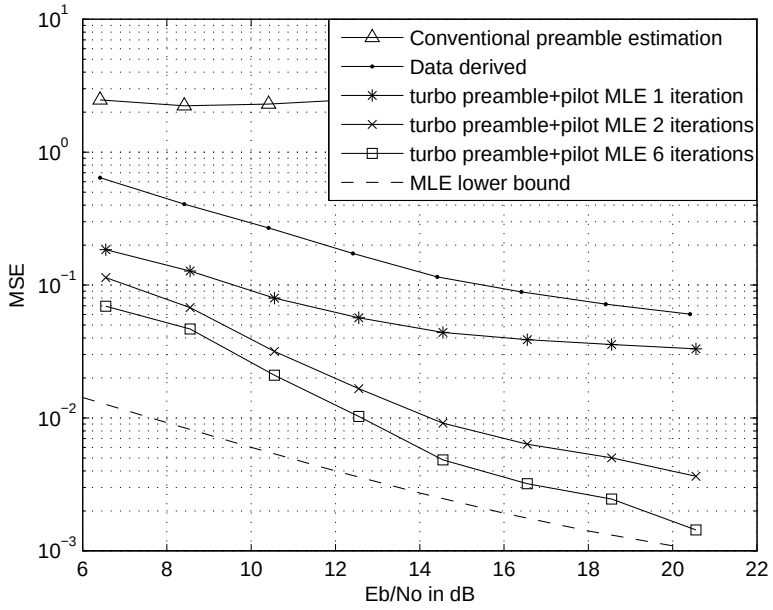

Figure 3.9: Downlink MSE performance between OFDM receiver with iterative turbo channel estimation and OFDM receiver with conventional preamble channel estimation and data derived channel estimation

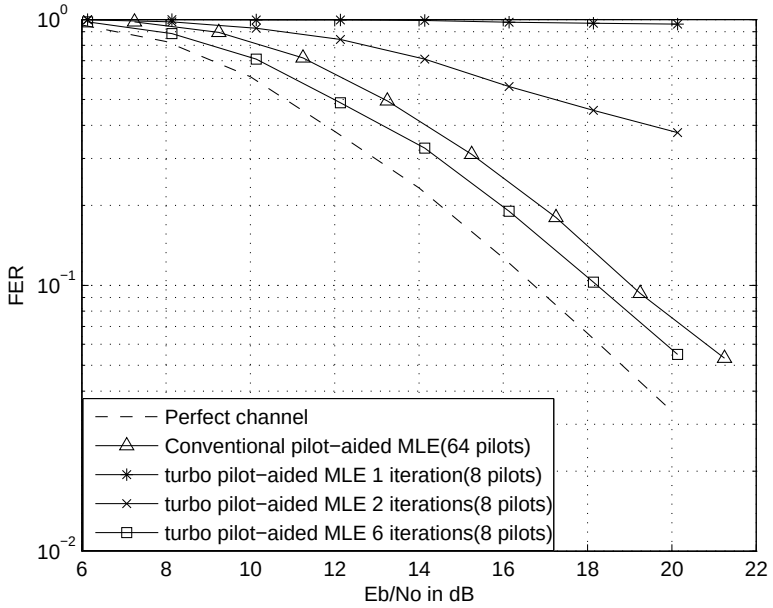

Figure 3.10: Uplink FER performance between OFDM receiver with iterative turbo channel estimation and OFDM receiver with conventional preamble channel estimation and data derived channel estimation

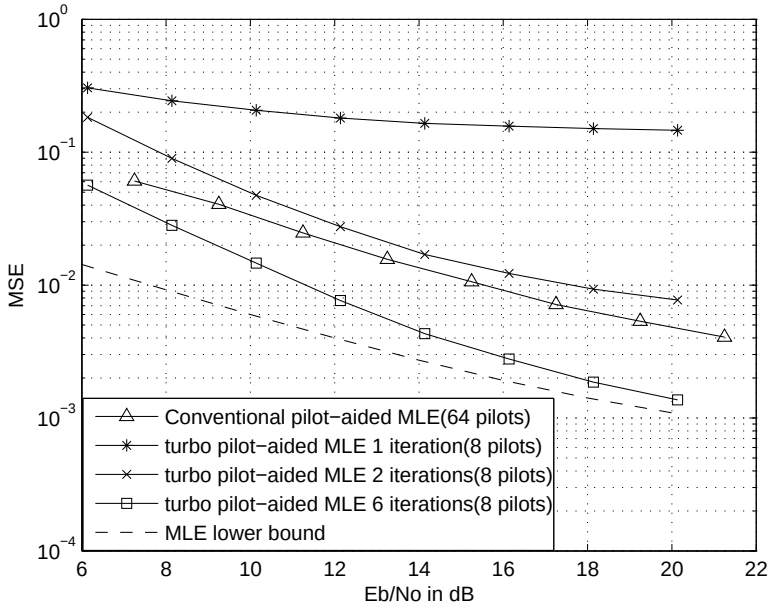

Figure 3.11: Uplink MSE performance between OFDM receiver with iterative turbo channel estimation and OFDM receiver with conventional preamble channel estimation and data derived channel estimation

are used for pilots in the other. In the first iteration, the iterative channel estimator has poor performance due to fewer pilots available for initial coarse estimation stage. However, as decoded soft data symbols are available for channel estimation in the later iterations, the iterative channel estimator outperforms the pilot-aided estimation with 64 inserted pilots. This demonstrates the advantage of iterative channel estimator in both SNR and throughput. The mean square error for both methods shown in Fig. 3.11 confirms the channel estimator performance.

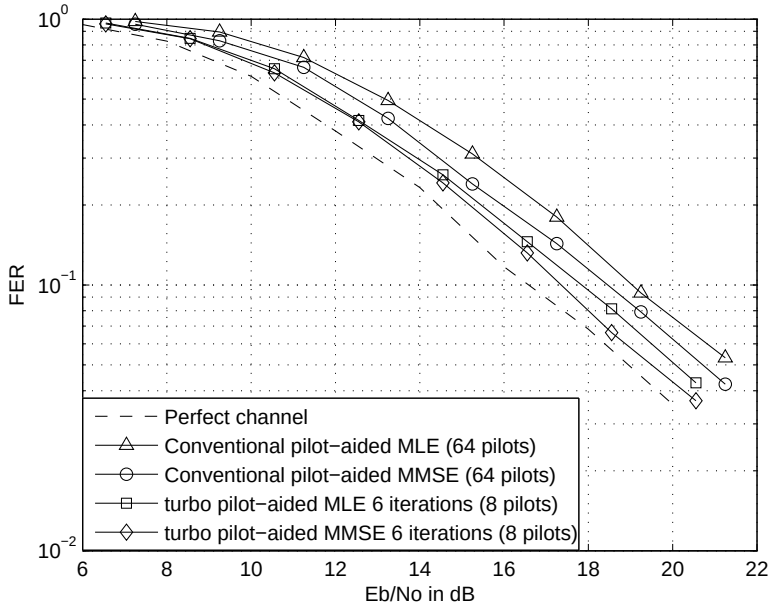

Figure 3.12: Uplink FER performance between OFDM receiver with iterative turbo MLE/MMSE channel estimation and OFDM receiver with conventional MLE/MMSE channel estimation

Fig. 3.12 and Fig. 3.13 show the uplink FER and MSE for the iterative receiver and that with pilot-aided MLE/MMSE channel estimation. It can be seen that the iterative turbo channel estimation performs 1dB better with much fewer pilots. This observation shows that in high Doppler environment, the iterative receiver maintains the system throughput and has a SNR gain over advanced channel estimation filters.

3.6.4 Performance under Vehicle Mobility

In addition to the 333kmh vehicular speed case, the performances of the iterative receiver at 120kmh and 60kmh are presented. Fig. 3.14 shows the FER performance comparison for various vehicular speeds. The performance improves for receivers

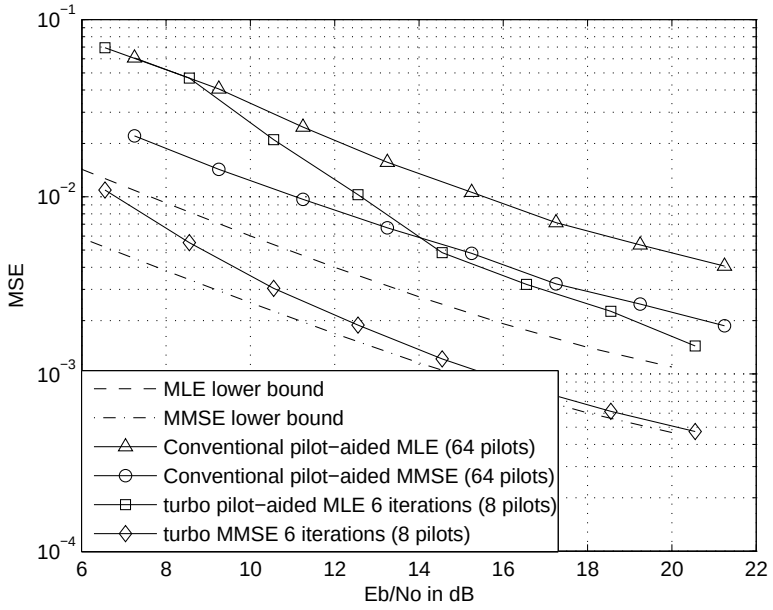

Figure 3.13: Uplink MSE performance between OFDM receiver with iterative turbo MLE/MMSE channel estimation and OFDM receiver with conventional MLE/MMSE channel estimation

with preamble based and data derived channel estimation as the vehicular speed decreases. However, in all scenarios, the iterative receiver has a significant performance gain over other methods. It is also interesting to note that in this paper we assume ten data symbols per frame for simulations, while in the IEEE standard 802.16 [16, 17] the frame length can increase up to 16 symbols. In that case, the channel variation can be considerable even at the vehicular speed of 60kmh and a more significant improvement can be achieved by our iterative receiver.

3.6.5 Performance with Carrier Frequency Offset

Furthermore, the effect of CFO is considered as in the realistic OFDM systems [16, 17] due to channel delays and the difference between transmitter and receiver oscillators. The IEEE standard 802.16 [17] says residual CFO of up to 4% of the subcarrier spacing is present after synchronization and acquisition, which causes ICI and degrades the system performance. Fig. 3.15 shows the FER performance of the iterative receiver with up to 4% residual CFO. This residual CFO is generated from an uniform distribution [22] over $[-0.04, 0.04]$. It can be observed that the degradation ranges from a fraction of a decibel (dB) for the 60kmh case to around 1dB for the 333kmh case, compared to that of the CFO-free system. To address a

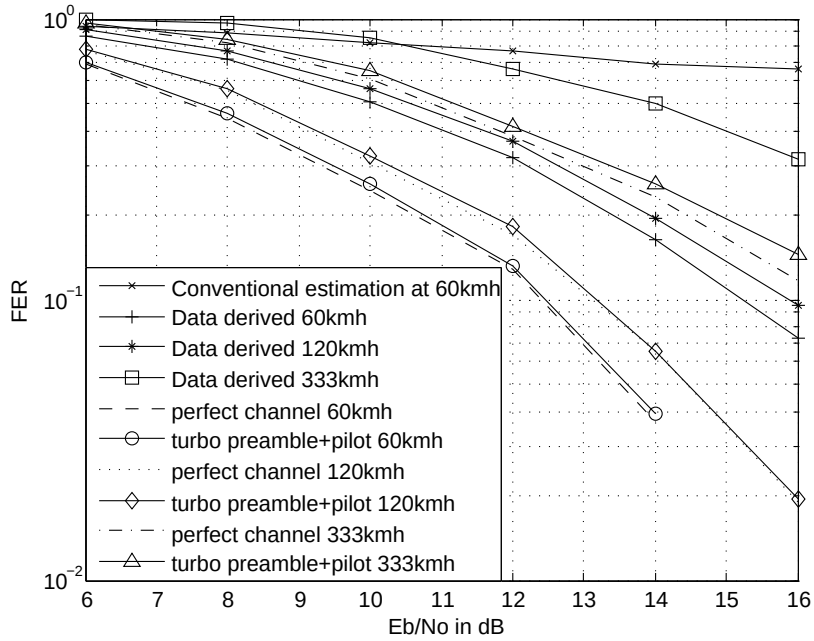

Figure 3.14: Frame error rate performance between OFDM receiver with iterative turbo channel estimation and OFDM receiver with conventional preamble channel estimation and data derived channel estimation at different mobilities.

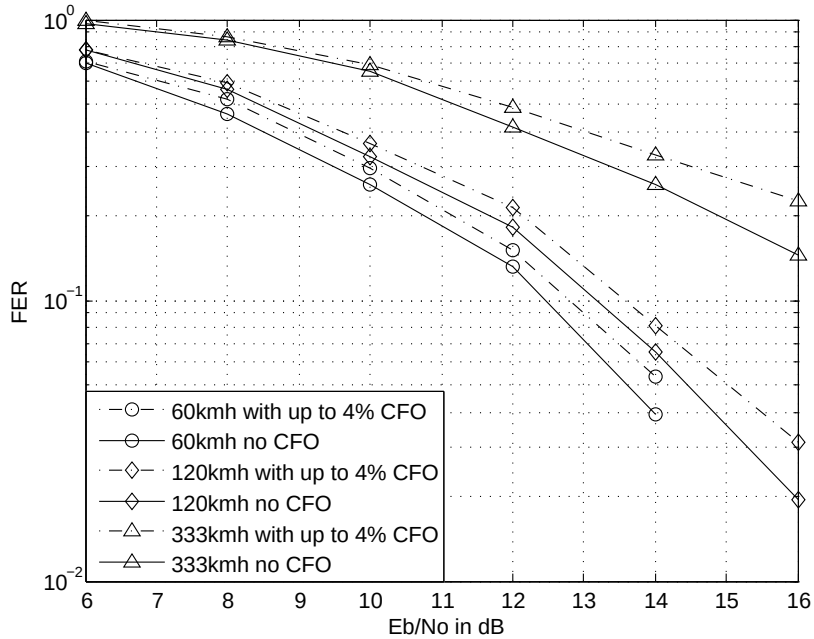

Figure 3.15: Frame error rate performance of iterative receiver with up to 4% residual CFO.

more significant CFO, we can either employ a separate synchronization module to perform frequency error estimation and compensation, or mitigate the resultant ICI

by advanced interference reduction algorithms [45]. Discussion on these approaches is beyond the scope of this paper.

To summarize, compared to OFDM receiver with existing channel estimation techniques, the OFDM receiver with iterative turbo channel estimation can approach the MSE lower bounds. It approaches performance of perfect CSI even with a small number of preambles and pilots in a rapid dispersive fading channel, which makes it an efficient solution in terms of both SNR and throughput. Furthermore, the iterative receiver is robust w.r.t residual CFO in practical OFDM systems.

3.7 Summary and Contributions

This chapter has investigated the problem of OFDM transmission in a rapid dispersive fading channel. In such a highly mobile environment, the wireless channel undergoes fast variations both in time and frequency. In order to track the fast varying channel, large number of pilot tones are usually inserted to the OFDM symbol for existing receivers, which incurs huge SNR and throughput loss. An iterative turbo channel estimation technique, which makes use of preamble, pilot and decoded soft data information for channel estimation is developed to improve the frame and bit error rate performance for a given signal to noise ratio while maximizing the system throughput at the same time. The channel estimation is conducted by three estimation stages, where a frequency-domain and time-domain combining strategy is developed to combine the channel estimates from above signals in an efficient and low complexity manner. Numerical results and MSE analysis have shown that, compared to the OFDM receiver with existing conventional channel estimation, the OFDM receiver with iterative turbo channel estimation can approach the performance with nearly perfect CSI at various mobility scenarios. In addition to the improvement in both SNR and throughput benefits, the receiver is robust to frequency error and has low computational complexity which means it is possible to implement in hardware.

Some specific contributions made in this chapter are as follows. First of all, the system model for the SISO-OFDM system model is investigated, the degradation from ICI due to realistic mobile radio channel is fully analyzed from theoretical perspective and validated through simulations. The effect of ICI in the channel estimation problem is modeled as Gaussian random process so that the system model for the channel estimation of the OFDM system is reformulated and simpli-

fied by combining the power of ICI with the white noise as effect noise. And the ML channel estimator and MMSE channel estimator are investigated and the MSE for MLE and MMSEE are analyzed through first and second order statistics of the channel estimator. The literature review on the conventional and iterative channel estimation techniques are presented.

Secondly, an iterative turbo channel estimator for the OFDM system is developed. The iterative turbo channel estimator consists of three estimation stages, namely the initial coarse estimation stage, iterative estimation stage, and the final estimation stage. The initial coarse estimation is performed in the first iteration, the pilot estimation is performed. More specifically, in the downlink transmission, the preamble estimation is performed, and channel tracking through linear filtering is performed after the preamble estimation to obtain the channel estimation at the data subcarriers. On the other hand, in the uplink transmission, pilot-aided channel estimation is performed at the pilot subcarriers, and the linear interpolation is performed among the channel estimates from pilot subcarriers to obtain the channel estimates at the data subcarriers. After the initial coarse estimation, the data detection and decoding are performed. The soft coded information is fed back from channel decoder for the next iteration.

The iterative estimation is performed from the second iteration onwards. The channel estimates can be obtained through pilots and soft coded data symbols. The frequency-domain combining and time-domain combining are developed to explore the frequency-domain and time-domain correlations. The moving average windows along frequency and time directions are introduced to perform the combining. In the frequency-domain combining, the channel estimates from the pilot and data subcarriers are weighted in such a way the ratio of the pilot weights and the data weights are evolved adaptively over iterations. More specifically, at the beginning, the channel estimates from the soft coded data symbols are less weighted than the pilot symbols because the soft coded data symbols are less reliable than the pilot symbols due to the initial coarse channel estimation. Over iterations, the reliability or the energy of the soft coded data symbols improves, and eventually the soft coded data symbols can act as the pilot symbols. Hence, the wights between the pilot and data symbols are adjusted adaptively. The time-domain combining is similar to the frequency-domain combining, where the adjacent data symbols rather than the adjacent subcarriers are combined.

The final estimation is performed in the last iteration, where the soft coded data symbols can act as the pilot symbols eventually. If the channel statistics are

not available at the receiver, the MLE is applied to perform the linear filtering to improve the channel estimates. On the other hand, if the channel statistics are known at the receiver, the MMSEE is employed.

Thirdly, the analysis of the lower MSE bounds that the iterative turbo channel estimation can achieve is presented. Theoretically, the iterative MMSEE has lower MSE than the iterative MLE where the additional gain is from the exploration of the channel statistics, which is usually difficult to obtain in the practical system. Furthermore, the complexity in terms of complex multiplications that the iterative turbo channel estimation requires are analyzed. Compared to the conventional MLE or MMSE estimation, the additional complexity from the iterative channel estimation remains low, which is very feasible for practical implementation.

Finally, the performances of the receivers with the iterative turbo channel estimation and the conventional channel estimation techniques are compared. The numerical and analytical results show that the developed technique can approach the performance of systems with perfect CSI with much fewer preamble and pilots symbols compared to existing channel estimation methods. Therefore, under same system configuration, the iterative receiver improve the system performance over the time and frequency selective fading channel while maintaining the system throughput. Furthermore, the iterative receiver outperforms the conventional receivers under pedestrian, low, intermediate, and high mobilities. And with marginal performance degradation, the iterative receiver is robust to within 4% carrier frequency offset after frequency acquisition.

Chapter 4

Iterative Receiver for MIMO-OFDM system

4.1 Introduction

In Chapter 3, a receiver with novel iterative turbo channel estimation technique is presented, which shows how the near-optimal channel estimation and data detection performance can be achieved in the realistic mobile radio channel environment. In this Chapter, the previous work is extended to MIMO-OFDM systems. A novel low complexity channel estimator with time-domain and frequency-domain combining of channel estimates from preamble, pilots and soft decoded data information is proposed to track the dynamics of channel frequency response. This channel estimator is integrated with a MRC receiver for the Alamouti STC system and an interference canceler for the system with spatial multiplexing.

4.2 Conventional MIMO-OFDM Receivers

The transmitting and receiving scheme on each subcarrier in the OFDM system can be considered as an independent MIMO model. Hence, the receiver design is on a per subcarrier basis. For the Alamouti STC system, the conventional MRC receiver is attractive due to it's low computational complexity. On the other hand, the receiver for the SM system is much more complicated. With a ZF receiver, a straight forward matrix inversion is needed, while the linear MMSE receiver provides improved detection with the knowledge of MIMO channel statistics.

4.2.1 Conventional Alamouti STC-OFDM Receiver

In this section, the conventional Alamouti STC-OFDM Receiver [14, 47] is derived from first principles. The same approach will be utilized in the derivation of the developed iterative receiver for Alamouti STC-OFDM in Section 4.3.1.

Due to the space-time block encoder and channel invariant assumption in the Alamouti STC system, symbols from different transmitting antennas need to be orthogonal to each other. In Chapter 2 Section 2.3.3, the system model for 2×1 Alamouti STC is given by equation (2.21), which is represented here as:

$$\mathbf{Y}_m = \mathbf{H}_m \cdot \mathbf{X}_m + \mathbf{W}_m, \tag{4.1}$$

where

$$\mathbf{Y}_m = \begin{bmatrix} Y^0_{i-1,m} \\ (Y^0_{i,m})^* \end{bmatrix}, \tag{4.2}$$

$$\mathbf{H}_m = \begin{bmatrix} H^{0,0}_m & H^{0,1}_m \\ (H^{0,1}_m)^* & -(H^{0,0}_m)^* \end{bmatrix}, \tag{4.3}$$

$$\mathbf{X}_m = \begin{bmatrix} X_{i-1,m} \\ X_{i,m} \end{bmatrix}, \tag{4.4}$$

and

$$\mathbf{W}_m = \begin{bmatrix} W^0_{i-1,m} \\ (W^0_{i,m})^* \end{bmatrix}. \tag{4.5}$$

Assuming that the transmitted symbols $\mathbf{X}_m$ are equiprobable, and the noise vector $\mathbf{W}_m$ is assumed to be a multivariate white Gaussian noise, the optimal detector is the ML detector, which is given by:

$$\widehat{\mathbf{X}}_m = \arg\min_{\widehat{\mathbf{X}}_m} \|\mathbf{Y}_m - \mathbf{H}_m \widehat{\mathbf{X}}_m\|^2. \tag{4.6}$$

Generally speaking, the ML detector will search the entire signal constellation, which has prohibitive computational complexity in practical implementation. Nevertheless, if we examine the channel matrix $\mathbf{H}_m$ carefully, the columns of $\mathbf{H}_m$ are orthogonal to each other regardless of what the channel fading coefficients are, i.e. by taking the product of the first column $\mathbf{H}^0_m$ and the second column $\mathbf{H}^1_m$ of matrix $\mathbf{H}_m$, we have

$$(\mathbf{H}^0_m)^H \mathbf{H}^1_m = \begin{bmatrix} (H^{0,0}_m)^* & H^{0,1}_m \end{bmatrix} \cdot \begin{bmatrix} H^{0,1}_m \\ -(H^{0,0}_m)^* \end{bmatrix}$$

$$= \quad 0. \tag{4.7}$$

This property of the Alamouti STC is very desirable for the data detection because the MIMO system can be considered as a multiple access system employing orthogonal spreading code. Then each transmitted coded data symbol is considered as a user in the multiple access environment, i.e. equation (4.1) can be reformulated as

$$\mathbf{Y}_m = \mathbf{H}_m^0 \cdot X_{i-1,m} + \mathbf{H}_m^1 \cdot X_{i,m} + \mathbf{W}_m. \tag{4.8}$$

Hence, similar to the multiple access system, the linear combiner (or matched filter) output can be obtained as:

$$\begin{aligned} \widehat{\mathbf{Y}}_m &= \mathbf{H}_m^H \cdot \mathbf{Y}_m \\ &= \mathbf{H}_m^H \cdot \mathbf{H}_m \mathbf{X}_m + \mathbf{H}_m^H \mathbf{W}_m \\ &= \sum_{t=0}^{1} |H_m^{0,t}|^2 \mathbf{X}_m + \mathbf{W}_m^{'}, \end{aligned} \tag{4.9}$$

where

$$\begin{aligned} \mathbf{H}_m^H \cdot \mathbf{H}_m &= \begin{bmatrix} |H_m^{0,0}|^2 + |H_m^{0,1}|^2 & 0 \\ 0 & |H_m^{0,0}|^2 + |H_m^{0,1}|^2 \end{bmatrix} \\ &= \sum_{t=0}^{1} |H_m^{0,t}|^2 \cdot \mathbf{I}_2, \end{aligned} \tag{4.10}$$

and the noise at the output of linear combiner is

$$\begin{aligned} \mathbf{W}_m^{'} &= \begin{bmatrix} (\mathbf{H}_m^0)^H \mathbf{W}_m \\ (\mathbf{H}_m^1)^H \mathbf{W}_m \end{bmatrix} \\ &= \begin{bmatrix} (H_m^{0,0})^* W_{i-1,m}^0 + H_m^{0,1} (W_{i,m}^0)^* \\ (H_m^{0,1})^* W_{i-1,m}^0 - H_m^{0,0} (W_{i,m}^0)^* \end{bmatrix}. \end{aligned} \tag{4.11}$$

As the channel fading coefficients $H_m^{0,0}$ and $H_m^{0,1}$ from different wireless links are independent and identical distributed (i.i.d), the noise $\mathbf{W}_m^{'}$ at the output of the linear combiner has zero mean and scaled covariance matrix, i.e.

$$E\{\mathbf{W}_m^{'}\} = \mathbf{0} \cdot \mathbf{I}_2, \tag{4.12}$$

and

$$E\{\mathbf{W}_m^{'}(\mathbf{W}_m^{'})^H\} = \sigma_w^2 \sum_{t=0}^{1} |H_m^{0,t}|^2 \cdot \mathbf{I}_2. \tag{4.13}$$

In this case, the detection becomes

$$\widehat{\mathbf{X}}_m = \arg\min_{\widehat{\mathbf{X}}_m} \|\widehat{\mathbf{Y}}_m - \sum_{t=0}^{1} |H_m^{0,t}|^2 \cdot \widehat{\mathbf{X}}_m\|^2. \tag{4.14}$$

Hence, it follows immediately that by using this linear combining (or match filtering), the detection criteria (4.14) reduces to two separate decoding criteria for $X_{i-1,m}$ and $X_{i,m}$. And only two complex multiplications and one complex addition per symbol per subcarrier are required for decoding, which is linear with respect to N with order $\mathcal{O}(N)$. For example, consider a signal constellation with M points. The detection criteria in (4.6) requires $2^{2\log_2 M}$ point searches. On the other hand, the detection criteria in (4.14) only requires $2 \times 2^{\log_2 M}$ point searches, which reduce the computational complexity by $1 - 2^{1-\log_2 M}$. In QPSK, $M = 4$, the complexity reduction is 50%. In 16QAM, $M = 8$, the complexity reduction is 87.5%. In addition to the complexity reduction, the SNR E_s/N_0 at the output of the linear combiner (matched filtering) is given by:

$$\begin{aligned} \frac{E_s}{N_0} &= \frac{E_s(\sum_{t=0}^{1} |H_m^{0,t}|^2)^2}{\sigma_w^2 \sum_{t=0}^{1} |H_m^{0,t}|^2} \\ &= \frac{E_s \sum_{t=0}^{1} |H_m^{0,t}|^2}{\sigma_w^2}, \end{aligned} \tag{4.15}$$

where E_s is the energy of transmitted symbol per subcarrier per transmitting antenna, and N_0 is the double sided white noise spectral density. It is straight forward to observe that the energy of the transmitted symbol from different antennas are combined to improve the SNR E_s/N_0, hence, the receiver maximum ratio combining is obtained.

4.2.2 Conventional SM-OFDM Receiver

In this section, the conventional SM-OFDM Receivers [14,47] are derived from first principles. The same approach will be utilized in the derivation of the developed iterative receiver for SM-OFDM in Section 4.3.2.

In the SM-OFDM system, there is significant difference in the interference among transmitting antennas experienced in the detection, as the transmitted symbols are not repeated, unlike in the Alamouti scheme. In Chapter 2 Section 2.3.3, the system model for $N_T \times N_R$ SM-OFDM is given by equation (2.26), which is represented here as:

$$\begin{aligned} \mathbf{Y}_{i,m} &= \mathbf{H}_{i,m}\mathbf{X}_{i,m} + \mathbf{W}_{i,m} \\ &= \underbrace{\mathbf{H}^t_{i,m}X^t_{i,m}}_{\text{desired signal}} + \underbrace{\sum_{k\neq t}\mathbf{H}^k_{i,m}X^k_{i,m}}_{\text{interference}} + \mathbf{W}_{i,m}, \end{aligned} \tag{4.16}$$

where $\mathbf{H}^k_{i,m}$ is the k^{th} column of $\mathbf{H}_{i,m}$. Assuming that the transmitted symbol $X^t_{i,m}$ where $0 \leq t < N_T$ are equiprobable, the optimal detector is the joint ML detector, which is given by:

$$\widehat{\mathbf{X}}_{i,m} = \arg\min_{\widehat{\mathbf{X}}_{i,m}} \|\mathbf{Y}_{i,m} - \mathbf{H}_{i,m}\widehat{\mathbf{X}}_{i,m}\|^2. \tag{4.17}$$

The joint ML detector searches the entire signal space which is spanned by vector $\mathbf{X}_{i,m}$. Consider a signal constellation with M points, each transmitted symbol consists of $\log_2 M$ number of bits. The joint ML detector requires $2^{N_T \log_2 M}$-point search per subcarrier detection. If N is the total number of subcarriers, the final computational complexity is proportional to $N \times 2^{N_T \log_2 M}$. For example, consider a 2×2 SM-OFDM system with $N = 256$ subcarriers, and $M = 4$ for QPSK modulation, the joint ML detection requires 4096-point search. If the number of transmitted antennas is increased from $N_T = 2$ to $N_T = 4$, or the modulation scheme is changed from QPSK ($M = 4$) to 16QAM ($M = 8$), the joint ML detection requires a 65536-point search. Such exponential increase in the computational complexity is prohibitive for practical implementations.

To reduce the complexity, linear detectors are proposed. The matched filter (MF) receiver's objective is to match the channel gains for the transmitted symbol of interest, regardless of the interference from other transmitting symbols. The MF detector for transmitted symbol $X^t_{i,m}$ is given by:

$$\mathcal{F}_{MF} = (\mathbf{H}^t_{i,m})^H. \tag{4.18}$$

The output of MF detector is given by:

$$\widehat{\mathbf{Y}}_{i,m} = \mathcal{F}_{MF}\mathbf{Y}_{i,m}$$

$$= \underbrace{(\mathbf{H}_{i,m}^{t})^{H}\mathbf{H}_{i,m}^{t}X_{i,m}^{t}}_{\text{desired signal}} + \underbrace{\sum_{k\neq t}(\mathbf{H}_{i,m}^{t})^{H}\mathbf{H}_{i,m}^{k}X_{i,m}^{k}}_{\text{interference}} + (\mathbf{H}_{i,m}^{t})^{H}\mathbf{W}_{i,m}. \quad (4.19)$$

This is similar to the single-user detector in the multiple-access environment. Although the MF is optimal for a single user channel and does reduce the receiver complexity, it is no longer optimal in a multiple user channel as can be seen in (4.19). The detection rule reduced to individual $X_{i,m}^{t}$ for $0 \leq t < N_T$ with interference modeled as additional noise component. The average signal-to-interference-plus-noise ratio (SINR) E_s/I_0 at the output of the MF detector is obtained by taking the ratio of signal energy and average noise power with interference power, which is given by:

$$\frac{E_s}{I_0} = \frac{\sum_{t=0}^{N_T-1}|(\mathbf{H}_{i,m}^{t})^{H}\mathbf{H}_{i,m}^{t}|^2 E_s}{\sum_{t=0}^{N_T-1}\sum_{k\neq t}|(\mathbf{H}_{i,m}^{t})^{H}\mathbf{H}_{i,m}^{k}|^2 + \sigma_w^2(\mathbf{H}_{i,m}^{t})^{H}\mathbf{H}_{i,m}^{t}}. \quad (4.20)$$

Here it is evident that the MF receiver suffers severe interference from other transmitted symbols because the columns of the channel matrix for SM-OFDM system is not orthogonal to each other. Therefore, this massive interference reduces the SINR E_s/I_0 significantly and compromises the system performance..

To completely remove the interference, a zero forcing (ZF) receiver $\mathcal{F}_{ZF}$ uses a straight forward matrix inversion by assuming that $\mathbf{H}^{H}\mathbf{H}$ is invertible (unless $\mathbf{H}^{H}\mathbf{H}$ has singular value), which is given by:

$$\mathcal{F}_{ZF} = (\mathbf{H}_{i,m}^{H}\mathbf{H}_{i,m})^{-1}\mathbf{H}_{i,m}^{H}. \quad (4.21)$$

The output of the ZF detector is given by:

$$\begin{aligned}\widehat{\mathbf{Y}}_{i,m} &= \mathcal{F}_{ZF}\mathbf{Y}_{i,m} \\ &= \mathbf{X}_{i,m} + (\mathbf{H}_{i,m}^{H}\mathbf{H}_{i,m})^{-1}\mathbf{H}_{i,m}^{H}\mathbf{W}_{i,m} \\ &= \mathbf{X}_{i,m} + \mathbf{W}_{i,m}^{'}. \end{aligned} \quad (4.22)$$

$\mathbf{W}_{i,m}^{'}$ is the noise vector at the output of the ZF detector. It has zero mean and scaled covariance matrix, i.e.

$$E\{\mathbf{W}_{i,m}^{'}\} = (\mathbf{H}_{i,m}^{H}\mathbf{H}_{i,m})^{-1}\mathbf{H}_{i,m}^{H}E\{\mathbf{W}_{i,m}\}$$

$$= 0 \cdot \mathbf{I}_{N_T}, \tag{4.23}$$

and

$$\begin{aligned} E\{\mathbf{W}'_{i,m}(\mathbf{W}'_{i,m})^H\} &= (\mathbf{H}^H_{i,m}\mathbf{H}_{i,m})^{-1}\mathbf{H}^H_{i,m}E\{\mathbf{W}_{i,m}\mathbf{W}^H_{i,m}\}\mathbf{H}_{i,m}((\mathbf{H}^H_{i,m}\mathbf{H}_{i,m})^{-1})^H \\ &= \sigma^2_w((\mathbf{H}^H_{i,m}\mathbf{H}_{i,m})^{-1})^H \\ &= \sigma^2_w((\mathbf{H}^H_{i,m}\mathbf{H}_{i,m})^H)^{-1} \\ &= \sigma^2_w(\mathbf{H}^H_{i,m}\mathbf{H}_{i,m})^{-1}. \end{aligned} \tag{4.24}$$

Since the noise vector at the output of ZF detector is independent and identically distributed (i.i.d), the detection rule reduces to the single term $X^t_{i,m}$ for $0 \leq t < N_T$. Hence, the total number of search points reduced to $N \times 2^{\log_2 M}$. The average SNR E_s/N_0 at the output of the ZF detector is obtained by:

$$\begin{aligned} \frac{E_s}{N_0} &= \frac{E_s}{\frac{\sigma^2_w Tr((\mathbf{H}^H_{i,m}\mathbf{H}_{i,m})^{-1})}{N_T}} \\ &= \frac{E_s N_T}{\sigma^2_w Tr((\mathbf{H}^H_{i,m}\mathbf{H}_{i,m})^{-1})}, \end{aligned} \tag{4.25}$$

where $Tr(\cdot)$ is the trace operator. We can further simplify the equation (4.25) by taking the SVD on $\mathbf{H}^H_{i,m}\mathbf{H}_{i,m}$:

$$\mathbf{H}^H_{i,m}\mathbf{H}_{i,m} = \mathbf{U}\mathbf{\Lambda}\mathbf{U}^H, \tag{4.26}$$

where $\mathbf{\Lambda} = diag(\lambda_0, \lambda_1, \ldots)$ is the diagonal matrix with the eigenvalues of $\mathbf{H}^H_{i,m}\mathbf{H}_{i,m}$ as its diagonal elements, and $\mathbf{U}$ is the unitary matrix. The inverse of $\mathbf{H}^H_{i,m}\mathbf{H}_{i,m}$ is given by:

$$\begin{aligned} (\mathbf{H}^H_{i,m}\mathbf{H}_{i,m})^{-1} &= (\mathbf{U}\mathbf{\Lambda}\mathbf{U}^H)^{-1} \\ &= \mathbf{U}\mathbf{\Lambda}^{-1}\mathbf{U}^H. \end{aligned} \tag{4.27}$$

Substitute equation (4.27) into equation (4.25), the average SNR E_s/N_0 at the output of the ZF detector is given by:

$$\begin{aligned} \frac{E_s}{N_0} &= \frac{E_s N_T}{\sigma^2_w Tr(\mathbf{U}\mathbf{\Lambda}^{-1}\mathbf{U}^H)} \\ &= \frac{E_s N_T}{\sigma^2_w Tr(\mathbf{U}^H\mathbf{U}\mathbf{\Lambda}^{-1})} \end{aligned}$$

$$
\begin{aligned}
&= \frac{E_s N_T}{\sigma_w^2 Tr(\mathbf{\Lambda}^{-1})} \\
&= \frac{E_s N_T}{\sigma_w^2 \sum_{t=0}^{N_T-1} \frac{1}{\lambda_t}}.
\end{aligned} \tag{4.28}
$$

It can be observed that the SNR E_s/N_0 is dominated by the the summation of the inverse of the eigenvalues of $\mathbf{H}_{i,m}^H \mathbf{H}_{i,m}$. If the $\mathbf{H}_{i,m}^H \mathbf{H}_{i,m}$ has eigenvalues which are trivial, the SNR E_s/N_0 at the output of the ZF detector will suffer from significant noise enhancement, hence, the performance of the ZF detector degrades dramatically.

Another linear detector is the MMSE detector, which is given by:

$$
\mathcal{F}_{MMSE} = (\mathbf{H}_{i,m}^H \mathbf{H}_{i,m} + \frac{\sigma_w^2}{E_s} \mathbf{I}_{N_T})^{-1} \mathbf{H}_{i,m}^H. \tag{4.29}
$$

The output of MMSE detector is given by:

$$
\begin{aligned}
\widehat{\mathbf{Y}}_{i,m} &= \mathcal{F}_{MMSE} \mathbf{Y}_{i,m} \\
&= (\mathbf{H}_{i,m}^H \mathbf{H}_{i,m} + \frac{\sigma_w^2}{E_s} \mathbf{I}_{N_T})^{-1} \mathbf{H}_{i,m}^H \mathbf{H}_{i,m} \mathbf{X}_{i,m} \\
&\quad + (\mathbf{H}_{i,m}^H \mathbf{H}_{i,m} + \frac{\sigma_w^2}{E_s} \mathbf{I}_{N_T})^{-1} \mathbf{H}_{i,m}^H \mathbf{W}_{i,m}.
\end{aligned} \tag{4.30}
$$

Similar to the ZF detector, the detection rule still reduces to the single term $X_{i,m}^t$ for $0 \leq t < N_T$. The noise at the output of the MMSE detector is i.i.d, however, there is interference caused by the MMSE filtering. The average SINR E_s/I_0 at the output of the MMSE detector is obtained by [102, 103]:

$$
\begin{aligned}
\frac{E_s}{I_0} &= \frac{1}{N_T} \sum_{t=0}^{N_T-1} \frac{E_s |\mathcal{F}_{MMSE}^t \mathbf{H}_{i,m}^t|^2}{\sigma_w^2 |\mathcal{F}_{MMSE}^t|^2 + E_s \sum_{k \neq t} |\mathcal{F}_{MMSE}^k \mathbf{H}_{i,m}^t|^2} \\
&= \frac{\sum_{t=0}^{N_T-1} E_s}{\sum_{t=0}^{N_T-1} \sigma_w^2 [(\mathbf{H}_{i,m}^H \mathbf{H}_{i,m} + \frac{\sigma_w^2}{E_s} \mathbf{I}_{N_T})^{-1}]_{t,t}} - 1,
\end{aligned} \tag{4.31}
$$

where $\mathcal{F}_{MMSE}^t$ and $\mathbf{H}_{i,m}^t$ are the t^{th} column of $\mathcal{F}_{MMSE}$ and $\mathbf{H}_{i,m}^t$ respectively, and $[\cdot]_{t,t}$ is the t^{th} diagonal element in matrix $[\cdot]$. Hence, the SINR E_s/I_0 of MMSE

receiver is upper bounded as:

$$\begin{aligned}
\frac{E_s}{I_0} &\leq \frac{\sum_{t=0}^{N_T-1} E_s}{\sum_{t=0}^{N_T-1} \sigma_w^2 [(\mathbf{H}_{i,m}^H \mathbf{H}_{i,m} + \frac{\sigma_w^2}{E_s}\mathbf{I}_{N_T})^{-1}]_{t,t}} \\
&= \frac{E_s N_T}{\sum_{t=0}^{N_T-1} \sigma_w^2 [(\mathbf{H}_{i,m}^H \mathbf{H}_{i,m} + \frac{\sigma_w^2}{E_s}\mathbf{I}_{N_T})^{-1}]_{t,t}} \\
&= \frac{E_s N_T}{Tr(\sigma_w^2 (\mathbf{H}_{i,m}^H \mathbf{H}_{i,m} + \frac{\sigma_w^2}{E_s}\mathbf{I}_{N_T})^{-1})} \\
&= \frac{E_s N_T}{Tr(\sigma_w^2 (\mathbf{U}^H \Lambda \mathbf{U} + \frac{\sigma_w^2}{E_s}\mathbf{I}_{N_T})^{-1})} \\
&= \frac{E_s N_T}{\sigma_w^2 \sum_{t=0}^{N_T-1} (\lambda_t + \frac{\sigma_w^2}{E_s})^{-1}}
\end{aligned} \tag{4.32}$$

It can be observed that at high SINR E_s/I_0, i.e. $\frac{\sigma_w^2}{E_s} \approx 0$, the MMSE detector reduces to the ZF detector, and their SINRs are asymptotically the same.

4.2.3 Performance of MIMO-OFDM Receivers

In this section, we briefly present the performance of the MIMO-OFDM receivers as discussed in Section 4.2.1 and Section 4.2.2. We compare the MRC receiver for the Alamouti STC, and MF, ZF, and MMSE receivers for the SM over a 2×2 MIMO-OFDM system with 256 subcarriers. To fairly compare to the Alamouti STC MRC receiver, we also present the MRC receiver for a 2×1 MIMO-OFDM channel. QPSK modulation is used for the symbols in the SM-OFDM system, while 16QAM modulation is used for the symbols in the Alamouti STC-OFDM system. This is to ensure that both systems have the same spectral efficiency (equivalent effective data rate), which is defined as the number of bits transmitted per second per channel usage:

$$\rho = \frac{N_i \times \log_2 M}{T_i \times N_T}, \tag{4.33}$$

where N_i symbols with $\log_2 M$ bits per symbol are transmitted over T_i seconds and N_T physical channels. In 2×2 or 2×1 Alamouti STC-OFDM with 16QAM modulation, the parameters of interest are set to the following values, $N_i = 2$, $M = 4$, $T_i = 2$, $N_T = 2$, where $\rho = 2$ bits per second per channel usage. For 2×2 SM-OFDM with QPSK modulation, the parameters are set to, $N_i = 2$, $M = 2$,

$T_i = 1$, $N_T = 2$, where $\rho = 2$ bits per second per channel usage. The channel fading coefficients for each wireless link is assumed i.i.d(this is equivalent to using a large interleaver on the transmitted and receive symbols), and we assume that the receiver has full knowledge of the channel state information.

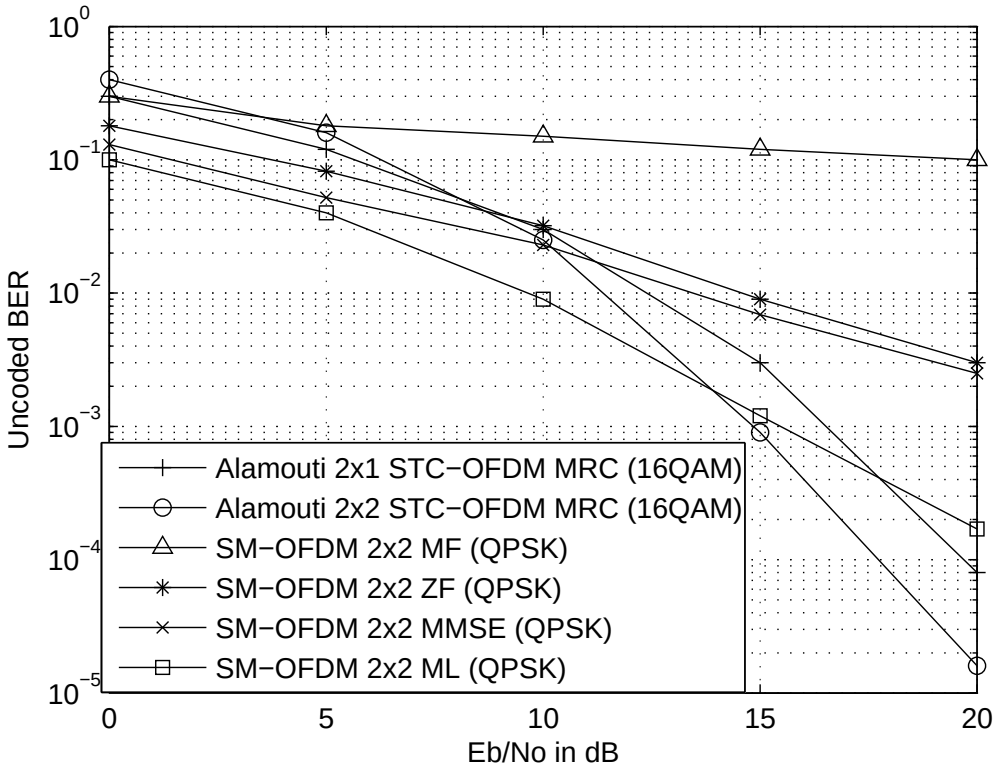

Figure 4.1: Uncoded BER performance for 2×1 and 2×2 Alamouti STC-OFDM MRC receiver, and 2×2 SM-OFDM MF, ZF and MMSE receiver

Fig. 4.1 shows the uncoded BER performance for the above mentioned receivers. It can be seen from the figure that the MF receiver has very poor performance compared to other receivers. This is expected because the MF receiver suffers from the massive multiple access interference from other transmitted symbols. Hence, it is not surprising that the error floor occurs at high SNR.

For other receivers, we can see that they have diverse performance in low and high SNR regions. In the low SNR region, SM-OFDM receivers perform better than the Alamouti STC-OFDM MRC receiver. On the other hand, at high SNR, the slope of the BER curve for Alamouti STC-OFDM MRC receiver is more favorable. This is because in the low SNR region, the channel is dominated by the noise term. The additional coding in the Alamouti STC scheme makes the performance even worse, which is similar to the performance between the coded and uncoded

system in the low SNR. In the high SNR region, the system is interference limited, the Alamouti STC scheme provides diversity of order 4, which is higher than the diversity of order 2 introduced by the SM scheme in the 2×2 environment. This observation suggests that the best MIMO scheme to use in practice depends on the channel SNR and the required throughput (spectral efficiency) as well as on other considerations such as the interference level. A possible solution is to design a scheme to combine [104] the Alamouti STC and SM systems to reach the best performance, which is out of the scope of this thesis.

We also observed that the 2×2 MRC receiver has better performance than the 2×1 case. This is because the additional diversity is obtained from another receive antenna. Furthermore, among SM-OFDM receivers, the ML receiver has the best performance because it is optimal in the sense that it extracts diversity gain in additional to the multiplexing gain [48]. The MMSE receiver improves the performance of ZF receiver slightly because it reduces the combined effect of interference the two parallel channels and additive noise. However, similar to the ZF receiver, the MMSE receiver does not exploit the channel diversity, hence, both the MMSE and ZF receivers are asymptotically close in the high SNR region.

4.3 Iterative Receiver for MIMO-OFDM

We have discussed the conventional non-iterative receivers for MIMO-OFDM system and assumed perfect channel state information in Section 4.2. In a practical system, the receiver has to estimate the channel. In this section, we develop joint iterative channel estimation and data detection receivers for MIMO-OFDM system over time and frequency dispersive fading channel.

4.3.1 Iterative Receiver for Alamouti STC-OFDM

The receiver is shown in Fig.4.2, with a space-time processing module performing MRC for Alamouti STC-OFDM system, and a MAP decoder that operates in an iterative fashion. The STC-OFDM channel matrix used in the data detection in the demapper module is updated by a low complexity novel channel estimation algorithm, which will be presented in the later section. In this section, we derive the soft MRC receiver for the 2×2 Alamouti STC-OFDM. In the 2×2 Alamouti

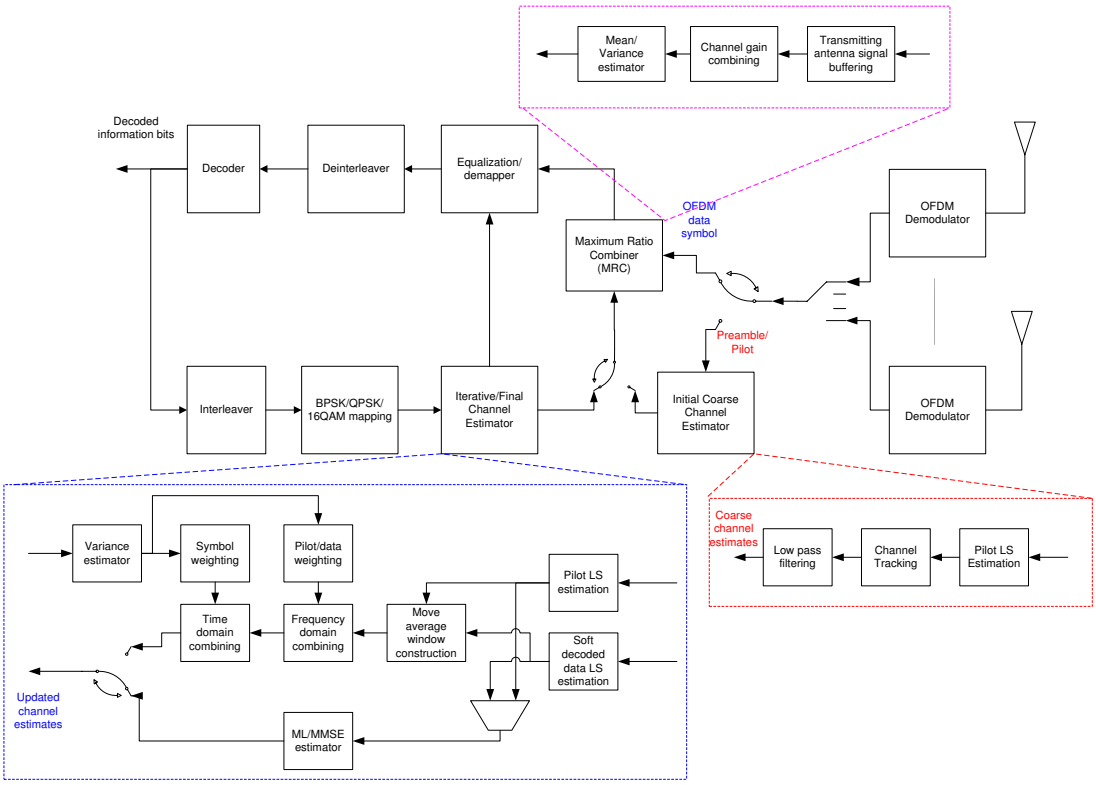

Figure 4.2: Iterative receiver for Alamouti STC-OFDM systems

STC system, the system model is also given by equation (4.1) with

$$\mathbf{Y}_m = \begin{bmatrix} Y^0_{i-1,m} \\ Y^1_{i-1,m} \\ (Y^0_{i,m})^* \\ (Y^1_{i,m})^* \end{bmatrix}, \tag{4.34}$$

$$\mathbf{H}_m = \begin{bmatrix} H^{0,0}_m & H^{0,1}_m \\ H^{1,0}_m & H^{1,1}_m \\ (H^{0,1}_m)^* & -(H^{0,0}_m)^* \\ (H^{0,0}_m)^* & -(H^{1,0}_m)^* \end{bmatrix}, \tag{4.35}$$

and

$$\mathbf{W}_m = \begin{bmatrix} W^0_{i-1,m} \\ W^1_{i-1,m} \\ (W^0_{i,m})^* \\ (W^1_{i,m})^* \end{bmatrix}. \tag{4.36}$$

Again, the columns of channel matrix $\mathbf{H}_m$ are orthogonal to each other, i.e. by taking the inner product of the first column $\mathbf{H}_m^0$ and the second column $\mathbf{H}_m^1$ of matrix $\mathbf{H}_m$, we have

$$\begin{aligned}(\mathbf{H}_m^0)^H\mathbf{H}_m^1 &= \begin{bmatrix} (H_m^{0,0})^* & (H_m^{1,0})^* & H_m^{0,1} & H_m^{0,0} \end{bmatrix} \cdot \begin{bmatrix} H_m^{0,1} \\ H_m^{1,1} \\ -(H_m^{0,0})^* \\ -(H_m^{1,0})^* \end{bmatrix} \\ &= 0. \end{aligned} \tag{4.37}$$

By using the same approach in Section 4.2.1, the output of linear combiner is given by:

$$\begin{aligned}\widehat{\mathbf{Y}_m^{MRC}} &= \mathbf{H}_m^H \cdot \mathbf{Y}_m \\ &= \mathbf{H}_m^H \cdot \mathbf{H}_m\mathbf{X}_m + \mathbf{H}_m^H\mathbf{W}_m \\ &= \sum_{r=0}^{1}\sum_{t=0}^{1} |H_m^{r,t}|^2\mathbf{X}_m + \mathbf{W}_m^{'}, \end{aligned} \tag{4.38}$$

where

$$\mathbf{H}_m^H \cdot \mathbf{H}_m = \sum_{r=0}^{1}\sum_{t=0}^{1} |H_m^{r,t}|^2 \cdot \mathbf{I}_2. \tag{4.39}$$

Then the mean and covariance matrix of the MRC linear combining output is obtained as:

$$\mu_m^{MRC} = \sum_{r=0}^{1}\sum_{t=0}^{1} |H_m^{r,t}|^2\mathbf{X}_{i,m}, \tag{4.40}$$

$$\mathcal{C}_m^{MRC} = \sigma_w^2 \sum_{r=0}^{1}\sum_{t=0}^{1} |H_m^{r,t}|^2 \cdot \mathbf{I}_2. \tag{4.41}$$

Data detection is performed by using a single-tap equalizer (this is essentially the multiplication by the conjugate of the channel value), also known as demapper module. It assumes the output of mean and variance esitmator is Gaussian distributed [105] as $\mathcal{N}(\mu_m^{MRC}, \mathcal{C}_m^{MRC})$. The demapper outputs LLR λ_1^e of the k^{th} coded bits c_k for MRC output as:

$$\lambda_1^e(c_k(\mathbf{X}_m)) = \ln \frac{\sum\limits_{\mathbf{S}_j \in U_k^+(\mathcal{A}^{N_T})} P(\mathbf{X}_m = \mathbf{S}_j|\widehat{\mathbf{Y}_m^{MRC}}, \mathbf{H}_m, \lambda_2^e)}{\sum\limits_{\mathbf{S}_j \in U_k^-(\mathcal{A}^{N_T})} P(\mathbf{X}_m = \mathbf{S}_j|\widehat{\mathbf{Y}_m^{MRC}}, \mathbf{H}_m, \lambda_2^e)}, \tag{4.42}$$

where the conditional probability $P(\mathbf{X}_m = \mathbf{S}_j|\widehat{\mathbf{Y}_m^{MRC}}, \mathbf{H}_m, \lambda_2^e)$ is proportional to its Gaussian p.d.f, i.e.

$$P(\mathbf{X}_m = \mathbf{S}_j|\widehat{\mathbf{Y}_m^{MRC}}, \mathbf{H}_m, \lambda_2^e) \sim \exp\{-\frac{1}{2\sigma_w^2 \sum_{r=0}^{1}\sum_{t=0}^{1}|H_m^{r,t}|^2}\|\widehat{\mathbf{Y}_m^{MRC}} - \mu_m^{MRC}\|^2\} \cdot \prod_{l\neq k} P(c_l(\mathbf{X}_m)), \quad (4.43)$$

and $\mathbf{S}_j = [S_j^0, S_j^1, \ldots, S_j^{N_T-1}]^T$ is the j^{th} signal vector in the signal constellation set $\mathcal{A}^{N_T}$, which contains all $2^{N_T \times \log_2 M}$ possible symbols. $U_k^+(\mathcal{A}^{N_T})$ is the constellation subset in $\mathcal{A}^{N_T}$ that contains all the symbols with k^{th} bit being 1, and $U_k^-(\mathcal{A}^{N_T})$ minus is the constellation subset in $\mathcal{A}^{N_T}$ that contains all the symbols with k^{th} bit being 0.

In the 2×2 Alamouti STC detection approach, due to the fact that the channel matrix has orthogonal columns, the MRC can be applied to data detection. As in the multiple access environment, OFDM symbols from different transmitting antennas do not interfere with each other. Therefore, the iterative structure is limited to the loop between the channel estimation and decoding. In other words, the soft decoded data information is fed back for channel re-estimation purposes only.

4.3.2 Iterative Receiver for SM-OFDM

In the SM-OFDM system, the columns in the channel matrix are not orthogonal to each other, i.e., the transmitting symbols from different transmitting antennas are interfering with each other at the receiving antenna. As discussed in Section 4.2.2, the MF receiver explores the MIMO diversity by combining the received energy from all transmitting antennas, however, it suffers from massive level of interference. The ZF receiver removes the interference completely, however, it does not explore the diversity benefits and suffers from large noise enhancement. The MMSE receiver makes the compromise between the interference and noise, however, it does not explore the benefits of MIMO diversity either. Therefore, in order to explore the MIMO diversity, remove the interference, and avoid noise enhancement at the same time, we apply the iterative parallel interference cancelation approach to perform data detection. The receiver is shown in Fig.4.3, with a space-time processing module performing MMSE detection, a parallel interference cancelation approach for the SM-OFDM system, and a MAP decoder that performs data decoding while also providing feedback information for the iterative detection technique. The

switch is shown to initially allow the selection of the MMSE detector for the first iteration and then select the interference canceler in subsequent iterations. In the following, we present an iterative algorithm for the detection of an OFDM received signal from multiple antennas, which performs data detection and decoding, while canceling interference.

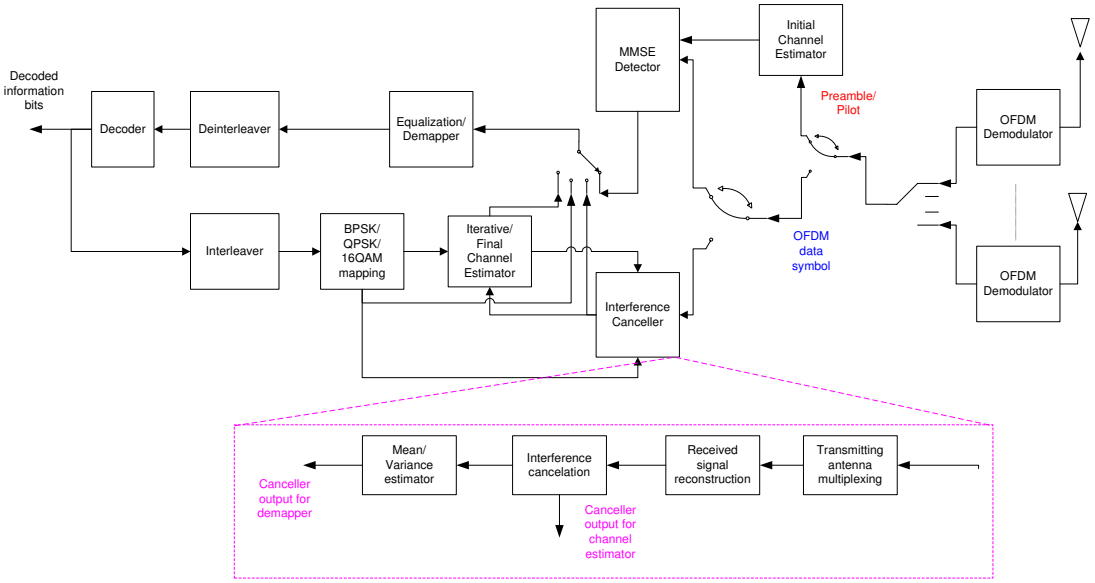

Figure 4.3: Iterative receiver for SM-OFDM systems

In the first iteration, MMSE filtering is performed to reduce the error to a reasonable level for further processing in the later iterations. Assuming that the channel state information is perfectly known and the transmitted data symbols are uncorrelated, the output of the MMSE filter for the signal transmitted by all transmitting antennas is given by:

$$\widehat{\mathbf{Y}_{i,m}^{MMSE}} = \mathcal{F}_{i,m}^{MMSE}\mathbf{Y}_{i,m}, \tag{4.44}$$

where the MMSE filter is given by:

$$\mathcal{F}_{i,m}^{MMSE} = [\mathbf{H}_{i,m}^{H}\mathbf{H}_{i,m} + \frac{\sigma_w^2}{E_d}\mathbf{I}_{N_R}]^{-1}\mathbf{H}_{i,m}^{H}, \tag{4.45}$$

where E_d is the channel data symbol energy. The mean and covariance matrix of MMSE filter output is obtained as:

$$\mu_{i,m}^{MMSE} = \mathcal{F}_{i,m}^{MMSE}\mathbf{H}_{i,m}\mathbf{X}_{i,m}, \tag{4.46}$$

$$\mathcal{C}_{i,m}^{MMSE} = \sigma_w^2[\mathbf{H}_{i,m}^H\mathbf{H}_{i,m} + \frac{\sigma_w^2}{E_d}\mathbf{I}_{N_R}]^{-1}. \tag{4.47}$$

Hence, the demapper outputs LLR λ_1^e of the k^{th} coded bits c_k for MMSE filter output as:

$$\lambda_1^e(c_k(\mathbf{X}_{i,m})) = \ln \frac{\sum\limits_{\mathbf{S}_j \in U_k^+(\mathcal{A}^{N_T})} P(\mathbf{X}_{i,m} = \mathbf{S}_j|\widehat{\mathbf{Y}_{i,m}^{MMSE}}, \mathbf{H}_{i,m}, \lambda_2^e)}{\sum\limits_{\mathbf{S}_j \in U_k^-(\mathcal{A}^{N_T})} P(\mathbf{X}_{i,m} = \mathbf{S}_j|\widehat{\mathbf{Y}_{i,m}^{MMSE}}, \mathbf{H}_{i,m}, \lambda_2^e)}, \tag{4.48}$$

where the conditional probability $P(\mathbf{X}_{i,m} = \mathbf{S}_j|\widehat{\mathbf{Y}_{i,m}^{MMSE}}, \mathbf{H}_{i,m}, \lambda_2^e)$ is proportional to its Gaussian p.d.f, i.e.

$$\begin{aligned} P(\mathbf{X}_{i,m} = \mathbf{S}_j|\widehat{\mathbf{Y}_{i,m}^{MMSE}}, \mathbf{H}_{i,m}, \lambda_2^e) \;&\sim \exp\{-\tfrac{1}{2}(\widehat{\mathbf{Y}_{i,m}^{MMSE}} - \mu_{i,m}^{MMSE})^H(\mathcal{C}_{i,m}^{MMSE})^{-1} \\ &\cdot(\widehat{\mathbf{Y}_{i,m}^{MMSE}} - \mu_{i,m}^{MMSE})\} \prod_{l\neq k} P(c_l(\mathbf{X}_{i,m})). \end{aligned} \tag{4.49}$$

From the second iteration onwards, to separate the desired signal from the interference signal, we define the $N_T \times 1$ interference cancelation vector as

$$\mathbf{e}^t = [0, 0, \ldots, 0, 1, 0, \ldots, 0]^T \tag{4.50}$$

such that all elements in $\mathbf{e}^t$ are zeros except the t^{th} element is 1. The interference vector can be constructed as:

$$\begin{aligned} \overline{\mathbf{X}}_{i,m}^t &= \mathbf{X}_{i,m} - X_{i,m}^t\mathbf{e}^t \\ &= [X_{i,m}^0, X_{i,m}^1, \cdots, X_{i,m}^{t-1}, 0, X_{i,m}^{t+1}, \cdots, X_{i,m}^{N_T-1}]^T, \end{aligned} \tag{4.51}$$

where the symbol of interest $X_{i,m}^t$ is removed. Then the parallel co-antenna interference canceler is performed as

$$\begin{aligned} \mathbf{Y}_{i,m}^{t,IC} &= \mathbf{Y}_{i,m} - \mathbf{H}_{i,m}\overline{\mathbf{X}}_{i,m}^t \\ &= \mathbf{Y}_{i,m} - \mathbf{H}_{i,m}(\mathbf{X}_{i,m} - X_{i,m}^t\mathbf{e}^t) \\ &= \underbrace{\mathbf{H}_{i,m}^t X_{i,m}^t}_{\text{desired signal}} + \underbrace{\sum_{k\neq t}\mathbf{H}_{i,m}^k(X_{i,m}^k - \widehat{X_{i,m}^k})}_{\text{residual interference}} + \mathbf{W}_{i,m}, \end{aligned} \tag{4.52}$$

where $\widehat{X_{i,m}^k}$ is the soft symbol of $X_{i,m}^k$. The residual interference term in equation (4.52) will vanish if the soft symbol is estimated perfectly, i.e. $\widehat{X_{i,m}^k} = X_{i,m}^k$. In

that case, the interference canceler will have interference free performance, i.e.

$$\mathbf{Y}_{i,m}^{t,IC} = \mathbf{H}_{i,m}^{t} X_{i,m}^{t} + \mathbf{W}_{i,m}, \tag{4.53}$$

where a linear combiner (matched filter) as discussed in Section (4.3.1) provides the optimal detection as:

$$\begin{aligned} Y_{i,m}^{t,IC-MF} &= \mathcal{F}_{i,m}^{MF} \mathbf{Y}_{i,m}^{t,IC} \\ &= (\mathbf{H}_{i,m}^{t})^{H} \mathbf{H}_{i,m}^{t} X_{i,m}^{t} + (\mathbf{H}_{i,m}^{t})^{H} \mathbf{W}_{i,m} \\ &= \sum_{r=0}^{N_R-1} |H_{i,m}^{r,t}|^2 X_{i,m}^{t} + (\mathbf{H}_{i,m}^{t})^{H} \mathbf{W}_{i,m}. \end{aligned} \tag{4.54}$$

Generally speaking, the reliability of the soft data symbols improves over iterations, which means the co-antenna interference can not be removed completely in the first few iterations. Hence, the residual interference has to be taken into the consideration. Similar to the first iteration, data detection is performed in the single-tap demapper by assuming the output of space-time processing module is Gaussian distributed as $\mathcal{N}(\mu_{i,m}^{t,IC}, \mathcal{C}_{i,m}^{t,IC})$. The mean of the interference canceler output is obtained by taking the expectation of equation (4.52) as:

$$\begin{aligned} \mu_{i,m}^{t,IC} &= E\{\mathbf{H}_{i,m}^{t} X_{i,m}^{t} + \sum_{k \neq t} \mathbf{H}_{i,m}^{k} (X_{i,m}^{k} - \widehat{X_{i,m}^{k}}) + \mathbf{W}_{i,m}\} \\ &= E\{\mathbf{H}_{i,m}^{t} X_{i,m}^{t}\} + \sum_{k \neq t} \mathbf{H}_{i,m}^{k} (\underbrace{E\{X_{i,m}^{k}\} - \widehat{X_{i,m}^{k}}}_{=0}) + E\{\mathbf{W}_{i,m}\} \\ &= \mathbf{H}_{i,m}^{t} X_{i,m}^{t}. \end{aligned} \tag{4.55}$$

To compute the covariance matrix $\mathcal{C}_{i,m}^{t,IC}$, firstly we compute the mean of the interference vector $\overline{\mathbf{X}}_{i,m}^{t}$, which is given by:

$$\begin{aligned} E\{\overline{\mathbf{X}}_{i,m}^{t}\} &= E\{\mathbf{X}_{i,m} - X_{i,m}^{t} \mathbf{e}^{t}\} \\ &= [\widehat{X_{i,m}^{0}}, \widehat{X_{i,m}^{1}}, \cdots, \widehat{X_{i,m}^{t-1}}, 0, \widehat{X_{i,m}^{t+1}}, \cdots, \widehat{X_{i,m}^{N_T-1}}]^{T}, \end{aligned} \tag{4.56}$$

and the covariance matrix of the interference vector $\overline{\mathbf{X}}_{i,m}^{t}$ is given by:

$$\begin{aligned} \overline{\mathcal{C}}_{i,m}^{t,IC} &= E\{(\overline{\mathbf{X}}_{i,m}^{t} - E\{\overline{\mathbf{X}}_{i,m}^{t}\})(\overline{\mathbf{X}}_{i,m}^{t} - E\{\overline{\mathbf{X}}_{i,m}^{t}\})^{H}\} \\ &= diag(\gamma_{i,m,0}^{2}, \gamma_{i,m,1}^{2}, \cdots, \gamma_{i,m,t-1}^{2}, 0, \gamma_{i,m,t+1}^{2}, \cdots, \gamma_{i,m,N_T-1}^{2}), \end{aligned} \tag{4.57}$$

where

$$\gamma^2_{i,m,k} = |X^k_{i,m}|^2 - |\widehat{X^k_{i,m}}|^2. \tag{4.58}$$

As shown in Chapter 2 Section 2.5, the energy of soft data symbol is computed as:

$$\begin{aligned} |\widehat{X^t_{i,m}}|^2 &= E_d |E\{\widehat{X^t_{i,m}}\}|^2 \\ &= E_d |\sum_{S_j \in \mathcal{A}} S_j \cdot P(\widehat{X^t_{i,m}} = S_j)|^2, \end{aligned} \tag{4.59}$$

where $\mathcal{A}$ is the signal constellation set with $2^{\log_2 M}$ signal points. For equal energy constellation, like BPSK and QPSK, the average signal power of the data symbol is given by:

$$\begin{aligned} |X^t_{i,m}|^2 &= |E\{X^t_{i,m}\}|^2 \\ &= E_d, \end{aligned} \tag{4.60}$$

For unequal energy constellation, like 16QAM or 64QAM, by using Jensen's inequality [106], the average signal power of of data symbols is given by:

$$\begin{aligned} |X^t_{i,m}|^2 &= |E\{X^t_{i,m}\}|^2 \\ &\leq E\{|\widehat{X}^t_{i,m}|^2\} \\ &= E_d \sum_{S_j \in \mathcal{A}} |S_j|^2 \cdot P(\widehat{X^t_{i,m}} = S_j). \end{aligned} \tag{4.61}$$

Hence, the covariance matrix $\mathcal{C}^{t,IC}_{i,m}$ can be obtained by:

$$\mathcal{C}^{t,IC}_{i,m} = \mathbf{H}_{i,m} \overline{\mathcal{C}}^{t,IC}_{i,m} \mathbf{H}^H_{i,m} + \sigma^2_w \mathbf{I}_{N_T}, \tag{4.62}$$

With the Gaussian distribution $\mathcal{N}(\mu^{t,IC}_{i,m}, \mathcal{C}^{t,IC}_{i,m})$, the demapper outputs LLR λ^e_1 of the k^{th} coded bits c_k for MMSE filter output as:

$$\lambda^e_1(c_k(\mathbf{X}^t_{i,m})) = \ln \frac{\sum\limits_{\mathbf{s}_j \in U^+_k(\mathcal{A})} P(X^t_{i,m} = S_j | \widehat{\mathbf{Y}^{IC}_{i,m}}, \mathbf{H}_{i,m}, \lambda^e_2)}{\sum\limits_{\mathbf{s}_j \in U^-_k(\mathcal{A})} P(X^t_{i,m} = S_j | \widehat{\mathbf{Y}^{IC}_{i,m}}, \mathbf{H}_{i,m}, \lambda^e_2)}, \tag{4.63}$$

where the conditional probability $P(X^t_{i,m} = S_j | \widehat{\mathbf{Y}^{IC}_{i,m}}, \mathbf{H}_{i,m}, \lambda^e_2)$ is proportional to its

Gaussian p.d.f, i.e.

$$P(X^t_{i,m} = S_j|\widehat{Y^{t,IC}_{i,m}}, \mathbf{H}_{i,m}, \lambda^e_2) \sim \exp\{-\tfrac{1}{2}(\widehat{\mathbf{Y}^{t,IC}_{i,m}} - \mathbf{H}^t_{i,m}X^t_{i,m})^H(\mathcal{C}^{t,IC}_{i,m})^{-1} \cdot(\widehat{\mathbf{Y}^{t,IC}_{i,m}} - \mathbf{H}^t_{i,m}X^t_{i,m})\} \prod_{l\neq k} p(c_l(X^t_{i,m})), \quad (4.64)$$

Furthermore, the post interference cancelation process can be performed to reduce the equalizer/demapper complexity. The IC-MF process is obtained by taking the linear combiner or MF on the output of the interference canceler, i.e.

$$\begin{aligned} Y^{t,IC-MF}_{i,m} &= \mathcal{F}^{MF}_{i,m}\mathbf{Y}^{t,IC}_{i,m} \\ &= (\mathbf{H}^t_{i,m})^H\mathbf{H}^t_{i,m}X^t_{i,m} + \sum_{k\neq t}(\mathbf{H}^t_{i,m})^H\mathbf{H}^k_{i,m}(X^k_{i,m} - \widehat{X^k_{i,m}}) \\ &\quad +(\mathbf{H}^t_{i,m})^H\mathbf{W}_{i,m}. \end{aligned} \quad (4.65)$$

Again, we compute the mean $\mu^{t,IC-MF}_{i,m}$ and covariance matrix $\mathcal{C}^{t,IC-MF}_{i,m}$ as:

$$\begin{aligned} \mu^{t,IC-MF}_{i,m} &= E\{(\mathbf{H}^t_{i,m})^H\mathbf{H}^t_{i,m}X^t_{i,m} + \sum_{k\neq t}(\mathbf{H}^t_{i,m})^H\mathbf{H}^k_{i,m}(X^k_{i,m} - \widehat{X^k_{i,m}}) \\ &\quad +(\mathbf{H}^t_{i,m})^H\mathbf{W}_{i,m}\} \\ &= E\{(\mathbf{H}^t_{i,m})^H\mathbf{H}^t_{i,m}X^t_{i,m}\} + \sum_{k\neq t}(\mathbf{H}^t_{i,m})^H\mathbf{H}^k_{i,m}(\underbrace{E\{X^k_{i,m}\} - \widehat{X^k_{i,m}}}_{=0}) \\ &\quad +E\{(\mathbf{H}^t_{i,m})^H\mathbf{W}_{i,m}\} \\ &= (\mathbf{H}^t_{i,m})^H\mathbf{H}^t_{i,m}X^t_{i,m}, \end{aligned} \quad (4.66)$$

and

$$\mathcal{C}^{t,IC-MF}_{i,m} = (\mathbf{H}^t_{i,m})^H(\mathbf{H}_{i,m}\overline{\mathcal{C}}^{t,IC}_{i,m}\mathbf{H}^H_{i,m} + \sigma^2_w\mathbf{I}_{N_T})\mathbf{H}^t_{i,m}. \quad (4.67)$$

Another post interference cancelation process is the IC-MMSE, which is obtained by taking the MMSE filtering on the output of the interference canceler, which is given by:

$$Y^{t,IC-MMSE}_{i,m} = (\mathcal{F}^{t,MMSE}_{i,m})^H\mathbf{Y}^{t,IC}_{i,m}. \quad (4.68)$$

The mean $\mu^{t,IC-MMSE}_{i,m}$ and covariance matrix $\mathcal{C}^{t,IC-MMSE}_{i,m}$ can be obtained as:

$$\mu^{t,IC-MMSE}_{i,m} = (\mathcal{F}^{t,MMSE}_{i,m})^H\mathbf{H}^t_{i,m}X^t_{i,m}, \quad (4.69)$$

and

$$\mathcal{C}_{i,m}^{t,IC-MMSE} = (\mathcal{F}_{i,m}^{t,MMSE})^H(\mathbf{H}_{i,m}\overline{\mathcal{C}}_{i,m}^{t,IC}\mathbf{H}_{i,m}^H + \sigma_w^2\mathbf{I}_{N_T})\mathcal{F}_{i,m}^{t,MMSE}. \tag{4.70}$$

4.4 Iterative Channel Estimation for MIMO-OFDM System

In Chapter 3 Section 3.3, we have developed a low complexity iterative turbo channel estimation technique for the SISO-OFDM systems. In this Section, we extend it to a MIMO-OFDM system. With the soft decoded data symbol fed back from MAP decoder, the channel frequency response at each symbol is updated by a novel iterative channel estimation approach, where channel estimates from preamble, pilot and soft coded data symbols are frequency and time combined in two stages, which are referred to as initial coarse estimation stage, and iterative estimation stage. We assume that OFDM symbols are transmitted continuously on a frame by frame basis. Each frame consists of a preamble followed by a number of data symbols. The data symbols have pilot tones inserted as specified in [17].

4.4.1 Initial Coarse Estimation Stage

In practical MIMO-OFDM systems, adjacent pilot tones are allocated and the multiple transmitting antennas are usually configured in on/off mode so that there is no interference when the pilot tones are transmitted. For example, in the 2×2 MIMO-OFDM system, the even indexed subcarriers are dedicated for the first antenna to transmit pilot symbols, and the odd indexed subcarriers are dedicated for the second antenna to transmit pilot symbols. Therefore, at each receiver antenna, each subcarrier only receives reference signal from one transmitting antenna so that there is no interference. In this case, the channel frequency response between each transmitting and receiving wireless link can be obtained at those dedicated subcarriers. Signal processing techniques can be applied to obtain the channel frequency response for the subcarriers that were not used in the transmission.

The initial coarse estimation stage is performed at the first iteration. Extended from Chapter 3 Section 3.3.2, channel estimate between the r^{th} receiving antenna and t^{th} transmitting antenna at pilot subcarrier p for the i^{th} OFDM symbol can be obtained by the LS approach:

$$\widehat{H_{i,p}^{r,t}} = H_{i,p}^{r,t} + W_{i,p}^{\prime r}, \tag{4.71}$$

where E_p is the energy of preamble/pilot symbol, $H_{i,p}^{r,t}$ is the true channel frequency response, and $W_{i,p}^{'r}$ is the estimation error at the output of the LS channel estimator. As shown in Section 3.3.2, the estimation error is Gaussian distributed $\mathcal{N}(0, \frac{\sigma_w^2}{E_p})$. To obtain the channel frequency response at the non-transmitting subcarriers, linear interpolation is performed between two subcarriers where the pilot tones are transmitted. More specifically, $\widehat{H_{i,p}^{r,t}}$ and $\widehat{H_{i,p+2}^{r,t}}$ are the channel estimates from two adjacent pilots. The channel estimate $\widehat{H_{i,m}^{r,t}}$ at subcarrier m, which is between pilot subcarrier p and $p+2$, is given by:

$$\widehat{H_{i,m}^{r,t}} = \left[\begin{array}{cc} 1 - \frac{m-p}{2} & \frac{m-p}{2} \end{array} \right] \cdot \left[\begin{array}{c} \widehat{H_{i,p}^{r,t}} \\ \widehat{H_{i,p+2}^{r,t}} \end{array} \right], \tag{4.72}$$

For OFDM data symbols, channel tracking is applied to obtain the initial coarse channel estimates. The initial channel estimates for the i^{th} data symbol is given by:

$$\begin{aligned} \widehat{\mathbf{H}_i} &= \widehat{\mathbf{H}_{i-1}} + \mathcal{F}(\Delta\widehat{\mathbf{H}_{i-1,i,p}}) \\ &= \widehat{\mathbf{H}_{i-1}} + \mathbf{F}(\widehat{\mathbf{H}_{i,p}} - \widehat{\mathbf{H}_{i-1,p}}), \end{aligned} \tag{4.73}$$

where $\widehat{\mathbf{H}_{i,p}}$ is the channel estimates at pilot subcarriers. $\mathcal{F}(\cdot)$ is the interpolation filter, which can be FFT based [25], MMSE based [29], or linear interpolation based [101].

4.4.2 Iterative Estimation Stage

Because the decoding data information from previous iterations may not be reliable, the energy of soft decoded data symbol may be less than the unity. If the soft decoded data symbol is directly applied in LS estimation, the so obtained channel estimates are subject to a bias due to the unreliable decoding information. To overcome this problem, a moving average window (MAW) around the subcarrier of interest is defined, and the average energy of the soft data symbols within the MAW is computed to normalize the LS channel estimation. Hence, using the LS approach in Chapter 3 Section 3.3, channel estimation between the r^{th} receiving antenna and t^{th} transmitting antenna at data subcarrier d for i^{th} OFDM symbol can be modeled as:

$$\widehat{H_{i,d}^{r,t}} \approx H_{i,d}^{r,t} \sqrt{|\widehat{X_{i,d\in\Theta}^{t}}|^2} + W_{i,d}^{'r}, \tag{4.74}$$

where

$$|\widehat{X^t_{i,d\in\Theta}}|^2 = E\{\widehat{X^t_{i,d\in\Theta}}(\widehat{X^t_{i,d\in\Theta}})^*\}, \tag{4.75}$$

is the average energy of soft coded data information in the MAW Θ, and $W'^r_{i,d}$ is the summation of residual interference and white noise, which is given by:

$$W'^r_{i,d} = \sum_{k\neq t}[H^{r,k}_{i,d}(X^t_{i,d} - \widehat{X^t_{i,d}})\frac{(\widehat{X^t_{i,d}})^*}{\sqrt{|\widehat{X^t_{i,d\in\Theta}}|^2}}] + \frac{W^r_{i,d}(\widehat{X^t_{i,d}})^*}{\sqrt{E_d|\widehat{X^t_{i,d\in\Theta}}|^2}}. \tag{4.76}$$

In equation (4.76), $H^{r,k}_{i,d}$ is the true channel frequency response from other transmitting and receiving wireless link, which is not available in the practical system. Hence, to truly represent the system, we model the true channel frequency response as:

$$H^{r,k}_{i,d} = \widehat{H^{r,k}_{i,d}} + \Delta\widehat{H^{r,k}_{i,d}}, \tag{4.77}$$

where $\widehat{H^{r,k}_{i,d}}$ is the channel estimate at the output of the LS channel estimator and $\Delta\widehat{H^{r,k}_{i,d}}$ is the channel estimation error, which can be approximated as a Gaussian random process [107] with distribution $\mathcal{N}(0, \sigma^2_{\Delta\widehat{H}})$ obtained from the previous iteration. Substitute equation (4.77) into equation (4.76), we have

$$W'^r_{i,d} = \sum_{k\neq t}[(\widehat{H^{r,k}_{i,d}} + \Delta\widehat{H^{r,k}_{i,d}})(X^t_{i,d} - \widehat{X^t_{i,d}})\frac{(\widehat{X^t_{i,d}})^*}{\sqrt{|\widehat{X^t_{i,d\in\Theta}}|^2}}] + \frac{W^r_{i,d}(\widehat{X^t_{i,d}})^*}{\sqrt{E_d|\widehat{X^t_{i,d\in\Theta}}|^2}}. \tag{4.78}$$

We can compute the mean and variance of $W'^r_{i,d}$ as:

$$\begin{aligned} E\{W'^r_{i,d}\} &= \sum_{k\neq t}[(\widehat{H^{r,k}_{i,d}} + \Delta\widehat{H^{r,k}_{i,d}})\underbrace{(E\{X^t_{i,d}\} - \widehat{X^t_{i,d}})}_{=0}\frac{(\widehat{X^t_{i,d}})^*}{\sqrt{|\widehat{X^t_{i,d\in\Theta}}|^2}}] \\ &\quad + \frac{E\{W^r_{i,d}\}(\widehat{X^t_{i,d}})^*}{\sqrt{E_d|\widehat{X^t_{i,d\in\Theta}}|^2}} \\ &= 0, \end{aligned} \tag{4.79}$$

and

$$E\{|W'^r_{i,d}|^2\} = E\{|\sum_{k\neq t}[(\widehat{H^{r,k}_{i,d}} + \Delta\widehat{H^{r,k}_{i,d}})(X^t_{i,d} - \widehat{X^t_{i,d}})\frac{(\widehat{X^t_{i,d}})^*}{\sqrt{|\widehat{X^t_{i,d\in\Theta}}|^2}}]$$

$$
\begin{aligned}
&+\frac{W_{i,d}^{r}(\widehat{X_{i,d}^{t}})^{*}}{\sqrt{E_d|\widehat{X_{i,d\in\Theta}^{t}}|^2}}|^2\}\\
&= \sum_{k\neq t}(|\widehat{H_{i,d}^{r,k}}|^2+\sigma_{\Delta\widehat{H}}^2)(|X_{i,d}^{k}|^2-|\widehat{X_{i,d}^{k}}|^2)+\frac{\sigma_w^2}{E_d}\\
&= \sigma_{e_H}^2+\frac{\sigma_w^2}{E_d}. \qquad (4.80)
\end{aligned}
$$

After LS estimation, channel estimates from both pilot and soft decoded data information are ready for the frequency-domain combining. Assuming that within the MAW, the channel frequency response is highly correlated, i.e. $H_{i,p}^{r,t}\approx H_{i,d}^{r,t}$, the weighted average for the channel frequency response at particular subcarrier m of interest is given by:

$$
\begin{aligned}
\widetilde{H}_{i,m}^{r,t} &= \omega_p\sum_{p\in\Theta}\widehat{H}_{i,p}^{r,t}+\omega_d\sum_{d\in\Theta}\widehat{H}_{i,d}^{r,t}\\
&= (N_p\omega_p+N_d\omega_d\sqrt{|\widehat{X_{i,d\in\Theta}^{t}}|^2})H_{i,m}^{r,t}+(\omega_p\sum_{p\in\Theta}W_{i,p}^{'r}+\omega_d\sum_{d\in\Theta}W_{i,d}^{'r}), \qquad (4.81)
\end{aligned}
$$

where N_p and N_d are the number of pilot and data symbols within the MAW. To minimize the estimate variance

$$
E\{|\omega_p\sum_{p\in\Theta}W_{i,p}^{'r}+\omega_d\sum_{d\in\Theta}W_{i,d}^{'r}|^2\}=N_p\omega_p^2\frac{\sigma_w^2}{E_p}+N_d\omega_d^2(\sigma_{e_H}^2+\frac{\sigma_w^2}{E_d}), \qquad (4.82)
$$

the optimal weight values $\{\omega_p,\omega_d\}$, can be obtained by solving the following Lagrange multiplier problem:

$$
\begin{aligned}
\{\omega_p,\omega_d\} &= \arg\min_{\omega_p,\omega_d}\{(N_p\omega_p^2\frac{\sigma_w^2}{E_p}+N_d\omega_d^2(\sigma_{e_H}^2+\frac{\sigma_w^2}{E_d}))\\
&\quad +\lambda(N_p\omega_p+N_d\omega_d\sqrt{|\widehat{X_{i,d\in\Theta}^{t}}|^2}-1)\}, \qquad (4.83)
\end{aligned}
$$

where λ is the Lagrange multiplier. Hence, the optimal weights $\{\omega_p,\omega_d\}$ are given by:

$$
\omega_p=\frac{1+E_d\frac{\sigma_{e_H}^2}{\sigma_w^2}}{N_p(1+E_d\frac{\sigma_{e_H}^2}{\sigma_w^2})+N_d\frac{E_d}{E_p}|\widehat{X_{d\in\Theta}^{t}}|^2}, \qquad (4.84)
$$

and

$$
\omega_d=\frac{\sqrt{|\widehat{X_{i,d\in\Theta}^{t}}|^2}}{N_p\frac{E_p}{E_d}(1+E_d\frac{\sigma_{e_H}^2}{\sigma_w^2})+N_d|\widehat{X_{i,d\in\Theta}^{t}}|^2}. \qquad (4.85)
$$

It can be seen that the optimal weights $\{\omega_p, \omega_d\}$ are dependent on the number of pilot and data symbols within the MAW, the energy of pilot and data symbols, the energy of the soft decoded data symbol, the residue interference variance, and noise variance. Therefore, the combining is performed in perfect proportion to the reliability of the available information. As the iterations proceed, the available *a priori* information on data signals improves, the weights associated with the data-aided channel estimates increase accordingly, where the decoding data serve as virtual reference signals.

To further reduce the noise, time-domain MAW combining is applied to the channel frequency response from consecutive symbols. Assuming that channel frequency response between consecutive symbols are highly correlated, i.e. $H_{i,m}^{r,t} \approx H_{i-1,m}^{r,t}$, by applying similar approach, the optimization problem can be defined as:

$$\begin{aligned} \widehat{\widetilde{H_{i,m}^{r,t}}} &= \alpha\widetilde{H_{i-1,m}^{r,t}} + \beta\widetilde{H_{i,m}^{r,t}} \\ &= (\alpha+\beta)H_{i,m}^{r,t} + \underbrace{(\alpha W_{i-1,m}^{''r} + \beta W_{i,m}^{''r})}_{\mathcal{N}(0,\alpha^2\sigma^2_{w_{i-1,m}^{''r}} + \beta^2\sigma^2_{w_{i,m}^{''r}})}, \end{aligned} \tag{4.86}$$

where α and β are the solution of following optimization problem

$$\{\alpha,\beta\} = \underset{\alpha,\beta}{\operatorname{argmin}}\{(\alpha^2\sigma^2_{w_{i-1,m}^{''r}} + \beta^2\sigma^2_{w_{i,m}^{''r}}) + \lambda(\alpha+\beta-1)\}, \tag{4.87}$$

and $\sigma^2_{w_{i-1,m}^{''r}}$ and $\sigma^2_{w_{i,m}^{''r}}$ are the output of the variance estimator after the frequency-domain combining for the $(i-1)^{th}$ and i^{th} OFDM symbol respectively. Ignoring the index i and m for brevity, these noise variance terms are obtained by substituting the equations (4.84) and (4.85) into equation (4.82) as:

$$\begin{aligned} \sigma^2_{w^{''r}} &\approx N_p\omega_p^2\frac{\sigma_w^2}{E_p} + N_d\omega_d^2(\sigma^2_{e_H} + \frac{\sigma_w^2}{E_d}) \\ &\approx \frac{N_p\sigma_w^2(1+E_d\frac{\sigma^2_{e_H}}{\sigma_w^2})^2}{(N_p(1+E_d\frac{\sigma^2_{e_H}}{\sigma_w^2}) + N_d\frac{E_d}{E_p}|\widehat{X^t_{d\in\Theta}}|^2)^2} + \frac{N_d(\sigma^2_{e_H}+\frac{\sigma_w^2}{E_d})|\widehat{X^t_{d\in\Theta}}|^2}{(N_p\frac{E_p}{E_d}(1+E_d\frac{\sigma^2_{e_H}}{\sigma_w^2}) + N_d|\widehat{X^t_{i,d\in\Theta}}|^2)^2}. \end{aligned} \tag{4.88}$$

Hence, the optimal weighing factors α and β are obtained as:

$$\alpha = \frac{\sigma^2_{w_i^{''r}}}{\sigma^2_{w_{i-1}^{''r}} + \sigma^2_{w_i^{''}}}, \tag{4.89}$$

$$\beta = \frac{\sigma^2_{w''^r_{i-1}}}{\sigma^2_{w''^r_{i-1}} + \sigma^2_{w''^r_i}}, \tag{4.90}$$

This process will continue for a number of iterations. The advantage of this iterative method is that when the data decoding becomes more and more reliable as iterations progress, soft coded data information acts as new "pilots". Using the information symbols is beneficial as their total power over a frame is significantly more than that of the pilot symbols therefore adding noticeably to the channel estimation performance, and thus the data detection performance.

4.4.3 Final Estimation Stage

The final estimation stage is performed on the last iteration. Similar in the SISO-OFDM system, we have the option of MLE and MMSEE for the final channel estimation. In the case of MLE, the channel estimate is given by:

$$\begin{aligned}
\widehat{\mathbf{H}^{r,t}_{i,MLE}} &= \mathbf{G}(\mathbf{G}^H\mathbf{G})^{-1}\mathbf{G}^H\widetilde{\mathbf{H}^{r,t}_{i,IC-LS}} \\
&= \mathbf{G}(\mathbf{G}^H\mathbf{G})^{-1}\mathbf{G}^H[(\mathbf{X}^t_i)^H\mathbf{X}^t_i]^{-1}(\widehat{\mathbf{X}^t_i})^H\mathbf{Y}^{r,IC}_i \\
&= \frac{1}{N}\mathbf{G}\mathbf{G}^H(\widehat{\mathbf{X}^t_i})^{-1}\mathbf{Y}^{r,IC}_i,
\end{aligned} \tag{4.91}$$

where $\widehat{\mathbf{X}^t_i}$ is soft coded OFDM symbol vector at t^{th} transmitting antenna from the last second iteration with pilot tones, $\widetilde{\mathbf{H}^{r,t}_{i,IC-LS}}$ is the LS channel estimates vector after interference cancelation, and $\mathbf{Y}^r_i$ is the output of interference canceler at the r^{th} receiving antenna. In the case of MMSEE, the channel estimate is given by:

$$\begin{aligned}
\widehat{\mathbf{H}^{r,t}_{i,MMSE}} &= \mathbf{G}\mathbf{R}_{\mathbf{h'h'}}(\mathbf{G}^H\mathbf{G}\mathbf{R}_{\mathbf{h'h'}} + \sigma^2_{w'}\mathbf{I_L})^{-1}\mathbf{G}^H\widetilde{\mathbf{H}^{r,t}_{i,IC-LS}} \\
&= \mathbf{G}\mathbf{R}_{\mathbf{h'h'}}(N\mathbf{R}_{\mathbf{h'h'}} + \sigma^2_{w'}\mathbf{I_L})^{-1}\mathbf{G}^H\widetilde{\mathbf{H}^{r,t}_{i,IC-LS_{LS}}} \\
&= \mathbf{G}\mathbf{R}_{\mathbf{h'h'}}(N\mathbf{R}_{\mathbf{h'h'}} + \sigma^2_{w'}\mathbf{I_L})^{-1}\mathbf{G}^H(\widehat{\mathbf{X}^t_i})^{-1}\mathbf{Y}^{r,IC}_i.
\end{aligned} \tag{4.92}$$

4.4.4 Mean Square Error Analysis of Iterative Channel Estimation

Similar to the SISO-OFDM system, we can analyze the MSE of the developed iterative turbo channel estimation technique. Again, it is difficult to analyze the MSE of the iterative channel estimation technique because of the exchange of soft information and MAP decoder. Instead, the MSE lower bounds are calculated for

MLE and MMSEE in Section 4.4.3. In the case of the MLE, the MSE lower bound can be obtained as:

$$MSE_{MLE} = \frac{1}{N_R N_T} \sum_{r=0}^{N_R-1} \sum_{t=0}^{N_T-1} \frac{\sigma_{w'}^2 L^{r,t}}{N}. \tag{4.93}$$

In the case of MMSEE, the MSE can be obtained as:

$$MSE_{MMSE} = \frac{1}{N_R N_T} \sum_{r=0}^{N_R-1} \sum_{t=0}^{N_T-1} \frac{\sigma_{w'}^2}{N} \sum_{l=0}^{L^{r,t}-1} \frac{1}{1+\sigma_{w'}^2/(N\alpha_l^{r,t})}. \tag{4.94}$$

4.5 Complexity of Iterative Receiver for MIMO-OFDM Systems

Similar in Section 3.5, the computational complexity of the iterative receiver is measured by the number of valued multiplications. And only the complexity of the detector is compared because the complexity of the decoder is common to every iterative receiver. In the 2×1 Alamouti STC-OFDM system, the MRC linear combiner requires two multiplications per symbol per subcarrier for detection, hence, the overall complexity for the MRC linear combiner is proportional to $2 \times 2N \times N_{itr}$, where N is the total number of OFDM subcarriers and N_{itr} is the total number of iterations. In the 2×2 Alamouti STC-OFDM system, the MRC linear combiner requires four multiplications per symbol per subcarrier for the detection, and the overall complexity is proportional to $4 \times 2N \times N_{itr}$. Therefore, in both MIMO configurations for the Alamouti STC-OFDM systems, the complexity of the MRC receiver is $\mathcal{O}(N)$.

For the iterative receivers in the $N_R \times N_T$ SM-OFDM system, the MMSE detector in the first iteration requires $\mathcal{O}(N_T^3)$ complexity to obtain the MMSE filtering coefficients per symbol per subcarrier, and total $N \times (N_R + \mathcal{O}(N_T^3))N_T$ computational complexity to perform the filtering. From the second iteration onwards, the interference canceler requires $N_T(N_T-1)N_R$ complex multiplications per subcarrier to perform cancelation as shown in equation (4.52). For the IC-MF receiver, an additional $N_T \times N_R$ multiplications per subcarrier are required for the matched filtering. Furthermore, for the IC-MMSE receiver, an additional $N_T \times N_R + \mathcal{O}(N_T^3)$ multiplications per subcarrier are required for the MMSE filtering. Table 4.1 summarizes the computational complexity of the iterative receivers for MIMO-OFDM systems. It can be seen that all the iterative receivers have a complexity of $\mathcal{O}(N)$.

Table 4.1: Computational Complexity for Receivers in MIMO-OFDM Systems

Receivers	Computational Complexity in Multiplications
2×1 MRC	$2 \times 2N \times N_{itr}$
2×2 MRC	$4 \times 2N \times N_{itr}$
MMSE+IC	$N \times [(N_R + \mathcal{O}(N_T^3))N_T + (N_T(N_T-1)N_R)(N_{itr}-1)]$
MMSE+IC-MF	$N \times [(N_R + \mathcal{O}(N_T^3))N_T + (N_T(N_T-1)N_R + N_T N_R)(N_{itr}-1)]$
MMSE+IC-MMSE	$N \times [(N_R + \mathcal{O}(N_T^3))N_T +$ $(N_T(N_T-1)N_R + N_T N_R + N_T\mathcal{O}(N_T^3))(N_{itr}-1)]$
Conventional ML	$N \times 2^{N_T N_R}$

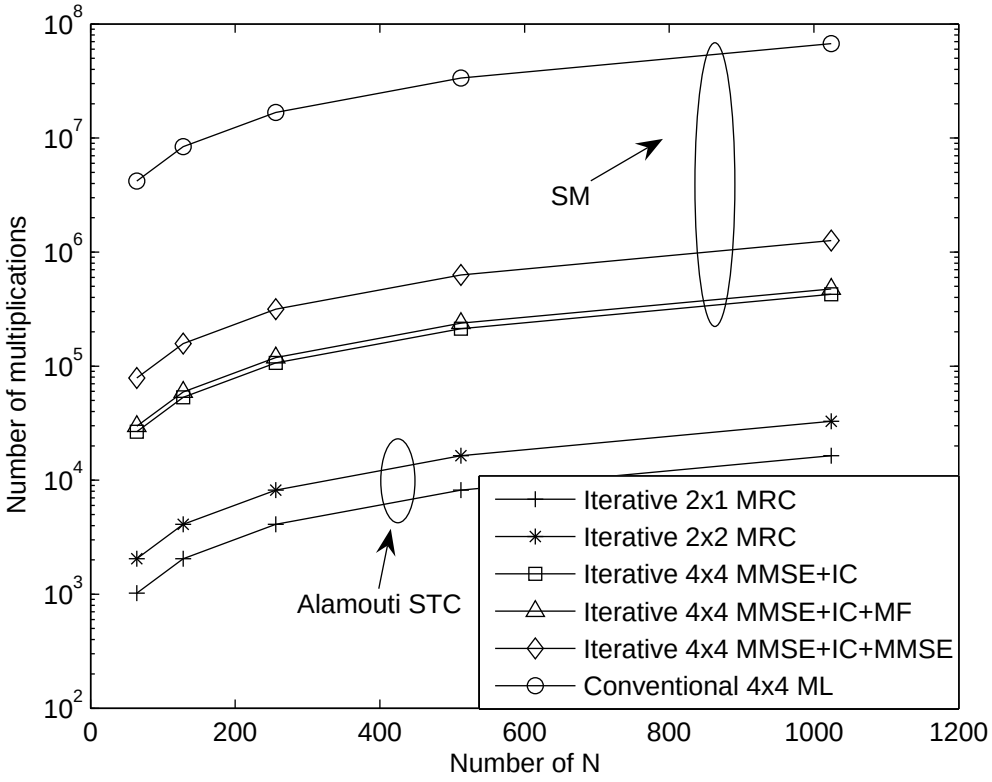

Figure 4.4: Complexity for MIMO-OFDM receivers

Fig. 4.4 shows the complexity of MIMO-OFDM receivers including both iterative receivers and conventional ML receiver. Among all the iterative receivers, the MRC receiver is the simplest receiver due to the orthogonal space-timing coding property, while the iterative receivers for the spatial multiplexing system are a bit complex. Nevertheless, compared to the ML receiver which has exponential complexity with respect to the number of transmitting antennas, receiving antennas, memory of the channel, and order of the data modulation, the iterative receivers have lower

complexity and therefore are more favorable for realization.

The complexity of the iterative channel estimation for the MIMO-OFDM system can be obtained from the iterative channel estimation in the SISO-OFDM system. Each transmitting and receiving wireless link requires separate channel estimation. In the initial estimation stage, pilot estimation requires $N_p \times N_R N_T$ multiplications. To obtain the coarse channel frequency response at data tones, the linear interpolation between pilot tones requires $(N - N_p) \times N_R N_T$ multiplications. In the iterative estimation stage, the soft data channel estimation requires $(N - N_p) \times N_R N_T$ multiplications. The calculation of ω_p, ω_d coefficients requires $N \times N_\Theta^{FD} \times N_R N_T$ multiplications, frequency-domain filtering requires $N \times N_\Theta^{FD} \times N_R N_T$ multiplications. The calculation of α, β coefficients requires a single multiplication per transmitting and receiving link. The time-domain filtering requires $2N \times N_R N_T$ multiplications. Therefore, there in total $(N_{itr} - 2) \times (3N - N_p + 2N \times N_\Theta^{FD} + 1) \times N_R N_T$ multiplications.

In the final estimation stage, the soft data channel estimation requires $(N - N_p)$ multiplications. MLE operation requires $\mathcal{O}(N^2)$ multiplications and MMSE operation requires $\mathcal{O}(N^3)$. Therefore, the total complexity is $N + O(N^2) \times N_R N_T$ for MLE and $N + \mathcal{O}(N^3) \times N_R N_T$ for MMSE estimator. Table 4.2 summarizes the number of multiplications involved in each stage. It can be seen that if the final estimation stage is excluded, the complexity of initial coarse estimation stage and iterative estimation stage is in the order of $\mathcal{O}(N)$. Compared to conventional MLE or MMSE estimation, the additional complexity from iterative channel estimation remains low.

4.6 Numerical Results

4.6.1 Simulation Setup

We consider an IEEE standar802.16e 2×2 MIMO Mobile WiMAX [17] compliant OFDM system with $N = 256$ subcarriers, and 8 pilot tones. 200 subcarriers are used, CP length is 64. The carrier frequency is 3.5GHz, and the bandwidth is 2.5MHz. There are 4 OFDM data symbols per frame transmission. The energy of each pilot symbol is the same as each data symbol. The 3GPP spatial channel model (SCM) [108] urban micro scenario is adopted in the simulation. The mobile speeds are 3kmh and 120kmh, which corresponds to pedestrian and vehicular environment. We also include an extreme vehicle speed of 333kmh for some comparisons. A rate-1/2 $(171, 133)_8$ convolutional code is used for channel coding.

Table 4.2: Computational Complexity for Iterative Channel Estimation in MIMO-OFDM System

Operations	First Stage	Second Stage (per iteration)	Final Stage
Pilot Estimation	$N_p \times N_R N_T$	0	0
Soft Data Estimation	0	$(N - N_p) \times N_R N_T$	$(N - N_p) \times N_R N_T$
Linear Interpolation	$(N - N_p) \times N_R N_T$	0	0
ω_p, ω_d Calculation	0	$N \times N_\Theta^{FD} \times N_R N_T$	0
Frequency-domain Filtering	0	$N \times N_\Theta^{FD} \times N_R N_T$	0
α, β Calculation	0	$N_R N_T$	0
Time-domain Filtering	0	$2N \times N_R N_T$	0
ML Estimation	0	0	$\mathcal{O}(N^2) \times N_R N_T$
MMSE Estimation	0	0	$\mathcal{O}(N^3) \times N_R N_T$
Total for each stage	$\mathcal{O}(N)$	$\mathcal{O}(N)$	$\mathcal{O}(N^2) or \mathcal{O}(N^3)$

The modulation scheme is 16QAM for STC system, and QPSK for SM system to maintain the same throughput. The total number of iterations is set to 4. The frequency-domain MAW size is set to 7 to ensure that the correlation of channel frequency response within the MAW is sufficient high. Similar to Chapter 3, we demonstrated the performance under the simulation environment that frame by frame transmission is adopted, which is the same setup as the practical system. The FER performance of the iterative receiver is compared to that of the conventional MRC receiver for Alamouti STC system and MMSE receiver for SM system, both employing one-shot preamble channel estimation. We refer to the proposed iterative receivers as "turbo..." or "iterative..", the conventional receivers as "conventional...", and the receiver performance with perfect CSI as "Perfect...".

4.6.2 Performance in the Alamouti STC-OFDM System

Fig. 4.5 shows the FER performances of MRC receivers for both QPSK and 16QAM modulations at 3kmh. The iterative receiver performs joint channel re-estimation and MRC data detection. It can be seen that with iterative channel estimation, the iterative MRC receiver outperforms the conventional MRC receiver with one-shot preamble channel estimation by 2dB. And the performances are only 0.5dB away from the the performance of the MRC receiver with perfect CSI.

Fig. 4.6 shows the FER performance of MRC receivers for QPSK modulation at various mobilities. We also include the conventional MRC receiver at the mo-

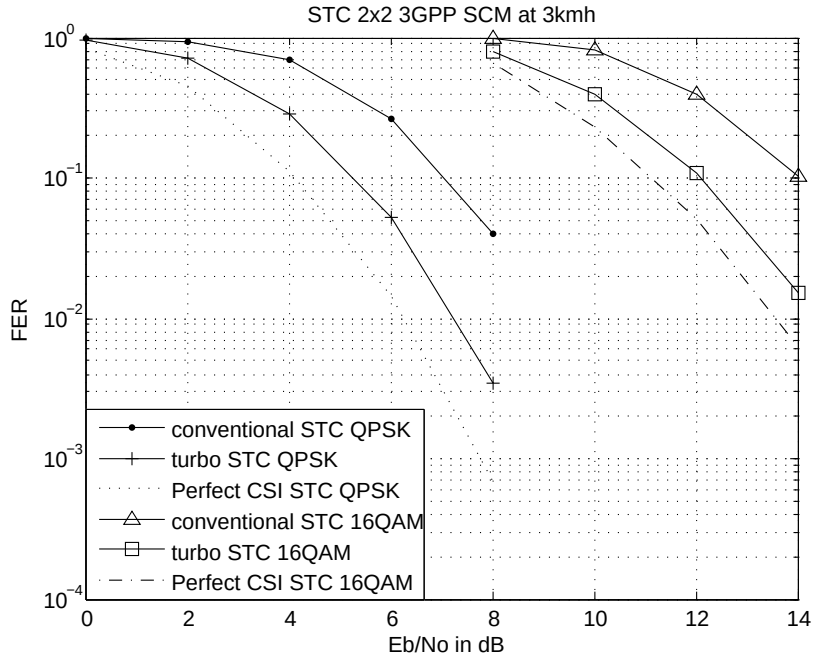

Figure 4.5: FER performance of the 2×2 Alamouti STC-OFDM MRC receivers for QPSK and 16QAM modulation at 3kmh

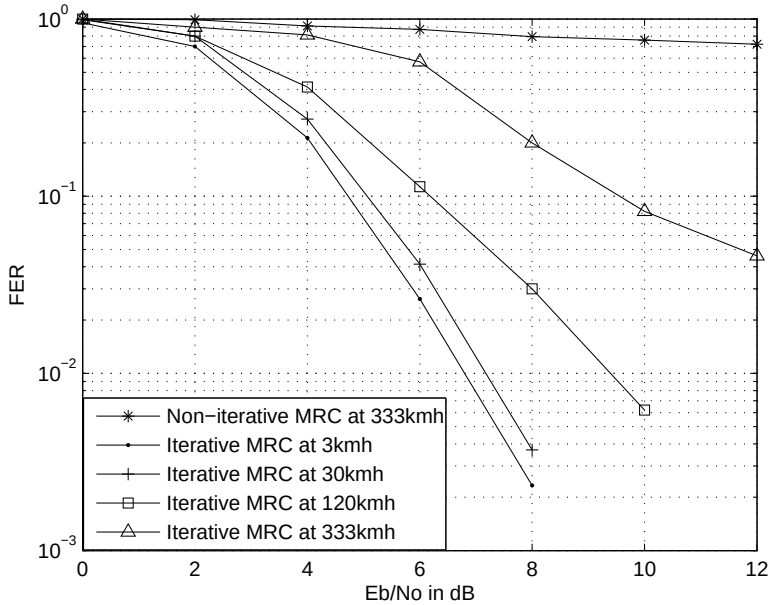

Figure 4.6: FER performance of the 2×2 Alamouti STC-OFDM MRC receivers for QPSK modulation at various mobilities

bility of 333kmh. It can be seen that the performance of the receiver performance degrades as the mobility increases. This is because as the mobile speed goes higher

and higher, the channel variation becomes more and more significant among OFDM symbols. The space-time coding techniques are developed based on the assumption that the channel response between two consecutive data symbols is constant, which is approximately true under a very low mobility environment. At high mobility environments, this assumption does not hold. As we can observe that the performance fades away from the low mobility case. Nevertheless, the iterative receiver still works at high mobility of 333kmh compared to the conventional receiver, which completely fails in such high mobility.

4.6.3 Performance in the SM-OFDM System

Fig. 4.7 and Fig. 4.8 show the FER performances of various receivers discussed in Section 4.3 in SM-OFDM system for QPSK modulation at 3kmh and 120kmh, respectively. We also include the conventional MMSE receiver as discussed in Section 4.2.2, which employs one-shot preamble channel estimation. It can be observed that at pedestrian speed (3km/hr), the conventional MMSE receiver works fine even without the updated CSI because the channel undergoes slow fading. The iterative receivers outperform the conventional receiver by 2dB at an operating point with a $FER = 10^{-2}$. Their performance is less than 1dB away from the performance if the CSI is known.

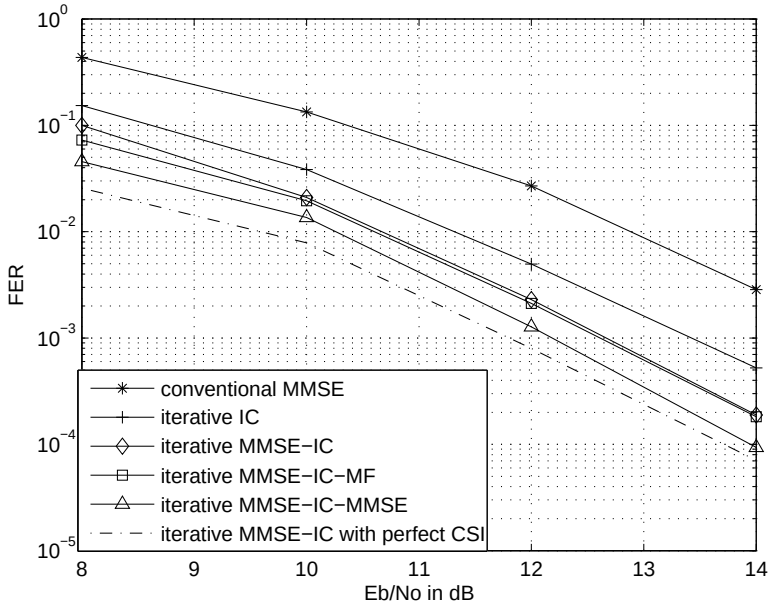

Figure 4.7: FER performance of the 2×2 SM-OFDM receivers for QPSK modulation at 3kmh

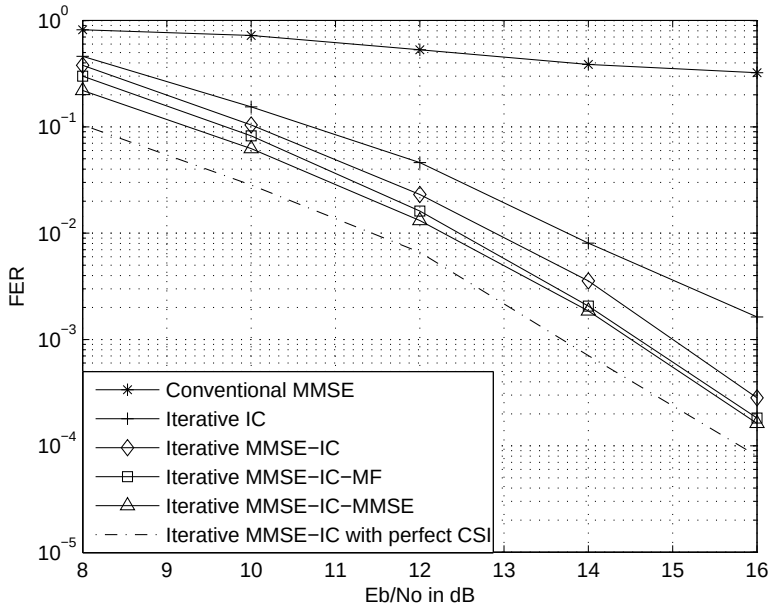

Figure 4.8: FER performance of the 2×2 SM-OFDM receivers for QPSK modulation at 120kmh

On the other hand, at high vehicular speed, the one-shot preamble channel estimation is not sufficient for the conventional MMSE receiver, and the massive interference in the SM-OFDM system results in the failure. The iterative receivers perform well with 1dB away from the performance under perfect CSI. Furthermore, among the iterative receivers, the additional signal processing, such as MMSE, etc., does provide an additional 2dB gain compared to just using the interference canceler.

Furthermore, Fig. 4.9 shows the MSE performance at 12dB between conventional channel estimation and iterative channel estimation at 3kmh and 120kmh. At both pedestrian and vehicular speeds, the iterative channel estimation outperforms the conventional one-shot channel estimation. At high mobility, the channel varies significantly due to the short coherence time, the channel estimates from the preamble in the conventional one-shot channel estimation shows a high MSE for the OFDM symbols after preamble. The iterative receiver, however, tracks the channel variations in every OFDM symbol, where the MSE remains lower for consecutive OFDM symbols.

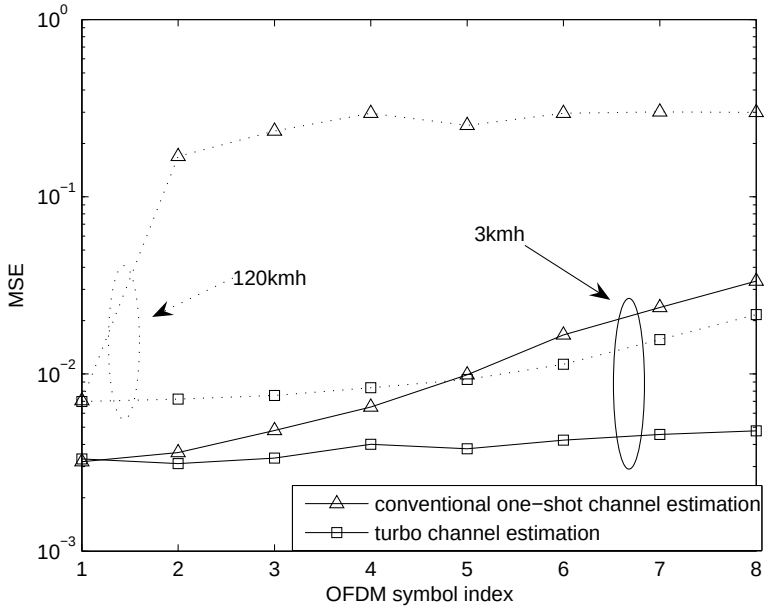

Figure 4.9: MSE performance at 12dB in the conventional channel estimator and iterative channel estimator at 3kmh and 120kmh

4.6.4 Comparison of the Performances of Receivers under Same Spectrum Efficiency

Fig. 4.10 compares the FER performances of the conventional and the iterative receivers for SM system and Alamouti STC system at same spectrum efficiency, i.e. 4bits/s/Hz. In SM system, the iterative receiver performs joint channel re-estimation and interference cancelation. It can be seen that 2dB gain is obtained over MMSE receiver with conventional one-time preamble channel estimation, and 6dB gain over conventional Alamouti STC receiver. Fig. 4.11 shows the FER performances among conventional almouti STC receiver, MMSE SM receiver and iterative receiver at 120kmh. At such high mobility, the channel does not stay stationary any more, but varies significantly from symbol to symbol within one data packet. The conventional Alamouti STC receiver completely fails under these conditions. The conventional SM MMSE receiver in this case performs better than the conventional Alamouti STC receiver, however, the performance degrades from that for the pedestrian case (3km/hr). Nevertheless, the iterative receiver is more robust to high mobility environment and achieves more than 6dB gain over the conventional receivers.

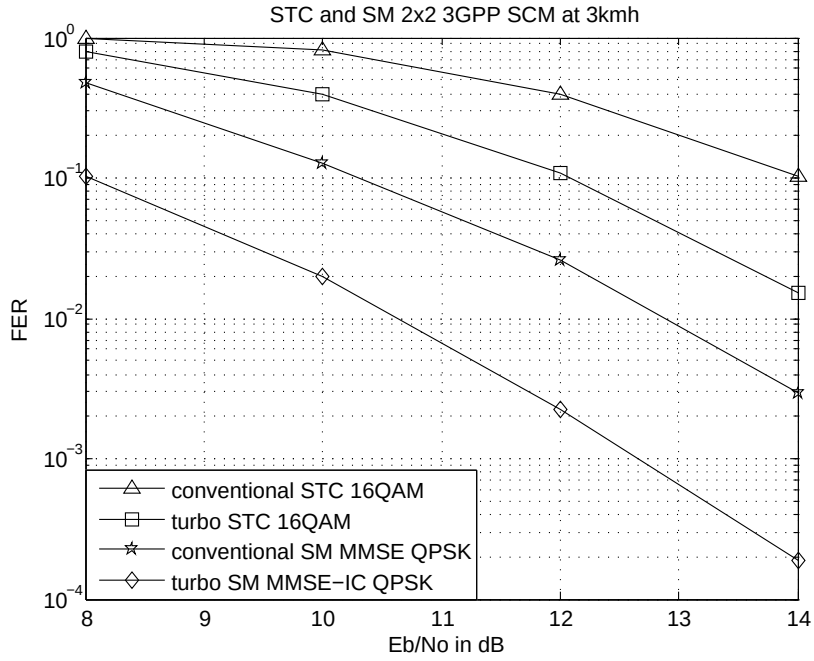

Figure 4.10: FER performance comparisons among conventional MRC receiver, MMSE receiver and iterative receiver at 3kmh

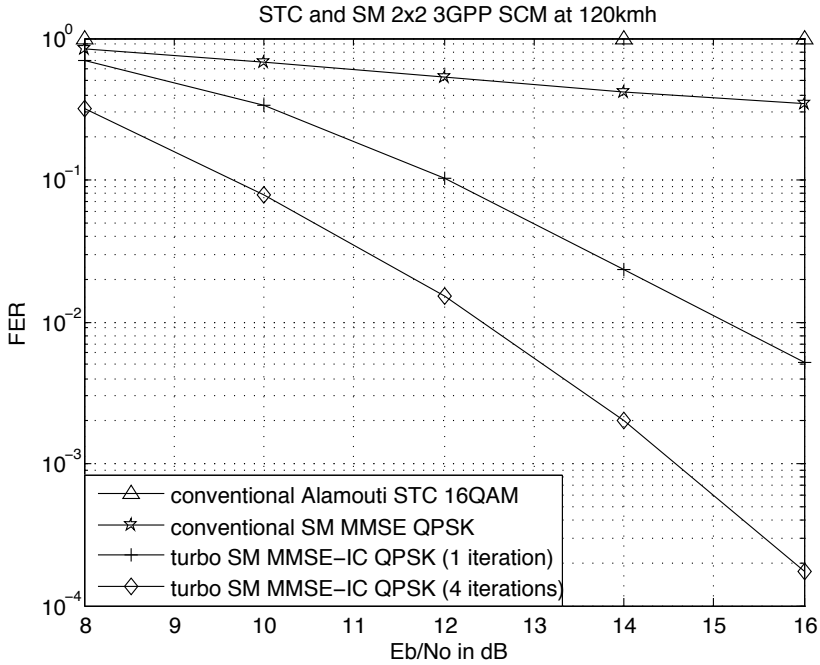

Figure 4.11: FER performance comparisons among conventional MRC receiver, MMSE receiver and iterative receiver at 120kmh

4.7 Summary and Contributions

This chapter has developed iterative receivers for practical MIMO-OFDM systems. In MIMO-OFDM systems, the received signal at each receiving antenna is the

superposition of the fading signals from all transmitting antennas. The massive interference makes data detection a challenging problem. For the Alamouti STC-OFDM system, an iterative linear MRC receiver is developed. For the SM-OFDM system, interference canceler based iterative receivers with post-processing are developed. As discussed in previous chapters, channel estimation is a very critical and fundamental problem for the receiver design, especially for the system operated under various mobility environment. The conventional MIMO-OFDM receiver usually employs one-shot channel estimation, which is designed for static mobile environment. Such time variation and frequency variation of the channel response degrade the performance of the conventional receivers. As shown before, the primary advantage of the proposed iterative channel estimation technique is to further improve the channel estimates with data decoding information in dynamic channel environment. Extended from Chapter 3, a novel low complexity channel estimator is developed. It tracks the dynamics of channel frequency response through time-domain and frequency-domain combining of channel estimates from preamble, pilots and soft decoded data information. This channel estimator is integrated with iterative receivers.

Some specific contributions made in this chapter are as follows. First of all, the system model for the MIMO-OFDM is investigated from the extension of the SISO-OFDM system model. And the conventional MRC receiver in the Alamouti STC-OFDM system is investigated. The MRC receiver makes use of the orthogonal property of the channel matrix produced by the space-time encoder, hence, optimal detection can be obtained through linear operations. Such approach is analogous to the single user detection in the synchronous multiple access environment. The conventional MF, ZF and MMSE receivers in the SM-OFDM system are studied. The channel matrix in SM-OFDM system does not have the orthogonal property, hence, the receiver for SM system is much more complicated. MF receiver simply combines the energy from multiple receiving antennas. It suffers severe interferences from other transmitting symbols because the columns of the channel matrix for SM-OFDM system is not orthogonal to each other. ZF receiver uses a straight forward matrix inversion. The linear MMSE receiver provides improved detection with the knowledge of MIMO channel statistics. It makes the compromise between the MF and ZF receivers.

Secondly, an iterative linear MRC receiver for Alamouti STC-OFDM system is developed. The channel state information is updated in each iteration, and the linear combining is performed on the updated channel estimates to improve the

performance. Furthermore, an interference canceler receiver with post-processing for the SM-OFDM system is developed. The MMSE filtering is performed in the first iteration, followed by the interference cancelation in the remaining iterations. In addition, several post interference cancelation processes, such as IC-MF and IC-MMSE are also developed.

Thirdly, a low complexity iterative channel estimator is integrated with the iterative receivers. Similar to the SISO-OFDM systems, the iterative channel estimator consists of three estimation stages, namely the initial coarse estimation stage, iterative estimation stage, and the final estimation stage. It performs time-domain and frequency-domain combining of channel estimates from preamble, pilots and soft decoded data information to track the dynamics of channel frequency response. The theoretical lower bounds of the MSE that the iterative channel estimation can achieve is derived. And the complexity in terms of complex multiplications that the iterative receiver requires is analyzed.

Finally, the performances of the iterative receivers and the conventional receivers are compared. The numerical and analytical results show that the iterative receivers have 2dB gain compared to the conventional receivers in pedestrian low mobility condition and more than 6dB gain in vehicular high Doppler environment. Among the iterative receivers, the post-processing provides further 2dB performance improvement from the interference canceler. Furthermore, the iterative channel estimation technique is robust in high mobility environment where the conventional receiver fails due to poor channel estimation.

Chapter 5

Iterative Receiver on Sphere Decoder

5.1 Introduction

In this Chapter, the iterative receiver techniques based on a new sphere decoder are presented for the spatial multiplexed MIMO system. The Algorithms I and II in [68] are extended to iterative reception by including accumulated *a priori* information metric in the enumeration process. Furthermore, we develop two novel schemes for the SE algorithm by utilizing the *a priori* information. These two novel schemes aim to improve the performance and reduce the computational complexity even further over iterations. It is worth mentioning that as previous chapters have demonstrated the iterative channel estimation approach in great detail, in this chapter, we move to the detection method itself by assuming the MIMO system model is generic and spatially multiplexed while the channel estimation is perfect. We remove the focus including channel estimation, and concentrate our analysis on how to utilize the data information to improve the overall detection-decoding sensitivity while reducing the complexity at the same time. The derived low complexity data-driven sphere decoder can be applied to any specific system that needs interference mitigation. It may not be necessarily limited to MIMO system, for example, a multi-user DS-CDMA system could also use this technique. Iterative channel estimation could be easily added to the techniques discussed in this Chapter.

5.2 Modified Linear MIMO Model for Sphere Decoder Detections

The MIMO spatial multiplexing system considered in this Chapter is shown in Fig. 5.1. There are N_T transmitting antennas and N_R receiving antennas. The information bits $\{\mathbf{b}\}$ are first encoded into coded bits sequences $\{\mathbf{d}\}$. These coded bits are interleaved into a new sequence $\{\mathbf{c}\}$, mapped into M-ary complex symbols sequence of $\{\mathbf{x}\}$ represented by a vector $\mathbf{x} = [x_0, x_1, \cdots, x_{N_T-1}]^T$.

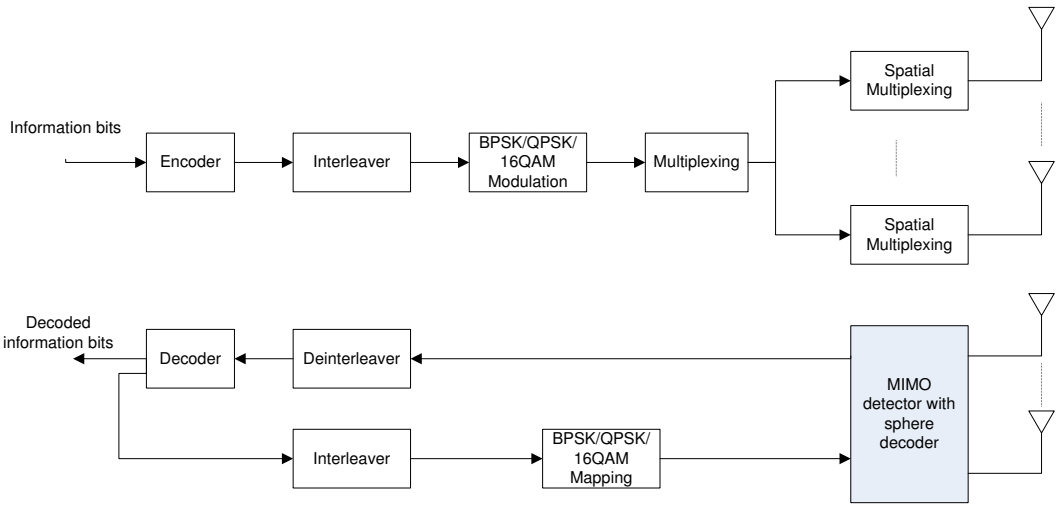

Figure 5.1: MIMO spatial multiplexing transmitter and iterative receiver with sphere decoder

Assuming that each transmitting and receiving antenna link undergoes independent flat fading, the system model can be expressed as:

$$\mathbf{y} = \mathbf{hx} + \mathbf{w}, \tag{5.1}$$

where $\mathbf{y}$ is the received signal defined as $N_R \times 1$ vector $\mathbf{y} = [y_0, y_1, \cdots, y_{N_R-1}]^T$. $\mathbf{h}$ is $N_R \times N_T$ channel matrix. $\mathbf{w}$ is $N_R \times 1$ AWGN vector with covariance $\sigma_w^2 \mathbf{I}_{N_R}$.

It is worth noting that the system model in Fig. 5.1 is in the complex signal representation, and the real and imaginary parts of the model are assumed as independent to each other. Generally speaking, the sphere decoder algorithms perform tree search through the signal space. Hence, it is more convenient to reformulate the system model from a complex value representation to a real value representation. Therefore, by defining the $2N_R \times 1$ vector $\mathbf{Y}$, $2N_T \times 1$ vector $\mathbf{X}$,

$2N_R \times 1$ vector $\mathbf{W}$ as:

$$\mathbf{Y} = \begin{bmatrix} \Re(\mathbf{y})^T & \Im(\mathbf{y})^T \end{bmatrix}^T, \tag{5.2}$$

$$\mathbf{X} = \begin{bmatrix} \Re(\mathbf{x})^T & \Im(\mathbf{x})^T \end{bmatrix}^T, \tag{5.3}$$

$$\mathbf{W} = \begin{bmatrix} \Re(\mathbf{w})^T & \Im(\mathbf{w})^T \end{bmatrix}^T, \tag{5.4}$$

and $2N_R \times 2N_T$ matrix $\mathbf{H}$ as:

$$\mathbf{H} = \begin{bmatrix} \Re(\mathbf{h}) & -\Im(\mathbf{h}) \\ \Im(\mathbf{h}) & \Re(\mathbf{h}) \end{bmatrix}, \tag{5.5}$$

where $\Re(\cdot)$ and $\Im(\cdot)$ denote the real and imaginary parts of the argument, the real-domain signal representation of the system model can be expressed as:

$$\mathbf{Y} = \mathbf{HX} + \mathbf{W} \tag{5.6}$$

The MIMO detector based on the original sphere decoder algorithm maximizes the likelihood of the transmitted signal being detected. It is equivalent to minimizing the Euclidian Distance of the transmitted signal and received signal given that the channel is known, which is given as:

$$\widehat{\mathbf{X}} = \arg\max_{\mathbf{X}\in\mathcal{U}} P(\mathbf{Y}|\mathbf{X}) = \arg\min_{\mathbf{X}\in\mathcal{U}} \|\mathbf{Y} - \mathbf{HX}\|^2, \tag{5.7}$$

where $\mathcal{U}$ is the signal subset of dimension $2N_T$. As in the sphere decoder algorithms, not all signal vectors in the complete constellation set $\mathcal{A}$ are examined, only a partial constellation set $\mathcal{U}$, where $\mathcal{U} \in \mathcal{A}$ is employed in the detection. In this Chapter, the sphere decoder is modified to estimate the MAP probability of transmitted signal sequence given by:

$$\widehat{\mathbf{X}} = \arg\max_{\mathbf{X}\in\mathcal{U}} P(\mathbf{X}|\mathbf{Y}) = \arg\max_{\mathbf{X}\in\mathcal{U}} \frac{P(\mathbf{Y}|\mathbf{X})P(\mathbf{X})}{P(\mathbf{Y})}, \tag{5.8}$$

where $P(\mathbf{X})$ is the *a priori* information, which is sourced from the *a-posteriori* probabilities of the channel decoder in the previous iteration. Because the *a priori* information is not available in the first iteration, sphere decoding based on the ML metric (5.7) is employed in the MIMO detector in Fig. 5.1. From the second iteration onwards, the MAP detection metric (5.8) is employed. In each iteration, the MIMO detector selects the most reliable points $\{\widehat{\mathbf{X}}\}$ to form a list $\mathcal{U}$ to compute

the extrinsic LLR of the coded bit as:

$$\begin{aligned}\lambda_1^e(d_k(\widehat{\mathbf{X}})) &= \frac{1}{2}\sum_{\widehat{\mathbf{X}}\in\mathcal{U}_k^+}(-\frac{1}{\sigma_w^2}\|\mathbf{Y}-\mathbf{H}\widehat{\mathbf{X}}\|^2+\mathbf{d}_{\backslash k}^T\lambda_{\mathbf{2},\backslash\mathbf{k}}^{\mathbf{e}}) \\ &\quad -\frac{1}{2}\sum_{\widehat{\mathbf{X}}\in\mathcal{U}_k^-}(-\frac{1}{\sigma_w^2}\|\mathbf{Y}-\mathbf{H}\widehat{\mathbf{X}}\|^2+\mathbf{d}_{\backslash k}^T\lambda_{\mathbf{2},\backslash\mathbf{k}}^{\mathbf{e}}),\end{aligned} \tag{5.9}$$

where $d_k(\widehat{\mathbf{X}})$ is the k^{th} coded bit in sequence $\{d\}$, representing the sphere decoder enumerated transmitted symbol vector $\widehat{\mathbf{X}}$. $\mathcal{U}_k^+$ and $\mathcal{U}_k^-$ denote the subset of $\mathcal{U}$ for which $d_k(\widehat{\mathbf{X}})$ is $+1$ and -1 respectively. $\mathbf{d}_{\backslash k}$ is obtained from sequence $\mathbf{d}$ by removing the k^{th} coded bit. $\lambda_{2,\backslash k}^e$ is the extrinsic LLR of sequence $\mathbf{d}_{\backslash k}$ from the channel decoder. After MIMO detection, the sequence of extrinsic LLRs $\{\lambda_1^e\}$ of coded bits is deinterleaved and passed through the channel decoder to complete one iteration.

5.3 The Original FP and SE Algorithms

The sphere decoder algorithms were developed initially to solve the lattice coding problem for the pulse amplitude modulation (PAM) signals. In this section, we give an brief overview of the sphere decoder.

As the name suggested, a geometrical searching sphere $(\mathbf{X}_o, C)$ is defined, where $\mathbf{X}_o$ is the center of the sphere and $\sqrt{C}$ is the radius of the sphere in the signal space. In sphere decoding, the primary objective is to examine the signal points within the searching sphere and find the signal point which is closest to the transmitted signal. Hence, we need to know where to start (the center of the sphere), and how far we should search (the radius of the sphere). Theoretically, the center of the sphere can be anywhere in the signal space, and the radius of the sphere can be as large as infinity, while judicious choice of there two parameters can significantly speed up the search process.

The sphere decoder algorithms [66, 67] determine the center of the sphere from the unconstrained ML estimate of transmitted signal from the observed received signal, i.e.

$$\mathbf{X}_o = (\mathbf{H}^H\mathbf{H})^{-1}\mathbf{H}^H\mathbf{Y}. \tag{5.10}$$

Substituting equation (5.10) into equation (5.7), we have:

$$\widehat{\mathbf{X}} = \arg\min_{\mathbf{X}\in\mathcal{U}}\|\mathbf{Y}-\mathbf{H}\mathbf{X}\|^2$$

$$\begin{aligned} &= \arg\min_{\mathbf{X}\in\mathcal{U}}\{(\mathbf{X}-\mathbf{X}_o)^H\mathbf{H}^H\mathbf{H}(\mathbf{X}-\mathbf{X}_o)+\mathcal{K}\} \\ &= \arg\min_{\mathbf{X}\in\mathcal{U}}\{(\mathbf{X}-\mathbf{X}_o)^H\mathbf{H}^H\mathbf{H}(\mathbf{X}-\mathbf{X}_o)\}, \end{aligned} \tag{5.11}$$

where

$$\mathcal{K} = \mathbf{Y}^H(\mathbf{I}_{2N_R} - \mathbf{H}(\mathbf{H}^H\mathbf{H})^{-1}\mathbf{H}^H)\mathbf{Y} \tag{5.12}$$

is a constant which is independent to $\widehat{\mathbf{X}}$, and $\mathcal{U}$ is collection of the candidates $\mathbf{X}$ within the searching sphere such that

$$(\mathbf{X}-\mathbf{X}_o)^H\mathbf{H}^H\mathbf{H}(\mathbf{X}-\mathbf{X}_o) \leq C. \tag{5.13}$$

The sphere decoder algorithms first use the Cholesky factorization [109] to find an upper triangular matrix $\mathbf{Q}$ such that $\mathbf{Q}^H\mathbf{Q} = \mathbf{H}^H\mathbf{H}$ whereby equation (5.13) can be expressed as:

$$\sum_{i=0}^{2N_T-1} Q_{i,i}^2(X_i - [X_o]_j + \sum_{j=i+1}^{2N_T-1}\frac{Q_{i,j}}{Q_{i,i}}(X_j - [X_o]_j))^2 \leq C. \tag{5.14}$$

Then, the sphere decoder algorithms start from the top level, i.e. $i = 2N_T - 1$, by ignoring the terms related to $i = 0, 1, \ldots, 2N_T - 2$, and the equation (5.14) is simplified to:

$$Q_{2N_T-1,2N_T-1}^2(X_{2N_T-1} - [X_o]_{2N_T-1})^2 \leq C. \tag{5.15}$$

The solution of X_{2N_T-1} is upper bounded by

$$\mathcal{L}_{2N_T-1} := \left\lfloor [X_o]_{2N_T-1} + \frac{\sqrt{C}}{Q_{2N_T-1,2N_T-1}} \right\rfloor \tag{5.16}$$

and lower bounded by

$$\mathcal{V}_{2N_T-1} := \left\lceil [X_o]_{2N_T-1} - \frac{\sqrt{C}}{Q_{2N_T-1,2N_T-1}} \right\rceil, \tag{5.17}$$

where $\lfloor\cdot\rfloor$ and $\lceil\cdot\rceil$ are the floor and ceiling operators to find the nearest integer. With the lower and upper bounds, X_i can be obtained by selecting one of the possible values from this interval. It is worth noting that in the above upper triangular approach (Cholesky factorization), the precision of the previous value affects the accuracy of the next value. In this case, once X_{2N_T-1} is fixed, it will affect of the selection of next level X_{2N_T-2}. To see this influence clearly, we keep the top two

levels $i = 2N_T - 1, 2N_T - 2$, and ignoring the rest levels $i = 0, 1, \ldots, 2N_T - 3$, the equation (5.14) is simplified to:

$$Q^2_{2N_T-2,2N_T-2}(X_{2N_T-2} - [X_o]_{2N_T-2} + \frac{Q_{2N_T-2,2N_T-1}}{Q_{2N_T-2,2N_T-2}}(X_{2N_T-1} - [X_o]_{2N_T-1}))^2 + Q^2_{2N_T-1,2N_T-1}(X_{2N_T-1} - [X_o]_{2N_T-1})^2 \leq C. \quad (5.18)$$

Similarly, the solution of X_{2N_T-2} is upper bounded by

$$\mathcal{L}_{2N_T-2} := \left\lfloor [X_o]_{2N_T-1} + \frac{\sqrt{C - \vartheta_{2N_T-2}} - \zeta_{2N_T-2}}{Q_{2N_T-2,2N_T-2}} \right\rfloor \quad (5.19)$$

and lower bound by

$$\mathcal{V}_{2N_T-2} := \left\lceil [X_o]_{2N_T-1} - \frac{\sqrt{C - \vartheta_{2N_T-2}} - \zeta_{2N_T-2}}{Q_{2N_T-2,2N_T-2}} \right\rceil, \quad (5.20)$$

where

$$\vartheta_{2N_T-2} = Q^2_{2N_T-1,2N_T-1}(X_{2N_T-1} - [X_o]_{2N_T-1})^2 \quad (5.21)$$

and

$$\zeta_{2N_T-2} = Q_{2N_T-2,2N_T-1}(X_{2N_T-1} - [X_o]_{2N_T-1}). \quad (5.22)$$

The sphere decoder algorithms now choose a possible value within the new interval.

Based on above discussion, the FP and SE algorithms are the enumeration strategies for the sphere decoder, or in other words, they are the tree search algorithms on how to select the values in the interval. The FP enumeration algorithm starts from the lower bound and search the entire interval till the upper bound. On the other hand, The SE algorithm starts from the middle point of the interval (center of the searching sphere $\mathbf{X}_o$) and search the points near the middle point through a zig-zag order. In summary, the main differences of FP and SE algorithms are the number of nodes they visit at each dimension and the way that they perform the search. It has been reported in the literature that the SE algorithm is more efficient than the FP algorithm [68]. However, the SE algorithm may not cover all points in the interval, hence, it has performance loss compared to the FP algorithm.

No matter which algorithm is used, the idea of the sphere decoder algorithms is to construct a search tree, whose nodes at each level representing the lattice points in each dimension lying inside the sphere with certain radius. The algorithms start

from the top level of the tree (first dimension in the signal space), then search towards the next level. At each level, the algorithms scan the possible nodes, if the node is within the sphere, the algorithms will go to its offsprings in the lower levels, otherwise if the node is outside the sphere, that node and its offsprings in the lower level will be pruned.

5.4 Iterative MIMO Detection with Modified FP and SE Sphere Decoder

The authors in [68] looked at the sphere decoding from the viewpoint of stack sequential decoding algorithm [93] and developed two new sphere decoding algorithms. Algorithm I in [68] is based on FP enumeration by updating the upper bound at each level to avoid enumerating previously examined partial paths. Algorithm II in [68] is used to perform SE enumeration with pre-processing and ordering. Numerical results shows significant reductions in the computational complexity with near ML detection performance compared to previously proposed sphere decoding algorithms. However, the output of the FP and SE algorithms in [68] is the lattice point of minimum Euclidean Distance to the received signal, which is essentially the ML detection criteria as shown in equation (5.7). In this section, we modify the FP and SE algorithms to estimate the MAP probability of the received symbol sequence by introducing the accumulated *a priori* information metric in the tree search.

5.4.1 MAP Criteria Reformulation

Starting from the MAP criteria in equation (5.8), we assume that the transmitted symbols $X_0, X_1 \ldots, X_{2N_T-1}$ are independent, the *a priori* probability $P(\mathbf{X})$ can be expressed as:

$$P(\mathbf{X}) = \prod_{k=0}^{2N_T-1} P(X_k) = \exp(\sum_{k=0}^{2N_T-1} \ln P(X_k)). \tag{5.23}$$

Hence, the MAP criteria in equation (5.8) can be reformulated as:

$$\begin{aligned} \widehat{\mathbf{X}} &\approx \arg\max_{\mathbf{X}\in\mathcal{U}} P(\mathbf{Y}|\mathbf{X})P(\mathbf{X}) \\ &\approx \arg\max_{\mathbf{X}\in\mathcal{U}} \exp(-\frac{\|\mathbf{Y}-\mathbf{H}\mathbf{X}\|^2}{2\sigma_w^2} + \sum_{k=0}^{2N_T-1} \ln P(X_k)) \end{aligned}$$

$$\approx \quad \arg\min_{\mathbf{X}\in\mathcal{U}}(\|\mathbf{Y}-\mathbf{HX}\|^2 - 2\sigma_w^2 \sum_{k=0}^{2N_T-1} \ln P(X_k)). \tag{5.24}$$

The modified FP and SE algorithms narrow down the search region as:

$$\|\mathbf{Y}-\mathbf{HX}\|^2 - 2\sigma^2 \sum_{k=0}^{2N_T-1} \ln P(X_k) \leq C. \tag{5.25}$$

By performing QR decomposition, the channel matrix $\mathbf{H}$ can be expressed as:

$$\mathbf{H} = \begin{bmatrix} \mathbf{Q} & \mathbf{Q}' \end{bmatrix} \begin{bmatrix} \mathbf{R} \\ \mathbf{0} \end{bmatrix}. \tag{5.26}$$

where $\mathbf{Q}$ is a $2N_R \times 2N_T$ unitary matrix, $\mathbf{Q}'$ is $2N_R \times (2N_R - 2N_T)$ unitary matrix, $\mathbf{R}$ is a $2N_T \times 2N_T$ upper triangular matrix, and $\mathbf{0}$ is $(2N_R - 2N_T) \times 2N_T$ zero matrix. Knowing that:

$$\begin{bmatrix} \mathbf{Q} & \mathbf{Q}' \end{bmatrix}^H \begin{bmatrix} \mathbf{Q} & \mathbf{Q}' \end{bmatrix} = \mathbf{I}_{2N_R}, \tag{5.27}$$

Take (5.26) into (5.25), we have

$$\begin{aligned} \| \begin{bmatrix} \mathbf{Q} & \mathbf{Q}' \end{bmatrix} (\mathbf{Y}-\mathbf{HX})\|^2 - 2\sigma_w^2 \sum_{k=0}^{2N_T-1} \ln P(X_k) &\leq C \\ \|\mathbf{Q}^H\mathbf{Y}-\mathbf{RX}\|^2 - 2\sigma_w^2 \sum_{k=0}^{2N_T-1} \ln P(X_k) &\leq C \\ \|\mathbf{Y}'-\mathbf{RX}\|^2 - 2\sigma_w^2 \sum_{k=0}^{2N_T-1} \ln P(X_k) &\leq C - \|\mathbf{Q}'^H\mathbf{Y}\|^2, \end{aligned} \tag{5.28}$$

where $\mathbf{Y}' = \mathbf{Q}^H\mathbf{Y}$. By expanding the term $\|\mathbf{Y}'-\mathbf{RX}\|^2$, we can further simplify (5.28) as follows:

$$\sum_{k=0}^{2N_T-1} |Y_k^{'} - \sum_{j=k}^{2N_T-1} R_{k,j}X_j|^2 - 2\sigma_w^2 \sum_{k=0}^{2N_T-1} \ln P(X_k) \leq C^{'}, \tag{5.29}$$

where $C^{'}$ is the newly defined sphere radius.

5.4.2 Iterative MIMO Detection with Modified FP Algorithm

In this Section, we present the iterative MIMO detection with modified FP algorithm. Fig. 5.2 illustrates the algorithm flow. The modules highlighted are modified for the new algorithm. The algorithm can be summarized in the following six steps, and the detailed description of each step is presented afterwards.

- Step 1: Initialization
- Step 2: Compute bounds
  - Compute the accumulated *a priori* information metric
  - Compute the branch metric
  - Compute the path metric
  - Compute lower and upper bounds
- Step 3: Enumerate the tree node
- Step 4: Go to next or upper level if out of bounds
- Step 5: Update the Node
- Step 6: Found candidate signal vector
  - Save the vector
  - Update bounds
  - Go to upper level

The algorithm starts from Step 1 Initialization, which initializes all the parameters required for the tree node search. These parameters include the received signal and upper triangular matrix from preprocessing, the search sphere radius, branch metric, path metric, and the accumulated *a priori* information metric, etc. Then the search starts from the top level of the tree and computes the lower and upper bounds for the tree node enumeration in Step 2. We include the computation of the accumulated *a priori* information metric in addition to the branch metric and path metric. And the *a priori* information is also utilized in the computation of the boundaries.

In Step 3, the tree node is enumerated in an ascending order starting from the lower bound. Step 4 directs the search one level up or one level down depending

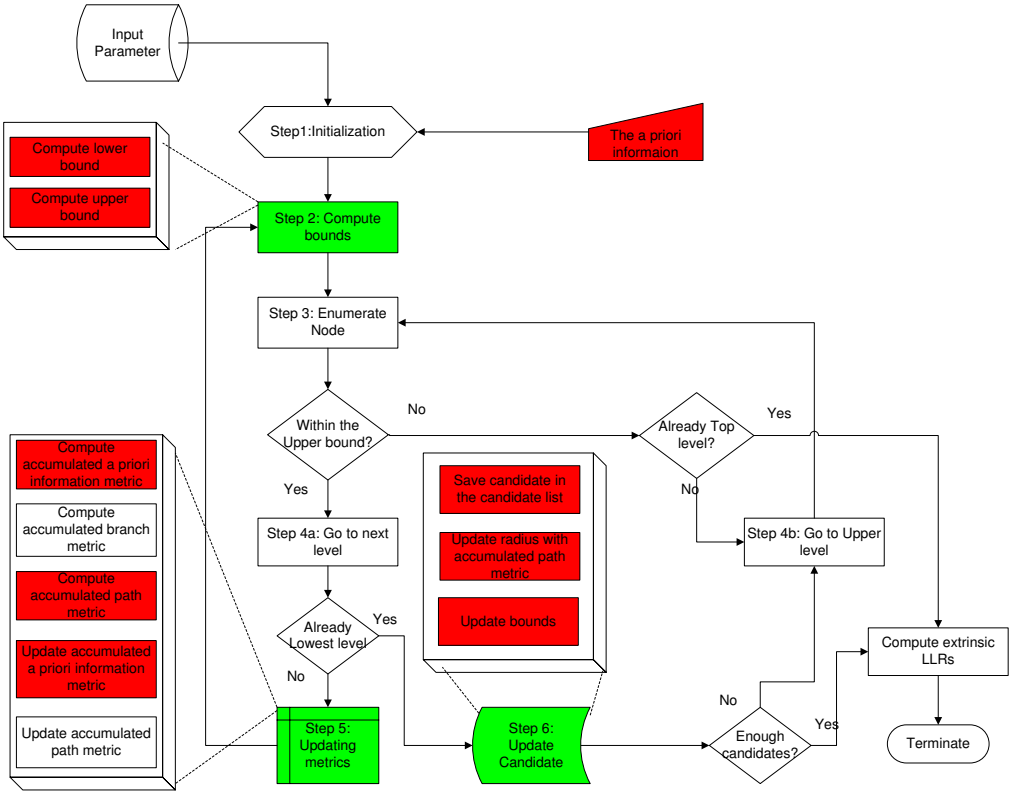

Figure 5.2: Algorithm flow chart for iterative MIMO detection with modified FP algorithm

on whether the enumerated node is within the boundaries. Step 5 updates the accumulated *a priori* information metric, the branch metric, and the path metric if the tree node survives. Once the search reaches the lowest level with surviving tree node, it means a candidate signal vector is found. Step 6 saves the candidate signal vector and continue to search other possible candidates.

Mathematically, given $\mathbf{Y}'$, $\mathbf{R}$, the *a priori* information $P(\widehat{\mathbf{X}})$, and the radius C', the modified FP algorithm can be outlined as follows:

1. Set tree search level index $i := 2N_T - 1$, path metric $\vartheta_i := 0$, branch metric $\zeta_i := 0$, accumulated *a priori* information metric $\delta_i := 0$, constellation index $\lambda_j := 0, j \in [0, 2N_T - 1]$, constellation set Φ, and current radius $d := C'$.

2. If $(d < \vartheta_i)$
   Go to Step 4.
   Else {
   Compute the lower bound $\mathcal{L}_i := \left\lceil \frac{Y_i' - \zeta_i - \sqrt{d - \vartheta_i}}{R_{i,i}} \right\rceil$,

Compute the upper bound $\mathcal{V}_i := \left\lfloor \frac{Y_i^{'} - \zeta_i + \sqrt{d - \vartheta_i}}{R_{i,i}} \right\rfloor$,
$\lambda_i := idx(\mathcal{L}_i, \Phi) - 1$, $idx(\cdot)$ is the operator that finds the index in constellation set Φ.}

3. $\lambda_i := \lambda_i + 1$, $\widehat{X}_i := \Phi(\lambda_i)$
   If $(\widehat{X}_i \leq \mathcal{V}_i)$
   $\widehat{X}_i$ Within the interval, go to Step 5.
   Else
   $\widehat{X}_i$ Outside the interval, go to Step 4.

4. If $(i == 2N_T - 1)$
   Go to Step 7.
   Else
   Go back to upper level $i := i + 1$, then go to Step 3.

5. If $(i > 0)$ {
   Update branch metric $\zeta_{i-1} := \sum_{k=i}^{2N_T - 1} R_{i-1,k} \widehat{X}_k$,
   Update accumulate a priori information metric $\delta_i := \delta_{i-1} + 2\sigma_w^2 \ln P(\widehat{X}_i)$
   Update path metric $\vartheta_{i-1} := \vartheta_i + |Y_i^{'} - \zeta_i - R_{i,i}\widehat{X}_i|^2 - \delta_i$,
   Go to next level $i := i - 1$, then go to Step 2. }
   Else if$(i == 0)$
   Go to Step 6.

6. If $(d > \vartheta_i + |Y_i^{'} - \zeta_i - R_{i,i}\widehat{X}_i|^2 - \delta_i)$ {
   Updating the radius $d := \vartheta_i + |Y_i^{'} - \zeta_i - R_{i,i}\widehat{X}_i|^2 - \delta_i$,
   Save $\widehat{\mathbf{X}}$ in candidate list $\mathcal{U}$,
   Go back to upper level $i := i + 1$, then go to Step 7.}

7. If ($C^{'}$ is within Upper bound)
   If(List has less points as required)
   Increase the radius $C^{'}$, then go to Step 1.
   Else
   Terminate.

The new algorithm differs from the original FP algorithm in that it includes *a priori* information metric δ_i accumulated along the way of tree search. The path metric ϑ_i is determined not only by the accumulated branch metric ζ_i, but also the additional accumulated priori information metric δ_i. If the visited nodes diverge from the transmitted signal, δ_i is likely to grow, which in turn leads to an increasing

path metric ϑ_i and a dramatically reduced search radius in $(i+1)^{th}$ level. Therefore, invalid paths will be identified and pruned at an early stage, and the number of tree nodes visited will be reduced.

5.4.3 Iterative MIMO detection with modified SE algorithm

In this Section, we present the iterative MIMO detection with modified SE algorithm. Fig. 5.3 illustrates the algorithm flow as described above. The algorithm is summarized as follows, and the detailed description of each step is presented afterwards.

- Step 1: Initialization
- Step 2: Enumerate the tree node
  - Compute the ZF-DFE estimate
  - Compute the *a priori* information metric
  - Compute the branch metric
  - Compute the path metric
- Step 3: Tree node check with Updates
  - Within the sphere, accumulate the three metrics
  - Outside the sphere, go to Step 6
  - Outside the sphere and no more neighbor node, go to upper level
- Step 4: Go to next or upper level if outside the sphere or no more neighbor node
- Step 5: A candidate signal vector is found, save the vector and go to upper level
- Step 6: Zig-zag visit neighbor node

Similar to the modified FP algorithm, the modified SE algorithm starts from Step 1 Initialization. In Step 2, the algorithm computes the ZF-DFE estimate and the metrics. We include the computation of the accumulated *a priori* information metric in addition to the computation of the branch metric and path metric. In Step 3, the tree node is checked to see whether it is within the search radius.

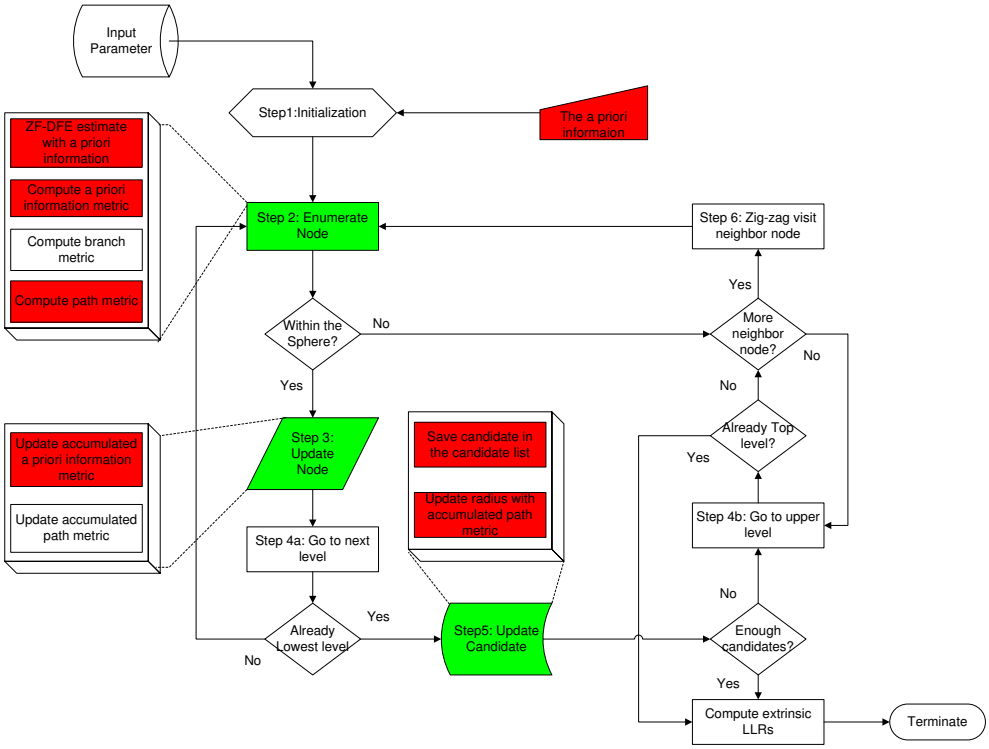

Figure 5.3: Algorithm flow chart for iterative MIMO detection with modified SE algorithm

Compared to the original SE algorithm [67,68], the *a priori* information is utilized in the computation of the accumulated path metric, which is compared with the search radius to determine whether the tree node is within the sphere. Step 4 directs the tree search one level up or one level down or zig-zag in the same level depending on whether the enumerated node is within the sphere. At the same time, it updates the accumulated *a priori* information metric, the branch metric, and the path metric if the new tree node is enumerated. Once the tree search reaches the lowest level and the tree node is survived, it means a candidate signal vector is found. Step 5 saves the candidate signal vector and continues to search for other possible candidates. Step 6 performs the zig-zag searching of the neighboring tree node.

Mathematically, given $\mathbf{Y}'$, $\mathbf{R}$, the *a priori* information $P(\widehat{\mathbf{X}})$, and the radius C', the modified SE algorithm can be outlined as follows:

1. Set tree search level index $i := 2N_T - 1$, path metric $\vartheta_i := 0$, branch metric $\zeta_i := 0$, accumulated *a priori* information metric $\delta_i := 0$, zig-zag search index $\lambda_j := 0, j \in [0, 2N_T - 1]$, radius increasing index $\Delta := 0$, and current radius

$d := C'$.

2. If (the node is first time visited) {
   Compute the ZF-DFE estimate of transmitted symbol at level i as $\widehat{X}_i = \langle (Y_i^{'} - \zeta_i)/R_{i,i} \rangle$, where $\langle \cdot \rangle$ is operator that finds the nearest constellation point.
   Create zig-zag lookup table Φ_i for constellation point $\widehat{X}_i$. Define $|\Phi_i|$ as the number of possible zig-zag points.
   Compute the accumulated *a priori* information metric $\delta_i := \delta_{i-1} + 2\sigma_w^2 \ln P(\widehat{X}_i)$.
   }
   Else If ($\lambda_i == |\Phi_i| - 1$)
   If ($i == 2N_T - 1$)
   Go to Step 7.
   Else
   Reset the zig-zag scan $\lambda_i := 0, \widehat{X}_i = \Phi_i(\lambda_i)$,
   Go back to upper level $i := i + 1$, then go to Step 6.
   Else
   go to Step 6.

3. If (the current radius is less than the path metric at level i, i.e. $d < \vartheta_i + |Y_i^{'} - \zeta_i - R_{i,i}\widehat{X}_i|^2 - \delta_i$)
   Out of sphere, go to Step 4.
   Else If ($i > 0$) {
   Update branch metric $\zeta_{i-1} := \sum_{k=i}^{2N_T-1} R_{i-1,k}\widehat{X}_k$,
   Update path metric $\vartheta_{i-1} := \vartheta_i + |Y_i^{'} - \zeta_i - R_{i,i}\widehat{X}_i|^2 - \delta_i$,
   Go to next level $i := i - 1$, then go to Step 2. }
   Else If ($i == 0$)
   go to Step 5.

4. If($i == 2N_T - 1$)
   If ($\lambda_i < |\Phi_i| - 1$)
   Perform zig-zag scan $\lambda_i := \lambda_i + 1$, $\widehat{X}_i = \Phi_i(\lambda_i)$.
   Else
   Go to Step 7.
   Else
   Go back to upper level $i := i + 1$, then go to Step 6.

5. A point within the sphere is found, save $\widehat{\mathbf{X}}$ in the candidate list $\mathcal{U}$. Update the radius $d := \vartheta_i + |Y_i^{'} - \zeta_i - R_{i,i}\widehat{X}_i|^2 - \delta_i$, then go back to upper level $i := i + 1$, go to Step 6.

6. Perform zig-zag scan $\lambda_i := \lambda_i + 1$,
   while(No zig-zag scan available, i.e. $\lambda_i > |\Phi_i| - 1$) {
   Reset zig-zag scan $\lambda_i := 0$,
   Go back to upper level $i := i + 1$.
   If $(i > 2N_T - 1)$
   Go to Step 7.
   Perform zig-zag scan $\lambda_i := \lambda_i + 1$. }
   Compute the accumulated *a priori* information metric $\widehat{X}_i = \Phi_i(\lambda_i)$, $\delta_i := \delta_{i-1} + 2\sigma_w^2 \ln P(\widehat{X}_i)$, go to Step 3.

7. If ($C^{'}$ is within Upper bound)
   If(List has less points as required)
   Increase the radius $C^{'}$, $\Delta := \Delta + 1$, go to Step 1.
   Else
   Terminate.

Unlike the modified FP algorithm using the lower and upper boundary adaption to prune the less likely path, the modified SE algorithm eliminates the path by making the comparison between the current available sphere radius and the path metric. A large path metric ϑ_i is more likely to be outside the available sphere radius. Hence, further searches starting from less reliable enumerated nodes to its children nodes will not be likely.

5.5 Further Modifications on Iterative SE Algorithm

The SE algorithm has a drawback that there is a performance loss due to the poor performance of the ZF-DFE estimate of the symbol at each level of the tree search. The authors in [68] proposed many pre-processing algorithms to enhance the initial estimate, such as those using ordered ZF-DFE and MMSE estimates, at a cost of increasing complexity for the pre-processing. Similarly, the authors in [59] proposed to initialize the K-best sphere decoder by LMMSE estimate rather than the conventional QR decomposition. However, the LMMSE detection requires a

matrix inversion, which is still considered as the operation with highest complexity. In this section, we present two novel schemes to improve the ZF-DFE estimate by utilizing the *a priori* information. These two novel schemes aim to improve the performance and reduce the computational complexity even further over iterations.

5.5.1 Improved ZF-DFE Estimate Based on Approximated *a priori* Information

In Step 2, the ZF-DFE estimate of transmitted signal at i^{th} level depends on the ML metric, which will affect the convergence of the tree search and introduce performance loss [68]. With iterative detection and decoding, the ZF-DFE estimates based on the MAP metric will be more accurate. Hence, the objective of this novel scheme is to incorporate the *a priori* information, derived from the channel decoder output, to obtain more accurate ZF-DFE estimates. The *a priori* information metric $-2\sigma_w^2 \sum_{k=0}^{2N_T-1} \ln P(X_k)$ as shown in equation (5.25) is, however, in the logarithm form, which has infinite order in Taylor's expansion. This means that a polynomial with infinite order has to be solved, which is impractical.

Nevertheless, it can be seen that in (5.28), $\|\mathbf{Y}' - \mathbf{R}\mathbf{X}\|^2$ is in quadratic form. Intuitively, if the *a priori* information metric can be approximated in the quadratic form as shown in [74], the ZF-DFE estimates can still be obtained by backward substitutions, which is a practical solution. Hence, by expressing the *a priori* information metric in the Taylor's series and ignoring the higher order terms, we have the following:

$$-2\sigma_w^2 \sum_{k=0}^{2N_T-1} \ln P(X_k) \approx \mathbf{X}^H \alpha \mathbf{X} + \beta^H \mathbf{X} + \gamma, \tag{5.30}$$

where α is $2N_T \times 2N_T$ diagonal matrix with diagonal elements being the quadratic coefficients, β is $2N_T \times 1$ vector contains linear coefficients, and $\gamma = \sum_{k=0}^{2N_T-1} \gamma_k$ is the scalar coefficient. Hence, the left hand side of (5.28) can be reformulated as:

$$\begin{aligned} \mathcal{J} &= (\mathbf{Y}' - \mathbf{R}\mathbf{X})^H (\mathbf{Y}' - \mathbf{R}\mathbf{X}) + \mathbf{X}^H \alpha \mathbf{X} + \beta^H \mathbf{X} + \gamma \\ &= \mathbf{X}^H (\mathbf{R}^H \mathbf{R} + \alpha)\mathbf{X} - (\mathbf{Y'}^H \mathbf{R} - 0.5\beta^H)\mathbf{X} \\ &\quad -\mathbf{X}^H (\mathbf{R}^H \mathbf{Y}' - 0.5\beta) + \mathbf{Y'}^H \mathbf{Y}' + \gamma. \end{aligned} \tag{5.31}$$

The optimal solution can be obtained by taking the derivative of $\mathcal{J}$ with respect

to $\mathbf{X}$ as follows:

$$\frac{\partial \mathcal{J}}{\partial \mathbf{X}} = -2(\mathbf{R}^H\mathbf{Y}' - 0.5\beta) + 2(\mathbf{R}^H\mathbf{R} + \alpha)\mathbf{X} = 0. \tag{5.32}$$

By taking the QR decomposition $(\mathbf{R}^H\mathbf{R}+\alpha) = \mathbf{UV}$, (5.32) can be solved by using a ZF-DFE estimate as:

$$\mathbf{V}\widehat{\mathbf{X}} = \mathbf{Y}'', \tag{5.33}$$

where $\mathbf{U}$ is $2N_T \times 2N_T$ unitary matrix, $\mathbf{V}$ is $2N_T \times 2N_T$ upper triangular matrix, and $\mathbf{Y}'' = \mathbf{U}^{-1}(\mathbf{R}^H\mathbf{Y}' - 0.5\beta)$. Therefore, the ZF-DFE estimate of X_i at level i of tree search in Step 2 can be reformulated as:

$$\widehat{X}_i = \langle (Y_i^{''} - \zeta_i^{'})/V_{i,i} \rangle, \tag{5.34}$$

where the branch metric is given by $\zeta_i^{'} := \sum_{k=i}^{2N_T-1} V_{i-1,k}\widehat{X}_k$.

The coefficients of α, β, and γ can be obtained by following the LS approximation approach [106]. More specifically, we have the following minimization problem:

$$\begin{aligned} \{\alpha, \beta, \gamma\} &= \arg\min(\| - 2\sigma_w^2 \sum_{k=0}^{2N_T-1} \ln P(X_k) \\ &\quad -(\mathbf{X}^H\alpha\mathbf{X} + \beta^H\mathbf{X} + \gamma)\|^2). \end{aligned} \tag{5.35}$$

The signals transmitted at different tree search level i are independent to each other, hence, the coefficients of α_i, β_i, and γ_i at the i^{th} level can be obtained by solving the following three equations:

$$\alpha_i \sum_{k=0}^{M-1} \widehat{X}_k^2 + \beta_i \sum_{k=0}^{M-1} \widehat{X}_k + \gamma_i M = -2\sigma_w^2 \sum_{k=0}^{M-1} \ln P(\widehat{X}_k), \tag{5.36}$$

$$\alpha_i \sum_{k=0}^{M-1} \widehat{X}_k^3 + \beta_i \sum_{k=0}^{M-1} \widehat{X}_k^2 + \gamma_i \sum_{k=0}^{M-1} \widehat{X}_k = -2\sigma_w^2 \sum_{k=0}^{M-1} \widehat{X}_k \ln P(\widehat{X}_k), \tag{5.37}$$

$$\alpha_i \sum_{k=0}^{M-1} \widehat{X}_k^4 + \beta_i \sum_{k=0}^{M-1} \widehat{X}_k^3 + \gamma_i \sum_{k=0}^{M-1} \widehat{X}_k^2 = -2\sigma_w^2 \sum_{k=0}^{M-1} \widehat{X}_k^2 \ln P(\widehat{X}_k), \tag{5.38}$$

where M is the size of signal enumeration set. For QPSK, $M = 2$. For 16QAM,

$M = 4$. The solution is given by:

$$\alpha_i = \frac{-2\sigma_w^2 \sum_{k=0}^{M-1} \ln P(\widehat{X}_k) \sum_{k=0}^{M-1} \widehat{X}_k^2 + 2\sigma_w^2 M \sum_{k=0}^{M-1} \widehat{X}_k^2 \ln P(\widehat{X}_k)}{(\sum_{k=0}^{M-1} \widehat{X}_k^2)^2 - M \sum_{k=0}^{M-1} \widehat{X}_k^4}, \tag{5.39}$$

$$\beta_i = -\frac{2\sigma_w^2 \sum_{k=0}^{M-1} \widehat{X}_k \ln P(\widehat{X}_k)}{\sum_{k=0}^{M-1} \widehat{X}_k^2}, \tag{5.40}$$

$$\gamma_i = -\frac{2\sigma_w^2 \sum_{k=0}^{M-1} \ln P(\widehat{X}_k) + \alpha_i \sum_{k=0}^{M-1} \widehat{X}_k^2}{M}. \tag{5.41}$$

Substituting α, β and γ back in to equation (5.31), we can solve equation (5.32)-(5.33). Finally, we summarize the Step 2 in Section 5.4.3 as follows:

2) If (the node is visited for the first time) {
    If (first iteration)
        Compute the ZF-DFE estimate as $\widehat{X}_i = \langle (Y_i^{'} - \zeta_i)/R_{i,i} \rangle$.
    Else {
        Compute α, β, and γ.
        Compute the ZF-DFE estimate as $\widehat{X}_i = \langle (Y_i^{''} - \zeta_i^{'})/V_{i,i} \rangle$.
    }
    Create zig-zag lookup table Φ_i for constellation point $\widehat{X}_i$.
    Define $|\Phi_i|$ as the number of possible zig-zag points.
    Compute the accumulated *a priori* information metric $\delta_i := \delta_{i-1} + 2\sigma_w^2 \ln P(\widehat{X}_i)$.
}
Else If ($\lambda_i == |\Phi_i| - 1$)
    If ($i == 2N_T - 1$)
        Go to Step 7.
    Else
        Reset zig-zag scan $\lambda_i := 0, \widehat{X}_i = \Phi_i(\lambda_i)$,
        Go back to upper level $i := i + 1$, then go to Step 6.
Else
    Go to Step 6.

5.5.2 Improved Tree Search Based on Starting Node *a priori* Zig-Zag Trial

The approach in this scheme is to make a trial on another constellation point rather than the ZF-DFE estimate. In sphere decoding, randomly picking points at the starting node of the tree search may not be an efficient approach. Hence, we can do this on *a priori* zig-zag trial basis to visit the neighboring constellation point of ZF-DFE estimate. The idea is to select the starting node with the best *a priori* probability among the nodes around the original ZF-DFE estimates. The algorithm is summarized in the following steps:

- Compute the ZF-DFE estimates
- Examine the *a priori* probability of the ZF-DFE estimates
- Perform zig-zag trial to visit the neighboring nodes of the ZF-DFE estimates
- Examine the *a priori* probability of the neighboring nodes around the ZF-DFE estimates
- Select the starting node associating with the highest *a priori* probability for the subsequent tree search

Subsequently, Step 2 in Section 5.4.3 can be modified as follows:

2) If (the node is visited for the first time) {
Compute the ZF-DFE estimate of transmitted symbol at level i as $\widehat{X}_i = \langle (Y_i^{'} - \zeta_i)/R_{i,i} \rangle$. Create zig-zag lookup table Φ_i for constellation point $\widehat{X}_i$. Define $|\Phi|$ as the number of possible zig-zag points.
If ($i == 2N_T - 1$) {
while ($\lambda_i < |\Phi_i|$) {
$\lambda_i := \lambda_i + \Delta + 1$, $X_i = \Phi_i(\lambda_i)$.
Compute the *a priori* probability of X_i, i.e. $P(X_i)$
$\widehat{X}_i = X_i$ if X_i has higher *a priori* probability $P(X_i)$.
}
}
Compute the accumulated *a priori* information metric $\delta_i := \delta_{i-1} + 2\sigma_w^2 \ln P(\widehat{X}_i)$.
}
Else If ($\lambda_i == |\Phi_i| - 1$)
If ($i == 2N_T - 1$)

Go to Step 7.

Else

Reset zig-zag scan $\lambda_i := 0, \widehat{X}_i = \Phi_i(\lambda_i)$,

Go back to upper level $i := i + 1$, then go to Step 6.

Else

Go to Step 6.

5.6 Complexity of Iterative Receiver with Sphere Decoder

The sphere decoder algorithms are developed for the so-called *integer least-square* problem, which is to find the "closest" lattice point to the transmitted signal in either finite or infinite sense. Compared to the standard least square problem, the solution of *integer least-square* is much more difficult because the solution can only be found through searching over the discrete signal space rather than the simple pseudo-inverse approach. In fact, the solution of the *integer least-square* problem is generally NP hard, both in a worst case sense as well as an average sense. Therefore, it is very difficult to find the exact complexity for the sphere decoder algorithms. Nevertheless, [65, 110] suggested that the complexity of the sphere decoder algorithms are proportional to the number of lattice points visited. And in general, the sphere decoding algorithms have the worst case and average complexity that is exponential in the number of searching dimension $2N_T$. However, in communication applications, the transmitting signal is within a finite alphabet, and the received signal is the lattice point perturbed by the additive noise with known statistics. Hence, the expected complexity is a relevant figure of merit. The authors in [110] concluded that over a wide range of SNRs including the high SNR region, the expected complexity of the sphere decoder is polynomial (often roughly cubic).

By examining the sphere decoder algorithm carefully, we observed that the complexity of sphere decoders depends on three factors. The first factor is the noise variance (σ^2) or SNR. The second factor is the signal constellation type. And the third factor is the search radius. The SNR determines how noisy the wireless channel is, the signal constellation determines the enumeration range of the possible signal point, and the search radius determines how far we are going to search in the signal space. For a system with fixed configuration, the first two factors are out of the design control, only the third factor varies between algorithms. The

iterative sphere decoder algorithms in this Chapter is the variation to the standard sphere decoder mentioned in [65]. The main difference is the accumulated *a priori* information metric δ_i. Rearranging equation (5.25), we have

$$\|\mathbf{Y}-\mathbf{HX}\|^2 \leq C + \underbrace{2\sigma_w^2 \sum_{k=0}^{2N_T-1} \ln P(X_k)}_{\delta_{2N_T-1}}. \tag{5.42}$$

It can be observed that once the search radius is determined, the accumulated *a priori* information metric adjusts the radius in each search dimension. Obviously, depending on how the points are enumerated, such adjustment can be either enlarge the radius or shrink the radius, subject to the reliability of the visited node in each iteration. Following the similar approach in [65], we have a rough estimate on complexity of the iterative receivers over iterations, which is on the average number of nodes visited in each iteration. For QPSK modulation, we have

$$\mathcal{C}^n \approx \sum_{i=0}^{N_T-1} \sum_{j=0}^{2i} \begin{pmatrix} 2i \\ j \end{pmatrix} \Gamma\left(\frac{C+\delta_{2N_T-1}^{n-1}}{\sigma^2+j}, N_R-N_T+i\right), \tag{5.43}$$

and for 16QAM modulation, we have

$$\mathcal{C}^n \approx \sum_{i=0}^{N_T-1} \sum_{m} \frac{1}{2^{2i}} \sum_{j=0}^{2i} \begin{pmatrix} 2i \\ j \end{pmatrix} \phi_{2ij}(m) \Gamma\left(\frac{C+\delta_{2N_T-1}^{n-1}}{\sigma^2+j}, N_R-N_T+i\right), \tag{5.44}$$

where n means the n^{th} iteration, $\Gamma(\cdot,\cdot)$ is the normalized gamma function, and $\phi_{2ij}(m)$ is the coefficient of ϕ^m in the polynomial $(1+\phi+\phi^4+\phi^9)^j(1+2\phi+\phi^4)^{2i-j}$. Some remarks are worth noting. Firstly, the above analysis on the complexity does not take the preprocessing into account. We assume that the preprocessing operations, like QR decomposition, ZFE computation, etc., are common to all sphere decoding algorithms. Secondly, the actual addition and multiplication operations to determine which nodes to visit are not included in the complexity analysis. We believe that the number of these operations are not going to make significant influence on the complexity analysis because the number of nodes visited is the dominant factor in the system complexity. Thirdly, in the iterative sphere decoder algorithms, the accumulated *a priori* information metric is only available after each iteration. To estimate the average number nodes visited in the tree search, we need to know the radius of the search sphere at the current iteration, which is not available. Hence, we use the accumulated *a priori* information metric from the

previous iteration instead. Finally, although equation (5.43) and (5.44) give the rough estimation on the average number of nodes visited for the iterative sphere decoder, we do expect the accumulated *a priori* information metric to help improve the path metric so that the most invalid nodes and branches would be identified and pruned at an early stage. In this case, the number of tree nodes visited would be reduced over iterations.

5.7 Numerical Results

5.7.1 Simulation Setup

We consider a 4×4 MIMO spatial multiplexing system. The channel model for each transmit and receive antenna are independent flat Rayleigh fading channel. A rate-1/2 $(171, 133)_8$ convolutional code is used for channel coding. Each block of information bits has the length of 9216. The modulation includes QPSK and 16QAM. The data-driven sphere decoder techniques in this Chapter focuses on the detection method itself, which is MIMO block by block operated. We therefore use bit error rate as the most suitable performance metric. We compared the BER and complexity for the original sphere decoder algorithms and the iterative sphere decoder algorithms. We refer to the original FP and SE algorithm in [68] as "FP ML" and "SE ML" respectively, the iterative FP algorithm in Section 5.4.2 as "FP MAP", and the iterative SE algorithm in Section 5.4.3 as "SE MAP". The computation load is measured by the number of visited nodes in the tree search, which dominates the system complexity and indicates the convergence speed of algorithms.

5.7.2 Performance of Receivers with Sphere Decoder

Fig. 5.4 shows the BER performance for original FP and SE algorithms, and the iterative FP and SE algorithms after 4 iterations. It can be observed that the iterative sphere decoding algorithms have a 2dB gain for QPSK modulation, and 3dB gain for 16QAM modulation over the original sphere coding algorithms at an operating point $BER = 10^{-4}$. This observation suggests that the iterative receiver with proposed sphere decoding algorithms can achieve significant performance gain over the standard sphere decoders for the non-iterative receivers. Regarding the performance of different sphere decoding algorithms, it can be seen that the FP algorithm outperforms the SE algorithm by 0.5dB in QPSK and 1.5dB in 16QAM.

This is because the SE algorithms only visit the ZF-DFE estimate and its surrounding points, and go to the next dimension once a suitable point is found. Intuitively, if the ZF-DFE estimate is poor or is far away from the true transmitted signal, the performance of SE algorithms degrades. On the other hand, the FP algorithms visit all points between the lower and upper boundaries so that the FP algorithms cover more signal point candidate in the searching sphere. Hence, naturally, the FP algorithms have high probability to find the better candidates of the transmitted signal.

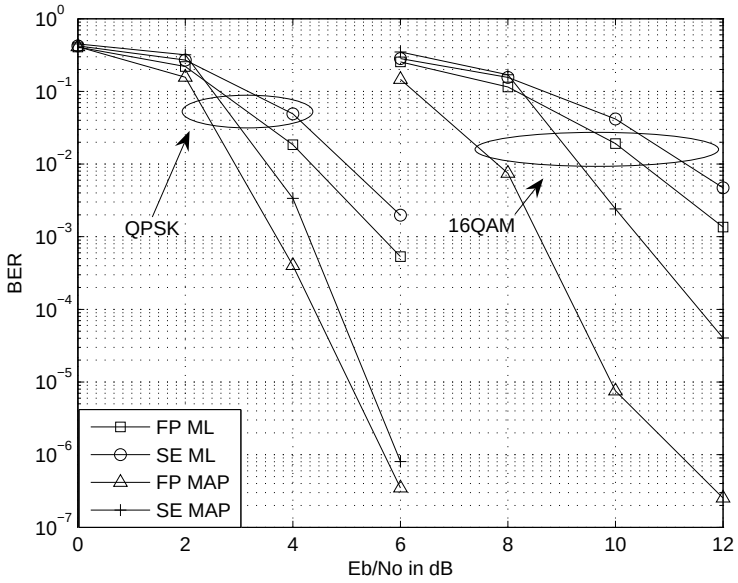

Figure 5.4: BER performance for original FP and SE algorithms, iterative FP and SE algorithms in a 4×4 MIMO spatial multiplexing system with QPSK and 16QAM modulation

Fig. 5.5 shows computation complexity for the iterative FP and SE algorithms over SNRs with 16QAM modulation. It can be seen that FP algorithm generally has higher complexity than the SE algorithm. Again, this is because the FP algorithm enumerates all the points within the admissible interval, while SE algorithm only searches the points around the ZF-DFE estimate. Therefore, a favorable complexity reduction can be obtained by the SE algorithm with performance loss compared to the FP algorithm shown in Fig. 5.4. As expected, by employing the *a priori* information, the complexity of modified algorithms can be further reduced over iterations because the additional *a priori* information metric improves the search by adjusting the overall path metric in addition to the Euclidian Distance. It helps identify and discard the inaccurate search path so that the unnecessary search

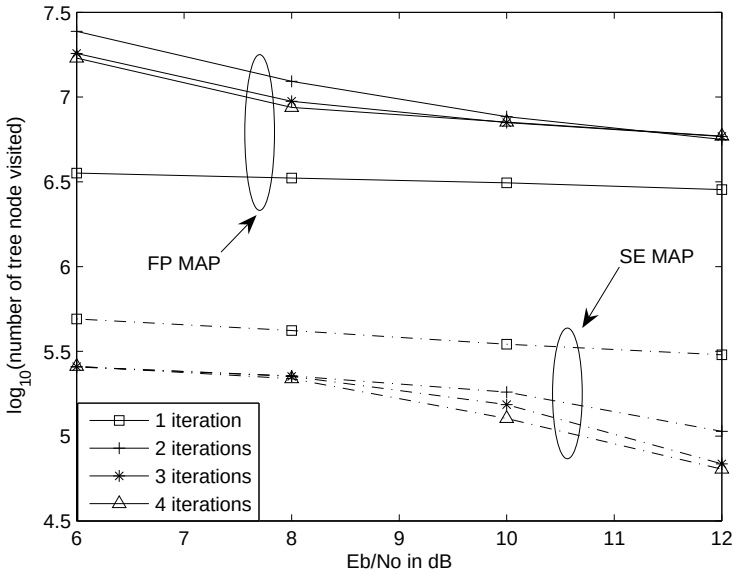

Figure 5.5: Computation complexity for iterative FP and SE algorithms over SNRs in a 4×4 MIMO spatial multiplexing system with 16QAM modulation

efforts can be saved.

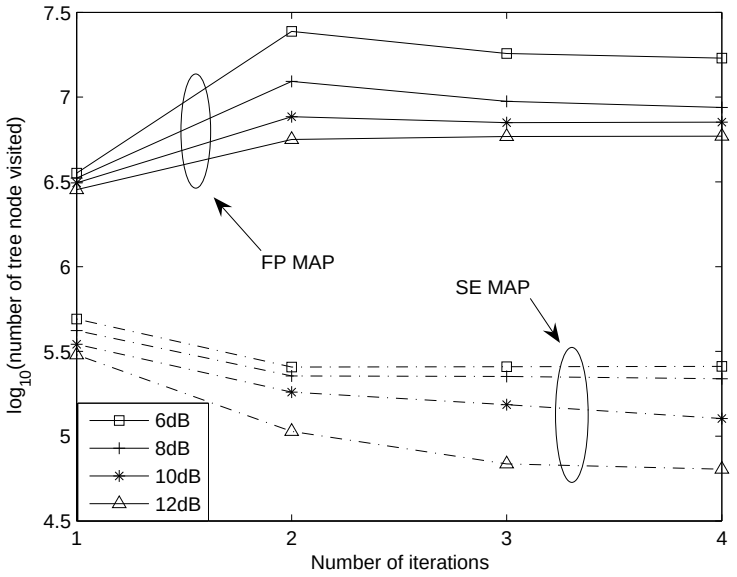

Figure 5.6: Computation complexity for iterative FP and SE algorithms over iterations in a 4×4 MIMO spatial multiplexing system with 16QAM modulation

Fig. 5.6 shows the computation complexity for the iterative FP and SE algorithms over iterations with 16QAM modulation. It is interesting to notice that

for the iterative FP algorithm, the complexity of the second iteration is higher than that for the first iteration in the low SNR region, and this difference becomes smaller as the SNR goes higher. However, this effect is not the case for the iterative SE algorithm. This is because the enumeration in the FP algorithm always starts from the lower bound and ends at higher bound. The lower/upper bound is random in the sense of the choice of the search radius. The actual transmitted signal may be far away from the lower and upper bounds, which results in a significant mismatch between the enumerated point starting from the lower/upper bound and the *a priori* information. This phenomenon leads to loose lower and upper bounds and slows down the tree search. Such effects become marginal with more stable priori information in the high SNR region as show in Fig. 5.6. Alternatively, for the iterative SE algorithm, the zig-zag tree search started from the ZF-DFE estimate, which is the unconstraint ML estimate without the *a priori* information. Then the ZF-DFE estimate is fine tuned by the *a priori* information. This is because the random nature of the lower/upper bounds subject to the search radius is avoided so that the significant mismatch between the ZF-DFE estimate and the *a priori* information is minimized.

5.7.3 Performance Comparison among SE Algorithms

In this section, we compare the performance among the SE algorithms. The scheme with improved ZF-DFE estimate based on quadratic approximated *a priori* information in 5.5.1 is referred as "Updated ZF-DFE MAP", and the scheme with improved tree search based on starting point *a priori* zig-zag trial in 5.5.2 is referred as "Zig-zag ZF-DFE MAP". #2 and #4 at the end of the legend means the 2^{nd} and 4^{th} iteration respectively, where # represents the number of iterations.

Fig. 5.7 shows BER performance for original "SE ML" algorithm and proposed iterative SE algorithms after 4 iterations. By picking up the operating point at BER of 10^{-4}, both schemes and the "Zig-zag ZF-DFE MAP" algorithms could improve the performance of the "SE MAP" algorithm even further for both modulation schemes. As an example, in the 16QAM modulation, the "Updated ZF-DFE MAP" has a 1dB gain over the "SE MAP". Such improvement becomes more significant when higher data modulation scheme is employed. This is because in lower modulation schemes, for example in QPSK modulation, the constellation point choices {-1,1} are limited in each level of the tree search. The "SE MAP" algorithm is good enough to pick the reliable points within the sphere. On the other hand, in higher modulation schemes, such as 16 QAM, the constellation point choices for

each level has increased to a larger set {-3,-1,1,3}. The performance loss due to a poor ZF-DFE estimate becomes more significant. The two schemes improve the ZF-DFE estimate so that additional performance gain can be obtained.

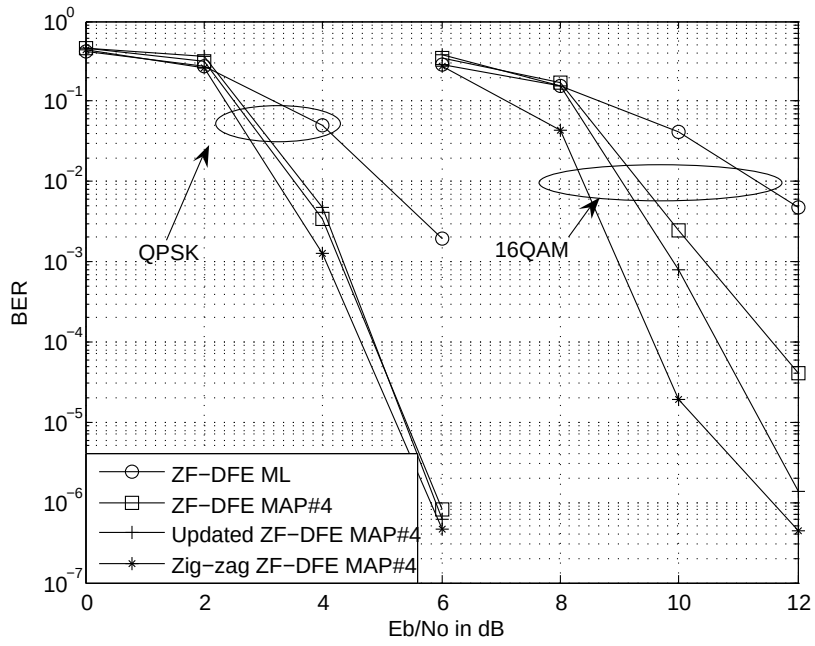

Figure 5.7: BER performance for the SE algorithms in a 4×4 MIMO spatial multiplexing system with QPSK and 16QAM modulation

Furthermore, compare Fig. 5.7 and Fig. 5.4, we observed that the "Zig-zag ZF-DFE MAP" algorithm have 2dB improvement over the "SE MAP" algorithm, which bring the performance gap within 0.5dB compared to the "FP MAP" algorithm. This is a significant improvement for the iterative SE algorithms in the sense that the iterative SE algorithms can approach the performance of the iterative FP algorithms while providing a significant complexity reduction.

Fig. 5.8 shows computation complexity for the SE algorithms with 16QAM modulation. As expected, by employing the *a priori* information, the complexity of the iterative SE algorithms can be further reduced over iterations because the *a priori* information metric in Step 3 and Step 5 adjusts the overall path metric adaptively according to the reliability of the enumerated point. Furthermore, the two modified iterative SE algorithms reduce the complexity even further in each iteration. This is expected because the better ZF-DFE estimate generates more reliable accumulated *a priori* information metric. The more reliable *a priori* information leads to not only a further performance gain shown in Fig. 5.7, but also fast convergence for sphere decoding over iterations.

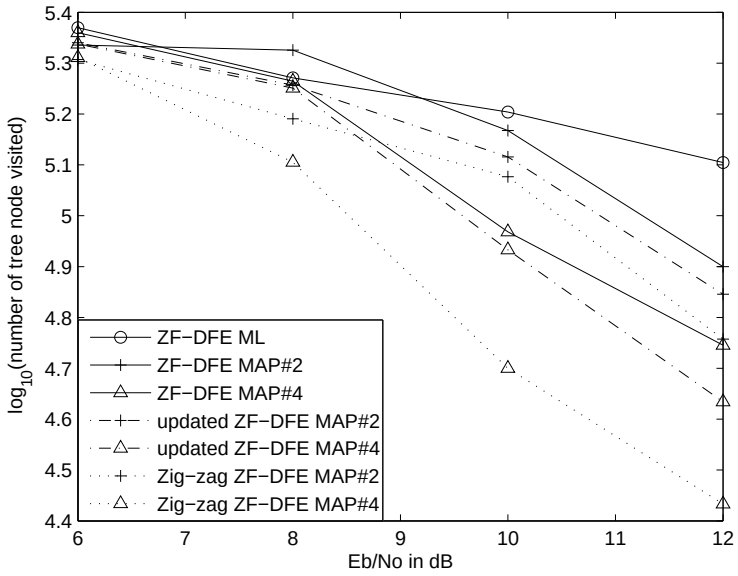

Figure 5.8: Computation complexity for SE algorithms over iterations in a 4×4 MIMO spatial multiplexing system with 16QAM modulation

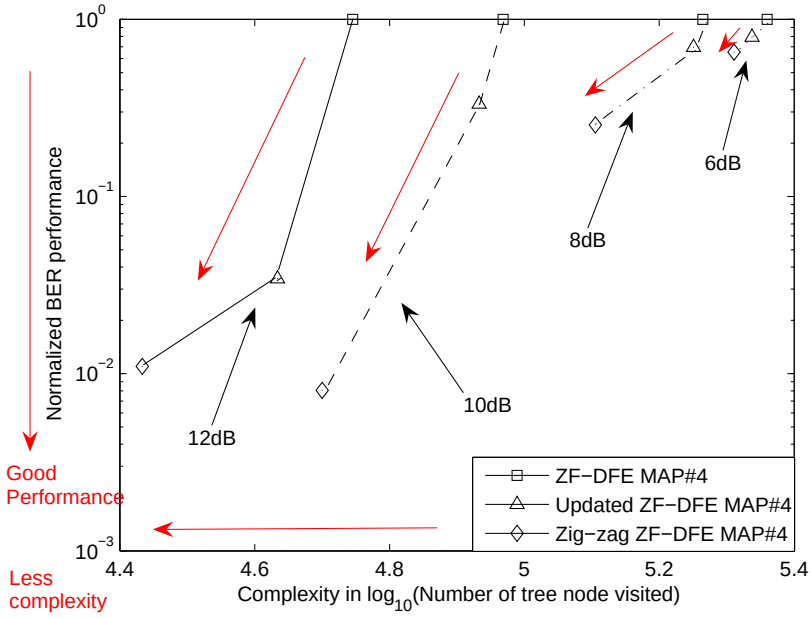

Figure 5.9: Normalized BER performance against complexity for the iterative SE algorithms at the 4^{th} iteration with 16QAM modulation

Finally, Fig. 5.9 shows the normalized BER performance against complexity among the iterative SE algorithms proposed in this chapter at the 4^{th} iteration with the 16QAM modulation. We take the BER performance of the "SE MAP"

algorithm as the reference to illustrate the performance and complexity benefits from the "Updated ZF-DFE MAP" and "Zig-zag ZF-DFE MAP" schemes. It can be seen that at different SNR points, the performance and complexity curves are moving towards the left and lower corner of the figure, which means the "Updated ZF-DFE MAP" scheme and the "Zig-zag ZF-DFE MAP" scheme improve the BER performance and achieve further complexity reduction from "ZF-DFE MAP" algorithm. It is worth mentioning the original SE algorithm, although it is not shown in the figure, only shows complexity reduction as SNR goes up. However, the iterative SE algorithms show both performance gain and complexity reduction.

5.8 Summary and Contributions

This chapter has investigated the FP and SE sphere decoder algorithms for the iterative receiver in the MIMO spatial multiplexing system configuration. The iterative FP and SE algorithms are developed by taking into account the *a priori* information to estimate the MAP probability of the received symbol sequence. In addition, two novel schemes are developed to further improve the performance and reduce the complexity over iterations for the iterative SE algorithm. Hence, significant performance gain can be achieved from iterative MAP approach over the conventional ML approach and complexity reduction can be obtained from SE algorithms.

Some specific contributions made in this chapter are as follows. First of all, the system model for sphere decoder algorithms in the MIMO spatial multiplexing system is investigated. A modified linear MIMO model for sphere decoder detection is presented. The conventional system model in the complex domain is modified to be in the real domain. The ML and MAP detection criteria are modified to suit the sphere decoder algorithms. Based on the modified system model, the literature review on the sphere decoder algorithms are presented. The original FP and SE algorithms in [68] are presented to illustrate the tree search steps to perform sphere decoding. The main difference between the FP and SE algorithms is the signal enumeration strategy.

Secondly, the iterative FP and SE algorithms is developed. The main advantage of the iterative algorithms compared to original algorithms is to include *a priori* information metric δ_i, which serves the accumulated *a priori* probability for the nodes visited along the way of tree search.

Thirdly, two novel schemes are developed for iterative SE algorithm to fur-

ther improve the performance and reduce the complexity over iterations. The first scheme is to improve the ZF-DFE estimate by using the quadratic approximation to the *a priori* information, the second scheme is to improve the tree search by employing a starting point with *a priori* zig-zag trial. Furthermore, a rough estimation on complexity of the iterative receivers over iterations are presented. This complexity estimation is measured on the average number of nodes visited in each iteration.

Finally, simulation results show that at least 2dB gain can be obtained for the QPSK modulation and 3dB gain can be obtained for the 16QAM modulation from the iterative MAP approach. And the iterative FP algorithms outperforms the iterative SE algorithms by 0.5dB in QPSK and 1.5dB in 16QAM. Among the iterative SE algorithms, the two novel schemes could improve the performance further up to 2dB in the 16QAM modulation. In addition to the bit error rate performance, the simulation results regarding the complexity show that the FP algorithms have the highest complexity, in both ML and MAP approach. Significant complexity reduction can be obtained from the SE algorithms with minor performance loss compared to FP algorithm. And the two novel schemes can also improve the complexity reduction over iterations even further.

Chapter 6

Iterative Receiver on Markov Chain Monte Carlo Methods

6.1 Introduction

In this Chapter, two novel MCMC methods for the MIMO detector, namely RSS-MCMC detector and the FST-MCMC, are presented. First of all, two reliability constraints are developed to separate the reliable bits from the unreliable bits. Then the reliable bits are treated as interference. The RSS-MCMC cancels the interference from the reliable bits obtained from the previous iteration while running the MCMC on the unreliable samples. Similar to RSS-MCMC, the FST-MCMC also works on the unreliable signal set by flipping the "ill conditioned" bits so that the Markov chain could visit more states. Both RSS-MCMC and FST-MCMC improve the performance at high SNR while the RSS-MCMC also reduces the complexity from drawing less samples in the Gibbs sampler. Similar to Chapter 5, in this chapter, we move to the detection method itself by assuming MIMO system is generic spatial multiplexed and the channel estimation is perfect.

6.2 Modified Linear MIMO Model for MCMC Methods

The MIMO spatial multiplexing system considered in this Chapter is shown in Fig. 6.1. The system model is as same as the one presented in Section 5.2. The modified linear MIMO model is obtained by separating the real and imaginary part of the complex system model, as shown in equation (5.1)-(5.6). At the iterative

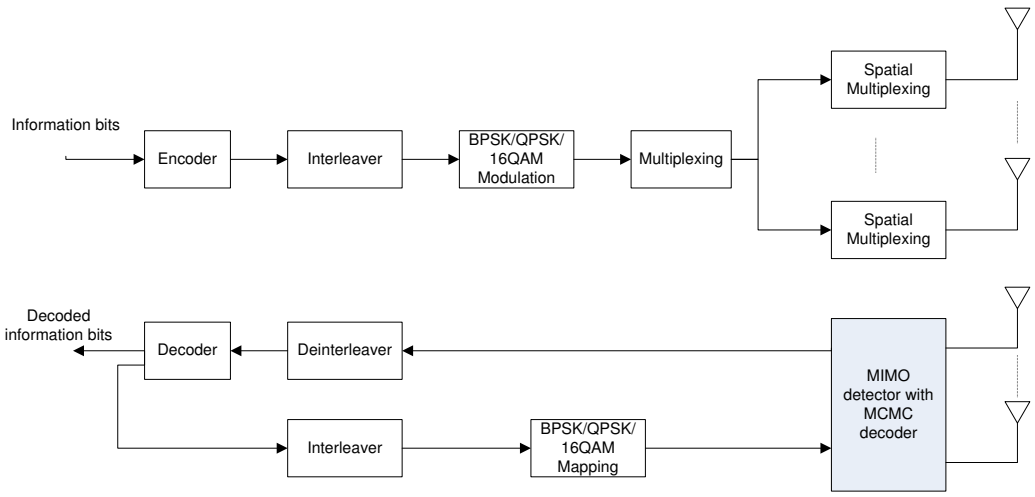

Figure 6.1: MIMO spatial multiplexing transmitter and iterative receiver with MCMC detector

receiver, in the first iteration, there is no *a priori* information, the MIMO detector performs the detection based on the ML criteria as:

$$\widehat{\mathbf{X}} = \arg\max_{\mathbf{X}\in\mathcal{U}} p(\mathbf{Y}|\mathbf{X}) = \arg\min_{\mathbf{X}\in\mathcal{U}} \|\mathbf{Y} - \mathbf{H}\mathbf{X}\|^2, \tag{6.1}$$

where $\mathcal{U}$ is the candidate signal set of dimension $2N_T$ collected by the MCMC processor. From the second iteration onwards, the sequence $\mathbf{X}$ can be divided into two sets, namely the reliable signal set $\mathbf{X}_R$ and unreliable signal set $\mathbf{X}_U$. The reliable signal set $\mathbf{X}_R$ contains the bits that satisfy the reliability constraint, are considered as correctly detected in the previous iteration. Similarly, the unreliable signal set $\mathbf{X}_U$ contains the bits that not satisfy the reliability constraint and are considered as unknown. Therefore, the system can be expressed as:

$$\begin{aligned} \mathbf{Y} &= \mathbf{H}\cdot\mathbf{diag}(\mathbf{e})\cdot\mathbf{X} + \mathbf{H}(\mathbf{I}_{2N_T} - \mathbf{diag}(\mathbf{e}))\mathbf{X} + \mathbf{N} \\ &= \mathbf{H}\mathbf{X}_U + \mathbf{H}\mathbf{X}_R + \mathbf{N}, \end{aligned} \tag{6.2}$$

where $\mathbf{X}_U = \mathbf{diag}(\mathbf{e})\mathbf{X}$, $\mathbf{X}_R = (\mathbf{I}_{2N_T} - \mathbf{diag}(\mathbf{e}))\mathbf{X}$, $\mathbf{diag}(\cdot)$ is the diagonal function, and $\mathbf{e}$ is the $2N_T \times 1$ vector which contains the position of the unreliable bits. In this Chapter, the RSS-MCMC method treats the reliable signal set $\mathbf{X}_R$ as the

interference and that can be deterministically removed as:

$$\begin{aligned}\mathbf{Y}_U &= \mathbf{Y} - \mathbf{H}\widehat{\mathbf{X}_R} \\ &= \mathbf{H}\mathbf{X}_U + \mathbf{H}(\mathbf{X}_R - \widehat{\mathbf{X}_R}) + \mathbf{N}, \end{aligned} \tag{6.3}$$

where $\widehat{\mathbf{X}_R}$ is the estimated soft data symbol vector for the reliable signal set. The MIMO detector's aim is to maximize *a posteriori* probability of transmitted signal sequence in the unreliable signal set $\mathbf{X}_U$ as:

$$\widehat{\mathbf{X}_U} = \arg \max_{\mathbf{X}_U \in \mathcal{U}_U} P(\mathbf{X}_U|\mathbf{Y}_U) = \arg \max_{\mathbf{X} \in \mathcal{U}_U} \frac{P(\mathbf{Y}_U|\mathbf{X}_U)P(\mathbf{X}_U)}{P(\mathbf{Y}_U)}, \tag{6.4}$$

where $P(\mathbf{X}_U)$ is considered as the *a priori* information fed back from channel decoder, and $\mathcal{U}_U$ is the candidate list $\mathcal{U}_U$ that the RSS-MCMC processor selects points $\{\widehat{X_{U,i}}\}$ for the unreliable signal set from the completed signal constellation set. The the RSS-MCMC processor computes the extrinsic LLR of the coded bit as:

$$\begin{aligned}\lambda^e_{1,U}(d_k(\widehat{\mathbf{X}_U})) &= \frac{1}{2} \sum_{\widehat{\mathbf{X}_U} \in \mathcal{U}^+_{U,k}} (-\frac{1}{\sigma_w^2}\|\mathbf{Y} - \mathbf{H}\widehat{\mathbf{X}_U}\|^2 + \mathbf{d}^T_{U,\backslash k}\lambda^{\mathbf{e}}_{\mathbf{2},\mathbf{U},\backslash \mathbf{k}}) \\ &\quad -\frac{1}{2} \sum_{\widehat{\mathbf{X}_U} \in \mathcal{U}^-_{U,k}} (-\frac{1}{\sigma_w^2}\|\mathbf{Y} - \mathbf{H}\widehat{\mathbf{X}_U}\|^2 + \mathbf{d}^T_{U,\backslash k}\lambda^{\mathbf{e}}_{\mathbf{2},\mathbf{U},\backslash \mathbf{k}}), \end{aligned} \tag{6.5}$$

where $d_k(\widehat{\mathbf{X}_U})$ is the k^{th} coded bit in sequence $\{\mathbf{d}\}$ representing the RSS-MCMC detector enumerated transmitted symbol vector $\widehat{\mathbf{X}_U}$. $\mathcal{U}^+_{U,k}$ and $\mathcal{U}^-_{U,k}$ denote the subset of $\mathcal{U}_U$ for which $d_k(\widehat{\mathbf{X}_U})$ is $+1$ and -1 respectively. $\mathbf{d}_{U,\backslash k}$ is obtained from sequence $\mathbf{d}_U$ by removing the k^{th} coded bit. $\lambda^e_{2,U,\backslash k}$ is the extrinsic LLR of sequence $\mathbf{d}_{U,\backslash k}$ from the channel decoder. After MIMO detection, the sequence of extrinsic LLR $\{\lambda^e_{1,U}\}$ of coded bits is deinterleaved and passed on to the channel decoder to complete one iteration.

6.3 Markov Chain Monte Carlo Method

In this section, we give an brief overview of the conventional Markov Chain Monte Carlo (MCMC) [80] technique. The derivation from the first principle will be used in later sections when we present two new MCMC methods. MCMC is a family of algorithms that simulate the pseudo-random samples from a target probability distribution. The basic idea behind MCMC method is that one can achieve the

sampling from a target distribution $p(\theta)$ by running a Markov chain whose steady state probability distribution approaches $p(\theta)$. In practice, how to realize such a Markov chain is an active research area in the literature, where two basic MCMC algorithms are most often used, namely the Metropolis-Hastings algorithm [111, 112] and the Gibbs sampler algorithm [113–117]. In this thesis, we focus on the latter because the Gibbs sampler algorithm is more practical in the implementation.

Assuming we want to estimate $\Theta = \{\theta_i\}$, where $0 \leq i < I-1$. Using the Gibbs sampler, θ_i updates its value with a new sample drawn from the conditional distribution $p(\theta_i|\Theta\backslash\theta_i)$. This process starts from the random sample $\theta^{(0)}$ at 0^{th} round, which is randomly generated with uniform distribution, the Gibbs sampler algorithm is implemented as follows:

1. Given $\Theta^{(n)} = (\theta_0^{(n)}, \theta_1^{(n)}, \ldots, \theta_{I-1}^{(n)})$.

2. For $i = 0, 1, \ldots, I-1$,
   Draw sample $\theta_i^{(n+1)}$ from the conditional distribution
   $p(\theta_i|\Theta\backslash\theta_i) = p(\theta_i|\theta_0^{(n+1)}, \ldots, \theta_{i-1}^{(n+1)}, \theta_{i+1}^{(n)}, \ldots, \theta_{I-1}^{(n)})$.

3. When $n \to \infty$, the distribution of Θ converges to $p(\Theta)$.

It can be shown that by performing above the steps, the Monte Carlo integral can be replaced by the summation for any target function $f(\cdot)$ such that:

$$\begin{aligned} E\{f(\Theta)\} &= \int_{\Theta} f(\Theta)p(\Theta)d\Theta \\ &= \int_{\theta_0}\int_{\theta_1}\cdots\int_{\theta_{I-1}} f(\Theta)p(\theta_i|\Theta\backslash\theta_i)d\theta_0 d\theta_1\cdots d\theta_{I-1} \\ &\approx \frac{1}{N}\sum_{n=0}^{N-1} f(\Theta^{(n)}). \end{aligned} \tag{6.6}$$

The multi-dimensional integral is avoided in the equation (6.6) by translating the integration as the summation through empirical average [118, 119]. As shown in Step 3 above, the estimate of the distribution of Θ becomes more accurate as number of samples N goes infinity. Hence, the MCMC method adopting equation (6.6) normally requires a very long "burn-in" period, for example, a few hundreds of samples to get the accurate distribution [79]. Nevertheless, the equation (6.6) suggests that a reasonable N is good enough to make the approximation.

Moreover, numerical studies show that the dimension of Θ and the number of samples N are weakly related [79] in the sense that even though the dimension of Θ increases, the number of samples N as required by the Markov chain remains

almost unchanged. The conclusion is the exponential growth of the computational complexity in performing a multi-dimensional integral may be avoided by using the Monte Carlo method. Such a property is very desirable for the practical MIMO or multiple access systems.

A practical approximation that has been motivated by the *Importance Sampling* [119] results in a better evaluation of Monte Carlo integral than the approach in equation (6.6). The idea is to perform a weighted empirical average [80] as:

$$E\{f(\Theta)\} \approx \frac{\sum_{n=0}^{N-1} p(\Theta^{(n)}) f(\Theta^{(n)})}{\sum_{n=0}^{N-1} p(\Theta^{(n)})}, \tag{6.7}$$

where $p(\Theta^{(n)})$ is the marginal distribution of the n^{th} instance of Θ as Gibbs sampler walks through. Marginal distribution $p(\Theta^{(n)})$ represents the reliability of the n^{th} instance of Θ, and it can be computed as:

$$\begin{aligned} p(\Theta^{(n)}) &= \int_{\theta_0^{(n+1)}} \int_{\theta_1^{(n+1)}} \cdots \int_{\theta_{I-1}^{(n)}} p(\theta_i|\Theta\backslash\theta_i) d\theta_0^{(n+1)} d\theta_1^{(n+1)} \cdots d\theta_{I-1}^{(n)} \\ &= p(\theta_i|\Theta\backslash\theta_i) \prod_{j=0}^{i-1} p(\theta_j^{(n+1)}) \prod_{k=i+1}^{I-1} p(\theta_k^{(n)}), \end{aligned} \tag{6.8}$$

where $p(\theta_j^{(n+1)})$ and $p(\theta_k^{(n)})$ can be obtained from the extrinsic LLR λ_2^e in the iterative receiver. From Appendix A.2, we can simplify the equation (6.8) as:

$$\begin{aligned} p(\Theta^{(n)}) &= p(\theta_i|\Theta\backslash\theta_i) \prod_{j=0}^{i-1} \frac{1}{2} \left\{ 1 + (2\theta_j^{(n+1)} - 1) \tanh \frac{\lambda_2^e(j)}{2} \right\} \\ &\quad \cdot \prod_{k=i+1}^{I-1} \frac{1}{2} \left\{ 1 + (2\theta_k^{(n)} - 1) \tanh \frac{\lambda_2^e(k)}{2} \right\}. \end{aligned} \tag{6.9}$$

The samples required by "importance sampling" approximation are very less [79,119] by performing above weighted empirical average, which does not need the "burn-in" period as required by equation (6.6). In this thesis, we are utilizing the MCMC method with "importance sampling". Furthermore, we also average over multiple Markov chains, which improve the convergence of MCMC method from diversity side point of view.

6.4 MIMO detector with RSS-MCMC and FST-MCMC Methods

Studies in [79, 81] revealed that at high SNR, a high portion of the coded bits can be detected in the first few iterations. The LLRs of these bits have large values such that some of the transition probabilities in the underlying Markov chain may become very small. As a result, the Markov chain may be divided into a number of nearly disjoint chains between which transitions rarely happen. Hence, the Gibbs sampler has less chance to visit sufficient points. This phenomenon is undesired for the stochastic approach of MCMC, which requires a large number of samples in order to cover the whole state space defined by the transmitted signal. In this section, we develop two novel MCMC methods for MIMO detection, namely the Reduced State Space MCMC (RSS-MCMC) method, and Forced State Transition MCMC (FST-MCMC) method. In the RSS-MCMC method, our approach is to remove the interference from the bits with reliable LLR values. Then we draw random samples only for unreliable bits associated with unreliable LLR values in the system with less interference. On the other hand, in the FST-MCMC method, we flip the bits that did not change for a long time to force the Markov chain to cover more states.

6.4.1 Reliability Constraints for Extrinsic LLRs

Defining an accurate reliable signal set is crucial, as otherwise canceling those signals leads to error propagation. Hence, we first develop the reliability constraints to construct the reliable signal set. Recall that the structure of iterative detection and decoding consists of two constituent decoders. The extrinsic information are exchanged between these two constituent decoders. Let us first look at the decoder employed as the MIMO detector. As discussed in Section 6.2, the output of MIMO detector (Extrinsic LLR) is given by:

$$\begin{aligned}\lambda_1^e(d_k(\widehat{\mathbf{X}})) &= \frac{1}{2}\sum_{\widehat{\mathbf{X}}\in\mathcal{U}_k^+}(-\frac{1}{\sigma_w^2}\|\mathbf{Y}-\mathbf{H}\widehat{\mathbf{X}}\|^2+\mathbf{d}_{\backslash k}^T\lambda_{\mathbf{2},\backslash\mathbf{k}}^{\mathbf{e}}) \\ &\quad -\frac{1}{2}\sum_{\widehat{\mathbf{X}}\in\mathcal{U}_k^-}(-\frac{1}{\sigma_w^2}\|\mathbf{Y}-\mathbf{H}\widehat{\mathbf{X}}\|^2+\mathbf{d}_{\backslash k}^T\lambda_{\mathbf{2},\backslash\mathbf{k}}^{\mathbf{e}}), \qquad (6.10)\end{aligned}$$

where $\mathbf{X}_R$ and $\mathbf{X}_U$ are considered together in the full signal set $\mathbf{X}$. Using the $\max - \log$ approximation [120, 121], the equation (6.10) is simplified to:

$$\begin{aligned}
\lambda_1^e(d_k(\widehat{\mathbf{X}})) &\approx \frac{1}{2}\max_{\widehat{\mathbf{X}}\in\mathcal{U}_k^+}\left\{-\frac{1}{\sigma_w^2}\|\mathbf{Y}-\mathbf{H}\widehat{\mathbf{X}}\|^2+\mathbf{d}_{\backslash k}^T\lambda_{\mathbf{2},\backslash\mathbf{k}}^{\mathbf{e}}\right\} \\
&\quad -\frac{1}{2}\max_{\widehat{\mathbf{X}}\in\mathcal{U}_k^-}\left\{-\frac{1}{\sigma_w^2}\|\mathbf{Y}-\mathbf{H}\widehat{\mathbf{X}}\|^2+\mathbf{d}_{\backslash k}^T\lambda_{\mathbf{2},\backslash\mathbf{k}}^{\mathbf{e}}\right\} \\
&\approx \frac{1}{2\sigma_w^2}\left\{-\|\mathbf{Y}-\mathbf{H}\widehat{\mathbf{X}_{\max}^+}\|^2+\|\mathbf{Y}-\mathbf{H}\widehat{\mathbf{X}_{\max}^-}\|^2\right\} \\
&\quad +\frac{1}{2}\left\{(\mathbf{d}_{\max,\backslash k}^+)^T\lambda_{\mathbf{2},\backslash\mathbf{k}}^{\mathbf{e}}-(\mathbf{d}_{\max,\backslash k}^-)^T\lambda_{\mathbf{2},\backslash\mathbf{k}}^{\mathbf{e}}\right\}, \qquad (6.11)
\end{aligned}$$

where $\widehat{\mathbf{X}_{\max}^+}$ and $\widehat{\mathbf{X}_{\max}^-}$ are the signal vector candidates with the k^{th} bit to be 1 and 0 in $\mathcal{U}_k^+$ and $\mathcal{U}_k^-$ respectively to perform the $\max\{\cdot\}$.

Assuming that the RSS-MCMC detector has consistent detection performance, i.e. $\widehat{\mathbf{X}_{\max}^+}$ and $\widehat{\mathbf{X}_{\max}^-}$ are only different at the k^{th} bit, and $\mathbf{d}_{\max,-k}^+ = \mathbf{d}_{\max,-k}^-$ because the k^{th} bit is excluded in the *a priori* coded bit sequence $\mathbf{d}$. We can further simplify the equation (6.11) as:

$$\begin{aligned}
\lambda_1^e(d_k(\widehat{\mathbf{X}})) &\approx \frac{1}{2\sigma_w^2}\left\{-\|\mathbf{Y}-\sum_{j\neq k}\mathbf{H}_j\widehat{X_j}-\mathbf{H}_k\widehat{X_k^+}\|^2+\|\mathbf{Y}-\sum_{j\neq k}\mathbf{H}_j\widehat{X_j}-\mathbf{H}_k\widehat{X_k^-}\|^2\right\} \\
&\approx \frac{1}{\sigma_w^2}\left(\widehat{X_k^+}-\widehat{X_k^-}\right)\mathbf{H}_k^T\left(\mathbf{Y}-\sum_{j\neq k}\mathbf{H}_j\widehat{X_j}\right) \\
&\quad +\frac{1}{2\sigma_w^2}\|\mathbf{H}_k\|^2\left(|\widehat{X_k^-}|^2-|\widehat{X_k^+}|^2\right) \\
&\approx \frac{2}{\sigma_w^2}\mathbf{H}_k^T\left(\mathbf{Y}-\sum_{j\neq k}\mathbf{H}_j\widehat{X_j}\right) \\
&\approx \underbrace{\frac{2}{\sigma_w^2}\|\mathbf{H}_k\|^2}_{\mu}X_k+\underbrace{\frac{2}{\sigma^2}\mathbf{H}_k^T\mathbf{N}}_{\eta}, \qquad (6.12)
\end{aligned}$$

where we take the average over the signal constellation so that $E\{\widehat{X_k^+}-\widehat{X_k^-}\}=2$ and $E\{|\widehat{X_k^-}|^2-|\widehat{X_k^+}|^2\}=0$. μ can be viewed as the conditional mean of $\lambda_1^e(\widehat{\mathbf{X}}))$ as:

$$\begin{aligned}
\mu &= E\{\lambda_1^e(d_k(\widehat{\mathbf{X}}))|X_k\} \\
&\approx \frac{2}{\sigma_w^2}\|\mathbf{H}_k\|^2, \qquad (6.13)
\end{aligned}$$

and η is the additive noise with the conditional variance as:

$$\begin{aligned}\sigma_\eta^2 &= E\left\{\left(\lambda_1^e(d_k(\widehat{\mathbf{X}})) - E\{\lambda_1^e(d_k(\widehat{\mathbf{X}}))\}\right)^2 |X_k\right\} \\ &\approx \frac{4}{\sigma_w^2}\|\mathbf{H}_k\|^2. \end{aligned} \tag{6.14}$$

Above conditional mean and conditional variance relation complies with the Gaussian distributed assumption, which has been verified by the empirical observations from simulations in [122].

The decoder takes the output of the MIMO detector as shown in the equation (6.12) as the input, and generates the LLRs fed back (*a priori* information) to the MIMO detector. Unfortunately, the analytical treatment of the soft output of channel decoder is difficult. Nevertheless, the Gaussian distribution assumption in [122] states as follows. Firstly, for large interleavers the *a priori* information remain fairly uncorrelated from channel observation over many iterations. Secondly, the probability density function of the extrinsic information of channel decoder (*a priori* information of detector respectively) approach Gaussian-like distribution with increasing number of iterations.

Hence, with the Gaussian distribution assumption and the derivation in equation (6.12), the *a priori* information as an input to the MIMO detector can be modeled by applying an independent Gaussian random variable η with variance σ_η^2 and zero mean in conjunction with the known coded bit $d_k \in \{-1, 1\}$ as follows:

$$\lambda_1^e(d_k) = \mu \cdot d_k + \eta, \tag{6.15}$$

where the mean value μ satisfies the relation discussed above as

$$\mu = \frac{\sigma_\eta^2}{2}. \tag{6.16}$$

To obtain μ and σ_η^2, we can compute the second order statistics of LLRs, which is given by:

$$\begin{aligned} E\{|\lambda_1^e(d_k)|^2\} &= \mu^2 + \sigma_\eta^2 \\ &= \mu^2 + 2\mu. \end{aligned} \tag{6.17}$$

The solution of μ can be obtained by taking the positive root of equation (6.17):

$$\begin{aligned} \mu &= -1 + \sqrt{1 + E\{|\lambda_1^e(d_k)|^2\}} \\ &\approx \sqrt{E\{|\lambda_1^e(d_k)|^2\}}, \end{aligned} \tag{6.18}$$

if $E\{|\lambda_1^e(d_k)|^2\}$ is significant larger than one over iterations. And the solution of σ_η^2 is obtained as:

$$\begin{aligned} \sigma_\eta^2 &= 2\mu \\ &\approx 2\sqrt{E\{|\lambda_1^e(d_k)|^2\}}. \end{aligned} \tag{6.19}$$

Therefore, the conditional distribution of the *a priori* information given that $d_k = 1$ and $d_k = -1$ is Gaussian with $\mathcal{N}(\mu, \sigma_\eta^2)$ and $\mathcal{N}(-\mu, \sigma_\eta^2)$ respectively.

The next step is to construct the reliable signal set by determining whether the signals are correctly decoded. This is done by examining the sign and the absolute value of the LLRs. The larger the LLR value, the higher probability that the bit is decoded reliably. However, there is still an open question in the literature concerning how the value of the LLR corresponds to the level of reliability. In other words, given a LLR value, how do you determine whether the decoded bit is reliable or not?

With the conditional distribution of the *a priori* information, we can set up a threshold ρ on the LLR values. An inappropriate threshold ρ may cause error propagation. We link the threshold ρ with a confidence level, which is measured by the probability of error for the *a priori* information as follows:

Case $d_k = -1$:

$$\begin{aligned} P(error|d_k = -1) &= \int_{\rho}^{\infty} \frac{1}{\sqrt{2\pi\sigma_\eta^2}} \exp(-\frac{(\lambda_1^e + \mu)^2}{2\sigma_\eta^2}) d\lambda_1^e \\ &= \int_{\frac{\rho+\mu}{\sigma_\eta}}^{\infty} \frac{1}{\sqrt{2\pi}} \exp(-\frac{\gamma^2}{2}) d\gamma \\ &= \mathcal{Q}(\frac{\rho + \mu}{\sigma_\eta}), \end{aligned} \tag{6.20}$$

where $\mathcal{Q}(\cdot)$ is the Q-function. Then we can obtain the threshold ρ as:

$$\rho = \sigma_\eta \cdot \mathcal{Q}^{-1}(p(error|d_k = -1)) - \mu, \tag{6.21}$$

where $\mathcal{Q}^{-1}(\cdot)$ is the inverse of Q-function.

Case $d_k = 1$:

$$\begin{aligned} P(error|d_k = 1) &= \int_{-\infty}^{\rho} \frac{1}{\sqrt{2\pi\sigma_\eta^2}} \exp(-\frac{(\lambda_1^e - \mu)^2}{2\sigma_\eta^2}) d\lambda_1^e \\ &= \int_{\frac{-\rho+\mu}{\sigma_\eta}}^{\infty} \frac{1}{\sqrt{2\pi}} \exp(-\frac{\gamma^2}{2}) d\gamma \\ &= \mathcal{Q}(\frac{-\rho+\mu}{\sigma_\eta}). \end{aligned} \tag{6.22}$$

Similarly, the threshold ρ in this case is obtained as:

$$\rho = -\sigma_\eta \cdot \mathcal{Q}^{-1}(P(error|d_k = 1)) + \mu. \tag{6.23}$$

After combining the cases of $d_k = -1$ and $d_k = 1$, this threshold ρ as becomes the first reliability constraint on the *a priori* information, which can be obtained as:

$$\rho = |\sigma_\eta \cdot \mathcal{Q}^{-1}(P(error|d_k = \pm 1)) - \mu|. \tag{6.24}$$

It can be seen that this threshold ρ is adaptive to the pre-defined error probability, and first order and second order statistics of the *a priori* information over iterations. The coded bits with absolute LLR values greater than this threshold will be considered as reliable.

Furthermore, as discussed before, LLRs with large values result in disjoint Markov chains with less chance to visit the significant samples. The insufficient number of samples may generate ill-conditioned LLRs [72], which has large value but sign flipped. This can be explained by equation (6.5). We can rewrite the LLR in (6.5) as the summation of the ML LLR and the *a priori* LLR:

$$\lambda_1^e(d_k(\widehat{\mathbf{X}})) = \lambda_{1,ML}^e(d_k(\widehat{\mathbf{X}})) + \lambda_{1,AP}^e(d_k(\widehat{\mathbf{X}})), \tag{6.25}$$

where

$$\lambda_{1,ML}^e(d_k(\widehat{\mathbf{X}})) = \frac{1}{2}(\sum_{\widehat{\mathbf{X}} \in \mathcal{U}_k^+} -\frac{1}{\sigma_w^2}\|\mathbf{Y} - \mathbf{H}\widehat{\mathbf{X}}\|^2 + \sum_{\widehat{\mathbf{X}} \in \mathcal{U}_k^-} \frac{1}{\sigma_w^2}\|\mathbf{Y} - \mathbf{H}\widehat{\mathbf{X}}\|^2), \tag{6.26}$$

and

$$\lambda^{e}_{1,AP}(d_k(\widehat{\mathbf{X}})) = \frac{1}{2}\left(\sum_{\widehat{\mathbf{X}}\in\mathcal{U}_k^{+}} \mathbf{d}^{T}_{\backslash k}\lambda^{\mathbf{e}}_{\mathbf{2},\backslash\mathbf{k}} - \sum_{\widehat{\mathbf{X}}\in\mathcal{U}_k^{-}} \mathbf{d}^{T}_{\backslash k}\lambda^{\mathbf{e}}_{\mathbf{2},\backslash\mathbf{k}}\right). \tag{6.27}$$

The ML LLR is the measure of the Euclidian Distance between the enumerated coded bits and the actual transmitted coded bits, and the *a priori* LLR is the measure of likelihood of the coded bit of interest as seen by other interfering bits. The computation of LLR in (6.5) relies on ML LLR initially, and is gradually dominated by the *a priori* LLR. If we purely rely on the threshold as unique reliability constraint, once an LLR error occurs in the reliable signal set, the large sign flipped LLR value may dominate the computation of the *a priori* LLR for the current bit of interest, even though the ML LLR has the correct sign. This phenomenon is especially undesirable in MCMC, because the later drawn samples are influenced by the earlier drawn samples. Our investigation shows that the receiver suffers from error propagation as in the hard decision DFE. Therefore, we develop the second reliability constraint that the sign of the *a priori* LLR should be the same as the ML LLR as:

$$\lambda^{e}_{1,ML}(d_k(\widehat{\mathbf{X}})) \cdot \lambda^{e}_{1,AP}(d_k(\widehat{\mathbf{X}})) > 0. \tag{6.28}$$

This second reliability constraint ensures that only the coded bits with the *a priori* LLR enhancing the ML LLR over iterations are considered to be reliable. In practical implementations, the ML LLR from first iteration can be stored and doesn't have to be computed in every iteration. The *a priori* LLR in each iteration can be obtained by subtracting the ML LLR from first iteration in equation (6.5).

6.4.2 Reduced State Space(RSS) MCMC Method

Fig. 6.2 shows the Iterative MIMO spatial multiplexing receiver with RSS-MCMC detector, which consists of a pre-processor, interference canceler, Gibbs sampler, and the extrinsic LLR computation module. The pre-processor is the module which partitions the full signal set into the reliable and unreliable signal sets. The two criteria to judge the reliability of the coded bits based on their extrinsic LLRs are presented in Section 6.4.1. In this section, the interference canceler, Gibbs sampler, and the extrinsic LLR computation modules are presented.

The interference canceler module performs interference cancelation once the bits are determined as reliable by the pre-processor. The interference from the bits in the reliable signal set $\mathbf{X}_R = \{d_{r,1}, d_{r,2}\ldots\}$as constructed by the two reliability

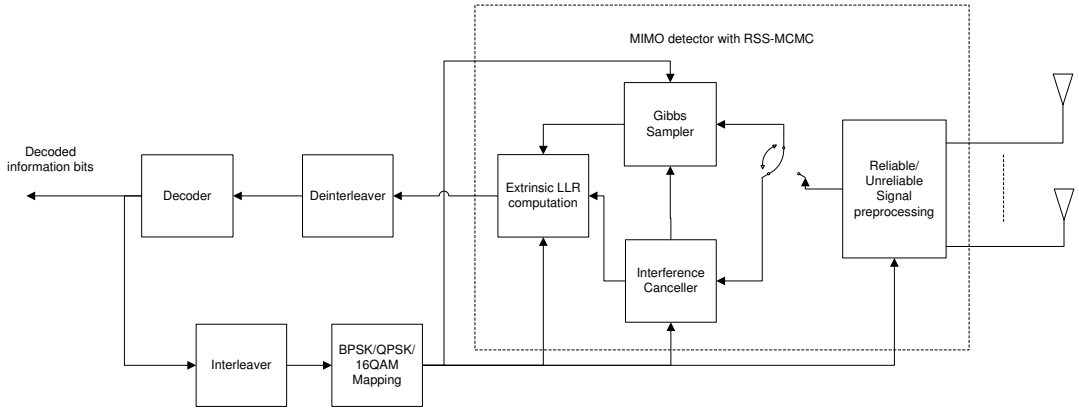

Figure 6.2: Iterative MIMO spatial multiplexing receiver with RSS-MCMC detector

constraints is first canceled from received signal. Extended from equation 6.2, the output of interference canceler can be obtain as:

$$\begin{aligned} \mathbf{Y^{IC}} &= \mathbf{Y} - \mathbf{H}\widehat{\mathbf{X}}_{\mathbf{R}} \\ &= \mathbf{H}\mathbf{X}_U + \underbrace{\mathbf{H}(\mathbf{X}_R - \widehat{\mathbf{X}}_{\mathbf{R}}) + \mathbf{N}}_{\mathcal{N}(0,\sigma_w^2\mathbf{I}_{2N_R})}. \end{aligned} \tag{6.29}$$

The residual interference and noise have zero mean and covariance matrix $\sigma^2\mathbf{I}_{2N_R}$ because the LLRs of the bits in the reliable signal set are large.

The Gibbs sampler takes the output of the interference canceler as its input and draws Markov chain samples for the coded bits in the unreliable signal set. Given $\mathbf{Y^{IC}}$ and the *a priori* information λ_2^e, the *a posterior* probability is evaluated as follows:

$$\begin{aligned} P(d_{u,k} = \pm 1|\mathbf{Y^{IC}}, \lambda_2^e) &= \sum_{\mathbf{X}_{U,\backslash k}} P(d_{u,k} = \pm 1, \mathbf{X}_{U,\backslash k}|\mathbf{Y^{IC}}, \lambda_2^e) \\ &= \sum_{\mathbf{X}_{U,\backslash k}} P(d_{u,k} = \pm 1|\mathbf{Y^{IC}}, \mathbf{X}_{U,\backslash k}, \lambda_2^e) \\ &\quad \cdot P(\mathbf{X}_{U,\backslash k}|\mathbf{Y^{IC}}, \lambda_2^e). \end{aligned} \tag{6.30}$$

Now if we treat

$$p(\Theta) = P(\mathbf{X}_{U,\backslash k}|\mathbf{Y^{IC}}, \lambda_2^e) \tag{6.31}$$

as the marginal distribution, and

$$f(\Theta) = P(d_{u,k} = \pm 1 | \mathbf{Y^{IC}}, \mathbf{X}_{U,\backslash k}, \lambda_2^e) \tag{6.32}$$

as the target function whose weighted sum is to be obtained, the estimate of the *a posterior* probability is obtained by evaluating equation 6.7 as:

$$P(d_{u,k} = \pm 1 | \mathbf{Y^{IC}}, \lambda_2^e) \approx \frac{\sum_{n=0}^{N-1} P(d_{u,k} = \pm 1 | \mathbf{Y^{IC}}, \mathbf{X}_{U,\backslash k}^{(n)}, \lambda_2^e) P(\mathbf{X}_{U,\backslash k}^{(n)} | \mathbf{Y^{IC}}, \lambda_2^e)}{\sum_{n=0}^{N-1} P(\mathbf{X}_{U,\backslash k}^{(n)} | \mathbf{Y^{IC}}, \lambda_2^e)}. \tag{6.33}$$

The next question is how the RSS-MCMC detector finds the density function $p(\Theta)$ and the target function $f(\Theta)$. We start from drawing random samples for the coded bits in the unreliable signal set $\mathbf{X}_U = \{d_{u,0}, d_{u,1}, \ldots, d_{u,I-1}\}$. The Gibbs sampler initializes the samples in $\mathbf{X}_U$ with equal probability of 0.5, and proceeds with drawing one sample in $\mathbf{X}_U$ at a time. The procedure is summarized as follows:

1. Initialize $\mathbf{X}_U$ randomly with equal probability.

2. for $n = 1$ to N
   draw $d_{u,0}^{(n)}$ from $P(d_{u,0} | d_{u,1}^{(n-1)}, d_{u,2}^{(n-1)}, \ldots, d_{u,I-1}^{(n-1)}, \mathbf{Y^{IC}}, \lambda_2^e)$
   draw $d_{u,1}^{(n)}$ from $P(d_{u,1} | d_{u,0}^{(n)}, d_{u,2}^{(n-1)}, \ldots, d_{u,I-1}^{(n-1)}, \mathbf{Y^{IC}}, \lambda_2^e)$
   draw $d_{u,2}^{(n)}$ from $P(d_{u,2} | d_{u,0}^{(n)}, d_{u,1}^{(n)}, d_{u,3}^{(n-1)}, \ldots, d_{u,I-1}^{(n-1)}, \mathbf{Y^{IC}}, \lambda_2^e)$
   $\vdots$
   draw $d_{u,k}^{(n)}$ from $P(d_{u,k} | d_{u,0}^{(n)} \ldots, d_{u,k+1}^{(n-1)}, \ldots, d_{u,I-1}^{(n-1)}, \mathbf{Y^{IC}}, \lambda_2^e)$
   $\vdots$
   draw $d_{u,I-1}^{(n)}$ from $P(d_{u,I-1} | d_{u,0}^{(n)} \ldots, d_{u,I-2}^{(n)}, \mathbf{Y^{IC}}, \lambda_2^e)$

It is worth noting that in the n^{th} sample $d_{u,k}^{(n)}$ is drawn based on the probability $P(d_{u,k} = \pm 1 | \mathbf{Y^{IC}}, \mathbf{X}_{U,\backslash k}^{(n)}, \lambda_2^e)$ that partially depends on the $(k-1)$ coded bits drawn in the n^{th} sample, and partially depends on the rest of the coded bits drawn in the $(n-1)^{th}$ sample. This probability is obtained by first computing the *a posterior* LLR:

$$\begin{aligned} \lambda_1^{(n)}(d_{u,k}) &= \ln \frac{P(d_{u,k} = +1 | \mathbf{Y^{IC}}, \mathbf{X}_{U,\backslash k}^{(n)}, \lambda_2^e)}{P(d_{u,k} = -1 | \mathbf{Y^{IC}}, \mathbf{X}_{U,\backslash k}^{(n)}, \lambda_2^e)} \\ &= \ln \frac{P(\mathbf{Y^{IC}} | \mathbf{X}_{U,\backslash k}^{(n)}, d_{u,k} = +1) P(\mathbf{X}_{U,\backslash k}^{(n)}, d_{u,k} = +1 | \lambda_2^e)}{P(\mathbf{Y^{IC}} | \mathbf{X}_{U,\backslash k}^{(n)}, d_{u,k} = -1) P(\mathbf{X}_{U,\backslash k}^{(n)}, d_{u,k} = -1 | \lambda_2^e)} \end{aligned}$$

$$
\begin{aligned}
&= \ln \frac{P(\mathbf{Y^{IC}}|\mathbf{X}^{(n)}_{U,\backslash k}, d_{u,k}=+1)}{P(\mathbf{Y^{IC}}|\mathbf{X}^{(n)}_{U,\backslash k}, d_{u,k}=-1)} + \ln \frac{P(\mathbf{X}^{(n)}_{U,\backslash k}, d_{u,k}=+1|\lambda^e_2)}{P(\mathbf{X}^{(n)}_{U,\backslash k}, d_{u,k}=-1|\lambda^e_2)} \\
&= \ln \frac{P(\mathbf{Y^{IC}}|\mathbf{X}^{(n)}_{U,\backslash k}, d_{u,k}=+1)}{P(\mathbf{Y^{IC}}|\mathbf{X}^{(n)}_{U,\backslash k}, d_{u,k}=-1)} + \underbrace{\ln \frac{P(\mathbf{X}^{(n)}_{U,\backslash k}|\lambda^e_{2,\backslash k})}{P(\mathbf{X}^{(n)}_{U,\backslash k}|\lambda^e_{2,\backslash k})}}_{=0} \\
&\quad + \underbrace{\ln \frac{P(d_{u,k}=+1|\lambda^e_2(d_{u,k}))}{P(d_{u,k}=-1|\lambda^e_2(d_{u,k}))}}_{\lambda^e_2(d_{u,k})} \\
&= \ln \frac{P(\mathbf{Y^{IC}}|\mathbf{X}^{(n)}_{U,\backslash k}, d_{u,k}=+1)}{P(\mathbf{Y^{IC}}|\mathbf{X}^{(n)}_{U,\backslash k}, d_{u,k}=-1)} + \lambda^e_2(d_{u,k}). \qquad (6.34)
\end{aligned}
$$

The computation of $P(\mathbf{Y^{IC}}|\mathbf{X}^{(n)}_{U,\backslash k}, d_{u,k}=\pm 1)$ follows the equation (6.29) as follows:

$$
P(\mathbf{Y^{IC}}|\mathbf{X}^{(n)}_{U,\backslash k}, d_{u,k}=\pm 1) = \mathcal{K} \exp(-\frac{\|\mathbf{Y^{IC}} - \mathbf{H}\mathbf{X}^{(n)}_{U,d_k=\pm 1}\|^2}{2\sigma_w^2}), \qquad (6.35)
$$

where $\mathcal{K}$ is a constant. Once $\lambda^{(n)}_1(d_{u,k})$ is obtained, we have

$$
P(d_{u,k}=\pm 1|\mathbf{Y^{IC}}, \mathbf{X}^{(n)}_{U,\backslash k}, \lambda^e_2) = \frac{(1-d_{u,k})\exp(-\lambda^{(n)}_1(d_{u,k})) + 1 + d_{u,k}}{2\left(1+\exp(-\lambda^{(n)}_1(d_{u,k}))\right)}. \qquad (6.36)
$$

After going through the above procedure, N important samples [79] are drawn for the bits in the unreliable set. These important samples will be used in computing extrinsic LLR in a later stage.

The final step is to compute the extrinsic LLR for each coded bit in the unreliable signal set, which is performed in the extrinsic LLR computation module. Starting from equation (6.33), we have:

$$
\lambda_1(d_{u,k}) \approx \ln \frac{\sum_{n=0}^{N-1} P(d_{u,k}=+1|\mathbf{Y^{IC}}, \mathbf{X}^{(n)}_{U,\backslash k}, \lambda^e_2) P(\mathbf{X}^{(n)}_{U,\backslash k}|\mathbf{Y^{IC}}, \lambda^e_2)}{\sum_{n=0}^{N-1} P(d_{u,k}=-1|\mathbf{Y^{IC}}, \mathbf{X}^{(n)}_{U,\backslash k}, \lambda^e_2) P(\mathbf{X}^{(n)}_{U,\backslash k}|\mathbf{Y^{IC}}, \lambda^e_2)}. \qquad (6.37)
$$

We can further expand $P(\mathbf{X}^{(n)}_{U,\backslash k}|\mathbf{Y^{IC}}, \lambda^e_2)$ as:

$$
P(\mathbf{X}^{(n)}_{U,\backslash k}|\mathbf{Y^{IC}}, \lambda^e_2) = \frac{P(\mathbf{X}^{(n)}_{U,\backslash k}, \mathbf{Y^{IC}}|\lambda^e_2)}{P(\mathbf{Y^{IC}}|\lambda^e_2)}
$$

$$= \frac{P(\mathbf{Y^{IC}}|\mathbf{X}^{(n)}_{U,\backslash k}, \lambda_2^e) P(\mathbf{X}^{(n)}_{U,\backslash k}|\lambda_2^e)}{P(\mathbf{Y^{IC}}|\lambda_2^e)}, \tag{6.38}$$

and expand $P(d_{u,k} = \pm 1|\mathbf{Y^{IC}}, \mathbf{X}^{(n)}_{U,\backslash k}, \lambda_2^e)$ by Bayes' rule as:

$$P(d_{u,k} = \pm 1|\mathbf{Y^{IC}}, \mathbf{X}^{(n)}_{U,\backslash k}, \lambda_2^e) = \frac{P(\mathbf{Y^{IC}}|\mathbf{X}^{(n)}_{U,\backslash k}, d_{u,k} = \pm 1) P(d_{u,k} = \pm 1)}{P(\mathbf{Y^{IC}}|\mathbf{X}^{(n)}_{U,\backslash k}, \lambda_2^e)}. \tag{6.39}$$

Substituting equation (6.38) and (6.39) into equation (6.37), we have

$$\begin{aligned}
\lambda_1(d_{u,k}) &\approx \ln \frac{\sum_{n=0}^{N-1} P(\mathbf{Y^{IC}}|\mathbf{X}^{(n)}_{U,\backslash k}, d_{u,k} = +1) P(\mathbf{X}^{(n)}_{U,\backslash k}|\lambda_2^e) P(d_{u,k} = +1)}{\sum_{n=0}^{N-1} P(\mathbf{Y^{IC}}|\mathbf{X}^{(n)}_{U,\backslash k}, d_{u,k} = -1) P(\mathbf{X}^{(n)}_{U,\backslash k}|\lambda_2^e) P(d_{u,k} = -1)} \\
&\approx \ln \frac{\sum_{n=0}^{N-1} P(\mathbf{Y^{IC}}|\mathbf{X}^{(n)}_{U,\backslash k}, d_{u,k} = +1) P(\mathbf{X}^{(n)}_{U,\backslash k}|\lambda_2^e)}{\sum_{n=0}^{N-1} P(\mathbf{Y^{IC}}|\mathbf{X}^{(n)}_{U,\backslash k}, d_{u,k} = -1) P(\mathbf{X}^{(n)}_{U,\backslash k}|\lambda_2^e)} + \ln \frac{P(d_{u,k} = +1)}{P(d_{u,k} = -1)} \\
&\approx \ln \frac{\sum_{n=0}^{N-1} P(\mathbf{Y^{IC}}|\mathbf{X}^{(n)}_{U,\backslash k}, d_{u,k} = +1) P(\mathbf{X}^{(n)}_{U,\backslash k}|\lambda_2^e)}{\sum_{n=0}^{N-1} P(\mathbf{Y^{IC}}|\mathbf{X}^{(n)}_{U,\backslash k}, d_{u,k} = -1) P(\mathbf{X}^{(n)}_{U,\backslash k}|\lambda_2^e)} + \lambda_2^e(d_{u,k}).
\end{aligned} \tag{6.40}$$

Hence, the extrinsic LLR for the k^{th} coded bits in the unreliable signal set is obtained as:

$$\begin{aligned}
\lambda_1^e(d_{u,k}) &\approx \lambda_1(d_{u,k}) - \lambda_2^e(d_{u,k}) \\
&\approx \ln \frac{\sum_{n=0}^{N-1} P(\mathbf{Y^{IC}}|\mathbf{X}^{(n)}_{U,\backslash k}, d_{u,k} = +1) P(\mathbf{X}^{(n)}_{U,\backslash k}|\lambda_2^e)}{\sum_{n=0}^{N-1} P(\mathbf{Y^{IC}}|\mathbf{X}^{(n)}_{U,\backslash k}, d_{u,k} = -1) P(\mathbf{X}^{(n)}_{U,\backslash k}|\lambda_2^e)} \\
&\approx \ln \frac{\sum_{n=0}^{N-1} P(\mathbf{Y^{IC}}|\mathbf{X}^{(n)}_{U,\backslash k}, d_{u,k} = +1) \prod_{j \neq k} P\left(d_{u,j}^{(n)}|\lambda_2^e(d_{u,j}^{(n)})\right)}{\sum_{n=0}^{N-1} P(\mathbf{Y^{IC}}|\mathbf{X}^{(n)}_{U,\backslash k}, d_{u,k} = -1) \prod_{j \neq k} P\left(d_{u,j}^{(n)}|\lambda_2^e(d_{u,j}^{(n)})\right)} \\
&\approx \ln \frac{\sum_{n=0}^{N-1} P(\mathbf{Y^{IC}}|\mathbf{X}^{(n)}_{U,\backslash k}, d_{u,k} = +1) \prod_{j \neq k} \frac{1}{2} \left\{1 + (2d_{u,j}^{(n)} - 1) \tanh \frac{\lambda_2^e(d_{u,j}^{(n)})}{2}\right\}}{\sum_{n=0}^{N-1} P(\mathbf{Y^{IC}}|\mathbf{X}^{(n)}_{U,\backslash k}, d_{u,k} = -1) \prod_{j \neq k} \frac{1}{2} \left\{1 + (2d_{u,j}^{(n)} - 1) \tanh \frac{\lambda_2^e(d_{u,j}^{(n)})}{2}\right\}}.
\end{aligned}$$

(6.41)

The most significant difference between the RSS-MCMC and conventional MCMC detectors is that the statistically significant samples can be drawn in an interference reduced system rather than over the entire signal space. In the RSS-MCMC detector, interference from reliable bits is removed in (6.29), which results a MIMO system with less interference, whereby the Gibbs sampler performance can be improved. If all the bits are reliable, the RSS-MCMC detector is an interference canceler. On the other hand, if all the bits are unreliable, the RSS-MCMC detector is the same as conventional MCMC detector. Otherwise, if the bits are partially reliable, the RSS-MCMC detector is the hybrid conventional MCMC detector and interference canceler.

6.4.3 Force State Transitions (FST) MCMC Method

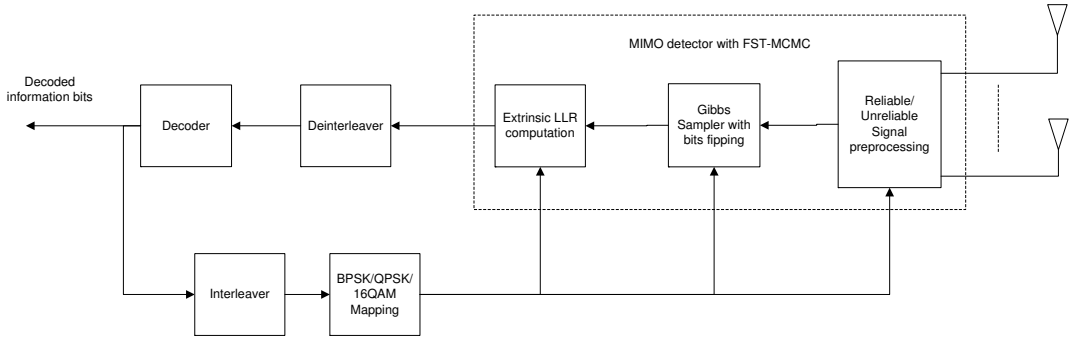

Figure 6.3: Iterative MIMO spatial multiplexing receiver with FST-MCMC detector

Fig. 6.3 shows the Iterative MIMO spatial multiplexing receiver with FST-MCMC detector, which consists of a pre-processor, Gibbs sampler with bit flipping, and the extrinsic LLR computation module. The pre-processor and the extrinsic LLR computation modules are the same as the RSS-MCMC detector. Hence, in this section, the Gibbs sampler with bit flipping is presented for the FST-MCMC detector.

As discussed before, the problem of Gibbs sampler at high SNR is that the LLRs of the coded bits may have large values so that the transition probability in the underlying Markov chain may becomes very small. Hence, the Markov chain would

stay in the same state no matter how many samples are drawn. In this section, we develop a forced state transitions MCMC method. In this method, we force the Markov chain to move by manually changing some coded bits which stay the same for a long period of time. In the MCMC methods, the event that the Markov chain changes state occurs when a certain bit d_k is to be drawn by the Gibbs sampler will differ from the previous sample, i.e. $d_k^{(n)} \neq d_k^{(n-1)}$. The Gibbs sampler draws the sample according to the conditional probability $P(d_k|\mathbf{Y}, \mathbf{X}_{\backslash k}^{(n)}, \lambda_2^e)$, which is directly related to the *a posterior* LLR in a non-linear manner. A small value of LLR indicates that the coded bit is more likely to change state, while a large value of the LLR indicates that the coded bits will stay the same. Obviously, the coded bits that remain the same are normally associated with large LLR values.

In Section 6.4.1, it has been shown that the LLRs can be assumed as Gaussian distributed with conditional mean μ and conditional variance σ_η^2. The decision error would occur at the tail of the Gaussian distribution, which falls into two cases. In the first case, the LLR value is small and the sign of the LLR is flipped. The Gibbs sampler will take care of this case because the coded bit associated with such small LLR value will likely to be changed in the next sample so that the Markov chain can visit more states. In the second case, the LLR value is large and sign of the LLR is flipped. In this case, the coded bit associated with such large LLR value will less likely to be changed in the next sample so that the Markov chain would be trapped in the current state and never move forward. Hence, the FST-MCMC method is going to flip these "ill conditioned" coded bits to force the Markov chain to move to next state.

Similar to the RSS-MCMC method, the FST-MCMC method will first partition the full signal set into the reliable signal set and unreliable signal set. The reliable signal signal set will keep as it is. For the unreliable signal set, the FST-MCMC method will check the following two criteria:

1. The coded bit has not been changed for the last m samples.

2. Its ML metric and the *a priori* metric is not consistent.

Then the FST-MCMC method will flip the bit once these two conditions are true, and continue with the Gibbs sampler. The FST-MCMC method is summarized as follows:

1. Partition $\mathbf{X}$ into $\mathbf{X}_R$ and $\mathbf{X}_U$.

2. Initialize $\mathbf{X}$ randomly with equal probability.

3. for $n = 1$ to N
   for $k = 0$ to $I - 1$
   draw $d_k^{(n)}$ from $P(d_k | d_0^{(n)} \ldots, d_{k+1}^{(n-1)}, \ldots, d_{I-1}^{(n-1)}, \mathbf{Y^{IC}}, \lambda_2^e)$
   If $(d_k \in \mathbf{X}_U)$
   check the criterion 1.
   check the criterion 2.
   If (both criteria are true)
   flip the coded bit $d_k^{(n)}$.

4. Compute the extrinsic LLRs for all coded bits.

The FST-MCMC is different from the RSS-MCMC method in such a way that we keep the reliable bits while try to flip the unreliable bits as long as they are trapped in the same state and would never move forward for a long period of time.

6.5 Complexity of MIMO Detector with MCMC Methods

The complexity of the MIMO detector with MCMC methods is dominant by the number of samples drawn by the Gibbs sampler. It is worth noting that the exact complexity analysis is difficult because some parameters are *a priori* unknown and approximations are varying depending on a particular hardware realization. Nevertheless, we present a rough estimate in terms of the floating point operations. We consider a $N_T \times N_R$ MIMO spatial multiplexing system. Assuming that the iterative receiver with N_{itr} iterations consists of κ parallel Markov chains and each Markov chain has N samples to be drawn by the Gibbs sampler. For M-ary modulation in the MCMC, $N_T \log_2 M$ coded bits are considered as one sample, hence, there are altogether $N \times N_T \log_2 M$ coded bits are drawn by the Gibbs sampler per Markov chain in each iteration.

In the pre-processing module, the main complexity is on the computation of μ and σ_η^2 to obtain the statistical distribution of the *a priori* information. The pre-processor requires $2NT \log_2 M + 1$ operations. Then it requires 1 more multiplication to obtain σ_η^2. Lastly, 4 operations are required to obtain the threshold. Therefore, there are all together $2NT \log_2 M + 6$ operations for the pre-processing module.

In the Gibbs sampler module, the Gibbs sampler assigns a random bit with equal probability in the initialization. This operation requires a random variable

with uniform distribution. This random variable with uniform distribution can be implemented by a linear feedback shift register circuit, which counts as one operation per coded bit. In the drawing sample process, for each coded bit, the Gibbs sampler requires $8N_RN_T + 8N_R + 2$ floating point operations to compute $P(\mathbf{Y}|\mathbf{X}_{\backslash k}^{(n)}, d_k \pm 1)$. Then it requires three operations for the computation of $\lambda_1^{(n)}(d_k)$ and three operations to compute $P(d_k \pm 1|\mathbf{Y}, \mathbf{X}_{\backslash k}^{(n)}, \lambda_2^e)$. Finally, the Gibbs sampler requires one operation from a random variable to draw a coded bit.

In the extrinsic LLR computation module, the main complexity is the realization of equation (6.41). The computation of $P(\mathbf{Y}|\mathbf{X}_{\backslash k}^{(n)}, d_k \pm 1)$ has been performed in the Gibbs sampler module. It needs to be stored in the memory and have no additional complexity. The computation of the *a priori* probability requires $2 \times 6(N_T \log_2 M - 1)$ operations. And the product of $N_T \log_2 M - 1$ such *a priori* probabilities together with $P(\mathbf{Y}|\mathbf{X}_{\backslash k}^{(n)}, d_k \pm 1)$ requires $2N_T \log_2 M$ multiplications. A further $2N$ summations are included in the calculation for the numerator and denominator. Finally, two more operations are required to obtain the extrinsic LLR for a coded bit.

Hence, the complexity of the MCMC methods is summarized as follows:

- Pre-processor: $2N_T \log_2 M + 6$ per iteration.
- Gibbs sampler
  - Initialization: $N_T \log_2 M$ per iteration.
  - Draw sample: $N \times (8N_T^2N_R + 8N_TN_R + 9N_T) \log_2 M$ per iteration.
- Extrinsic LLR computation: $N_T \log_2 M \times (14N_T \log_2 M - 10 + 2N)$ per iteration.

Fig. 6.4 shows the number of multiplications per Markov chain against the number of antennas in the pre-processor, Gibbs sampler, and the extrinsic LLR computation, respectively. The number of receiving antennas is the same as the number of transmitting antennas, and there are five samples per Markov chain, i.e.$N = 5$. It can be seen that the main complexity is from the Gibbs sampler, while the complexity for the pre-processor and the extrinsic LLR computation is much lower. Furthermore, the complexity of the individual modules is not sensitive to the increase of the number of antennas.

By counting the entire Markov chain and summing the number of operations for all iterations from above three modules, we have the complexity estimation for

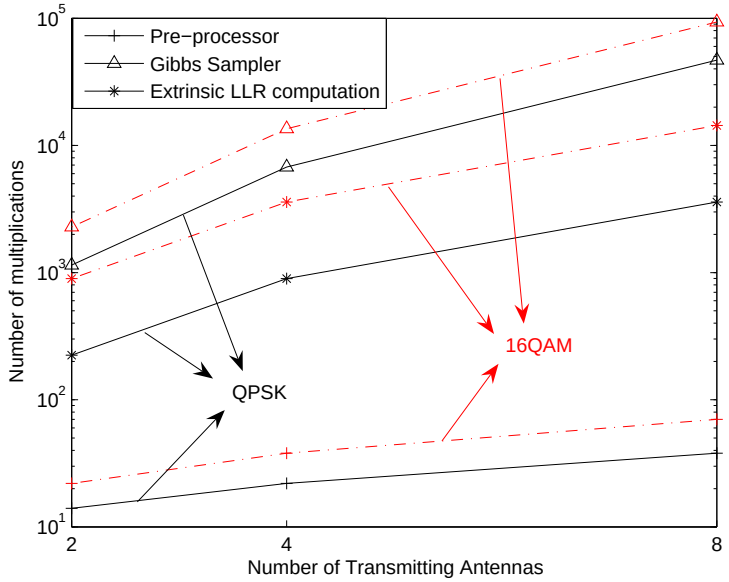

Figure 6.4: Number of multiplications per Markov chain in pre-processor, Gibbs sampler, and extrinsic LLR computation against the number of antennas with QPSK and 16QAM modulation

the MCMC methods as:

$$\mathcal{C} \approx \kappa(N_T \log_2 M(14N_T \log_2 M + 8NN_TN_R + 8NN_R + 11N - 7) + 6)N_{itr}. \quad (6.42)$$

Fig. 6.5 shows the total number of multiplications against the number of samplers per Markov chain for various number of antennas with QPSK and 16QAM modulation. Similarly, the number of receiving antennas is the same as the number of transmitting antennas. There are four parallel Markov chains, and four turbo iterations in the receiver, i.e.$\kappa = 4$ and $N_{itr} = 4$. It can be seen that the total complexity of the MCMC methods is approximately linear to the number of samples in the Markov chain, the order of the modulations, and the number of antennas. Hence, the exponential growth of the complexity that is commonly encountered in the conventional MIMO detectors can be avoided by using the MCMC methods developed in this thesis.

Some remarks are worth noting. Firstly, the above complexity analysis is generalized for both RSS-MCMC and FST-MCMC methods. In the RSS-MCMC method, the interference canceler module reduces the complexity of the Gibbs sampler because the reliable coded bits are removed, and only the unreliable bits are taken into the Gibbs sampler module. Compared to the Gibbs sampler, the

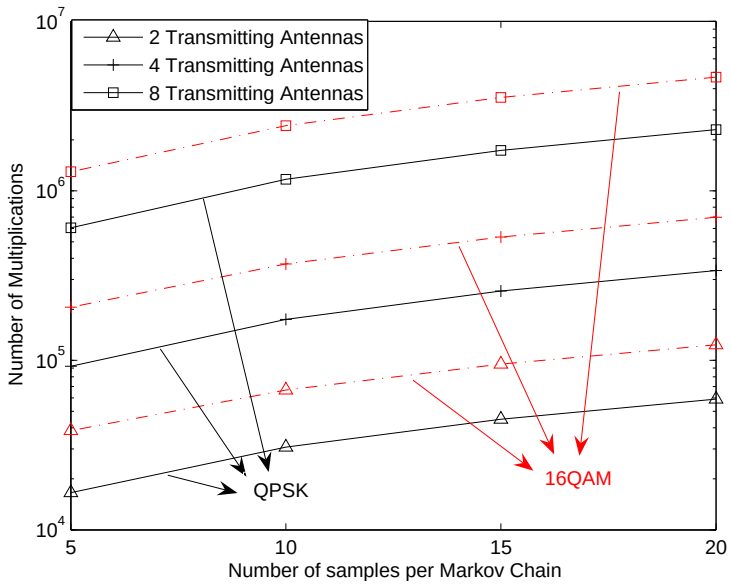

Figure 6.5: Total number of multiplications against the number of samplers per Markov chain for various transmitting antennas with QPSK and 16QAM modulation

complexity of the interference canceler is much less. Hence, we do expect the RSS-MCMC method will have significant complexity reduction. Secondly, the FST-MCMC method has the Gibbs sampler with bit flipping module rather than the interference canceler. We expect the Gibbs sampler with bit flipping to have the same complexity as the conventional Gibbs sampler because the complexity of the bit flipping is very low. Hence, unlike the RSS-MCMC method, there is no complexity reduction from the FST-MCMC method.

6.6 Numerical Results

6.6.1 Simulation Setup

We consider a 4×4 MIMO spatial multiplexing system and compare the BER for the iterative receivers with the conventional MCMC detector [79] and the iterative receiver with the RSS-MCMC detector and FST-MCMC detector. We also present the complexity reduction that the iterative receiver with RSS-MCMC detector can obtain over the iterative receiver with conventional MCMC detector.

For all MCMC methods, we run 20 samples in multiple Markov chains. In the conventional MCMC detector and the RSS-MCMC detector, we run four parallel

Markov chains, and within a Markov chain, there are five samples for each coded bit. Unless otherwise stated, the threshold ρ is selected to achieve 10^{-4} coded bit error rate. The complexity reduction is measured by the number of the drawn samples in the RSS-MCMC detector over the total number of samples drawn in the conventional MCMC detector. In the FST-MCMC detector, we run two parallel Markov chains, and within each Markov chain, there are 10 samples for each coded bit. This is because if we run four Markov chain with five samples each for FST-MCMC, the number of consecutive samples to determine whether to flip the coded bit should be less than five, which is useless for FST-MCMC because the Markov chain would not be in the "ill conditioned" state. Hence, we employ less parallel Markov chains but with more samples per Markov chain.

The channel model for each transmit and receive antenna are independent flat Rayleigh fading channel. A rate-1/2 $(171, 133)_8$ convolutional code is used for channel coding. The modulation includes QPSK and 16QAM. We refer to the conventional MCMC detector in [79] as "Conventional MCMC", and the RSS-MCMC method and the FST-MCMC method developed in this chapter as "RSS-MCMC" and "FST-MCMC" respectively. "itr 2", "itr 3", and "itr 4" denote the 2^{nd}, 3^{rd} and 4^{th} iteration.

6.6.2 Performance of Iterative Receivers with MCMC Methods

In this section, we present the BER performance of the iterative receivers with MCMC methods. As similar to Chapter 5, the modified MCMC methods in this Chapter focus on the detection method itself, hence, we think that bit error rate is the most suitable performance metric. Fig. 6.6 shows the BER performance for the iterative receivers with the conventional MCMC detector and with the RSS-MCMC detector over 4 iterations. It can be seen that in the QPSK modulation, the RSS-MCMC detector has slightly better performance than the conventional MCMC detector, although it is not noticeable in the 4^{th} iteration. In the case of 16QAM, the RSS-MCMC detector improves the performance over the conventional MCMC detector. This is because the RSS-MCMC detector performs detection on the undetermined bits in a MIMO system with less interference after canceling the interference from the reliable bits. At high SNR, the conventional MCMC detector shows degraded performance in the 3^{rd} and 4^{th} iteration, such undesired phenomenon has been observed in [79, 81]. Nevertheless, the RSS-MCMC detector does not show the error floor.

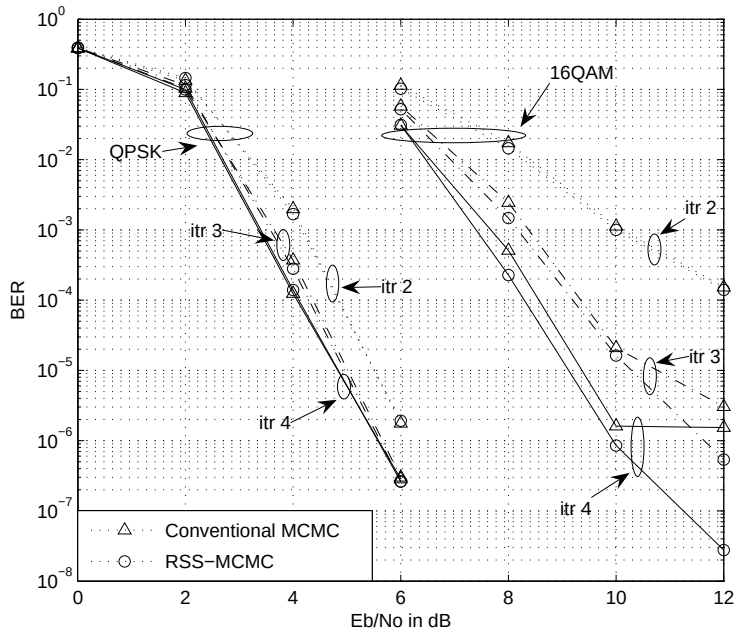

Figure 6.6: BER performance for the iterative receivers with the conventional MCMC detector, and with the RSS-MCMC detector in a 4×4 MIMO spatial multiplexing system with QPSK and 16QAM modulation

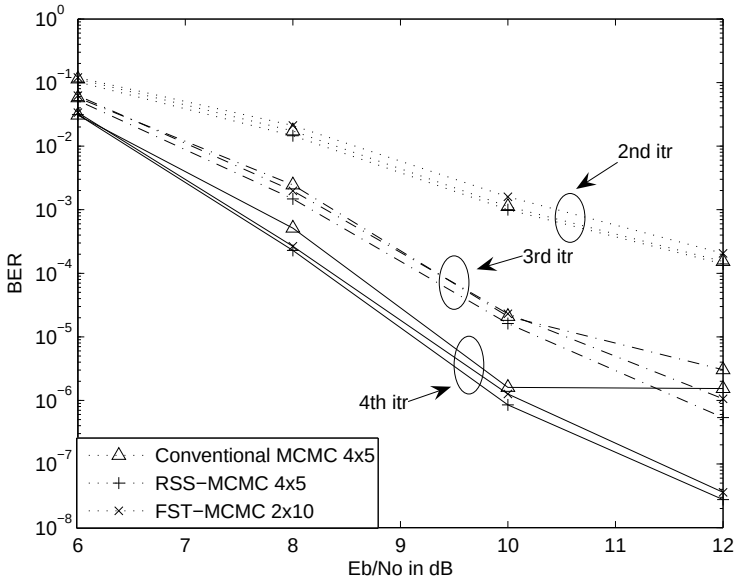

Figure 6.7: BER performance for the iterative receivers with the conventional MCMC detector, the RSS-MCMC detector, and the FST-MCMC detector in a 4×4 MIMO spatial multiplexing system with 16QAM modulation

Fig. 6.7 shows the BER performance for the iterative receivers with the conventional MCMC detector and with the FST-MCMC detector over 4 iterations for the 16QAM modulation. It can be seen that in the high SNR region, in the 2^{nd} iteration, there is no performance difference between the conventional MCMC detector and the FST-MCMC detector. However, in the 3^{rd} iteration, the conventional MCMC detector starts to show an error floor. And such degradation is even worse in the 4^{th} iteration. On the other hand, the FST-MCMC detector does not show any error floor in the 3^{rd} and 4^{th} iterations, which indicates that FST-MCMC detector is also robust in the high SNR region by forcing the Markov chain to visit more states when it is trapped in the "ill conditioned" states.

We also include the performance of the iterative receiver with the RSS-MCMC detector in Fig. 6.7. The FST-MCMC detector has the same performance compared with the RSS-MCMC detector. This observation shows that both methods solve the problem encountered by the conventional MCMC detector at high SNRs.

6.6.3 Computational Complexity for the RSS-MCMC Detector

In this section, we present the complexity for the RSS-MCMC detector, which is significantly reduced when compared to the conventional MCMC detector and FST-MCMC detector. Fig. 6.8 shows the complexity reduction when compared to the conventional MCMC detector over E_b/N_0 for the RSS-MCMC detector. In both QPSK and 16QAM modulation, there is no complexity reduction in the first iteration as the interference cancelation has not been employed because there is no *a priori* information available. In the 2^{nd} iteration, the complexity reduction from the reduced-state-space Gibbs sampler after interference cancelation reaches 30% for QPSK and 8% for 16QAM at 6dB. As the iterations proceed, more bits satisfy the reliability constraints. This can be observed in the 4^{th} iteration that more that 50% and 30% bits in QPSK and 16QAM respectively are considered as reliable. Furthermore, more complexity reduction can be achieved as the E_b/N_0 increases because more bits can be canceled as they are considered as reliable when E_b/N_0 improves.

Fig. 6.9 and Fig. 6.10 show the complexity reduction when compared to the conventional MCMC detector for the RSS-MCMC detector over iterations for QPSK and 16QAM modulation respectively. In both modulation schemes, there is a significant increase of the complexity reduction from the reduced-state-space Gibbs sampler after interference cancelation in the 2^{nd} and the 3^{th} iteration, while the

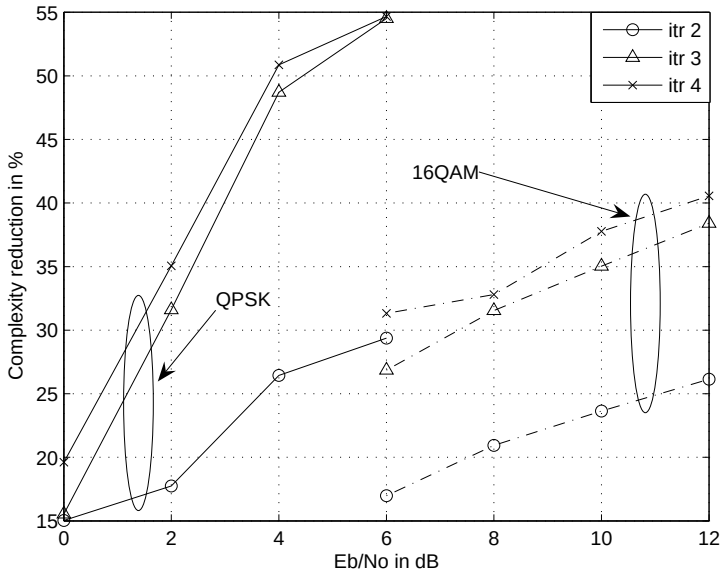

Figure 6.8: Complexity reduction from the reduced-state-space Gibbs sampler for the RSS-MCMC detector when compared to the conventional MCMC detector over E_b/N_0 with QPSK and 16QAM modulation

complexity reduction saturates in the 4^{th} iteration. This observation indicates that after four iterations, the LLRs converges to equilibrium and the further complexity reduction is marginal.

Table 6.1: Total complexity reductions in RSS-MCMC Detector

SNR	Reduction in QPSK	SNR	Reduction in 16QAM
0dB	12.5%	6dB	18%
2dB	22%	8dB	21.5%
4dB	31.5%	10dB	24.5%
6dB	35%	12dB	26%

Table 6.1 summarize the total complexity reductions. The total complexity reduction is the summation of complexity in each iteration including the first iteration. Generally, the complexity reduction in the QPSK modulation is more than that in the 16QAM modulation. It can be seen that 35% computation power can be saved in QPSK at 6dB, while 26% computation power can be saved in 16QAM at 12dB.

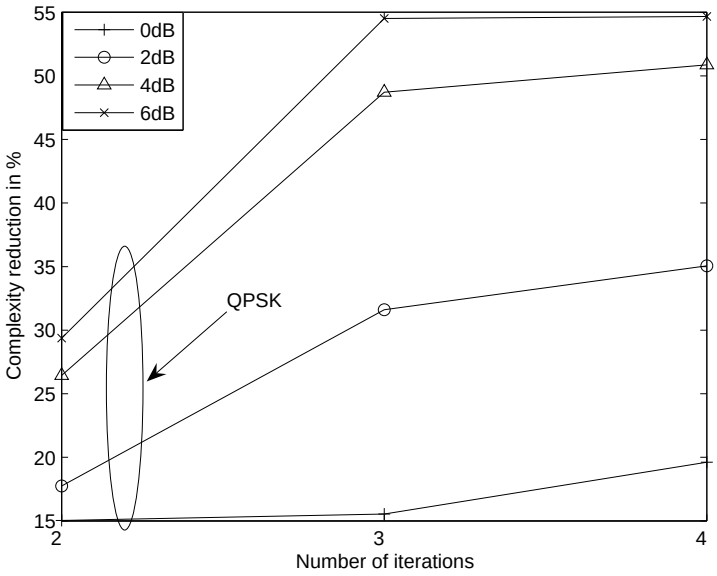

Figure 6.9: Complexity reduction from the reduced-state-space Gibbs sampler for the RSS-MCMC detector when compared to the conventional MCMC detector over iterations with QPSK modulation

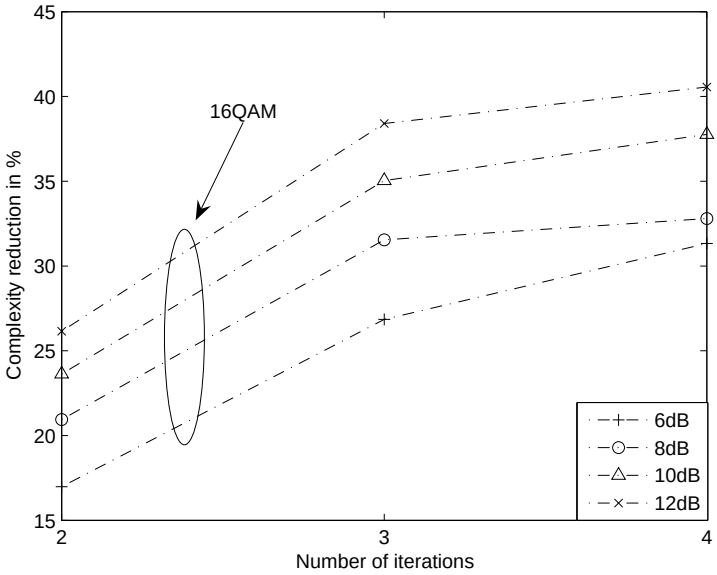

Figure 6.10: Complexity reduction from the reduced-state-space Gibbs sampler for the RSS-MCMC detector when compared to the conventional MCMC detector over iterations with 16QAM modulation

6.6.4 Performance and Complexity Tradeoff for RSS-MCMC Detector

As discussed in Section 6.5, the complexity reduction achieved by the RSS-MCMC method is due to the use of the reliable signal set, where the more reliable bits

are removed from the Gibbs sampler, thus saving significant computational complexity(ie. more computational effort is directed at less reliable bits, while reliable bits have less computational processing applied to them.). The larger the reliable signal set, the more the complexity reduction, thus the change in computational complexity with a changing E_b/N_0. And the criteria to partition the signal set is presented in Section 6.4.1. Also, at different E_b/N_0, as we move the threshold, we will achieve different levels of complexity reduction. If the threshold is high, the RSS-MCMC detector becomes the conventional MCMC detector. If the threshold is low, the RSS-MCMC detector tends towards the interference canceler. Consequently, the performance is varying with the level of complexity reduction. Hence, there is the performance and complexity tradeoff. In other words, optimal ρ values exist at different E_b/N_0 to provide the best BER performance with maximum complexity reduction.

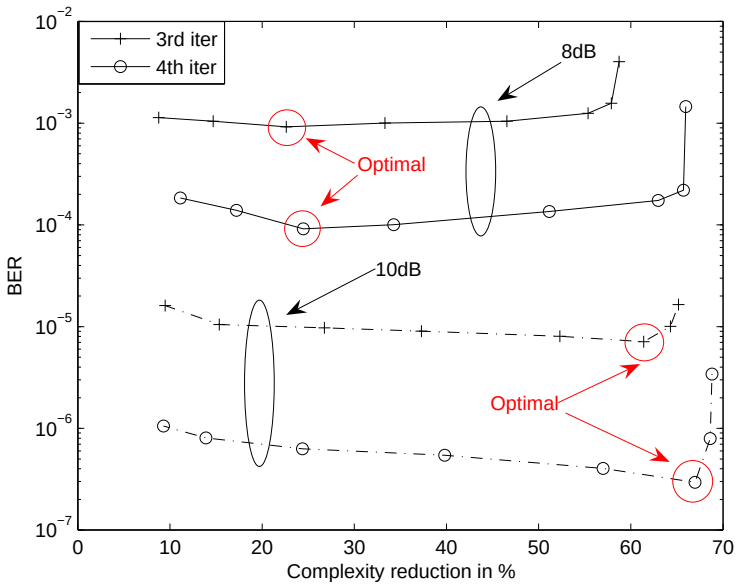

Figure 6.11: Complexity and performance tradeoff for the RSS-MCMC detector over iterations with 16QAM modulation at 8dB and 10dB

Fig. 6.11 shows the complexity and performance tradeoff for the RSS-MCMC detector over iterations with 16QAM modulation at 8dB and 10dB. It can be seen that this tradeoff is highly related to the SNR, and the optimal tradeoff point for different iterations is consistent. For example, at 8dB, the best BER performance occurs at 20% complexity reduction, while at 10dB, the best BER performance occurs at 65% complexity reduction. And the BER performances are getting worse when we are going far away from the optimal operating point.

Furthermore, we can also observe the trend of movement of the optimal point for different SNR regions, that is, the optimal point moves towards the right lower corner of the figure. This trend indicates that in the low SNR region, the extrinsic LLRs are less reliable, hence it's better for the Gibbs sampler to draw more samples rather than less because the MCMC method is good at detection at low SNR. On the other hand, in the high SNR region, the extrinsic LLRs are so reliable that the interference canceler can provide a system with less interference, the RSS-MCMC detector can have better performance compared to the conventional MCMC detector. In practical realization, we can either select the optimal ρ at different SNRs, or we can select suboptimal ρ for all SNRs so that the good BER performance and reasonable complexity reduction can be obtained.

6.7 Summary and Contributions

This chapter has investigated the iterative receivers with Markov Chain Monte Carlo methods for the MIMO system with spatial multiplexing. The MCMC detector with Gibbs sampler has shown the near capacity performance in the literature. However, the conventional MCMC detector suffers from error floor in the high SNR region. Two novel MCMC methods are developed to solve this problem. The reliability probelm of the LLRs is analyzed first followed by developing two reliability constraints to partition the full signal set into a reliable signal set and a unreliable signal set. Then the RSS-MCMC and FST-MCMC methods are presented. The RSS-MCMC method is to perform the reduced-state-space Gibbs sampler in a new system with less interference. And the FST-MCMC method forces the Markov chain to visit more states by manually flipping the "ill conditioned" bits.

Some specific contributions made in this chapter are as follows. First of all, the state-of-art iterative receiver with MCMC methods are reviewed. The conventional MCMC detector has degraded performance as SNR increases and suffers from error floor at high SNR. The system model for the iterative receiver with MCMC method in the MIMO spatial multiplexing system is investigated. A modified linear MIMO model for the MCMC detection is presented. The conventional system model in the complex domain is modified to be in the real domain. The ML and MAP detection criteria are modified to suit the MCMC detection. In addition, the fundamental of the MCMC integral and its approximation through importance sampling is introduced followed by the procedures that the Gibbs sampler draws samples.

Secondly, the theoretical analysis on the reliability of the extrinsic information exchanged between the detector and decoder in the turbo reception architecture is presented. The Gaussian Consistent assumption is employed to derive the conditional distribution of the LLRs. Based on this theoretical analysis, two reliability constraints are developed to separate the reliable signal from unreliable ones. The first constraint is to set up a threshold based on the statistical distribution of the extrinsic LLRs. The LLRs above the threshold will be passed to the second constraint. The second constraint is to test whether its ML metric and the *a priori* metric is consistent. Once these two constraints are satisfied, the coded bit associated with the extrinsic LLR is considered as reliable. This reliability test is done in a module called pre-processor.

Thirdly, the novel RSS-MCMC detector is presented, which consists of an interference canceler, a Gibbs sampler and an extrinsic LLR computation module. The approach is to remove the interference from the bits with reliable LLR values. Then the random samples are drawn only for unreliable bits in the new system with less interference. Furthermore, the FST-MCMC detector is presented, which consists of an a Gibbs sampler with bit flipping and an extrinsic LLR computation module. The approach is to flip the bits that did not change for a long time to force the Markov chain to cover more states. A rough estimation on complexity of the iterative receivers with MCMC methods is presented. This complexity estimation is measured on the floating point operations in all modules.

Finally, simulation results show that both RSS-MCMC and FST-MCMC methods outperform the conventional MCMC method, especially in the undesired error floor region at high SNR. Furthermore, the conventional MCMC method needs to draw random samples for all coded bits in the entire signal state space, while the RSS-MCMC method achieves further complexity reduction through interference cancelation and reduced-state-space Gibbs sampler. A performance and complexity tradeoff is also obtained for the RSS-MCMC method and provide a guidelines for the practical implementation.

Chapter 7

Conclusions and Future Research Directions

In this chapter we state the general conclusions drawn from this thesis. The summary of contributions can be found at the end of each chapter and are not repeated here. We also outline some future research directions arising from this work.

7.1 Conclusions

Modern wireless communications promise to support users with higher data rates in a dynamic mobile environment, where realistic mobile radio channel shows rapid dispersive nature in both time and frequency. Large amount of reference bits(pilot bits) are required in order to track such high mobility environment, however, the spectrum resource are occupied by the reference bits, which compromises the system throughput. Multiple antennas are employed to enhance the system capacity to achieve high data rates, however, the MIMO detector is far more complex than the SISO detector and imposes challenges in the receiver design in the sense of interference mitigation and detector complexity.

This thesis has utilized the Turbo principle in terms of iterative detection and decoding to the fundamental receiver design problems. From the signal processing point of view, the ultimate goal for the receiver design is to make the correct decision on the information data bits. The conventional receiver design paradigm considers the data as a passive parameter to be estimated, and completely rely on the the reference bits to estimate the channel parameters. Hence, the system performance is restricted by the availability of the reference signal, which becomes the limiting factor in the severe channel environment.

On the other hand, under the iterative receiver design paradigm, the evolution of the reliability of the data information over iterations enables the data-assisted channel estimation. Technically, the data information is represented as *a priori* probability, also known as the *soft* information, which is obtained from the channel decoder. This soft information is fed back to the respective receiver modules, for example, the channel estimator or the MIMO detector, as a semi-reference signal in parallel with the true reference signal, i.e. the preamble and pilot symbols, to operate simultaneously to achieve performance gain or complexity reductions in the overall system.

In this thesis, we addressed the important issues of efficient design of iterative receiver structures and algorithms for wireless communications. We developed low complexity iterative receivers with data-driven channel estimation and interference mitigation, which not only improve the receiver sensitivity, but also achieve significant complexity reduction compared to the conventional receivers. More precisely, we apply the iterative techniques to three areas of the receiver design. The first area is the mobility management with enhanced channel estimation in the SISO system. The second area is the interference mitigation with linear methods and channel estimation in the MIMO system. And the third area is the MIMO detection with performance enhancement and complexity reduction for nonlinear methods.

In the mobility management, we developed a novel three-stage iterative data-driven channel estimator. The frequency-domain combining and time-domain combining strategies utilizing the energy evolution and weighting between the soft data and reference signals. for SISO system. We first investigated the ICI caused by the mobility of the mobile radio channel at high speed, which could be a potential problem for the channel estimation. We analyzed the influence of the ICI and employed an approximation method to absorb the ICI into the effective noise. Then we illustrate the superior performance of the data-driven channel estimation in the practical OFDM system. The MSE analysis and complexity analysis show that the iterative receiver with channel estimation achieves ML and MMSE lower bounds with close to linear complexity after the second stage estimation. We compared the iterative data-driven channel estimator with the conventional pilot-aided MLE, MMSEE, and decision feedback channel estimators in both downlink and uplink of a practical system with fast mobility. The iterative data-driven channel estimator out performs the decision direct channel estimator by 2.5dB. It also out performs the conventional pilot-aided channel estimator by 1dB. It is worth mentioning that such performance gains are achieved by employing less reference signals, which

means that the macro cell coverage is maintained without losing system capacity in a highly dynamic channel environment. We also show the robustness of the iterative data-driven channel estimator if a maximum 4% carrier frequency offset is present in the system, where the degradation is only a fraction of decibel.

In the interference mitigation for the multiple antenna system, we developed a joint interference mitigation and channel estimation framework for interference limited system under highly dynamic channel environment. The novel iterative data-driven channel estimator performs time-domain combining and frequency-domain combining in MIMO configuration and cooperates with various linear detection methods so that both interference mitigation and channel estimation can be handled robustly in practical indoor and outdoor environment. In the Alamouti STC-OFDM system, we utilized the channel estimates combined from soft decoded data and reference signal to the iterative MRC receiver. The conventional MRC receiver has degraded performance as the mobility increases, and eventually fails because the assumption of the constant channel response between two consecutive data symbols no longer holds. Nevertheless, since the channel variations at high mobilities are tracked by the iterative data-driven channel estimation, the conventional Alamouti STC-OFDM system can be operated at high mobility environment with the iterative data-driven MRC receiver, where more than 8dB performance gains are obtained compared to the conventional MRC receiver. This is a great indication that the channel variation should be tracked in the realistic mobile radio environment.

Furthermore, in the SM-OFDM system, we developed a few iterative receivers with linear interference cancelation and data-driven channel estimation. We show that at low mobility, the iterative receiver can achieve a gain of 2dB compared to the conventional MMSE receiver at operating point of 10^{-2} frame error rate. On the other hand, at high mobility, the conventional MMSE receiver with one-shot channel estimation failed to operate, while the iterative receiver performed close to the optimal where the perfect CSI is known. In addition, post-processing provides a further 2dB gain over the pure interference cancelation at 10^{-3} frame error rate (in higher SNR region). This interesting finding indicates that it is necessary to have additional signal processing after interference cancelation if the system operates at higher SNR. We also showed the 16QAM modulated Alamouti STC-OFDM system and the QPSK modulated SM-OFDM system under the same spectral efficiency in a realistic mobile radio channel environment. We showed that the SM-OFDM system with lower modulation scheme is more robust than the Alamouti STC-

OFDM system with higher modulation. This is because the Alamouti STC based system assumes a stationary channel between data symbols, which is not realistic in channels with mobility.

In the second part of the thesis, we investigated the interference mitigation with nonlinear methods. The first nonlinear method we studied is the sphere decoder. Among the sphere decoder algorithms, FP and SE are two popular enumeration strategies, however, they are optimized for the ML solution, which does not take advantage of the MAP solution by using *a-priori* information. We introduced the accumulated *a priori* information metric and modified the FP and SE algorithms accordingly to make them suitable for an iterative receiver with MAP detection. 2dB gains for QPSK and 4dB gains for 16QAM are obtained from the iterative detection and decoding approach, and the complexity can be reduced by 10% over iterations in SE algorithm.

We also investigated the SE algorithm and found one drawback that the poor ZF-DFE estimates usually degrade the system performance. We developed two novel schemes to improve the ZF-DFE estimates by utilizing the *a priori* information. The first scheme is to obtain the update ZF-DFE estimates under MAP detection criteria. We first approximated the *a priori* information as a quadratic polynomial and included it in the ML cost function. Then we obtained the updated ZF-DFE estimates by solving this new cost function. The second scheme is to perform the *a priori* zig-zag method on the neighboring nodes of the original ZF-DFE estimates and select the nodes with the best *a priori* probability, where we perform the tree search from the new starting node. We show that another 2dB gain can be obtained, and the complexity can be further reduced by another 10% over iterations. Hence, the performance and complexity benefits from employing these two novel schemes indicate that more accurate estimate of the tree node at each level has significant impact on the tree search outcome and convergence. It is therefore valuable to employ the developed schemes in the sphere decoder receiver.

Finally, we studied another nonlinear method, known as the MCMC method. The conventional MCMC method suffers from an error floor at high SNR. The reason for this problem is the bits with high *a priori* probability dominate the Markov chain such that the Markov chain is trapped in the "ill conditioned" states and therefore cannot improve performance. This phenomenon challenged the fundamental idea behind the MCMC's statistical approach, that is that the Markov chain should cover as many states as possible in order to converge to the equilibrium distribution. We developed two novel MCMC methods, namely the RSS-MCMC

method and FST-MCMC method. The idea of the RSS-MCMC method is to get rid of the interference from reliable bits, then run the Markov chain only for the unreliable bits in the new system with less interference. On the other hand, the idea of the FST-MCMC method is to force the Markov chain to move by manually changing the "ill conditioned" bits. Before performing these two methods, we analyzed the reliability of the extrinsic information exchanged between the detector and decoder in the turbo reception architecture, and developed two reliability constraints to separate the reliable bits from the entire data vector. The first constraint is developed based on the distribution of the LLRs. The second constraint is developed based on the consistency of the ML and the *a priori* metric. We also define the "ill conditioned" bits in the FST-MCMC method as the bits in the unreliable signal set that do not change for a set period of time in the sample drawing process. We show that both methods can remove the error floor in the high SNR region. At low SNR marginal performance improvement can also be observed. In addition to the performance enhancement, we also show that the RSS-MCMC method can achieve further complexity reduction of 35% for QPSK at $\frac{E_b}{N_0} = 6$dB and 25% at $\frac{E_b}{N_0} = 12dB$ for 16QAM. Such complexity reduction is due to the Gibbs sampler which only needs to draw samples for the unreliable bits. These bits are partially from the entire signal space after interference cancelation. Last but not least, we investigated the performance and complexity trade-off by selecting various thresholds. Our preliminary performance and complexity trade-off chart provides a practical guideline on how to select optimal threshold for different SNRs.

7.2 Future Research Directions

In this section we outline a number of future research directions to arise from the work presented in this thesis.

In Chapter 3, we present the simulation of the iterative turbo receiver with channel estimation for SISO-OFDM system under the present of the residue CFO. And the results show that the iterative turbo channel estimation is robust to the residual CFO of up to 4% of the sub-carrier spacing. In practical OFDM system, synchronization with CFO compensation could be a challenging task. When the residual CFO becomes larger, the influence of the ICI caused by CFO becomes significant and cannot be simply absorbed by the central limited theorem into the effective noise. The best way to remove the effect of the ICI is to estimate the off-diagonal terms of the channel matrix and cancel them all. The estimation of all

off-diagonal items of channel matrix, however, results in a prohibitive complexity, especially when the number of subcarriers becomes larger. Although handling the problem of large CFO is out of the scope of this thesis, our primary investigation shows that the influence of the ICI has certain structure rather than being completely random. For example, the closer the neighboring subcarrier is to the subcarrier of interest, the higher the power of the ICI from that neighboring subcarrier. This phenomenon suggests that it is not necessary to estimate all off-diagonal terms of the channel matrix. It is sufficient to cancel the ICI from several neighboring subcarriers. Hence, the potential approach could be to develop a method to focus on the iterative channel estimation with the presence of the CFO.

In Chapter 4, we developed iterative receivers with channel estimation for a single user MIMO-OFDM system. A natural extension of this work is to investigate the multiuser MIMO-OFDM system, also known as MIMO-orthogonal frequency division multiple access (OFDMA) system. In the OFDMA system, users are allocated to different subcarriers, which can be either disjoint or overlapped. If the subcarrier allocation is disjoint, the iterative receiver developed in this thesis can be applied without any modification. However, if the subcarrier allocation is overlapped, massive interference is generated from different users in addition to that from multiple antennas, which makes the channel estimation even more complicated. Furthermore, if residual CFOs are presented, especially in the uplink, all users have different CFOs, no matter how the users are allocated, interference will be always there. Hence, the potential work can be on the iterative multiuser detection with channel estimation with or without the presence of CFO in the MIMO-OFDMA system.

Furthermore, for the Alamouti STC system, we have show that under high mobility environment, the realistic channel shows significant variation particularly in the time-domain. The assumption that the channel response between two consecutive data symbols is stationary does no longer hold. Therefore, the orthogonal property of the channel matrix is destroyed. In this case, the Alamouti STC system can be considered a SM system with time diversity (same symbols are transmitted twice in consecutive time interval). In Chapter 4, the performance gain we obtained from the iterative receiver is mainly from the channel re-estimation. The potential work can be on the employment of the interference cancelation approach rather than the MRC approach for the space-time coded system in high mobility environment.

In both Chapter 3 and 4, we illustrated the iterative receiver in the OFDM

system. The most important advantage of OFDM system over the single carrier system is the utilization of the frequency domain signal processing techniques. For example, the ISI problem caused by the multipath fading in the single carrier system is mitigated in the OFDM system because the multipath fading in the time-domain has been transferred into flat fading in the frequency-domain. However, the OFDM system still cannot solve the deep fading problem even with perfect channel estimation. Recently, a technique called channel shortening [123–127] has become popular in the literature. The idea is to pre-equalize the channel in the time-domain so that the channel frequency response looks flat in the frequency-domain. The time-domain equalization could be computationally expensive, the potential work could be on the rake-receiver approach with iterative frequency channel estimation and detection followed by multipath cancelation and rake combining in the time-domain.

In Chapter 5, we studied the sphere decoder algorithms which focus on the depth-first approach. Breadth-first sphere decoder algorithms, such as K-best sphere decoder [69, 128, 129], are also popular in the literature. Breadth-first sphere decoders are known to have fixed complexity with no-guaranteed performance. Juntti *et al.* [59] modified the conventional K-best sphere decoder [69] by initializing the K-best sphere decoder by LMMSE estimate. However, the LMMSE generally has higher complexity as discussed in the Chapter 3 and 4 of this thesis. It could be interesting to know how much performance gain and complexity reduction can be obtained if *a priori* information as developed in this thesis is employed in the breadth-first sphere decoder algorithm. It could be also interesting to see whether the depth-first and breadth-first algorithms can be combined into a hybrid sphere decoder for iterative receiver. Furthermore, in Chapter 6, the *a priori* information is utilized to qualify the reliable bits from the entire signal space. We can also apply the interference cancelation to the sphere decoder to form a RSS-SD method. Our preliminary results show that with the same performance, the complexity of RSS-SD method can be reduced significantly because the complex signal enumeration process is performed only on the unreliable bits.

In Chapter 6, for different SNR, there is a performance and complexity trade-off for the RSS-MCMC method. The optimal operating points for various SNR on the performance versus complexity curve are corresponding to different LLR reliability. In practical systems, in order to operate at the optimal performance and complexity, the threshold for the conditional LLR distribution has to be changed for different SNRs. Although simulations can be carried out to show the performance

and complexity curves for different system configurations, this is unrealistic for real systems. A more feasible solution is to pick a threshold and obtain the trade-off point with reasonable complexity with minor performance loss compared to the optimal solution. Hence, the last but not the least, other potential work could on the theoretical formulation of this optimization problem.

Finally, the development of the cost effect data-driven interference mitigation methods in Chapter 5 and 6 is based on a generic MIMO spatial multiplexed system and perfect channel estimation. This allows the developed methods to be applied to any system that needs interference mitigation. Future work can be focused on applying the advanced iterative non-linear detection methods developed in this thesis to a practical interference limited system. Furthermore, the iterative data-driven channel estimation developed in Chapter 3 and 4 could be integrated into a system where it could operate jointly with the advanced detection methods.

Appendix A

A.1 The Calculation of E_b/N_0

The E_b/N_0 calculation is defined as information bit energy E_b over the noise power spectral density N_0, as seen at the receiver. Considering the generalized SISO/MIMO system in Fig. A.1, given that $(E_b/N_0)_{dB}$ in dB scale, denoting the transmitted symbol energy as E_s, data modulation order as M, channel encoder rate as R_c, the number of transmitting antennas as N_T, and the number of receiving antennas as N_R, the noise variance is calculated in following steps:

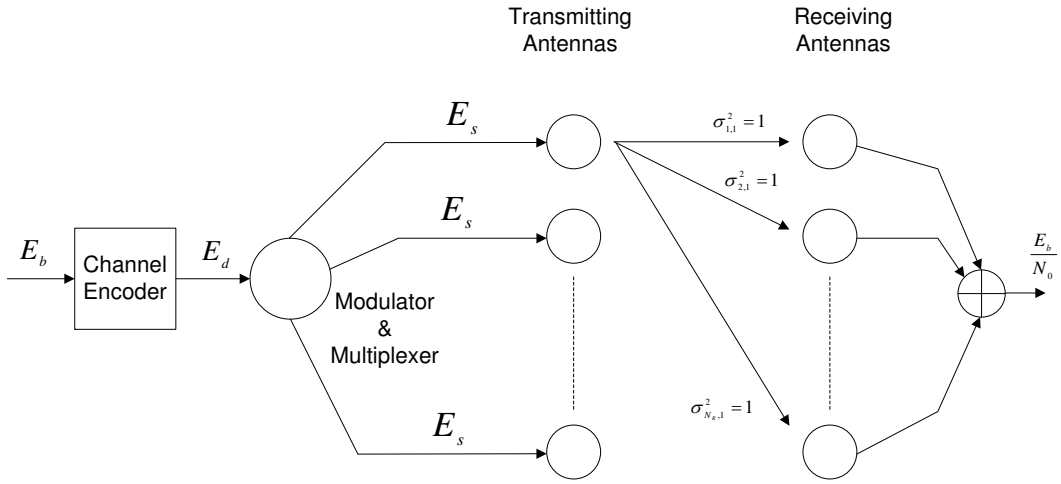

Figure A.1: Generalized SISO/MIMO system

Step 1 Assuming channel energy of each transmitting and receiving antenna link is normalized to one, and the data symbol stream at each transmitting antenna has the rate R, the average symbol energy at the receiver after combining all

the receiving antennas are given by:

$$\overline{E_s} = \frac{E_s \cdot R \cdot N_T \cdot N_R}{R \cdot N_T} = E_s \cdot N_R, \tag{A.1}$$

where the numerator is the total symbol energy collected at the receiver, and the denominator is the total number of symbols collected at the receiver.

Step 2 As the transmitted symbol is formed by $\log_2 M$ coded bits, hence, the average coded bit energy is given by:

$$\overline{E_d} = \frac{\overline{E_s}}{\log_2 M} = \frac{E_s \cdot N_R}{\log_2 M}. \tag{A.2}$$

Step 3 As the convolution encoder does not introduce additional energy for the information bit, the input and output energy of convolutional encoder should be conserved as:

$$E_b \cdot R = \frac{E_s \cdot N_R}{\log_2 M}. \tag{A.3}$$

Hence, the information bit energy can be expressed as:

$$E_b = \frac{E_s \cdot N_R}{R \cdot \log_2 M}. \tag{A.4}$$

Step 4 Known that the noise variance is defined as the double-sided noise power spectral density as:

$$\sigma^2 = \frac{N_0}{2} = \frac{E_b}{2} \cdot 10^{-\frac{(\frac{E_b}{N_0})_{dB}}{10}}, \tag{A.5}$$

substitute E_b in equation (A.4) into equation (A.5), the noise variance is obtained by:

$$\sigma^2 = \frac{E_s \cdot N_R}{2 \cdot R \cdot \log_2 M} \cdot 10^{-\frac{(\frac{E_b}{N_0})_{dB}}{10}}. \tag{A.6}$$

Therefore, in the computer simulation, given the SNR $\frac{E_b}{N_0}$ in dB scale, symbol energy E_s, the number of receiving antennas N_R, channel coder rate R, and data modulation order M, the noise variance can be calculated by equation (A.6).

Step 5 SNR can also be defined the transmitted symbol energy E_s over the noise power spectral density N_0, i.e. $\frac{E_s}{N_0}$, which is also known as intermediate SNR. Sometimes it is worth finding the SNR relationship between the information bit and transmitted symbol. From equation (A.4), such relationship can be

easily derived as:

$$(\frac{E_b}{N_0})_{dB} = (\frac{E_s}{N_0})_{dB} + 10\log_{10}\frac{N_R}{R \cdot \log_2 M}. \tag{A.7}$$

A.2 Estimation of Soft Symbol

As discussed in 2.5, the soft symbol is computed from the LLR values given by the *a priori* information. Here we derive the Bayesian estimate of the soft symbol for BPSK, QPSK and 16QAM modulation schemes. Let λ be the LLR value fed back from the channel decoder for the coded bit d, the probability of the coded bit d to be 1 and 0 can be expressed as:

$$\begin{aligned} P(d=1) &= \frac{e^{\lambda}}{1+e^{\lambda}} = \frac{e^{\lambda/2}}{e^{\lambda/2}+e^{-\lambda/2}} \\ &= \frac{1}{2}(1+\frac{e^{\lambda/2}-e^{-\lambda/2}}{e^{\lambda/2}+e^{-\lambda/2}}) \\ &= \frac{1}{2}(1+\tanh(\lambda/2)), \end{aligned} \tag{A.8}$$

$$P(d=0) = 1 - P(d=1) = \frac{1}{2}(1-\tanh(\lambda/2)). \tag{A.9}$$

In the case of BPSK, $d_0 = 1$ is mapping to $s = +1$, and $d_0 = 0$ is mapping to $s = -1$, hence, the soft symbol is given by:

$$\widehat{s} = 1 \cdot P(d_0 = 1) + (-1) \cdot P(d_0 = 0) = \tanh(\lambda_0/2). \tag{A.10}$$

In the case of Gray-coded QPSK, the complex QPSK symbol is formed by $\{d_0, d_1\}$, d_0 is mapped to real part and d_1 is mapped to imaginary part. As the QPSK symbol is Gray-coded, either the real part or the imaginary part is similar to individual BPSK case. Hence,

$$\Re\{\widehat{s}\} = \tanh(\lambda_0/2), \tag{A.11}$$

$$\Im\{\widehat{s}\} = \tanh(\lambda_1/2), \tag{A.12}$$

where $\Re\{\cdot\}$ and $\Im\{\cdot\}$ are the real and imaginary part of the complex number, respectively.

In the case of the 16-QAM, the complex 16-QAM symbol is formed by $\{d_0, d_1, d_2, d_3\}$, $\{d_0, d_1\}$ is mapped to real part and $\{d_2, d_3\}$ is mapped to imaginary part. The mapping is as follows: $\{1,1\} \rightarrow +3$, $\{0,1\} \rightarrow +1$, $\{0,0\} \rightarrow -1$, and $\{1,0\} \rightarrow -3$. Hence,

$$\begin{aligned} \Re\{\widehat{s}\} &= 3 \cdot P(d_0 = 1, d_1 = 1) + 1 \cdot P(d_0 = 0, d_1 = 1) \\ &\quad +(-1) \cdot P(d_0 = 1, d_1 = 0) + (-3) \cdot P(d_0 = 1, d_1 = 0) \end{aligned}$$

$$
\begin{aligned}
&= \frac{3}{4}(1+\tanh(\lambda_1/2))(1+\tanh(\lambda_0/2)) + \frac{1}{4}(1+\tanh(\lambda_1/2))(1-\tanh(\lambda_0/2)) \\
&\quad -\frac{1}{4}(1-\tanh(\lambda_1/2))(1-\tanh(\lambda_0/2)) - \frac{3}{4}(1-\tanh(\lambda_1/2))(1+\tanh(\lambda_0/2)) \\
&= \frac{1}{4}[8\tanh(\lambda_1/2) + 4\tanh(\lambda_1/2)\tanh(\lambda_0/2)] \\
&= \tanh(\lambda_1/2)[2+\tanh(\lambda_0/2)]. \qquad \text{(A.13)}
\end{aligned}
$$

Similarly,

$$
\begin{aligned}
\Im\{\widehat{s}\} &= 3\cdot P(d_2=1,d_3=1) + 1\cdot P(d_2=0,d_3=1) \\
&\quad +(-1)\cdot P(d_2=1,d_3=0) + (-3)\cdot P(d_2=1,d_3=0) \\
&= \frac{3}{4}(1+\tanh(\lambda_3/2))(1+\tanh(\lambda_2/2)) + \frac{1}{4}(1+\tanh(\lambda_3/2))(1-\tanh(\lambda_2/2)) \\
&\quad -\frac{1}{4}(1-\tanh(\lambda_3/2))(1-\tanh(\lambda_2/2)) - \frac{3}{4}(1-\tanh(\lambda_3/2))(1+\tanh(\lambda_2/2)) \\
&= \frac{1}{4}[8\tanh(\lambda_3/2) + 4\tanh(\lambda_3/2)\tanh(\lambda_2/2)] \\
&= \tanh(\lambda_3/2)[2+\tanh(\lambda_2/2)]. \qquad \text{(A.14)}
\end{aligned}
$$

Appendix B

B.1 Proof of Effective Noise Statistics in Pilot Symbol Channel Estimation for SISO-OFDM System

In Chapter 3 section 3.3.2, the effective noise in the pilot symbol channel estimation for SISO-OFDM System is given by:

$$\begin{aligned} W_P^{'}(p) &= \sum_{q \neq p} H_{p,q} X_P(q) X_P^*(p) \\ &\quad + \sum_{n \neq p,q} H_{p,n} \sqrt{\frac{E_d}{E_p}} X_d(n) X_P^*(p) + \frac{W(p) X_P^*(p)}{\sqrt{E_p}}, \end{aligned} \tag{B.1}$$

where the symbol index superscription (i) is dropped for brevity. Assuming that the pilot symbols $X_P(p)$, $X_P(q)$ the data symbol $X_d(n)$, and the noise sample $W(p)$ are independent, the expectation of $W_P^{'}(p)$ is given by:

$$\begin{aligned} E\{W_P^{'}(p)\} &= \sum_{q \neq p} H_{p,q} \underbrace{E\{X_P(q)\}}_{=0} \underbrace{E\{X_P^*(p)\}}_{=0} \\ &\quad + \sum_{n \neq p,q} H_{p,n} \sqrt{\frac{E_d}{E_p}} \underbrace{E\{X_d(n)\}}_{=0} \underbrace{E\{X_P^*(p)\}}_{=0} + \frac{E\{W(p)\}}{\sqrt{E_p}} \underbrace{E\{X_P^*(p)\}}_{=0} \\ &= 0, \end{aligned} \tag{B.2}$$

where the expectation of the pilot symbols and data symbols $E\{X_P(q)\} = E\{(X_P(p)) = E\{X_d(n)\} = 0$ as the symbols in the signal constellation set are equal probable.

Denote $\alpha = \sum_{q \neq p} H_{p,q} X_P(q) X_P^*(p)$, $\beta = \sum_{n \neq p,q} H_{p,n} \sqrt{\frac{E_d}{E_p}} X_d(n) X_P^*(p)$, and $\gamma =$

$\frac{W(p)X_P^*(p)}{\sqrt{E_p}}$, the variance of $W_P^{'}(p)$ can be obtained by:

$$\begin{aligned} E\{W_P^{'*}(p)W_P^{'}(p)\} &= E\{(\alpha+\beta+\gamma)^*(\alpha+\beta+\gamma)\} \\ &= E\{\alpha^*\alpha+\alpha^*\beta+\alpha^*\gamma+\beta^*\alpha+\beta^*\beta+\beta^*\gamma \\ &\quad +\gamma^*\alpha+\gamma^*\beta+\gamma^*\gamma\}, \end{aligned} \tag{B.3}$$

where

$$\begin{aligned} E\{\alpha^*\alpha\} &= E\{\sum_{q\neq p}\sum_{q^{'}\neq p} X_P(p)X_P^*(q)H_{p,q}^*H_{p^{'},q}X_P(q^{'})X_P^*(p)\} \\ &= \sum_{q\neq p} E\{H_{p,q}^*H_{p,q}\}\underbrace{E\{X_P(q)X_P^*(q)\}}_{=1}\underbrace{E\{X_P(p)X_P^*(p)\}}_{=1} \\ &= \sum_{q\neq p} E\{|H_{p,q}|^2\}, \end{aligned} \tag{B.4}$$

$$\begin{aligned} E\{\alpha^*\beta\} &= E\{\sqrt{\frac{E_d}{E_p}}\sum_{q\neq p}\sum_{n\neq p,q} X_P(p)X_P^*(q)H_{p,q}^*H_{p,n}X_d(n)X_P^*(p)\} \\ &= \sqrt{\frac{E_d}{E_p}}\sum_{q\neq p}\sum_{n\neq p,q} E\{H_{p,q}^*H_{p,n}\}\underbrace{E\{X_P(p)X_P^*(p)\}}_{=1}\underbrace{E\{X_P^*(q)\}}_{=0}\underbrace{E\{X_d(n)\}}_{=0} \\ &= 0, \end{aligned} \tag{B.5}$$

$$\begin{aligned} E\{\alpha^*\gamma\} &= E\{\sum_{q\neq p} X_P(p)X_P^*(q)H_{p,q}^*\frac{W(p)X_P^*(p)}{\sqrt{E_p}}\} \\ &= \frac{1}{\sqrt{E_p}}\sum_{q\neq p} E\{H_{p,q}^*\}\underbrace{E\{X_P(p)X_P^*(p)\}}_{=1}\underbrace{E\{X_P^*(q)\}}_{=0}\underbrace{E\{W(p)\}}_{=0} \\ &= 0, \end{aligned} \tag{B.6}$$

$$\begin{aligned} E\{\beta^*\alpha\} &= \sum_{q\neq p}\sum_{n\neq p,q}\sqrt{\frac{E_d}{E_p}}X_P(p)X_d^*(n)H_{p,n}^*H_{p,q}X_P(q)X_P^*(p) \\ &= \sqrt{\frac{E_d}{E_p}}\sum_{q\neq p}\sum_{n\neq p,q} E\{H_{p,q}H_{p,n}^*\}\underbrace{E\{X_P^*(p)X_P(p)\}}_{=1}\underbrace{E\{X_P(q)\}}_{=0}\underbrace{E\{X_d^*(n)\}}_{=0} \\ &= 0, \end{aligned} \tag{B.7}$$

$$\begin{aligned} E\{\beta^*\beta\} &= \sum_{n\neq p,q}\sum_{n'\neq p,q}\frac{E_d}{E_p}X_P(p)X_d^*(n)H_{p,n}^*H_{p,n'}X_d(n')X_P^*(p) \\ &= \frac{E_d}{E_p}\sum_{n\neq p,q}E\{H_{p,n}^*H_{p,n}\}\underbrace{E\{X_P(p)X_P^*(p)\}}_{=1}\underbrace{E\{X_d^*(n)X_d(n)\}}_{=1} \\ &= \frac{E_d}{E_p}\sum_{n\neq p,q}E\{|H_{p,n}|^2\}, \end{aligned} \tag{B.8}$$

$$\begin{aligned} E\{\beta^*\gamma\} &= E\{\sum_{n\neq p,q}\frac{\sqrt{E_d}}{E_p}X_P(p)X_d^*(n)H_{p,n}^*W(p)X_P^*(p)\} \\ &= \frac{\sqrt{E_d}}{E_p}\sum_{n\neq p,q}E\{H_{p,n}^*\}\underbrace{E\{X_P(p)X_P^*(p)\}}_{=1}\underbrace{E\{X_d^*(n)\}}_{=0}\underbrace{E\{W(p)\}}_{=0} \\ &= 0, \end{aligned} \tag{B.9}$$

$$\begin{aligned} E\{\gamma^*\alpha\} &= E\{\sum_{q\neq p}\frac{1}{\sqrt{E_p}}X_P(p)W^*(p)H_{p,q}X_P(q)X_P^*(p)\} \\ &= \frac{1}{\sqrt{E_p}}\sum_{q\neq p}E\{H_{p,q}\}\underbrace{E\{X_P(p)X_P^*(p)\}}_{=1}\underbrace{E\{W^*(p)\}}_{=0} \\ &= 0, \end{aligned} \tag{B.10}$$

$$\begin{aligned} E\{\gamma^*\beta\} &= E\{\sum_{n\neq p,q}\frac{\sqrt{E_d}}{E_p}X_P(p)W^*(p)H_{p,n}X_d(n)X_P^*(p)\} \\ &= \frac{\sqrt{E_d}}{E_p}\sum_{n\neq p,q}E\{H_{p,n}\}\underbrace{E\{X_P(p)X_P^*(p)\}}_{=1}\underbrace{E\{X_d^*(n)\}}_{=0}\underbrace{E\{W^*(p)\}}_{=0} \\ &= 0, \end{aligned} \tag{B.11}$$

and

$$\begin{aligned} E\{\gamma^*\gamma\} &= E\{\frac{1}{E_p}X_P(p)W^*(p)W(p)X_P^*(p)\} \\ &= \frac{1}{E_p}\underbrace{E\{X_P(p)X_P^*(p)\}}_{=1}\underbrace{E\{W^*(p)W(p)\}}_{=\sigma_w^2} \\ &= \frac{\sigma_w^2}{E_p}. \end{aligned} \tag{B.12}$$

Hence,equation (B.3) can be expressed by:

$$\begin{aligned} E\{W_P^{'*}(p)W_P^{'}(p)\} &= \sum_{q\neq p} E\{|H_{p,q}|^2\} + \frac{E_d}{E_p}\sum_{n\neq p,q} E\{|H_{p,n}|^2\} + \frac{\sigma_w^2}{E_p} \\ &= \frac{\sigma_{ICI}^2 + \sigma_w^2}{E_p}, \end{aligned} \tag{B.13}$$

where

$$\sigma_{ICI}^2 = E_p \sum_{q\neq p} E\{|H_{p,q}|^2\} + E_d \sum_{n\neq p,q} E\{|H_{p,n}|^2\} \tag{B.14}$$

is the power of ICI from other subcarriers rather than the p^{th} subcarrier of interest.

B.2 Proof of Effective Noise Statistics in Data Symbol Channel Estimation for SISO-OFDM System

In Chapter 3 Section 3.3.3, the effective noise in the data symbol channel estimation for SISO-OFDM System is given by:

$$\begin{aligned} W_d^{'}(m) &= \sum_{n\neq m} H_{m,n}\frac{X_d(n)\widehat{X}_d^*(m)}{\sqrt{|\widehat{X}_{d\in\Theta}|^2}} \\ &\quad + \sum_{p\neq m} H_{m,p}\frac{\sqrt{E_p}X_P(p)\widehat{X}_d^*(m)}{\sqrt{E_d|\widehat{X}_{d\in\Theta}|^2}} + \frac{W(m)\widehat{X}_d^*(m)}{\sqrt{E_d|\widehat{X}_{d\in\Theta}|^2}}, \end{aligned} \tag{B.15}$$

where the symbol index superscript (i) is dropped for brevity. Assuming that the pilot symbols $X_P(p)$, the data symbol $X_d(n)$ and $X_d(m)$, and the noise sample $W(m)$ are independent, the expectation of $W_d^{'}(m)$ is given by:

$$\begin{aligned} E\{W_d^{'}(m)\} &= \sum_{n\neq m} H_{m,n}\frac{\overbrace{E\{X_d(n)\}}^{=0}\widehat{X}_d^*(m)\}}{\sqrt{|\widehat{X}_{d\in\Theta}|^2}} \\ &\quad + \sum_{p\neq m} H_{m,p}\frac{\sqrt{E_p}\overbrace{E\{X_P(p)\}}^{=0}\widehat{X}_d^*(m)}{\sqrt{E_d|\widehat{X}_{d\in\Theta}|^2}} + \frac{\overbrace{E\{W(m)\}}^{=0}\widehat{X}_d^*(m)}{\sqrt{E_d|\widehat{X}_{d\in\Theta}|^2}} \\ &= 0. \end{aligned} \tag{B.16}$$

Denote $\alpha = \sum_{n\neq m} H_{m,n}\frac{X_d(n)\widehat{X}_d^*(m)}{\sqrt{|\widehat{X}_{d\in\Theta}|^2}}$, $\beta = \sum_{p\neq m} H_{m,p}\frac{\sqrt{E_p}X_P(p)\widehat{X}_d^*(m)}{\sqrt{E_d|\widehat{X}_{d\in\Theta}|^2}}$ and $\gamma = \frac{W(m)\widehat{X}_d^*(m)}{\sqrt{E_d|\widehat{X}_{d\in\Theta}|^2}}$, the variance of $W_d^{'}(m)$ can be obtained by:

$$\begin{aligned} E\{W_d^{'*}(m)W_d^{'}(m)\} &= E\{(\alpha+\beta+\gamma)^*(\alpha+\beta+\gamma)\} \\ &= E\{\alpha^*\alpha+\alpha^*\beta+\alpha^*\gamma+\beta^*\alpha+\beta^*\beta+\beta^*\gamma \\ &\quad +\gamma^*\alpha+\gamma^*\beta+\gamma^*\gamma\}, \end{aligned} \tag{B.17}$$

where

$$\begin{aligned} E\{\alpha^*\alpha\} &= E\{\sum_{n\neq m}\sum_{n^{'}\neq m}\frac{1}{|\widehat{X}_{d\in\Theta}|^2}\widehat{X}_d(m)X_d^*(n)H_{m,n}^*H_{m,n^{'}}X_d(n^{'})\widehat{X}_d^*(m)\} \\ &= \frac{1}{|\widehat{X}_{d\in\Theta}|^2}\sum_{n\neq m}E\{H_{m,n}^*H_{m,n}\}\underbrace{E\{X_d^*X_d(n)\}}_{=0}\underbrace{\widehat{X}_d(m)\widehat{X}_d^*(m)}_{\approx|\widehat{X}_{d\in\Theta}|^2} \\ &\approx \sum_{n\neq m}E\{|H_{m,n}|^2\}, \end{aligned} \tag{B.18}$$

$$\begin{aligned} E\{\alpha^*\beta\} &= E\{\sum_{n\neq m}\sum_{p\neq m}\frac{\sqrt{E_p}}{\sqrt{E_d}|\widehat{X}_{d\in\Theta}|^2}\widehat{X}_d(m)X_d^*(n)H_{m,n}^*H_{m,p}X_P(p)\widehat{X}_d^*(m)\} \\ &= \frac{\sqrt{E_p}}{\sqrt{E_d}|\widehat{X}_{d\in\Theta}|^2}\sum_{n\neq m}\sum_{p\neq m}E\{H_{m,n}^*H_{m,p}\}\underbrace{E\{X_d^*(n)\}}_{=0} \\ &\quad \cdot\underbrace{E\{X_P(p)\}}_{=0}\widehat{X}_d(m)\widehat{X}_d^*(m) \\ &= 0, \end{aligned} \tag{B.19}$$

$$\begin{aligned} E\{\alpha^*\gamma\} &= E\{\sum_{n\neq m}\frac{1}{\sqrt{E_d}|\widehat{X}_{d\in\Theta}|^2}\widehat{X}_d(m)X_d^*(n)H_{m,n}W(m)\widehat{X}_d^*(m)\} \\ &= \frac{1}{\sqrt{E_d}|\widehat{X}_{d\in\Theta}|^2}\sum_{n\neq m}E\{H_{m,n}\}\underbrace{E\{X_d^*(n)\}}_{=0}\underbrace{E\{W(m)\}}_{=0}\widehat{X}_d(m)\widehat{X}_d^*(m) \\ &= 0, \end{aligned} \tag{B.20}$$

$$E\{\beta^*\alpha\} = E\{\sum_{p\neq m}\sum_{n\neq m}\frac{\sqrt{E_p}}{\sqrt{E_d}|\widehat{X}_{d\in\Theta}|^2}\widehat{X}_d(m)X_P^*(p)H_{m,p}^*H_{m,n}X_d(n)\widehat{X}_d^*(m)\}$$

$$
\begin{aligned}
&= \frac{\sqrt{E_p}}{\sqrt{E_d}|\widehat{X}_{d\in\Theta}|^2} \sum_{p\neq m} \sum_{n\neq m} E\{H^*_{m,p} H_{m,n}\} \underbrace{E\{X^*_P(p)\}}_{=0} \\
&\quad \cdot \underbrace{E\{X_d(n)\}}_{=0} \widehat{X}_d(m) \widehat{X}^*_d(m) \\
&= 0, \qquad \text{(B.21)}
\end{aligned}
$$

$$
\begin{aligned}
E\{\beta^*\beta\} &= E\{\sum_{p\neq m} \sum_{q\neq m} \frac{E_p}{E_d|\widehat{X}_{d\in\Theta}|^2}(p) \widehat{X}_d(m) X^*_P(p) H^*_{m,p} H_{m,q} X_P(q) \widehat{X}^*_d(m)\} \\
&= \frac{E_p}{E_d|\widehat{X}_{d\in\Theta}|^2} \sum_{p\neq m} E\{H^*_{m,p} H_{m,p}\} \underbrace{E\{X^*_P(p) X_P(p)\}}_{=1} \underbrace{\widehat{X}_d(m)\widehat{X}^*_d(m)}_{\approx |\widehat{X}_{d\in\Theta}|^2} \\
&\approx \frac{E_p}{E_d} \sum_{p\neq m} E\{|H_{m,p}|^2\}, \qquad \text{(B.22)}
\end{aligned}
$$

$$
\begin{aligned}
E\{\beta^*\gamma\} &= E\{\sum_{p\neq m} \frac{\sqrt{E_p}}{E_d|\widehat{X}_{d\in\Theta}|^2} \widehat{X}_d(m) X^*_P(p) H^*_{m,p} W(m) \widehat{X}^*_d(m)\} \\
&= \frac{\sqrt{E_p}}{E_d|\widehat{X}_{d\in\Theta}|^2} \sum_{p\neq m} E\{H^*_{m,p}\} \underbrace{E\{W(m)\}}_{=0} \underbrace{X^*_P(p)}_{=0} \widehat{X}_d(m)\widehat{X}^*_d(m) \\
&= 0, \qquad \text{(B.23)}
\end{aligned}
$$

$$
\begin{aligned}
E\{\gamma^*\alpha\} &= E\{\sum_{n\neq m} \frac{1}{\sqrt{E_d}|\widehat{X}_{d\in\Theta}|^2} \widehat{X}_d(m) W^*(m) H_{m,n} X_d(n) \widehat{X}^*_d(m)\} \\
&= \frac{1}{\sqrt{E_d}|\widehat{X}_{d\in\Theta}|^2} \sum_{n\neq m} E\{H_{m,n}\} \underbrace{E\{W^*\}}_{=0} \underbrace{E\{X_d(n)\}}_{=0} \widehat{X}_d(m)\widehat{X}^*_d(m) \\
&= 0, \qquad \text{(B.24)}
\end{aligned}
$$

$$
\begin{aligned}
E\{\gamma^*\beta\} &= E\{\sum_{p\neq m} \frac{\sqrt{E_p}}{E_d|\widehat{X}_{d\in\Theta}|^2} \widehat{X}_d(m) W^*(m) H_{m,p} X_P(p) \widehat{X}^*_d(m)\} \\
&= \frac{\sqrt{E_p}}{E_d|\widehat{X}_{d\in\Theta}|^2} \sum_{p\neq m} E\{H_{m,p}\} \underbrace{E\{W^*\}}_{=0} \underbrace{E\{X_P(p)\}}_{=0} \widehat{X}_d(m)\widehat{X}^*_d(m) \\
&= 0, \qquad \text{(B.25)}
\end{aligned}
$$

and

$$\begin{aligned} E\{\gamma^*\gamma\} &= E\{\frac{1}{E_d|\widehat{X}_{d\in\Theta}|^2}\widehat{X}_d(m)W^*(m)W(m)\widehat{X}_d^*(m)\} \\ &= \frac{1}{E_d|\widehat{X}_{d\in\Theta}|^2}\underbrace{E\{W^*(m)W(m)\}}_{=\sigma_w^2}\underbrace{\widehat{X}_d(m)\widehat{X}_d^*(m)}_{\approx|\widehat{X}_{d\in\Theta}|^2} \\ &\approx \frac{\sigma_w^2}{E_d}. \end{aligned} \tag{B.26}$$

Hence,equation (B.17) can be expressed by:

$$\begin{aligned} E\{W_d^{'*}(m)W_d^{'}(m)\} &\approx \sum_{n\neq m}E\{|H_{m,n}|^2\}+\frac{E_p}{E_d}\sum_{p\neq m}E\{|H_{m,p}|^2\}+\frac{\sigma_w^2}{E_d} \\ &= \frac{\sigma_{ICI}^2+\sigma_w^2}{E_d}, \end{aligned} \tag{B.27}$$

where

$$\sigma_{ICI}^2 = E_d\sum_{n\neq m}E\{|H_{m,n}|^2\}+E_p\sum_{p\neq m}E\{|H_{m,p}|^2\} \tag{B.28}$$

is the power of ICI from other subcarriers rather than the m^{th} subcarrier of interest.

Appendix C

C.1 Proof of Cramér-Rao Lower Bound for Iterative Channel Estimation

In this Appendix, we first introduce the Minimum Variance Unbiased (MVU) estimator, then we calculate the Cramér-Rao Lower Bound (CRLB) of OFDM channel estimator and show that it equals the MSE of an iterative MLE and hence iterative MLE is the MVU. Defining a mathematical model (i.e. PDF) $p(\mathbf{x};\theta)$, where $\mathbf{x}$ is the observation data set with N samples and θ is the parameter of interest, according to estimation theory [97], an estimator being MVU estimator should satisfy following two conditions. Firstly, the estimator has to be unbiased, that is:

$$E\{\widehat{\theta}\} = \theta. \tag{C.1}$$

Secondly, the estimator has to have a minimum variance, i.e.

$$\widehat{\theta}_{MVU} = \arg\min_{\widehat{\theta}} E\{|\widehat{\theta} - E\{\widehat{\theta}\}|^2\}. \tag{C.2}$$

The variance of any unbiased estimator $\widehat{\theta}$ must be lower bounded by the CRLB, with the variance of the MVU estimator attaining the CRLB. The CRLB is defined as:

$$E\{|\widehat{\theta} - E\{\widehat{\theta}\}|^2\} \geq \frac{1}{-E[\frac{\partial^2 \ln p(\mathbf{x};\theta)}{\partial \theta^2}]}, \tag{C.3}$$

and

$$E\{|\widehat{\theta}_{MVU} - E\{\widehat{\theta}_{MVU}\}|^2\} = \frac{1}{-E[\frac{\partial^2 \ln p(\mathbf{x};\theta)}{\partial \theta^2}]}. \tag{C.4}$$

In some cases the MVU estimator may not exist. The MLE approach is an alternative method in cases where the PDF is known. With MLE the unknown

parameter is estimated by maximizing the PDF, i.e.

$$\widehat{\theta}_{MLE} = \arg\max_{\theta} = p(\mathbf{x};\theta). \tag{C.5}$$

It can be shown that $\widehat{\theta}_{MLE}$ is asymptotically unbiased:

$$\lim_{N\to\infty} E\{\widehat{\theta}_{MLE}\} = \theta, \tag{C.6}$$

and asymptotically efficient(it can achieve the CRLB):

$$\lim_{N\to\infty} E\{|\widehat{\theta}_{MLE} - E\{\widehat{\theta}_{MLE}\}|^2\} = CRLB. \tag{C.7}$$

In this Appendix, dropping the symbol time index i for brevity, equation (3.55) can be rewritten as:

$$\widehat{\mathbf{H}}_{MLE} = \mathbf{G}\mathbf{h}^{'} + \mathbf{G}(\mathbf{G}^H\mathbf{G})^{-1}\mathbf{G}^H(\widehat{\mathbf{X}^{'}})^{-1}\mathbf{W}^{'} = \mathbf{H}^{'} + \mathbf{W}^{''}, \tag{C.8}$$

and it can be observed that $\mathbf{H}^{'}$ is equivalent to a linear transform of $\mathbf{h}^{'}$, $\mathbf{W}^{''}$ is the effective noise with Gaussian distribution $\mathcal{N}(0, {\sigma_w^{'}}^2)$. Hence, the asymptotically unbiased property is satisfied as:

$$E\{\widehat{\mathbf{H}}_{MLE}\} = \mathbf{G}\mathbf{h}^{'} = \mathbf{H}^{'}. \tag{C.9}$$

To show the asymptotically efficient property of the MLE, we first compute the CRLB and compare it with the MSE of $\widehat{\mathbf{H}}_{MLE}$. Defining $\mathbf{H}_R^{'}$ and $\mathbf{H}'_I$ as the real and imaginary components of $\mathbf{H}^{'}$, and defining $\Xi = (\mathbf{H}_R^{'T}, \mathbf{H}_I^{'T})^T$, the $(i,j)^{th}$ element of Fisher information matrix for Ξ is given by:

$$[\mathbf{F}]_{i,j} = -E[\frac{\partial^2 \ln p(\widehat{\mathbf{H}}_{MLE};\Xi)}{\partial\Xi_i\partial\Xi_j}], \tag{C.10}$$

where $p(\widehat{\mathbf{H}}_{MLE};\Xi)$ is the probability density function of $\widehat{\mathbf{H}}_{MLE}$ given Ξ [97], which is computed as:

$$p(\widehat{\mathbf{H}}_{MLE};\Xi) = \frac{1}{(\pi{\sigma_w^{'}}^2)^N}\exp\{-\frac{1}{{\sigma_w^{'}}^2}(\widehat{\mathbf{H}}_{MLE} - \mathbf{G}\mathbf{h}^{'})^H(\widehat{\mathbf{H}}_{MLE} - \mathbf{G}\mathbf{h}^{'})\} \tag{C.11}$$

Hence, by substituting (C.11) into (C.10), the Fisher information matrix is obtained

as [98]:

$$\mathbf{F} = \frac{2}{\sigma_w^{'\,2}} \begin{bmatrix} \Re\{\mathbf{G}^H\mathbf{G}\} & -\Im\{\mathbf{G}^H\mathbf{G}\} \\ \Im\{\mathbf{G}^H\mathbf{G}\} & \Re\{\mathbf{G}^H\mathbf{G}\} \end{bmatrix}. \tag{C.12}$$

Then the inverse of Fisher information matrix is given by:

$$\mathbf{F}^{-1} = \frac{2}{\sigma_w^{'\,2}} \begin{bmatrix} \Re\{(\mathbf{G}^H\mathbf{G})^{-1}\} & -\Im\{(\mathbf{G}^H\mathbf{G})^{-1}\} \\ \Im\{(\mathbf{G}^H\mathbf{G})^{-1}\} & \Re\{(\mathbf{G}^H\mathbf{G})^{-1}\} \end{bmatrix}. \tag{C.13}$$

Therefore, the CRLB is given by:

$$\begin{aligned} CRLB(\widehat{\mathbf{H}}_{MLE}) &= Tr(\mathbf{G}\mathbf{F}^{-1}\mathbf{G}^H) \\ &= \sigma_w^{'\,2} Tr(\mathbf{G}(\mathbf{G}^H\mathbf{G})^{-1}\mathbf{G}^H) \\ &= \frac{\sigma_w^{'\,2}}{N} Tr(\mathbf{G}\mathbf{G}^H). \end{aligned} \tag{C.14}$$

which equals to the MSE of MLE in equation (3.59).

Bibliography

[1] M. K. Varanasi and B. Aazhang, "Near-optimal detection in synchronous code-division multiple-access systems," *IEEE Trans. Commun.*, vol. 39, pp. 725–736, May 1991.

[2] A. Viterbi, *CDMA: Principle of spread spectrum communications.* Addison-Wesley, 1995.

[3] S. Haykin and M. Moher, *Modern wireless communications.* Prentice Hall, 2005.

[4] J. Hagenauer, "The turbo principle: Tutorial introduction and state of the art," in *Proc. Int. Symp. Turbo Codes and Related Topics*, Brest, France, Sept 1997.

[5] F. Tarköy, "Iterative multiuser decoding for asynchronous users," in *Proc. Int. Symp. on Inform. Theory (ISIT)*, Ulm, Germany, Jun 1997, p. 30.

[6] M. C. Reed, C. B. Schlegel, P. D. Alexander, and J. A. Asenstorfer, "Iterative multiuser detection for CDMA: Near single user performance," *IEEE Trans. Commun.*, vol. 46, no. 12, pp. 1693–1699, Dec 1998.

[7] M. Moher, "An iterative multiuser decoder for near-capacity communications," *IEEE Trans. Commun.*, vol. 46, pp. 870–880, July 1998.

[8] C. Berrou, A. Glavieux, and P. Thitimajshima, "Near Shannon limit error-correction coding and decoding: Turbo codes," in *Proc. Int. Conf. on Communications (ICC)*, Geneva, Switzerland, 1993, pp. 1064–1070.

[9] C. Berrou and A. Glavieux, "Near optimum error-correcting coding and decoding: Turbo codes," *IEEE Trans. Commun.*, vol. 44, no. 10, pp. 1261–1271, Oct 1996.

[10] G. D. Forney, *Concatenated Codes.* MIT Press, 1966.

[11] "Orthogonal frequency division multiplexing," U.S.Patent, Tech. Rep. 34884555, 1970.

[12] L. J. Cimini, "Analysis andsimulation of a digital mobile channel using orthogonal frequency division multiplexing," *IEEE Trans. Commun.*, vol. 33, no. 7, pp. 665–675, July 1985.

[13] R. V. Nee and R. Prasad, *OFDM for wireless multimedia communications.* Artech House Publishers, 2000.

[14] H. Liu and G. Q. Li, *OFDM-Based Broadband Wireless Networks: Design and Optimization.* Wiley, 2005.

[15] *Part 11: Wireless LAN Medium Access Control (MAC) and Physical Layer (PHY) Specification: High-Speed Physical Layer in the 5GHz Band*, IEEE Std. 802.11a, 1999.

[16] *Local and Metropolitan Area Networks–Part 16, Air Interface for Fixed Broadband Wireless Access systems*, IEEE Std. 802.16a, 2003.

[17] *Draft 12: Local and Metropolitan Area Networks–Part 16, Air Interface for Fixed Broadband Wireless Access systems*, IEEE Std. 802.16e, 2005.

[18] P. Hoeher, S. Kaiser, and P. Robertson, "Two dimensional pilot symbol aided channel estimation by wiener filtering," in *Proc. IEEE ICASSP*, Munich, Germany, Apr 1997, pp. 1845–1848.

[19] B. Yang, K. B. Letaief, R. S. Cheng, and Z. Cao, "Channel estimation for OFDM transmission in multipath fading channels based on parametric channel modeling," *IEEE Trans. Commun.*, vol. 49, no. 3, pp. 467–479, Mar 2001.

[20] M. de Courville, P. Duhamel, P. Madec, and J. Palicot, "Blind equalization of ofdm systems basesd on minimization of a quadratic criterion," in *Proc. IEEE Int. Conf. Communications*, Dallas, U.S.A., Jun 1996, pp. 1318–1321.

[21] X. Wang and H. V. Poor, "Blind equalization and multiuser detection for CDMA communications in dispersive channels," *IEEE Trans. Commun.*, vol. 46, pp. 91–103, Jan 1998.

[22] B. Lu and X. Wang, "Bayesian blind turbo receiver for coded OFDM systems with frequency offset and frequency selective fading," *IEEE J. Select. Areas Commun.*, vol. 12, no. 19, pp. 2516–2527, Dec 2001.

[23] A. Dowler, A. Nix, and J. McGeehan, "Data-derived iterative channel estimation with channel tracking for a mobile fourth generation wide area OFDM system," in *Proc. IEEE GLOBECOM*, vol. 2, San Francisco, U.S.A., Dec 2003, pp. 804–808.

[24] R. Negi and J. Cioffi, "Pilot tone selection for channel estimation in a mobile OFDM system," *IEEE Trans. Consumer Electron.*, vol. 44, pp. 1122–1128, Aug 1998.

[25] J. J. V. de Beek, O. Edfors, M. Sandell, S. K. Wilson, and P. O. Börjesson, "On channel estimation in OFDM systems," in *Proc. IEEE VTC-Fall*, Chicago, U.S.A., July 1995, pp. 815–819.

[26] ——, "OFDM channel estimation by singular value decomposition," in *Proc. IEEE VTC*, Atlanta, U.S.A., Apr 1996, pp. 923–927.

[27] O. Edfors, M. Sandell, J. J. V. de Beek, S. K. Wilson, and P. O. Börjesson, "OFDM channel estimation by singular value decomposition," *IEEE Trans. Commun.*, vol. 46, pp. 931–939, July 1998.

[28] V. Mignone and A. Morello, "CD3-OFDM, a novel demodulation scheme for fixed and mobile receivers," *IEEE Trans. Commun.*, vol. 44, no. 12, pp. 1144–1151, Sept 1996.

[29] Y. Li, L. J. Cimini, and N. R. Sollenberger, "Robust channel estimation for OFDM systems with rapid dispersive fading channels," *IEEE Trans. Commun.*, vol. 46, no. 7, pp. 902–915, July 1998.

[30] A. Stamoulis, S. N. Diggavi, and N. Al-Dhahir, "Intercarrier interference in MIMO OFDM," *IEEE Trans. Signal Processing*, vol. 50, no. 10, pp. 2451–2464, Oct 2002.

[31] C. Y. Shin and E. J. Powers, "Double selective channel estimation for OFDM systems," in *Proc. IEEE Asilomar*, Pacific Grove, U.S.A., Nov 2005.

[32] T. Zemen and C. F. Mecklenbräuker, "Time-variant channel estimation using discrete prolate spheroidal sequences," *IEEE Trans. Signal Processing*, vol. 53, no. 9, pp. 3597–3607, Sep 2005.

[33] T. Zemen, C. F. Mecklenbräuker, J. Wehinger, and R. R. Müller, "Iterative joint time-variant channel estimation and multi-user detection for MC-CDMA," *IEEE Trans. Wireless Commun.*, vol. 5, no. 6, pp. 1469–1478, Jun 2006.

[34] J. Kim, C. W. Wang, and W. E. Stark, "Frequency domain channel estimation for OFDM based on slepian basis expansion," in *Proc. Int. Conf. on Communications (ICC)*, Glasgow, UK, Jun 2007, pp. 3011–3015.

[35] D. Slepian, "Prolate spheroidal wave functions, fourier analysis and uncertainty - V: The discrete case," *Bell Syst. Technical Journal*, vol. 57, no. 5, pp. 1371–1430, May-Jun 1978.

[36] G. B. Giannakis and C. Tepedelenlioglu, "Basis expansion models and diversity techniques for blind identification and equalization of time-varying channels," *Proc. IEEE*, vol. 86, no. 10, pp. 1969–1986, Oct 1998.

[37] X. Ma and G. B. Giannakis, "Maximum-diversity transmission of doubly selective wireless channels," *IEEE Trans. Inform. Theory*, vol. 49, no. 7, pp. 1832–1840, Jul 2003.

[38] P. Schniter, "Low-complexity estimation of double-selective channels," in *Proc. IEEE SPAWC*, Rome, Italy, Jun 2003, pp. 200–204.

[39] A. P. Kannu and P. Schniter, "Reduced complexity decision-directed pilot-aided tracking of double-selective channels," in *Proc. CISS*, Princeton, U.S.A., Mar 2004, pp. 915–920.

[40] Y. Li, N. Seshadri, and S. Ariyavisitakul, "Channel estimation for OFDM systems with transmitter diversity in mobile wireless channels," *IEEE J. Select. Areas Commun.*, vol. 17, no. 3, pp. 461–471, Mar 1999.

[41] Y. Li, "Simplied channel estimation for OFDM systems with multiple transmit antennas," *IEEE Trans. Wireless Commun.*, vol. 1, no. 1, pp. 67–75, Jan 2002.

[42] Y. Li, J. H. Winters, and N. R. Sollenberger, "MIMO-OFDM for wireless communications: Signal detection with enhanced channel estimation," *IEEE Trans. Commun.*, vol. 50, no. 9, pp. 1471–1477, Sept 2002.

[43] B. Song, W. Zhang, and L. Gui, "Iterative joint channel estimation and signal detection in MIMO OFDM system," in *Proc. IEEE WCNM*, Wuhan, China, Sept 2005, pp. 39–43.

[44] S. Y. Park, Y. G. Kim, and C. G. Kang, "Iterative receiver for joint detection and channel estimation in OFDM systems under mobile radio channels," *IEEE Trans. Veh. Technol.*, vol. 53, pp. 450–460, Mar 2004.

[45] S. Tomasin, A. Gorokhov, H. Yang, and J. P. Linnartz, "Iterative interference cancellation and channel estimation for mobile OFDM," *IEEE Trans. Wireless Commun.*, vol. 4, pp. 238–245, Jan 2005.

[46] *Third Generation Partnership Project; Technical Specification Group Radio Access Network: Physical Layer Aspects for Evolved UTRA*, 3GPP Std. TR 25.814, 2006.

[47] A. B. Gershman and N. D.Sidiropoulos, *Space-Time Processing for MIMO Communications*. Wiley, 2005.

[48] D. Gesbert, M. Shafi, D. Shiu, P. J. Smith, and A. Naguib, "From theory to practice: an overview of mimo space-time coded wireless systems," vol. 21, no. 3, pp. 281–302, Apr 2003.

[49] P. W. Wolniansky, G. J. Foschini, G. D. Golden, and R. A. Valenzuela, "V-blast: an architecture for realizing very high data rates over the rich-scattering wireless channel," in *Proc. URSI Int. Symp. Signals, Systems, and Electronics*, Pisa, Italy, 29 Sep-2 Oct 1998, pp. 295–300.

[50] L. Hanzo, C. H. Wong, and M. S. Yee, *Adaptive wireless transceivers*. Wiley, 2003.

[51] B. Muquet, E. Biglieri, A. Goldsmith, and H. Sari, *MIMO Techniques for mobile WiMAX systems*. SEQUANS communication white paper, 2006.

[52] S. M. Alamouti, "A simple transmit diversity technique for wireless communications," vol. 16, no. 4, pp. 1451–1458, Oct 1998.

[53] D. Tse and P. Viswanath, *Fundamentals of wireless communications*. Cambridge University Press, 2005.

[54] B. Lu, X. Wang, and Y. Li, "Iterative receivers for space-time block coded OFDM systems in dispersive fading channels," *IEEE Trans. Wireless Commun.*, vol. 1, pp. 213–225, Apr 2002.

[55] Y. Sun, Z. Xiong, and X. Wang, "EM-based iterative receiver design with carrier frequency offset estimation for MIMO OFDM systems," *IEEE Trans. Commun.*, vol. 53, no. 4, pp. 581–586, Apr 2005.

[56] J. Ylioinas and M. Juntti, "EM based iterative receiver for joint decoding and channel parameter estimation in space-frequency turbo coded OFDM," in *Proc. IEEE Int. Symp. Pers. Indoor. Mobile Radio Commun*, Helsinki, Finland, Sep 2006, pp. 1–5.

[57] ——, "An iterative receiver for joint detection, decoding, and channel estimation in turbo coded MIMO OFDM," in *Proc. Annual Asilomar Conf. signals. Syst. Comp*, Pacific Grove, CA, Nov 2007, pp. 1784–1796.

[58] ——, "Comparison of three list detectors in iterative decoding and channel estimation in MIMO OFDM," in *Proc. IEEE Tenth Int. Symp. on Spread Spectrum Techniques and Applications (ISSSTA)*, Bologna, Italy, Aug 2008, pp. 140–144.

[59] ——, "Iterative joint detection, decoding, and channel estimation in turbo coded MIMO-OFDM," *IEEE Trans. Veh. Technol.*, vol. 58, no. 4, pp. 1784–1796, May 2009.

[60] W. G. Song and J. T. Lim, "Channel estimation and signal detection for MIMO-OFDM with time varying channels," *IEEE Commun. Lett.*, vol. 10, pp. 540–542, Jul 2006.

[61] J. Moon, H. Jin, T. Jeon, and S. K. Lee, "Channel estimation for MIMO-OFDM systems employing spatial multiplexing," in *Proc. IEEE VTC-Fall*, Los Angeles, U.S.A., Sept 2004, pp. 3649–3654.

[62] D. Hu, L. Yang, Y. Shi, and L. He, "Optimal pilot sequence design for channel estimation in MIMO OFDM systems," *IEEE Commun. Lett.*, vol. 10, no. 1, pp. 1–3, Jan 2006.

[63] H. V. Poor and S. Verdú, "Probability of error in MMSE multiuser detection," *IEEE Trans. Inform. Theory*, vol. 43, pp. 858–871, May 1997.

[64] E. Viterbo and J. Boutros, "A universal lattice code decoder for fading channels," *IEEE Trans. Inform. Theory*, vol. 45, pp. 1639–1642, July 1997.

[65] B. Hassibi and H. Vikalo, "On the sphere-decoding algorithm I. expected complexity," *IEEE Trans. Signal Processing*, vol. 53, no. 8, pp. 2806–2818, Aug 2005.

[66] U. Fincke and M. Pohst, "Improved methods for calculating vectors of short length in a lattice, including a complexity analysis," *Math.Comput.*, vol. 44, no. 4, pp. 463–471, Apr 1985.

[67] C. P. Schnorr and M. Euchner, "Lattice basis reduction: Improved pratical algorithms and solving subset sum problems," *Math.Programming.*, vol. 66, pp. 181–191, 1994.

[68] M. Damen, H. Gamal, and G. Caire, "On maximum-likelihood detection and the search for the closest lattice point," *IEEE Trans. Inform. Theory*, vol. 49, no. 10, pp. 2389–2402, Oct 2003.

[69] Z. Guo and P. Nilsson, "Algorithm and implementation of the K-best sphere decodign for MIMO detection," *IEEE J. Select. Areas Commun.*, vol. 24, no. 3, pp. 491–503, Mar 2006.

[70] M. Myllylä, M. Juntti, and J. R. Cavallaro, "A list sphere detector based on dijkstra's algorithm for MIMO-OFDM system," in *Proc. IEEE Int. Symp. Pers. Indoor. Mobile Radio Commun*, Athens, Greece., Sep 2007, pp. 1–5.

[71] E. Agrell, T. Eriksson, A. Vardy, and K. Zeger, "Closest point search in lattices," *IEEE Trans. Inform. Theory*, vol. 45, pp. 2201–2214, Aug 2002.

[72] B. Hocheald and S. ten Brink, "Achieving near capacity on a multiple-antenna channel," *IEEE Trans. Commun.*, vol. 51, no. 3, pp. 389–399, Mar 2003.

[73] H. Vikalo, B. Hassibi, and T. Kailath, "Iterative decoding for MIMO channels via modified sphere decoding," *IEEE Trans. Wireless Commun.*, vol. 3, no. 6, pp. 2299–2311, Nov 2004.

[74] J. Choi, Y. Hong, and J. Yuan, "An approximate MAP-based iterative receiver for MIMO channels using modified sphere detection," *IEEE Trans. Wireless Commun.*, vol. 5, no. 8, pp. 2119–2126, Aug 2006.

[75] S. Verdú, "Minimun probability of error for asynchronous gaussian multiple-access channels," *IEEE Trans. Inform. Theory*, vol. 32, pp. 85–96, Jan 1986.

[76] ——, *Multiuser detection.* Cambridge Univ. Press, 1998.

[77] V. Buchoux, O. Cappe, and E. Moulines, "Turbo multiuser detection for coded DS-CDMA systems: a gibbs sampling approach," in *Proc. Thirty-Fourth Asilomar Conf. Signals, Systems and Computers*, Pacific Grove, U.S.A., 29 Oct.-1 Nov 2000, pp. 1426–1430.

[78] R.Chen, J. S. Liu, and X. Wang, "Convergence analysis and comparisons of markov chain monte carlo algorithms in digital communications," *IEEE Trans. Signal Processing*, vol. 50, no. 2, pp. 255–270, Feb 2002.

[79] B. Farhang-Boroujeny, H. Zhu, and Z. Shi, "Markov chain monte carlo algorithm for CDMA and MIMO communication systems," *IEEE Trans. Signal Processing*, vol. 54, no. 5, pp. 1896–1909, May 2006.

[80] C. R. Robert and G. Casella, *Monte Carlo Statistical Methods.* New York: Springer-Verlag, 1999.

[81] X. Mao, P. Amini, and B. Farhang-Boroujeny, "Markov chain monte carlo MIMO detection methods for high signal-to-noise ratio regimes," in *Proc. IEEE GLOBECOM*, Washington, U.S.A., 26-30 Nov 2007, pp. 3979–3983.

[82] H. Zhu, B. Farhang-Boroujeny, and R.-R. Chen, "On performance of shpere decoding and markov chain monte carlo detection methods," *IEEE Signal Processing Lett.*, vol. 12, no. 10, pp. 669–672, Oct 2005.

[83] M. Dangl, Z. Shi, and M. C. Reed, "Advanced markov chain monte carlo methods for iterative (turbo) multiuser detection," in *Proc. ISTC*, Munich, Germany, Apr 2006.

[84] T. S. Rappaport, *Wireless Communications, Principle and Practice.* Prentice-Hall, 1996.

[85] W. G. Jeon, K. H. Chang, and Y. S. Cho, "An equalization technique for orthogonal frequency-division multiplexing system in time-variant multipath channel," *IEEE Trans. Commun.*, vol. 47, pp. 27–32, Jan 1999.

[86] W. C. Jakes, *Microwave Mobile Communications.* IEEE Press, 1994.

[87] *Guidelines for evaluation of radio transmission technologies for IMT-2000*, ITU-T Std. M.1225, 1997.

[88] M. Russell and G. Stuber, "Interchannel interference analysis of OFDM in a mobile environment," in *Proc. IEEE VTC-Fall*, Chicago, U.S.A., 1995, pp. 820–824.

[89] M. Zhao, Z. Shi, and M. C. Reed, "Iterative turbo channel estimation for OFDM system over rapid dispersive fading channel," *IEEE Trans. Wireless Commun.*, vol. 7, no. 8, pp. 3174–3184, Aug 2008.

[90] X. D. Wang and H. V. Poor, "Iterative (turbo) soft interference cancellation and decoding for coded CDMA," *IEEE Trans. Commun.*, vol. 47, no. 7, pp. 1046–1061, July 1999.

[91] L. R. Bahl *et al.*, "Optimal decoding of linear codes for minimizing symbol error rate," *IEEE Trans. Inform. Theory*, vol. 20, pp. 284–287, Mar 1974.

[92] A. Viterbi, "Error bounds for convolutional codes and an asymptotically optimum decoding algorithm," *IEEE Trans. Inform. Theory*, vol. 13, no. 2, pp. 260–269, Apr 1967.

[93] A. Viterbi and J. Omura, *Principles of Digital Communications and Coding*. McGraw-Hill, 1979.

[94] J. G. Proakis, *Digital Communications*. McGraw-Hill, 2000.

[95] A. Papoulis and S. U. Pillai, *Probability, Random Variables and Stochastic Processes*. McGraw-Hill, 2002.

[96] Y. Qiao, S. Yu, P. Su, and L. Zhang, "Research on an interative algorithm of LS channel estimation in MIMO OFDM systems," *IEEE Trans. Broadcast.*, vol. 51, no. 1, pp. 149–153, Mar 2005.

[97] S. M. Kay, *Fundamentals of Statistical Signal Processing: Estimation Theory*. Englewood Cliffs, NJ: Prentice-Hall, 1993.

[98] M. Morelli and U. Mengali, "A comparison of pilot-aided channel estimation methods for OFDM systems," *IEEE Trans. Signal Processing*, vol. 49, no. 12, pp. 3065–3073, Dec 2001.

[99] K. E. Baddour and N. C. Beaulieu, "Robust doppler spread estimation in nonisotropic fading channels," *IEEE Trans. Wireless Commun.*, vol. 4, no. 6, pp. 2677–2682, Nov 2005.

[100] L. L. Scharf, *Statistical Signal Processing.* Addison-Wesley, 1991.

[101] R. M. Mersereau and T. C. Speake, "The processing of periodically sampled multidimensional signals," *IEEE Trans. Acoust., Speech, Signal Processing*, vol. ASSP-31, pp. 188–194, Feb 1983.

[102] S. Haykin, *Adaptive filter theory.* Prentice Hall, 1996.

[103] R. W. Heath, S. Sandhu, and A. Paulraj, "Antenna selection for spatial multiplexing system with linear receivers," *IEEE Commun. Lett.*, vol. 5, no. 4, pp. 142–144, Apr 2001.

[104] R. W. Heath and A. J. Paulraj, "Switching between diversity and multiplexing in MIMO systems," *IEEE Trans. Commun.*, vol. 53, no. 6, pp. 962–968, Jun 2005.

[105] Y. Li and X. G. Xia, "Iterative demodulation/decoding methods based on gaussian approximations for lattice based space-time coded systems," *IEEE Trans. Wireless Commun.*, vol. 5, no. 8, pp. 1976–1983, Aug 2006.

[106] E. Kreyszig, *Advanced Engineering Mathematics.* Peter Janzow, 1999.

[107] M. A. Dangl, C. Sgraja, and J. Lindner, "Block turbo equalization for imperfect channel state information," in *Proc. IEEE Int. Symp. Information Theory*, Adelaide, Australia, Sept 2005, pp. 2016–2020.

[108] *Spatial channel model for MIMO simulation*, 3GPP Std. TR. 25.996 V6.1.0, Sept 2003. [Online]. Available: http://www.3gpp.org/

[109] G. H. Golub and C. F. V. Loan, *Matrix computations.* Johns Hopkins, 1996.

[110] H. Vikalo and B. Hassibi, "On the sphere-decoding algorithm II. generalizations, second-order statistics, and application to communications," *IEEE Trans. Signal Processing*, vol. 53, no. 8, pp. 2819–2834, Aug 2005.

[111] M. Metropolis, A. W. Rosenbluth, A. H. Teller, and E. Teller, "Equations of state calculations by fast computing machines," *J. Chem. Phys.*, vol. 21, pp. 1087–1091, 1953.

[112] W. K. Hastings, "Monte Carlo sampling methods using Markov Chains and their applications," *Biometrika*, vol. 57, pp. 97–109, 1970.

[113] S. Geman and D. Geman, "Stochastic relaxation, Gibbs distribution, and the Bayesian restoration of images," *IEEE Trans. Pattern Anal. Machine Intell.*, vol. 6, pp. 721–741, Nov 1984.

[114] J. K. Ruanaidh and J. J. O'Ruanaidh, *Numeraical Bayesian Methods Applied to Signal Processing*. New York: Springer-Verlag, 1996.

[115] K. S. Chan, "Asymptotic behavior of the Gibbs sampler," *J. Amer. Stat. Assoc.*, vol. 88, pp. 320–326, 1993.

[116] J. S. Liu, W. H. Wong, and A. Hong, "Covariance structure and convergence rate of the Gibbs sampler with varioius scans," *J. Roy. Statist. Soc. Ser. B*, vol. 57, pp. 157–169, 1995.

[117] L. Dou and R. J. Hodgson, "Bayesian inference and Gibbs sampling in spectral analysis and parameter estimation: I," *Inverse Problems*, vol. 11, pp. 1069–1085, 1995.

[118] J. Hammersley and D. Handscomb, *Monte Carlo Methods*. New York: Methuen, 1964.

[119] G. Fishman, *Monte Carlo: concepts, algorithms and applications*. New York: Springer-Verlag, 1996.

[120] P. Robertson, E. Villebrun, and P. Hoeher, "A comparison of optimal and suboptimal MAP decoding algorithms operating in the log domain," in *Proc. IEEE Int. Conf. Communications (ICC)*, London, UK, Jun 1995, pp. 1009–1013.

[121] J. Hagenauer, P. Robertson, and L. Papke, "Iterative turbo decoding of systematic convolutional codes with the MAP and SOVA algorithms," in *Proc. ITG Symp. Source and Channel Coding*, Trondheim, Norway, 1994, pp. 21–29.

[122] S. ten. Brink, "Convergence behavior of iteratively decoded parallel concatenated codes," *IEEE Trans. Commun.*, vol. 49, no. 10, pp. 1727–1737, Oct 2001.

[123] R. K. Martin, J. Balakrishnan, W. A. Sethares, and C. R. Johnson, "A blind adaptive TEQ for multicarrier systems," *IEEE Signal Processing Lett.*, vol. 9, no. 11, pp. 341–343, Nov 2002.

[124] R. K. Martin, J. M. Walsh, and C. R. Johnson, "Low-complexity MIMO blind adaptive channel shortening," *IEEE Trans. Signal Processing*, vol. 53, no. 4, pp. 1324–1334, Apr 2005.

[125] N. A. Dhahir, "FIR channel-shortening equalizers for MIMO ISI channels," *IEEE Trans. Commun.*, vol. 49, no. 2, pp. 213–218, Feb 2001.

[126] J. Zhang, W. Ser, and J. Zhu, "Effective optimization method for channel shortening in OFDM systems," in *Proc. IEE Commun*, vol. 150, no. 2, Apr 2003, pp. 85–90.

[127] C. Toker, S. lambotharan, J. A. Chambers, and B. Baykal, "Joint spatial and temporal channel-shortening techniques for frequency selective fading MIMO channels," in *Proc. IEE Commun*, vol. 152, no. 1, Feb 2005, pp. 89–94.

[128] L. Wang, L. Xu, S. Chen, and L. Hanzo, "Generic iterative search-center-shifting K-best sphere decodign for rank-deficient SDM OFDM systems," *IEEE Eletronics Letters*, vol. 44, no. 8, pp. 552–553, Apr 2008.

[129] ——, "A priori-LLR-threshold-assisted K-best sphere detection for MIMO channels," in *Proc. IEEE VTC-Spring*, Singapore, May 2008, pp. 867–871.